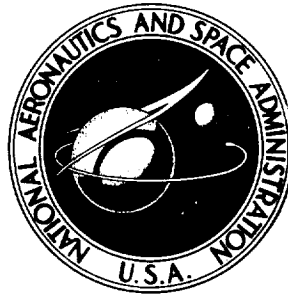


NASA CONTRACTOR  
REPORT



N73-21444  
NASA CR-2163

NASA CR-2163

CASE FILE  
COPY

HYDROGEN ENVIRONMENT  
EMBRITTLMENT OF METALS

*by R. P. Jewett, R. J. Walter, W. T. Chandler,  
and R. P. Frohberg*

*Prepared by*

ROCKETDYNE

DIVISION OF NORTH AMERICAN ROCKWELL

Canoga Park, Calif. 91304

*for*

NATIONAL AERONAUTICS AND SPACE ADMINISTRATION • WASHINGTON, D. C. • MARCH 1973



1. Report No. NASA CR-2163	2. Government Accession No.	3. Recipient's Catalog No.	
4. Title and Subtitle  HYDROGEN ENVIRONMENT EMBRITTLEMENT OF METALS		5. Report Date March 1973	
		6. Performing Organization Code	
7. Author(s) R. P. Jewett, R. J. Walter, W. T. Chandler and R. P. Frohberg		8. Performing Organization Report No.	
9. Performing Organization Name and Address  Rocketdyne Division of North American Rockwell 6633 Canoga Avenue Canoga Park, CA 91304		10. Work Unit No.	
		11. Contract or Grant No. NAS8-19(C)	
12. Sponsoring Agency Name and Address  National Aeronautics and Space Administration Washington, DC 20546		13. Type of Report and Period Covered Contractor Report	
		14. Sponsoring Agency Code	
15. Supplementary Notes			
16. Abstract  Hydrogen environment embrittlement refers to metals stressed while exposed to a hydrogen atmosphere. Tested in air, even after exposure to hydrogen under pressure, this effect is not observed on similar specimens. Much high-purity hydrogen is prepared by evaporation of liquid hydrogen, and thus has low levels for potential impurities which could otherwise inhibit or poison the absorbent reactions that are involved. High strength steels and nickel-base alloys are rated as showing extreme embrittlement; aluminum alloys and the austenitic stainless steels, as well as copper, have negligible susceptibility to this phenomenon.  The cracking that occurs appears to be a surface phenomenon, unlike that of internal hydrogen embrittlement.			
17. Key Words (Suggested by Author(s)) Hydrogen embrittlement, Hydrogen environment embrittlement, Testing in high pressure hydrogen, Effects of hydrogen environment on mechanical properties of metals, Crack behaviour in hydrogen		18. Distribution Statement  Unclassified - Unlimited	
19. Security Classif. (of this report) Unclassified	20. Security Classif. (of this page) Unclassified	21. No. of Pages 243	22. Price* \$3.00

\* For sale by the National Technical Information Service, Springfield, Virginia 22151



## FOREWORD

This report presents, describes, and discusses the nature of hydrogen-environment embrittlement. The embrittling effects of hydrogen have long been known, but it was relatively recent failures of large, high-pressure hydrogen storage vessels at NASA and NASA contractor facilities that served to focus attention specifically on hydrogen-environment embrittlement. The ensuing extensive investigations sponsored by NASA and other government agencies have considerably expanded the knowledge and understanding of this type of embrittlement.

Thus, in accordance with the NASA technology utilization program goal of "the rapid dissemination of information ... on technological developments ... which appear to be useful for general industrial application," this report was designed to acquaint a wide range of interested parties with hydrogen-environment embrittlement and to assist them in developing a course of action to deal with it.

For this report, a literature search was made and various investigators were personally contacted. The data were critically evaluated, collated, and compiled for their most effective presentation. Also included are discussions of the characteristics and proposed mechanisms for hydrogen-environment embrittlement, the extent and limitations of our understanding, associated problems and hazards, and possible means of preventing, minimizing, or compensating for hydrogen-environment embrittlement.



## ACKNOWLEDGMENTS

The study of hydrogen-environment embrittlement has grown initially from the work of a few investigators to a substantial group of investigations sponsored, for the most part, by NASA and other government agencies. The authors wish to acknowledge the help of the following individuals in obtaining the basic information:

W. Bryan McPherson	NASA-Marshall Space Flight Center
Samuel Snyder	NASA-Space Nuclear Propulsion Office, Washington
Dell P. Williams	NASA-Ames Research Center
James J. Lombardo	NASA-Space Nuclear Propulsion Office, Cleveland
Royce G. Forman	NASA-Manned Spacecraft Center
James A. Donovan	AEC-Savannah River Laboratory
Harris L. Marcus	North American Rockwell-Science Center
James C. Williams	North American Rockwell-Science Center
Peter P. Dessau	Aerojet-General Corporation
R. L. Kesterson	Westinghouse Astronuclear Laboratory
Robert P. Wei	Lehigh University
M. C. VanWanderham	Pratt & Whitney Aircraft
Joseph N. Masters	The Boeing Company
A. W. Loginow	United States Steel Corporation
Herbert H. Johnson	Cornell University



## CONTENTS

Foreword . . . . .	iii
Chapter 1. Introduction . . . . .	1
Operating Experiences . . . . .	1
Hydrogen and Metals . . . . .	4
Scope . . . . .	5
Chapter 2. Significance . . . . .	7
Availability of Low-Cost Liquid Hydrogen . . . . .	7
Usage Outlook . . . . .	8
The Overall Problem . . . . .	9
Chapter 3. Overview . . . . .	11
Internal Hydrogen Embrittlement . . . . .	13
Hydrogen-Environment Embrittlement . . . . .	17
Comparison . . . . .	19
Chapter 4. Early Work . . . . .	23
Early Service Failures Attributed to High-Pressure Hydrogen . . . . .	23
Mechanical Tests Performed in High-Pressure Hydrogen . . . . .	24
Recent Pressure Vessel Failures . . . . .	29
Chapter 5. Test Procedures . . . . .	31
Hydrogen Purification . . . . .	31
Pressurization and Line Flushing . . . . .	33
Mechanical Testing in Low-Pressure Hydrogen at Cryogenic and Ambient Temperatures . . . . .	35
Mechanical Testing in High-Pressure Hydrogen at Cryogenic and Ambient Temperatures . . . . .	37

Mechanical Testing in Hydrogen at Elevated Temperatures . . . . .	48
Chapter 6. Tensile Properties . . . . .	55
Room-Temperature Results . . . . .	57
Effect of Hydrogen Pressure . . . . .	76
Influence of Notch Severity . . . . .	81
Effect of Hold Time . . . . .	87
Effect of Temperature . . . . .	92
Embrittlement of Welds in Pressure Vessel Steels . . . . .	99
Effect of Hydrogen on Stress-Strain Curves . . . . .	103
Chapter 7. Other Mechanical Properties . . . . .	107
Creep and Stress Rupture . . . . .	107
Fatigue Properties . . . . .	107
Fracture Mechanics . . . . .	128
Crack Growth . . . . .	134
Chapter 8. Metallography . . . . .	149
Slightly Embrittled Specimens . . . . .	150
Severely Embrittled Specimens . . . . .	152
Extremely Embrittled Specimens . . . . .	159
Fractography of Specimens Fatigue Tested in Hydrogen . . . . .	164
Chapter 9. Preventive Measures . . . . .	169
Coatings . . . . .	169
Impurity Additions to Hydrogen . . . . .	174

Chapter 10. Discussion . . . . .	177
General . . . . .	177
Tensile Tests . . . . .	179
Surface Cracking in Hydrogen . . . . .	182
Crack Propagation in Hydrogen . . . . .	185
Effect of Hydrogen Environments on Other Properties . . . . .	189
Metals Susceptible to Hydrogen-Environment Embrittlement . . . . .	189
Effect of Various Parameters on Degree of Hydrogen-	
Environment Embrittlement . . . . .	191
Mechanism . . . . .	195
Chapter 11. Summary . . . . .	203
Chapter 12. Recommendations . . . . .	207
References . . . . .	211
Appendix: Work in Progress . . . . .	219



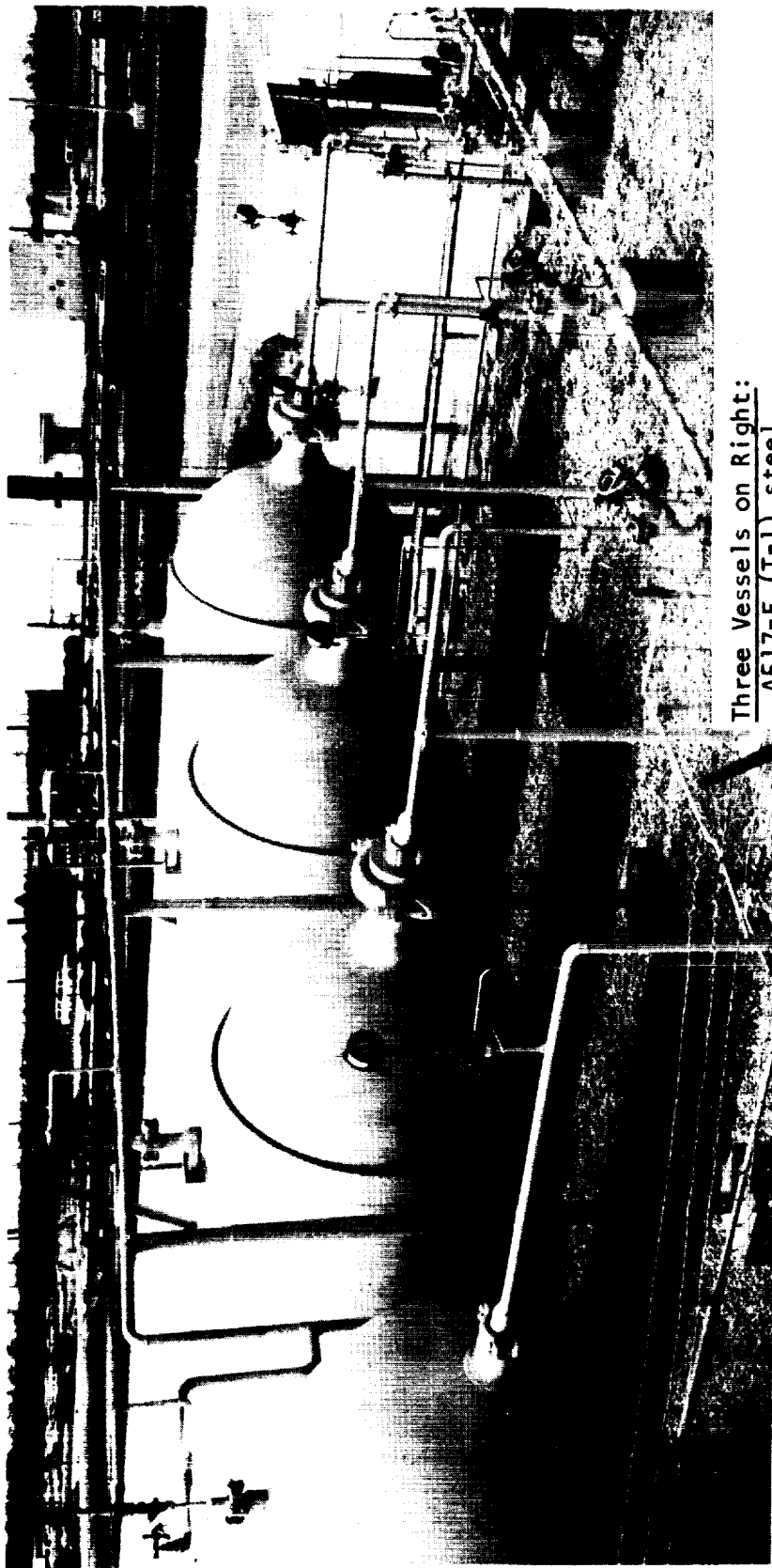
## CHAPTER 1. INTRODUCTION

### Operating Experiences

In 1965, a space program contractor experienced a failure of a large high-pressure hydrogen tank. Shortly afterward, a vessel failed at a NASA facility while being filled to rated pressure with gaseous hydrogen, and a total of six failures in five tanks occurred in less than 1 year. These were all pressure vessels which, according to general knowledge at that time, should not have failed.

These events were important because the failures were experienced in large, laminated (1500-cu ft volume or greater), thick-walled tanks designed to store gaseous hydrogen at 5000 to 10 000 psi, and the investment in a single tank could be as high as a quarter-million dollars. Fortunately, the failures were by leakage, or "whistlers," but the potential damage and loss of life caused by the explosion and fire of such an installation are staggering. A typical facilities installations is shown in Fig. 1.

In 1968, during the final stages of preparation for the Mariner '69 mission to Mars, it was realized that a nickel-base-alloy hydrogen tank was subject to the same environmental embrittling effects of gaseous hydrogen. Subsequent laboratory work showed that the threshold fracture toughness for the Inconel 718 alloy was reduced to 15 percent of its basic fracture toughness for the base metal and to 22 percent for weldments when tested in hydrogen. This dramatic reduction of fracture toughness in hydrogen, led to the replacement of Inconel 718 in these pressure vessels with an aluminum alloy, whose threshold fracture toughness was much less affected, thus reducing the probability of a tank failure and possible loss of an expensive mission to Mars.



Vessel on Left:

1146a steel,  
multiple-layer vessel,  
solid head  
(A.O. Smith)  
(CB&I)

Water Volume, ft<sup>3</sup> 1256  
Design Pressure, psi 5000

Added after other vessels reduced in pressure

Three Vessels on Right:

A517-F (T-1) steel,  
multiple-layer vessel,  
solid head

Water Volume, ft<sup>3</sup> 1375  
Length, feet 74

Inside Diameter, inches 60  
Outside Diameter, inches 71

Design Pressure, psi 6300  
Safety Factor 3 to 1

Working pressure reduced to 4500 psi

Figure 1. NASA/Mississippi Test Facility, Bay St. Louis, Mississippi

The alarming feature of these experiences was that the prior knowledge of hydrogen embrittlement was not adequate to explain these effects. The large storage vessels were made of low-strength structural grades of steel, normally considered unaffected by hydrogen. So also with Inconel 718 and other nickel-base alloys. The extensive work on delayed failure and internal-hydrogen embrittlement had shown that nickel-base alloys were unaffected by hydrogen except under the most severe hydrogen charging conditions. At that time, an awareness was just emerging regarding the differentiation of effects between ionic hydrogen in interstitial solution in the metal lattice and that of gaseous hydrogen external to and surrounding a nucleating and advancing crack front.

The many unique properties of hydrogen have led to widespread and increasing usage in nuclear programs, space programs and, in some cases, advanced aircraft programs. In addition to pure hydrogen, there are many cases where combustion or reaction products contain or produce hydrogen, and hardware must operate in these environments. Frequently, hardware development programs reveal the necessity for design changes during the component development stage, where adjustments for reduced load-carrying ability can be made. However, the penalty of a downrated or overweight piece of hardware in a high-performance system is too high to accept. Add to this the fact that a hardware development cycle which permits life and environment simulation--even in the laboratory--is not always available. Many times a system is unique, only one or two will be built, and a long life is required. The foregoing events and facts lead to only one conclusion. Since we must work with hydrogen, we must understand all the relationships between hydrogen and metals and the ultimate effects of these relationships on operating components and systems.

## Hydrogen and Metals

The relationship between hydrogen and metals may be broadly placed into three categories:

1. Hydrogen chemical reactions
2. Internal-hydrogen embrittlement
3. Hydrogen-environment embrittlement

The first two of these have been fairly well explored, while the third is the subject of this report. All three will be described briefly here and in more detail in Chapter 3, as sometimes there is confusion between these very different effects.

One case of hydrogen chemical reactions is typified by the long-recognized "steam reaction" in copper, in which hydrogen reacts with oxygen in solid copper to form  $H_2O$ . A similar situation occurs with steel, when carbon reacts with hydrogen in the lattice to form methane. In such cases, conditions of temperature, pressure, and chemical environment must be conducive to such reactions, and the resultant gas pressures lead to development of fissures, strength reduction, and cracking.

Another type of hydrogen reaction is found in the hydriding of the base metal or alloying constituents. Thus, under appropriate exposure conditions, metals such as titanium, columbium (niobium), and tantalum form hydrides. Since the properties of the hydride compound are so very different, the mechanical properties of the base metal or of an alloy containing these elements may degrade or, in the extreme cases, the metallic part may be converted to the hydride.

Internal-hydrogen embrittlement is the case where high-strength steels containing hydrogen in interstitial solid solution experience delayed failure in service. Many examples have been found in the manufacture of hardened springs, washers, etc. Perhaps the most dramatic cases were seen in the early 1950's when high-strength steel aircraft landing gear struts were under development. There were cases reported in which a test aircraft would successfully sustain one or more hard landings, imposing severe loads on the landing gear, but later would collapse while standing parked on the apron. This type of embrittlement has been studied in some detail, and the phenomenon of delayed failure due to hydrogen in high-strength steel has been well characterized. The principal characteristic of this effect is that hydrogen in solution is the cause of delayed failure, and the effect is essentially independent of its external environment during test or in service.

Hydrogen-environment embrittlement, as the name implies, takes place while the metal is stressed in hydrogen. A specimen exposed to high-pressure hydrogen, then tested in air does not exhibit this environmental effect. Thus, it was not until specimens were placed in pure hydrogen gas at pressures on the order of 10 000 psi and the specimen loaded to failure in this environment that the effect was isolated and reproduced. The experimental difficulties involved can be significant.

#### Scope

It is the purpose of this work to isolate and describe hydrogen-environment embrittlement as a separate and distinct effect of hydrogen on metals. Engineers

are generally acquainted with internal-hydrogen embrittlement. Too often they try to equate all hydrogen effects in metals or otherwise extend our understanding of internal-hydrogen embrittlement to explain hydrogen-environment embrittlement.

If the engineering community is to live with hydrogen (and it must), it is mandatory that it be clearly understood. Although other kinds of hydrogen effects exist, and may coexist with hydrogen-environment embrittlement, the presence of the latter as a separate phenomenon has been well established in the space program. There have already been inquiries about the characteristics of this phenomenon from other segments of industry, government, and the academic community. It is clear that a greater segment of the technical community will be working with hydrogen ..... and its effects ..... in the years to come.

## CHAPTER 2. SIGNIFICANCE

The hydrogen-environment embrittlement of metals and alloys is observed in gaseous hydrogen, particularly in high-purity, high-pressure hydrogen at room temperature. Thus, any application in which metals are exposed under these conditions may be vulnerable to this effect. These conditions have become far more commonplace in industry and government hardware and facilities with the growing use of liquid hydrogen in the space program.

The potential performance advantages of liquid hydrogen fuel/liquid oxygen oxidizer rocket engines have been well known since the beginning of modern rocketry. Aside from unfamiliarity and handling hazards, the loss due to boil-off during storage and handling were prohibitive and prevented early usage. It was not until the 1950's that several developments took place that formed a base from which large-scale production and use of liquid hydrogen could grow (Ref. 1).

### Availability of Low-Cost Liquid Hydrogen

Since hydrogen was first liquefied in 1896, it has been used in small quantities in universities and research institutes in cryogenic studies and basic studies of atomic structure. The quantities of liquid hydrogen required for this kind of work were limited, and there was no stimulus to large-scale production or price reduction.

With the emergence and growth of the space program in the 1950's, propellant chemists examined a large variety of fuels and oxidizers. The fuel then in common use was RP-1, an adaptation of jet engine fuel, which is essentially

kerosene. The vacuum specific impulse\* for the RP-1/liquid oxygen propellant combination is 340 seconds while, for liquid hydrogen/liquid oxygen, the specific impulse is 450 seconds. Thus, for high performance, hydrogen offers distinct advantages for chemical and nuclear rocket engines.

There were three major developments which provided liquid hydrogen in quantity: (1) the availability of hydrogen from a modified version of the Fischer-Tropsch process, the original goal of which was the synthesis of liquid gasoline; (2) the recognition of the ortho and para forms of hydrogen and, more important, the ability to convert ortho to the more stable para form. This permitted longer storage periods consistent with large-scale operations. Normally, liquid hydrogen boiloff losses were 1 percent/hour, which was excessive for widespread shipping, storage, and use; and (3) the invention of "super-insulation" which permitted piping, valving, and storage with a minimum of heat transfer.

#### Usage Outlook

It is clear that the space program will continue to use hydrogen, both in the chemical and nuclear rocket engines. Although there are very serious problems in developing a hydrogen-fueled, air-breathing engine, the fact remains that the potential performance payoff is handsome enough that most propulsion experts agree that it will ultimately become a reality. In the chemical synthesis of fuels and polymers, pure hydrogen has been in use for some time, and it can only be expected to grow.

It is not the liquid hydrogen *per se* which is of concern in hydrogen environment embrittlement. It is the fact that hydrogen is liquefied, thus freezing

---

\*Specific impulse is the ratio of thrust to the mass flowrate, and an overall measure of the efficiency of a jet or rocket engine.

the common contaminant gases such as oxygen, water, or nitrogen, and rendering the liquid hydrogen very pure. On boiling, the resultant gaseous hydrogen is of the highest purity. Thus, an adsorption-related effect, as hydrogen-environment embrittlement appears to be, is in no way poisoned or deterred by the presence of impurity elements. Thus, any user who works with liquid hydrogen boiloff, particularly at high pressures, is faced with the question of environment embrittlement for metal parts operating at high stress levels.

#### The Overall Problem

The recognition and concern for hydrogen-environment embrittlement is part of a growing recognition of the sometimes dramatic and even insidious effects of chemical environments on mechanical properties and hardware performance. The gross effects of corrosion and the less conspicuous effects of stress corrosion are generally well known, and designers are alert to them.

The presence of hydrogen, water vapor, and other gases can (and does) have a pronounced effect on crack initiation and crack growth rates. This in turn affects conventional mechanical properties, and can drastically reduce fracture toughness. Recognition of this is seen in the fracture mechanics approach to the design and development of high-performance hardware. The determination of plane strain fracture toughness in the identical proof and service media is essential to the realistic application of these concepts.

Thus, there is a growing awareness in science and engineering of the effects of environment on material properties and performance in real hardware situations. There is a rapidly increasing number of cases where behavior in

air or other convenient environment cannot be used to accurately predict performance. This is especially significant in those cases where high performance is necessary or where the cost of a development or service failure is prohibitive. With the trend toward precision design, there are penalties for overperformance as well as underperformance. This design philosophy is being adopted in a greater number of cases outside the aerospace industry, and is the direction in which our technology is moving.

The recognition and need for an understanding of hydrogen-environment embrittlement is a part of this growing awareness, and reaches out well beyond the space program in its ultimate impact.

### CHAPTER 3. OVERVIEW

There are three types of hydrogen embrittlement that have been identified for purposes of this report. They are classified as hydrogen-reaction embrittlement, internal-hydrogen embrittlement, and hydrogen-environment embrittlement. Many reviews have been published on hydrogen embrittlement, but none make this vital distinction between these types of embrittlement which will be described in this chapter.

There is no doubt that hydrogen-reaction embrittlement occurs by a different mechanism than the other two. There are similarities and differences between internal-hydrogen embrittlement and hydrogen-environment embrittlement. Many of the differences arise from the source of the hydrogen and how it is transported to the source of embrittlement. It is not resolved at this time whether the failure mechanisms are identical. In spite of over 3000 published papers on internal-hydrogen embrittlement, there is as yet no concensus on the exact failure mechanism for this type of embrittlement.

The oldest known type of hydrogen effect on a metal is that in which some form of chemical reaction occurs between the hydrogen gas and the metal. This type of reaction is prevalent in the petroleum industry in refinery operations and sour gas wells. It also has been encountered in other chemical industries where the use of gaseous hydrogen is required. Some of these instances are the manufacture of ammonia, methanol, edible oils, etc. The problems stem from the fact that all of these processes require the use of gaseous hydrogen, albeit not high-purity, at elevated temperatures and pressures.

The result of exposure of steels to high-pressure, high-temperature hydrogen is decarburization (with the formation of methane) and intergranular

cracking (Ref. 2). A severely attacked steel may undergo a reduction of tensile strength from 60 ksi down to 25 ksi with a concomitant decrease in the percent elongation from 30 percent to zero. The attack can be prevented by the appropriate choice of a steel containing carbide stabilizers. This type of hydrogen embrittlement has been studied by many investigators.

A similar type of hydrogen embrittlement is the well-documented "steam reaction" in tough pitch copper where hydrogen reacts with oxygen in solid copper to form water. This reaction, and the methane reaction in steel, can lead to extensive blistering.

In those materials that can absorb large quantities of hydrogen (e.g., titanium, columbium, tantalum, zirconium), embrittlement is associated with the formation of a hydride phase. Hydride phase formation can occur by a spontaneous transformation or can be strain-induced. Normally, embrittlement of these alloys is related to hydride formation, and is most severe at fast strain rates, except for the strain-induced transformation which can occur at slow strain rates. Delayed failure also can occur under sustained loading by the strain-induced transformation. The amount of hydrogen absorbed during exposure to gaseous hydrogen is a complex function of temperature. The hydrogen solubility decreases, but the rate of hydrogen absorption increases with increasing temperature. The embrittling hydride phases are most stable at low temperatures, at which comparatively low hydrogen contents may cause severe embrittlement. Hydrogen absorption and embrittlement at room temperature is dependent upon surface cleanliness, prior exposure to hydrogen, and hydrogen purity. Although embrittlement of the hydride formers is thought to be strictly from the hydride, experiments conducted by Bentle and Chandler (Ref. 3) indicate that columbium (niobium) and tantalum are

extremely embrittled when exposed to high-pressure hydrogen at temperatures in the range of 1000° to 1900°F, although the hydride is stable only to about 400°F.

### Internal Hydrogen Embrittlement

Observations of internal hydrogen embrittlement have been made in a number of metals and alloys; however, the vast majority of these observations have taken place in steels. A description of the effects of internal hydrogen in steels will illustrate the effects observed in other metals and alloys.

Internal hydrogen may be present in steels from a variety of sources, almost all of them related to processing. During the steelmaking process, part of whatever hydrogen may be in the melt will be trapped during solidification in the ingot and significant amounts of hydrogen may be retained in heavy sections. Pickling baths, during processing can and do, by virtue of the surface electrolytic reaction, deliver hydrogen ions to the metal surface. This permits ready transfer across that interface and buildup of hydrogen in the metal. Hydrogen can be picked up in a weld joint, and can be particularly severe in heavy sections, if combined water is present in welding flux.

Perhaps the most widely publicized origin of internal-hydrogen embrittlement is electroplating. Cadmium plating is frequently used to protect low-alloy, high-strength steel parts, and was identified as being responsible for delayed failure in springs, washers, and aircraft landing gears.

A more recently recognized source of ionic hydrogen is found in corrosion reactions. In the presence of water, a part of the corrosion reaction is the liberation and deposition of hydrogen on the metal surface, making it available to the corroded metal in solution, much as in the case of pickling.

In these instances hydrogen is present in dissociated form and it goes into the metal. The effects can be observed long after the sources are removed.

The presence of "fisheyes" or flakes in heavy steel forgings, castings, and weldments has been known for some time. This is a spontaneously occurring internal fissure, a form of delayed failure, and has been associated (Ref. 4) with stress in the presence of hydrogen. The decomposition of austenite into its several transformation products is a common origin of stress in heavy sections, although flaking may be traced to stress other than transformation stresses if hydrogen is present in the steel. Antiflaking thermal cycles have been devised to cool a heavy section under controlled conditions which eliminate transformation or other stresses.

The phenomenon known as delayed failure has been studied extensively, and early work dates back to the 1920's. This was first systematically studied and identified as a form of hydrogen embrittlement in 1955 (Ref. 5) and subsequently was clarified by Troiano and co-workers in 1960 (Ref. 6).

The now traditional representation of delayed failure due to internal hydrogen is shown in Fig. 2. The essential features as stated by Troiano (Ref. 6) are:

1. The notch tensile strength may be less than normal and directly reflects the loss of ductility due to hydrogen.
2. Delayed failure may occur over a wide range of applied stress.
3. There is only a slight dependence of the time to failure upon the applied stress.

4. Perhaps the most significant characteristic of this stress rupture relationship lies in the fact that there is a minimum critical value below which failure does not occur."

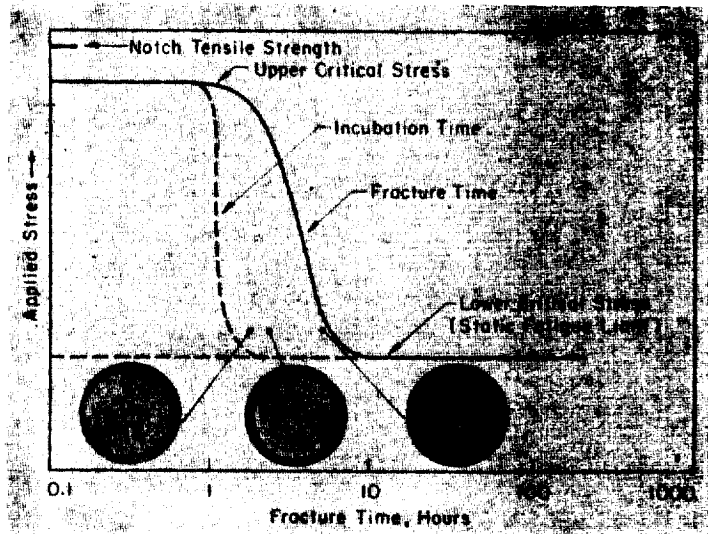


Figure 2. - Failure characteristics of a hydrogenated high-strength steel.

Another characteristic of this type of failure is that the crack initiates below the metal surface, in the region of highest stress concentration ahead of the root of the notch (Fig. 3). The crack continues to grow in a discontinuous fashion by repeating the nucleation step ahead of the notch. This takes place when the average hydrogen concentration in the metal is relatively low, and hydrogen diffuses to the region of triaxial stress concentration; at the root of a notch, a surface scratch, or a stress concentration region as encountered in real hardware.

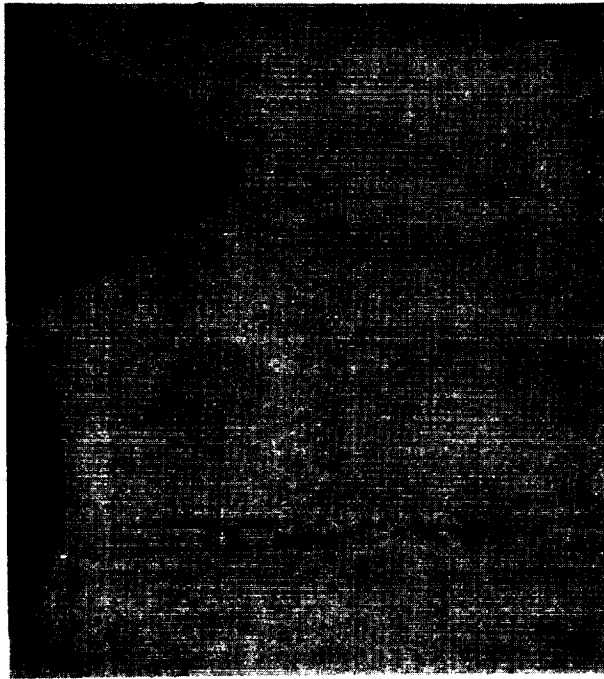


Figure 3. - Cracks observed in notched specimens sectioned after static loading.  
Longitudinal section at X 100.  
Top specimen - 0.001-in. notch radius  
Bottom specimen - 0.010-in. notch radius

Delayed failure occurs almost exclusively in martensitic steels heat treated to high-strength levels and subjected to conditions permitting hydrogen to enter the metal. Normally, hydrogen concentrations in the order of 1 to 5 ppm with appropriate stress conditions are adequate to cause this. In some other alloys, internal hydrogen embrittlement can be produced in the laboratory by severe artificial charging; however, the problem does not arise from normal metal processing.

Delayed failure may be avoided by eliminating hydrogen or reducing its level to a harmless value. Improved steelmaking and welding techniques, particularly for susceptible grades of steel, have virtually eliminated this origin of hydrogen. Pickling baths and procedures are controlled, and much work has been done in the area of electroplating to minimize the hydrogen deposited and to redistribute hydrogen in the part by postplating baking treatments.

#### Hydrogen-Environment Embrittlement

When early failures of bourdon tubes and similar parts subjected to service in high-pressure hydrogen were reported, it was evident from the circumstances of the failure that hydrogen was responsible. Such failures, although not realized at the time, did not fit the pattern which had already been established by flaking and delayed failure in statically loaded parts.

In 1965, when a very large investment in facilities tankage in the space program appeared threatened by failure in high-pressure gaseous hydrogen, a series of studies was undertaken to at least characterize the embrittling effects of high-pressure hydrogen. The first comprehensive report on this subject was by Walter and Chandler in February 1969 (Ref. 7).

This work was the first to recognize the wide variety of metals and alloys affected by gaseous hydrogen, and the authors established four categories of embrittlement upon exposure to hydrogen at 10 000 psi and room temperature.

These categories are:

1. Extreme Embrittlement. High-strength steels and nickel-base alloys are in this category. Embrittlement is characterized by a large decrease (from that in helium) of notch strength and notched and unnotched

ductility, and some decrease of unnotched strength. In unnotched specimens, failure is initiated by one surface crack which propagates into the specimen, leaving a thin shear lip around the periphery except at the location of the initiating crack.

2. Severe Embrittlement. This category contains the largest number of the metals tested, including ductile, lower-strength steels, pure nickel, and titanium alloys. Embrittlement is characterized by a considerable reduction of notch strength and notched and unnotched ductility, but no reduction of strength of unnotched specimens. Failure initiates from a series of surface cracks which, in some cases, are close enough to be continuous, and no shear lip is formed.
3. Slight Embrittlement. The metastable (tend to transform to martensite during deformation) Type 300 stainless steels, beryllium-copper, and commercially pure titanium are in this category. Embrittlement is characterized by a small decrease (from that in helium) in notch strength and notched ductility. Failure of unnotched specimens appears to initiate within the specimen, and shear lips are well formed. Very small, shallow, blunt surface cracks are frequently observed.
4. Negligible Embrittlement. Aluminum alloys, stable austenitic stainless steels, and copper are in this category. These materials were essentially unembrittled and no surface cracks were observed.

Contrary to prior experience with internal hydrogen, delayed failure was not observed. The embrittlement was immediate once a stress level greater than the yield strength was reached. There is ample evidence (to be developed

in subsequent chapters) that cracking originates at the surface, even in the case of notched specimens, where a high triaxial stress state exists at a point ahead of the notch.

The crack growth rate was found to be a function of temperature and pressure. The observed relationship has been attributed to a rate-controlling adsorption process (Ref. 8).

Perhaps the most disturbing feature of hydrogen-environment embrittlement is the large number of metals and alloys affected. It is easier to list those alloys unaffected (aluminum alloys, stable austenitic steels, pure copper) than those which exhibit the effect. Indeed, among those closest to the work, the feeling is that, in the absence of prior knowledge, it is safer to consider an alloy subject to hydrogen-environment embrittlement until experimental verification of immunity has been established.

#### Comparison

Table 1 shows a comparison between some of the characteristics of internal-hydrogen embrittlement and hydrogen-environment embrittlement. Excluded from this comparison is the embrittlement caused by a reaction between gaseous hydrogen and a metal.

Usually no effect of the hydrogen will be observed if tensile specimens, internally charged with hydrogen, are tested at ambient temperature immediately after charging. If, however, these specimens are held under a relatively low stress for a period of time, embrittlement will occur. This is not true in hydrogen-environment embrittlement. If a tensile specimen is tested in high-purity gaseous hydrogen at ambient temperature and pressure of 1 atmosphere or

TABLE 1  
 COMPARISON OF CHARACTERISTICS OF HYDROGEN-ENVIRONMENT EMBRITTLEMENT  
 AND INTERNAL HYDROGEN EMBRITTLEMENT (Ref. 9)

Parameter	Internal Hydrogen	Hydrogen Environment
Tensile Tests	Not Embrittled*	Embrittled
Delayed Failure Test	Embrittled	Not Embrittled
Crack Origin	Inside Metal	At Surface
Crack Rate Dependency	Hydrogen Diffusion	Probably Hydrogen Adsorption
Most Embrittled Materials	High-Strength Steels	High-Strength Steels and High-Strength Nickel-Base Alloys
Materials Not Embrittled	Low-Strength Steels, Austenitic Stainless Steels, and Nickel-Base Alloys	Austenitic Stainless Steels, Aluminum Alloys, Copper
Surface Cracking	Not Observed**	Observed in Unnotched Specimens

\*May be observed in high-strength steels with high hydrogen concentrations

\*\*Observed in some cases in martensitic-austenitic and martensitic steels (Ref. 10) and in nickel-base alloys (Ref. 11) when hydrogen is concentrated at the surface.

greater, immediate embrittlement occurs. The amount of embrittlement observed will depend on the type of specimen or alloy and the hydrogen pressure.

The origin of failure is different between the two types of embrittlement; with internal-hydrogen embrittlement, the crack origin is subsurface, as with most tensile tests. With hydrogen-environment embrittlement, the crack origin has been observed to be at the surface.

Probably the most striking difference between the alloys subjected to brittle failure in the two types of embrittlement is the behavior of nickel and nickel-base alloys. Inconel 718 and Rene' 41 (nickel-base alloys) were not embrittled by severe electrolytic charging (Ref. 12), while these alloys were among the most embrittled in 10 000-psi hydrogen. The high-strength steels are subject to both types of embrittlement. Stainless steels are not subject to either type of hydrogen embrittlement except those that transform to martensite after some deformation.

Again, it should be noted that many of the differences in characteristics between the two types of embrittlement arise from the difference in source of the hydrogen during embrittlement and the rate-controlling step for transport of the hydrogen.



## CHAPTER 4. EARLY WORK.

The embrittling effects of high-pressure hydrogen have been known for some time. It was not until recently, however, that hydrogen-environment embrittlement was identified as being distinct from internal-hydrogen embrittlement. The early tests were all designed with the latter type of hydrogen embrittlement in mind. Specimens were exposed to high-pressure hydrogen for a period of time, removed from the environment, and tested. It was not until the late 1950's that tests were conducted in a hydrogen environment. The early tests, while showing that an effect may exist, are of historic value and are summarized in this chapter.

### Early Service Failures Attributed to High-Pressure Hydrogen

There have been many service failures over the years attributed to high-pressure hydrogen. Bourdon gages were found to fragment within an hour or so after filling with hydrogen at pressures of 800 to 1000 atmospheres (11 800 to 14 700 psi) (Ref. 13). Mills and Edeskuty (Ref. 14) reported bourdon tube failures after room-temperature exposure to hydrogen for times as short as 1 minute and at pressures as low as 2/3 of the full-scale rating, even though these gages had been proof tested with oil and helium at full-scale pressure.

Dodge (Ref. 15) reported that an intensifier, which had been used repeatedly to pump oil at 4000 atmospheres (58 800 psi) and several times to compress nitrogen to the same pressure, failed within minutes when used to compress hydrogen at pressures not exceeding 3000 atmospheres (44 000 psi). Failure was defined as the development of very fine cracks that were barely visible to the eye.

Failures also have occurred in several pressure vessels when they were pressurized with high-pressure hydrogen. Bridgeman (Ref. 16) found that a Cr-V steel vessel used to contain hydrogen at 9000 atmospheres (132 000 psi) developed submicroscopic fissures which later developed into cracks visible to the eye, although the vessel had previously withstood liquids at 25 000 atmospheres (368 000 psi) pressure without damage.

Poulter (Ref. 17) reported that a 200-cu ft hydrogen cylinder, presumably with 2000-psi maximum pressure, failed after being in service 25 years. Examination of other hydrogen cylinders that had not failed showed small cracks extending from the inside surface to a depth of 25 percent of the wall thickness. Nitrogen pressure vessels which had been in service about the same length of time did not contain cracks.

#### Mechanical Tests Performed in High-Pressure Hydrogen

Prior to the early 1960's, the preponderance of tests performed in high-pressure hydrogen were carried out at elevated temperatures to study hydrogen attack on, or decarburization of steel. These tests were designed to measure decarburization effects and not hydrogen-environment embrittlement. Thus, the collection of elevated-temperature data plotted by Nelson (Ref. 18), i.e., the Nelson curves, showing safe operating conditions, are not applicable for predicting low-temperature compatibility of hydrogen with steels.

Room-temperature, high-pressure hydrogen burst tests were reported by the du Pont Chemical Co. as early as 1952 (Ref. 19). These tests were performed

using oil and hydrogen as the pressurizing media. It was stated that "the steels involved covered a variety of compositions, heat treatments, and wall thicknesses." The results are quoted as follows: "In the most striking instances these results showed that pressure vessels suitable for operation under oil at pressures in excess of 7000 atmospheres (103 000 psi) failed in a brittle fashion under hydrogen at pressures as low as 2000 atmospheres (29 400 psi) and in periods of time as short as a few minutes. Stainless-steel-lined vessels provided with continuous, shallow, spiral grooves to prevent hydrogen pressure buildup between the liner and vessel also were tested. It was found that with these liners the hydrogen pressure required for failure was the same as the oil pressure required for failure, indicating that the liner grooved-vessel approach was effective in preventing hydrogen embrittlement. Furthermore, the use of stainless-steel liners for periods up to several months was successful in eliminating brittle rupture."

Dodge and coworkers (Ref. 20 and 21) measured the susceptibility of various alloys to hydrogen embrittlement by measuring ductility after exposure to high-pressure hydrogen. Ductility was determined in air by measuring the number of 180° bends required for failure after exposure. The results of Van Ness and Dodge are given in Table 2 (Ref. 20). Perlmutter and Dodge extended this study to include approximately 50 metals at exposure conditions ranging from 7500 to 60 000 psi at room temperature. Some of their results for the more severely embrittled alloys are summarized in Table 2. These authors found no embrittlement for copper, zinc, titanium, and a number of their alloys, and for commercial grade 2-S aluminum, and only slight embrittlement for AISI types 321 and 430 stainless steels.

TABLE 2

## RESULTS OF BEND TESTS IN AIR AFTER EXPOSURE TO HIGH-PRESSURE HYDROGEN

(Number of 180° Bends)

Exposure Condition	Rimmed Low C Steel*	Alkili- Low C Steel*	Vitra- enamel*,** Monel*	K- Monel*	Armco Iron***	35% Cold-Rolled Haynes Alloy 25***	Cold Rolled Nichrome V***	K- Monel***
None	58	78	54	45	62	26		32
13 hr at 2000 atm (29 400 psi)	--	--	48	31				
13 hr at 2000 atm (29 400 psi)	39	80	43	--				
1 hr at 4000 atm (58 800 psi)	51	79	44	--				
18 hr at 4000 atm (5800 psi)	29	61	25	31	57			16
20 days at 7800 psig					20.2			
40 days at 7300 psig						16.5		
4 days at 15 400 psig							11.0	
2 days at 52 000 psig					61			
4 days at 52 000 psig					27.5	8.0	10.0	18
10 days at 52 000 psig					15.8	3.0	6.0	
19 days at 52 000 psig						0.2		
60 days at 52 000 psig							2.5	2

\*Ref. 20

\*\*Trade Name, U.S. Steel

\*\*\*Ref. 21

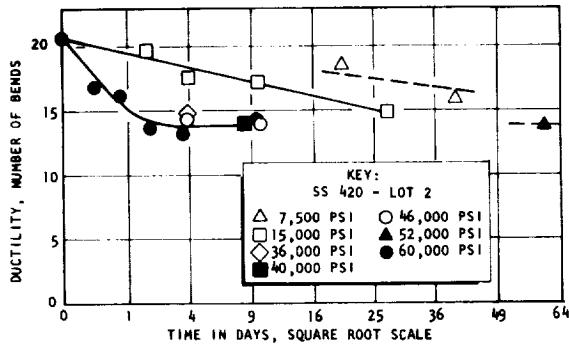
The results of Perlmutter and Dodge (Ref. 21) for AISI types 420 and 430 stainless steels and for coated alloys Alfer and Nifer\* are of interest. Figures 4a and 4b show the effect of exposure time in high-pressure hydrogen on the bend ductility in ambient-pressure air of AISI types 420 and 430 stainless steels, respectively. Embrittlement occurred immediately in the AISI type 420 stainless steel; whereas, a definite incubation period exists even at 60 000 psig for the type 430 stainless steel. The authors attributed this behavior to the greater amount of chromium present in the type 430 stainless steel. In the type 420 stainless steel, there was an "insufficient amount of chromium to form a stable oxide and, as a consequence, embrittlement begins to take place immediately upon exposure." Also of interest is the fact that the type 420 stainless steel "never loses its ductile character completely."

Figures 4c and 4d show the ductility behavior of Alfer and Nifer in air after exposure to high-pressure hydrogen. Perlmutter and Dodge again attribute this behavior to surface oxides.

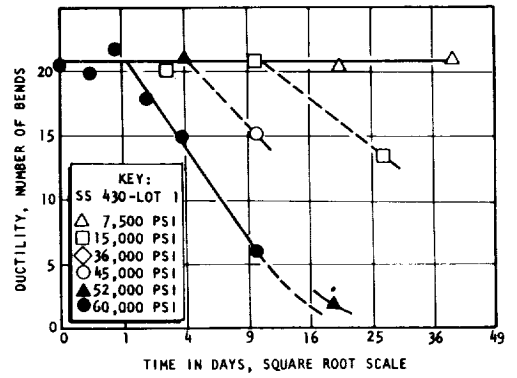
Alfer has a stable coating of oxide ( $Al_2O_3$  type); whereas, the Nifer does not. Further, aluminum is not embrittled by gaseous hydrogen but nickel is. Thus, Nifer is embrittled upon exposure to hydrogen and Alfer is not.

---

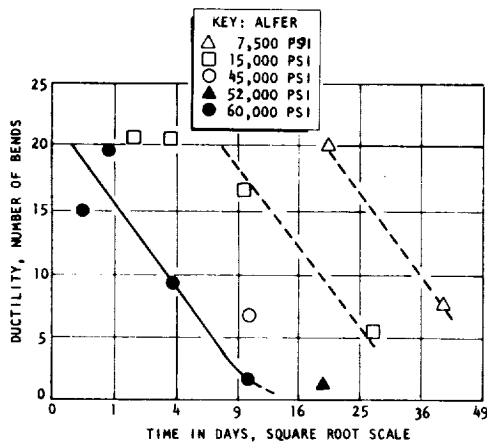
\*Alfer and Nifer, Metals Control Corp., are low-carbon steels clad with aluminum (containing 1.2% Si) and grade 330 nickel, respectively (cladding thickness, 10% on each side).



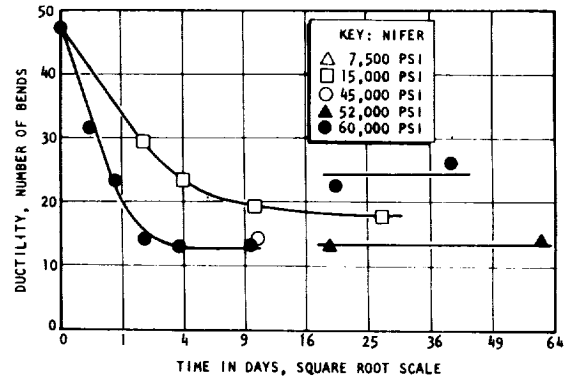
a. AISI type 420 stainless steel



b. AISI type 430 stainless steel



c. Alfer



d. Nifer

Figure 4. Ductility of various alloys exposed to hydrogen gas at room temperature(ref. 21)

The results of Perlmutter and Dodge for Haynes alloy 25 (~50% cobalt) show a difference in behavior between the annealed, 35% cold reduced, and 50% cold reduced conditions. The annealed material showed considerable resistance to embrittlement, and the 35% cold-reduced samples lost all their ductile character after 20 days exposure to hydrogen. The 50% cold-reduced samples were quite brittle in the as-received condition, but the ductility was further reduced in hydrogen.

Perlmutter and Dodge also performed additional tests at elevated temperatures, but the results reported are not sufficiently complete for analysis. They did report that tensile tests indicated that Armco Iron (~0.03% C) is embrittled at room temperature by 1000-atmospheres hydrogen and progressively more at higher temperatures. This result would indicate that pure iron is susceptible to hydrogen-environment embrittlement at elevated temperatures where there is insufficient carbon present to cause degradation of properties from chemical changes, viz., the methane reaction.

#### Recent Pressure Vessel Failures

More recently (1965), failures were reported by an aerospace contractor in 1300-cu ft, 5000-psig hydrogen storage vessels (Ref. 22). There were seven vessels in service at 5000 psig, four containing hydrogen and three containing nitrogen. In the hydrogen vessels, four failures occurred in three vessels in a 1-inch nozzle at the top of each vessel. These failures could not be predicted from the early work in hydrogen-environment embrittlement. The nozzles were fabricated from a low-alloy, 0.23-percent carbon steel with a 70-ksi

elastic limit, a 100-ksi ultimate tensile strength, and 23.5-percent elongation. These nozzles were welded into the approximately 6-inch-thick pressure vessel with a 1-inch weld surrounding the nozzle. The weld was not stress relieved and, because of the multilayer design of the pressure vessels, there were numerous stress raisers at the weld. Failure analysis of the last of the four failures showed that the failure initiated at the nozzle/weld interface, and propagated in a partially ductile, partially brittle manner through the nozzle. The weld and nozzle materials were found to be essentially free of defects and to have good mechanical properties. The failure stress analysis indicated that the internal stresses in the nozzle were a large fraction of the yield strength of the material. The nitrogen vessels have been in continuous operation under identical conditions at pressures up to 5000 psi. Another failure occurred in the weld area of a T-1 steel vessel being pressurized for the first time. The vessel was proof tested with water at 7500 psi and pressurized three times with nitrogen to 4200 psi prior to filling with hydrogen. The vessel was pressurized with hydrogen in a series of steps followed by depressurization. The last steps were 3500, 3800, and 3900 psi. On reaching 3900 psi, an audible failure occurred. On inspection of the vessel, a 50-inch-long crack was found which extended through the vessel along a longitudinal seam weld.

## CHAPTER 5. TEST PROCEDURES

Because the nature of hydrogen-environment embrittlement was little understood, it was some time before the necessity to conduct tests in the hydrogen environment was realized. This requirement has led to some unique testing facility problems.

### Hydrogen Purification

High hydrogen purity is important because impurities, particularly oxygen, decrease hydrogen-environment embrittlement. The inhibiting influence of impurities on hydrogen-environment embrittlement will be discussed in Chapter 9, Preventive Measures. Very high-purity hydrogen in the form of liquid hydrogen is used in rocket engine service; therefore, testing in the highest possible practical hydrogen purity is consistent with simulating actual service conditions.

The purity\* of bottled hydrogen ranges from 99.5 percent for that obtained from the electrolysis of water to 99.9995 percent obtained from the evaporation of liquid hydrogen. The less pure grades, less than  $-97^{\circ}\text{F}$  dew point, (1.96-ppm  $\text{H}_2\text{O}$ ), contain 4.0-ppm  $\text{N}_2$ , 0.5-ppm  $\text{O}_2$ , 1-ppm  $\text{CO}$  or  $\text{CO}_2$ , and 2-ppm total hydrocarbons. Contaminants in the highest-purity grade are mostly inert gases.

The most common method used for removing oxygen from gaseous hydrogen is by installation of a Deoxo Unit in the high-pressure hydrogen lines. This is a pressure vessel containing a catalyst which catalyzes the  $2 \text{H}_2 + \text{O}_2 \rightarrow 2 \text{H}_2\text{O}$  reaction. The manufacturer (Ref. 23) reports that the remaining oxygen impurity in gaseous hydrogen passed through the unit will be less than 1 ppm. Water

---

\*Information supplied by AIRCO, Division of Union Carbide.

vapor is removed downstream of the Deoxo Unit by means of a desiccant such as BaO, which has a high affinity for water and is not reduced by hydrogen.

A second method for purifying hydrogen is by cryogenic adsorbers. Activated charcoal, activated alumina, activated silica, and molecular sieves at  $-320^{\circ}\text{F}$ , will all scavenge  $\text{O}_2$ ,  $\text{N}_2$ , CO, and  $\text{CO}_2$  and other gases from hydrogen and helium. In flowing systems, these impurity gases are rapidly adsorbed in molecular sieves at  $-320^{\circ}\text{F}$  (Ref. 24) to partial pressures of less than 0.02 torr which, in high-pressure flowing hydrogen, results in  $\text{O}_2$ ,  $\text{N}_2$ , CO, and  $\text{CO}_2$  levels considerably below 1-ppm (Ref. 25). With static systems, even higher-purity levels are obtainable. The cryogenic adsorbers have the advantages of being easily installed in high-pressure systems.

The highest-purity hydrogen can be obtained by hydrogen evolution from metals which absorb large quantities of hydrogen. Hydrogen evolves from the hydride-forming metals (uranium, palladium, columbium, tantalum, and zirconium) at about  $1000^{\circ}\text{F}$ , which is considerably below the temperatures that other gases ( $\text{N}_2$  and  $\text{O}_2$ ) are evolved. The metals are first saturated with hydrogen by heating in a gaseous hydrogen environment. The lines are then evacuated and high-purity hydrogen is evolved by heating the hydrided metals.

For continuous hydrogen flow, a closed-end palladium alloy tube is used. Bottled hydrogen is maintained at the inside wall, and purified hydrogen is evolved at about  $350^{\circ}\text{C}$  ( $662^{\circ}\text{F}$ ) from the outside of the tube. Two companies market hydrogen purification units utilizing this principle. The maximum outlet pressure of these units is about 150 psig, and thus multistage compressors are needed for high-pressure service.

## Pressurization and Line Flushing

Experience has shown that contamination during pressurization and passage of hydrogen through pressure lines can be far in excess of the ordinary impurities present in bottled hydrogen unless considerable care is taken to avoid it. Oil-lubricated piston compressors are the most common means of pressurizing. These compressors contaminate the pressurized gases with oil, and an oil trap (molecular sieve) downstream of the compressor is needed to remove the oil.

Nonlubricated piston compressors also are available. Air, however, will pass through the sliding seals into the pressurized gas. The mechanism involves air adsorption on the shaft during the extension cycle, and the air is transferred into the high-pressure cavity during the compression cycle. To prevent this form of contamination, the compressor can be enclosed inside a cavity filled with hydrogen or an inert gas.

In diaphragm compressors, the gas being compressed is completely isolated from air or hydraulic oil because there are no sliding seals in this type of compressor. The gases are compressed by metal diaphragms which are flexed by a pulsating hydraulic pump. A series of static O-rings prevents the oil from leaking around the diaphragm periphery into the gas side. Thus, of the three types of compressors, the diaphragm type is preferred for maintaining purity during pressurization.

Air entrapment in high-pressure lines and test vessels is the main source of contamination in high-pressure systems. Unless air removal is systematic and thorough, the value of hydrogen purification is lost.

Methods used for removing air are (1) flowing hydrogen through the lines, (2) pressurization/depressurization, and (3) evacuation. Purging lines with flowing hydrogen is quite inefficient because of the large momentum difference between hydrogen (the lightest of molecules) and the air. The pressure cycling method is capable theoretically of removing all contaminating gases entrapped in the lines. However, adsorbed gases are not effectively removed by this technique. Evacuation is the only method that can ensure adequate removal of air. Unfortunately, high-pressure valves and fittings are not designed for vacuum, and experience indicates that the best vacuum that is reasonably obtainable is about 20 microns. Even at this level, considerable effort is needed to maintain a vacuum/high-pressure, leak-tight condition.

Flowing hydrogen and pressurization/depressurization are, of course, also capable of removing entrapped and adsorbed air molecules. Vacuum, however, does this most efficiently. In hardware application such as hydrogen-fueled propulsion systems, continuous flushing with flowing hydrogen should be every bit as effective for removing entrapped and adsorbed gases as the evacuation treatment. Thus, the final purity state from evacuation of test systems appears to most properly simulate that in flowing hydrogen systems.

The flushing procedure proved to be the most effective for high-pressure work is a combination of pressure and vacuum cycling. Greater embrittling effects were found with this procedure which has been adopted at Rocketdyne (Ref. 7). The system is initially evacuated, then purged by a series of pressure-vacuum cycles between 100 psig and 20 microns hydrogen. This is followed by several pressurization/depressurization cycles between the test pressure (3000 to 10 000 psi) and approximately 1-atmosphere pressure. For tests conducted below 3000 psi, several additional pressurizations/evacuations are substituted for the

higher-pressure pressurization/depressurization purgings. The resulting hydrogen purities of samples taken from the test cells following a mechanical test showed about 1-ppm N<sub>2</sub> and less than 0.5 ppm total of other gases (O<sub>2</sub>, A, CO, CO<sub>2</sub>, and CH<sub>4</sub>) (Ref. 26). A comparable pressure-vacuum cycle is employed by others (Ref. 27 and 28).

Considerable maintenance is required to maintain a vacuum leak-tight and pressure leak-tight system. Experience indicates that if the system is capable of being evacuated to 20 microns, it probably will be leak tight in the many pressure fittings, as indicated with a helium leak check with 10<sup>-7</sup> std cc/sec sensitivity.

To be sure that the hydrogen purity is adequate, the hydrogen present in the test vessel must be analyzed. Also, precaution must be taken to ensure that the sample represents the test environment. A sampling container (pressure vessel) is installed in the pressure system, the sampling container and pressure lines are evacuated several times as described above, and then are filled with the test environment. The standard analysis technique is by gas chromatography (Ref. 29). The hydrogen impurities are collected in a cryogenic trap of molecular sieves or activated charcoal, then released into a gas chromatography column.

#### Mechanical Testing in Low-Pressure Hydrogen at Cryogenic and Ambient Temperatures

The apparatus used for performing tests in low-pressure (less than 1 atmosphere) hydrogen are an adaptation of vacuum testing systems. An example of a versatile low-pressure test apparatus is that developed by Marcus and Stocker (Ref. 30). The apparatus is illustrated in Fig. 5, and is basically a high-vacuum system with gas inlet valves. The apparatus was constructed to follow

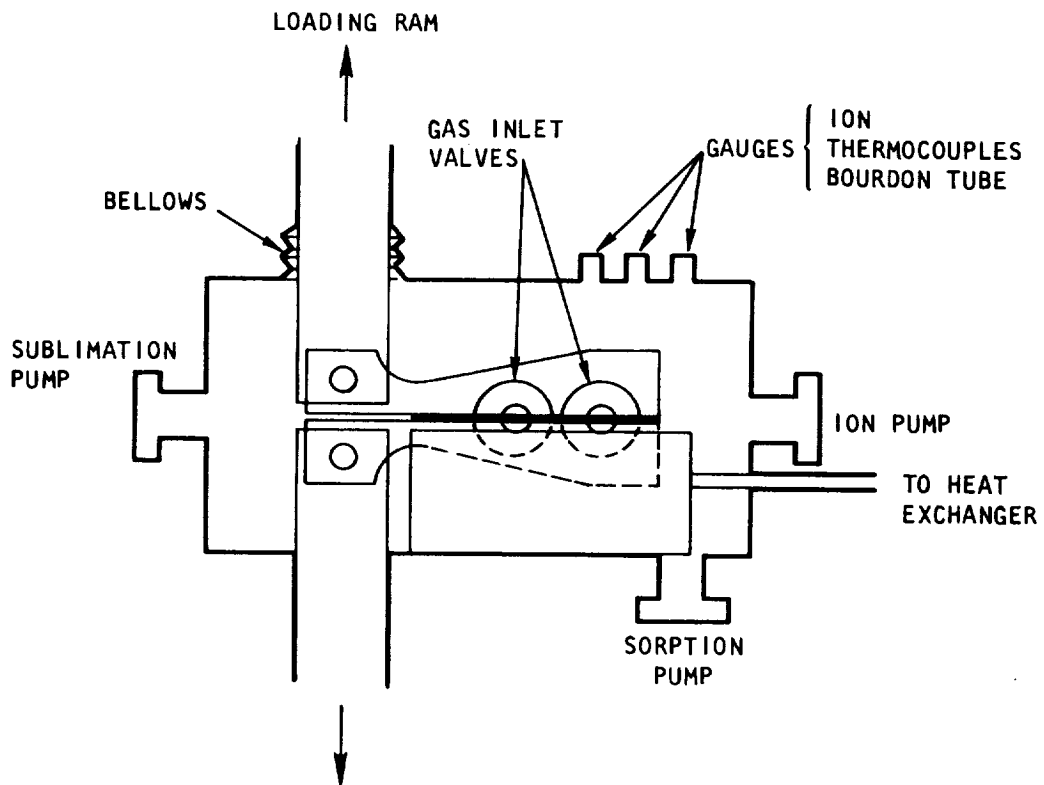


Figure 5. High-vacuum system used for performing tests in controlled low-pressure environments (ref. 30)

crack growth in low-pressure environments in the tapered double cantilever beam-type specimens shown in Fig. 5. Williams and Nelson (Ref. 31) used a similar apparatus.

Important features of the system used by Marcus and Stocker (Ref. 30) are (1) very high vacuum ( $10^{-10}$  torr), which is sufficient to eliminate effects due to other contaminating environments; (2) a heat exchanger that contacts the specimen and in which a precisely temperature-controlled fluid circulates; and (3) a bellows through which a tensile load is transmitted into the vessel without contaminating the environment.

The test procedure involves initial bakeout of the vessel at  $250^{\circ}\text{C}$  ( $482^{\circ}\text{F}$ ) and  $10^{-8}$  torr. The system then is cooled to the test temperature, and a specially prepared high-purity sample of hydrogen is introduced into the vessel. The influence of other gases, such as oxygen, on the hydrogen-environment effects can be tested by subsequent introduction of low partial pressures of these gases. The rate of crack extension is monitored optically through a glass port.

Other investigators (Ref. 32 and 33) have used a small environmental chamber which clamps to the test specimen as described in a subsequent section of this chapter.

#### Mechanical Testing in High-Pressure Hydrogen at Cryogenic and Ambient Temperatures

Testing in high-pressure environments has its own unique problems. Apparatus used can obviously be used at pressures down to 1 atmosphere. At high hydrogen pressures transmittal of the load from outside the vessel to the specimen is a

major consideration. Bellows that can withstand high internal pressures are too stiff for attachment to a loading ram. Thus, sliding seals are generally preferred for high-pressure systems.

The high pressure inside the vessel tends to force the loading ram back out of the vessel, and this load can be a significant percent of the total load applied to a specimen. This pressure force actually can be utilized as the sole tensile force for tensile testing specimens in high-pressure hydrogen. Figure 6 is a schematic representation of such an apparatus (Ref. 34). The test is conducted by slowly increasing the pressure until the specimen fails and is accelerated out the tube. A major deficiency of this test method is that the pressure and load cannot be varied independently without varying specimen size and, since embrittlement is a function of hydrogen pressure, it is difficult to interpret the test results.

The most common method of performing tensile tests in high-pressure hydrogen environments is by extending the test specimens through sliding seals at both vessel ends, as is illustrated in Fig. 7. This test concept was developed initially at Rensselaer Polytechnic Institute (Ref. 35) and has been used at Rocketdyne (Ref. 7) with modification to the sliding seal design to eliminate metal-to-metal contact. Elimination of metal-to-metal contact at the sliding seals reduced the sliding seal friction, and electrical isolation between the specimen and vessel made it possible to follow crack growth during the test by electrical resistivity measurements.

The test vessel can be placed in any mechanical testing machine. The loading device illustrated in Fig. 8 has been used for the tests conducted at

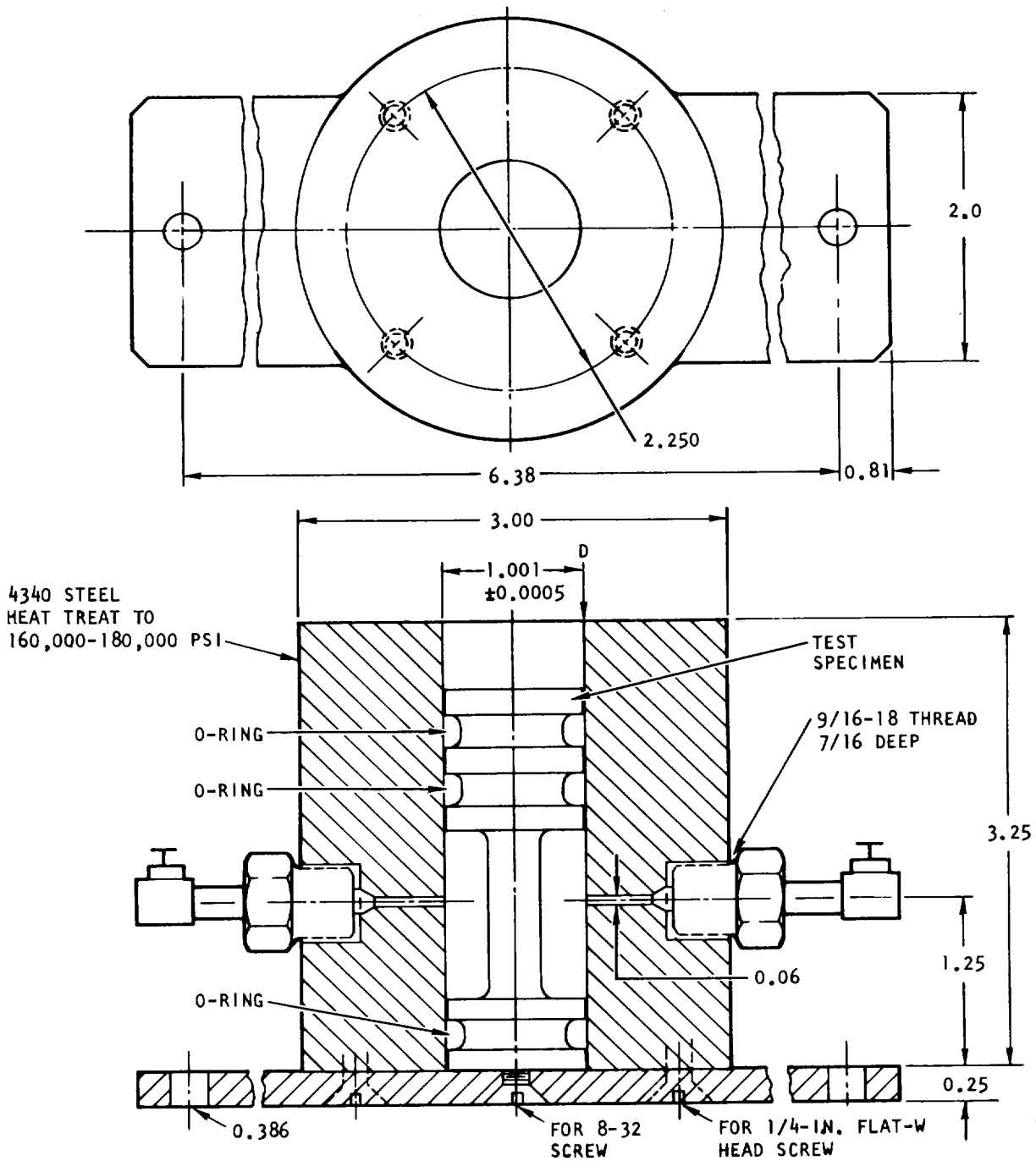


Figure 6. - Apparatus for tensile-testing specimens in high-pressure hydrogen.  
The system pressure is the only tensile force applied.

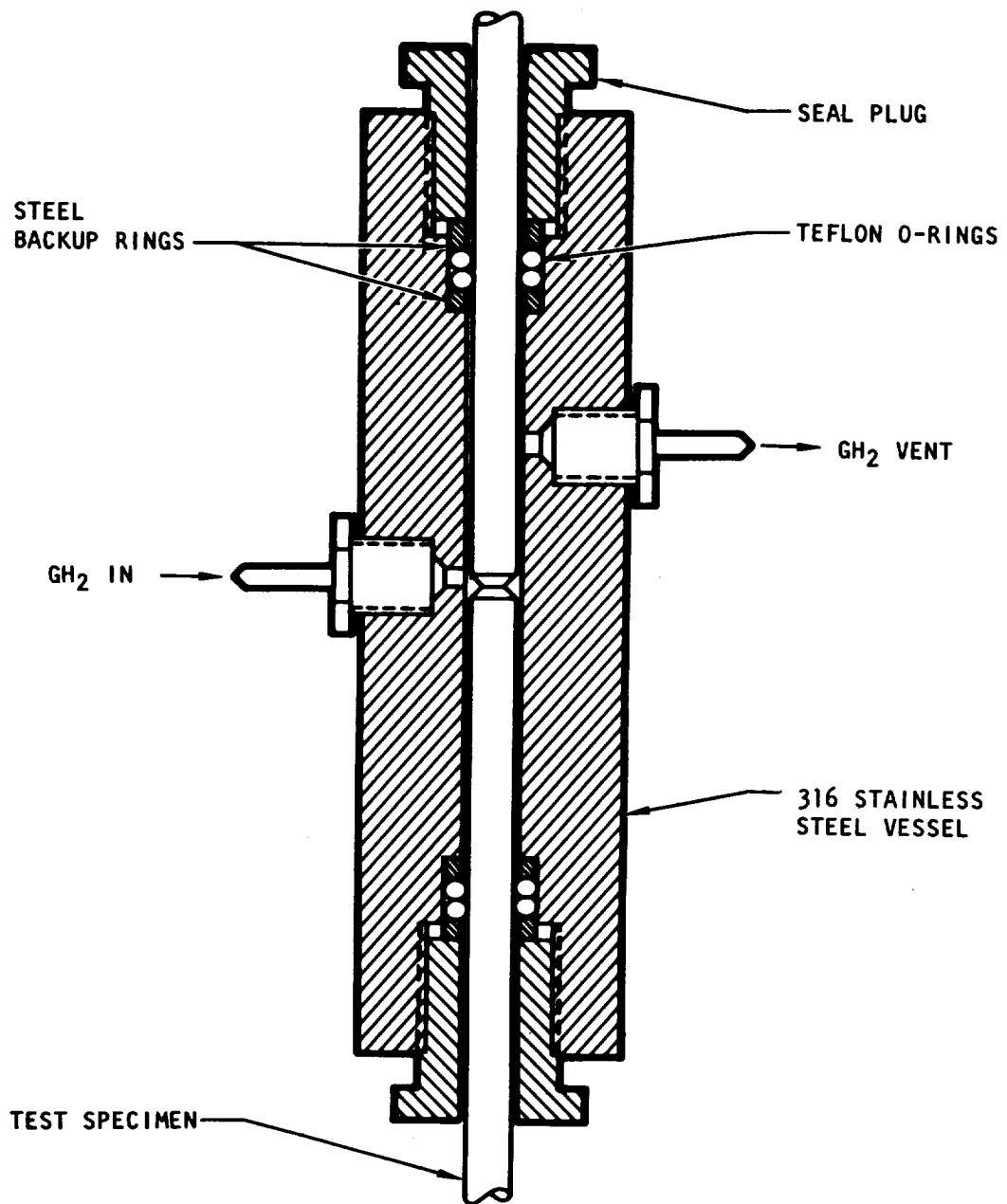


Figure 7. - Test vessel with cylindrical specimen (ref. 7).

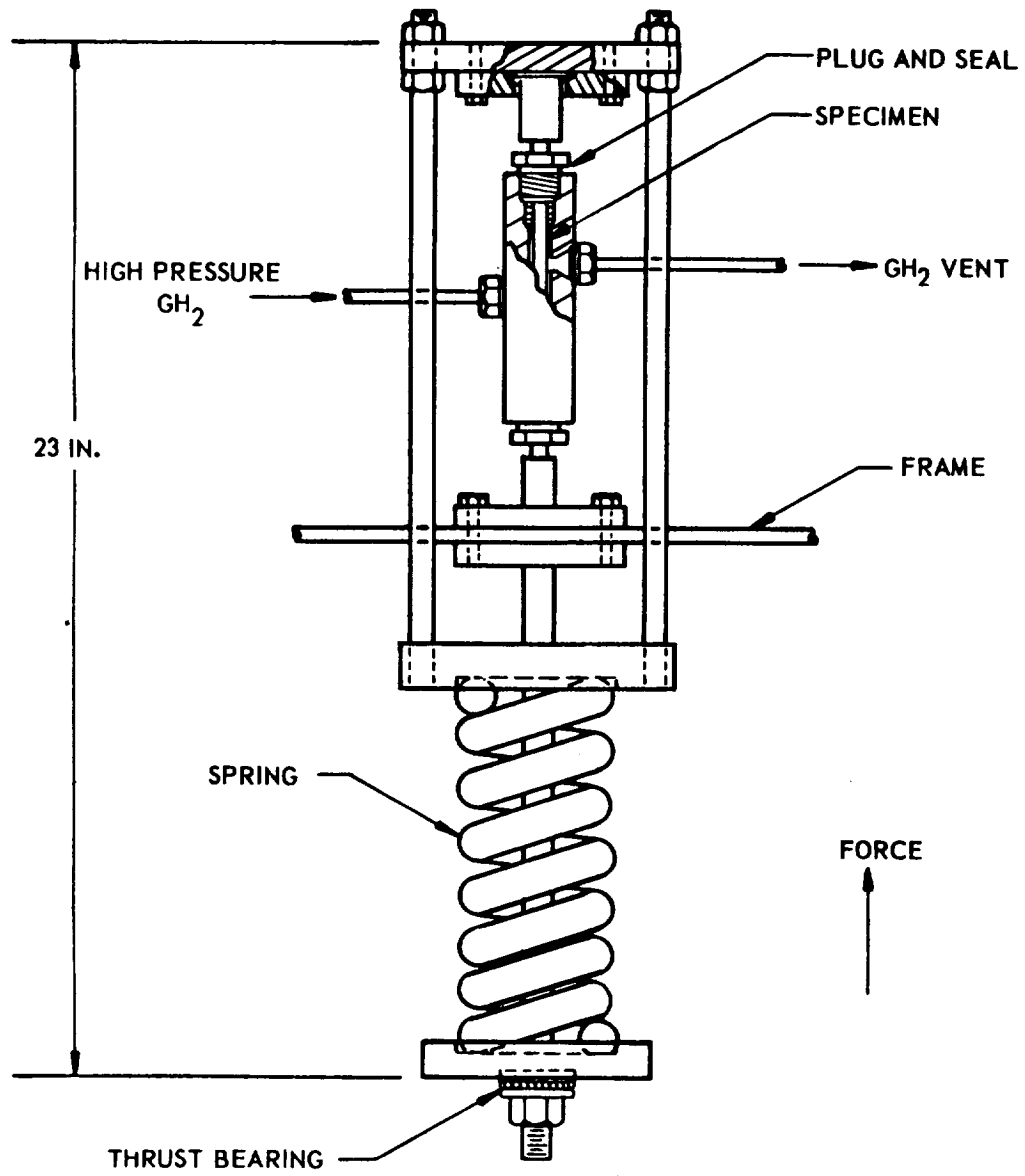


Figure 8. Test vessel and static-loading device (ref. 35).

Rensselaer Polytechnic Institute and Rocketdyne. It is very useful for conducting long-duration hold tests because several loading devices can be set up with specimens under load in the high-pressure environment at the same time. The tensile load is applied by compressing the spring, and the spring deflection is held by the nut riding on the thrust bearing.

Tensile tests are performed at Rocketdyne (Ref. 7) by compressing the spring with a hydraulic ram. Strain and load pacing are obtained by controlling the rate of travel of the hydraulic ram. Spring deflection is monitored for load pacing of notched specimens, and the cross-head motion is monitored for strain pacing of unnotched specimens. Load measurements are made by means of a load cell located between the hydraulic ram and the spring, and the load is recorded on a strip-chart recorder.

Calculation of the tensile load requires that the sliding seal friction and tensile load from the high-pressure gas be considered. The following equation is used to calculate the load at failure of unnotched specimens:

$$\text{Load} = \text{applied load} - \text{friction} + \text{pressure (specimen area at sliding seal - specimen area prior to necking)}$$

The maximum combined tensile load is assumed to occur prior to necking. For notched specimens, the final area at the base of the notch is used in place of the "area prior to necking" in the above equation.

A second effect of extending the specimen ends outside the pressure vessel is an increase of shear stress from the hydrostatic forces which act in two of the three principal directions. It can be shown that the two-dimensional pressure component increases the shear stress on the 45° maximum shear stress plane

to the same extent as the uniaxial applied tension load. That is, the specimen should have a 10 000-psi lower yield strength in 10 000-psi pressure than in 1-atmosphere pressure. This has been verified experimentally (Ref. 7) in tests conducted on 35 various engineering alloys in air (1 atmosphere), in 10 000-psi helium, and in 10 000-psi hydrogen.

The same technique of gripping the specimen outside the vessel has been used (Ref. 36) for testing sheet specimens. The vessel is clamped to the specimen as shown in Fig. 9. The center of the specimen is exposed to high-pressure hydrogen while the specimen ends are exposed to air. The same pressure and sliding seal effects discussed above on the cylindrical specimens are also applicable. The O-ring area is considerably larger for the sheet specimen than for the cylindrical specimens and, therefore, sliding friction is considerably higher during the sheet specimen tests.

For other types of specimens and/or tests, it is generally necessary to design the pressure vessel so that the entire specimen is inside the vessel and the loading ram extends into the vessel through sliding seals. Thus, the vessel contains the specimen and loading frame, and is comparatively large and expensive. Figure 10, a schematic of a vessel used to perform bend test fracture toughness measurements (Ref. 7), illustrates this point. The specimens were 1 x 2-1/2 x 14 inches and the vessel ID is 6 inches, while the inside length is 16 inches. The load was applied by means of a 65 000-pound loading ram that extended into the side (top of picture) of the vessel through sliding seals. A load cell located inside the pressure vessel is attached to the loading ram. Thus, the exact load applied to the specimens is measured directly without the need to compensate for sliding seal friction or for pressure effects.

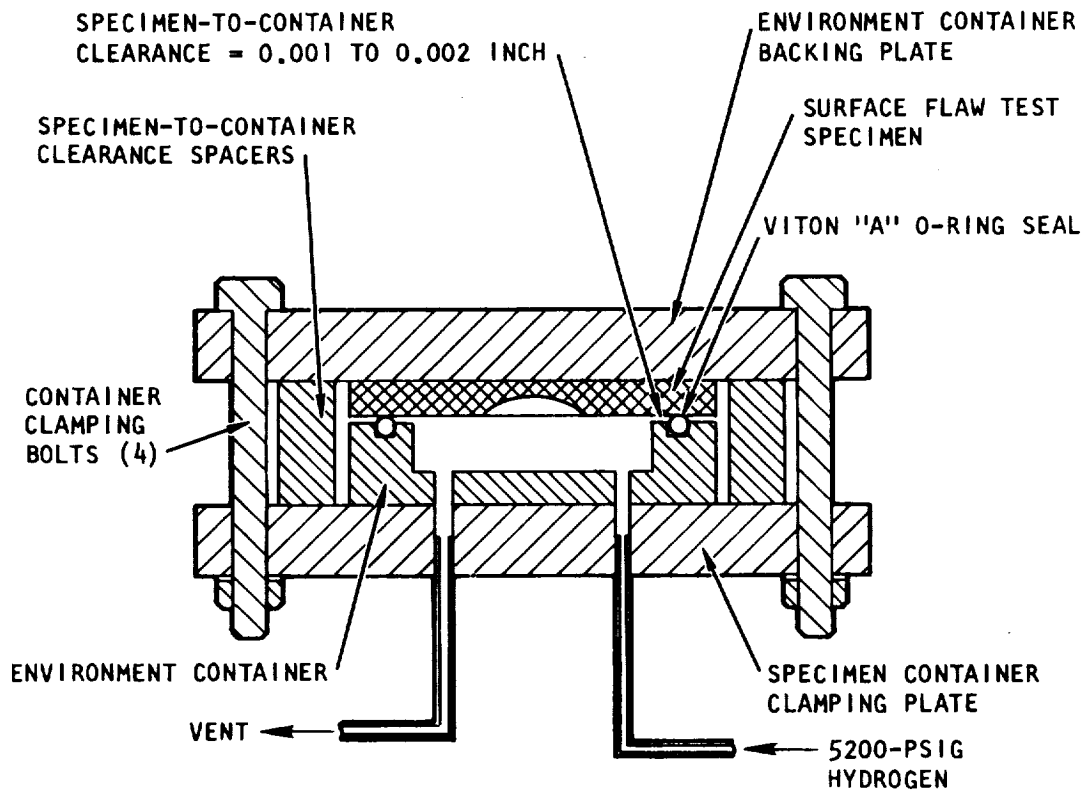


Figure 9. Sheet specimen clamped in frame with surface flaw exposed to 5200-psig hydrogen.

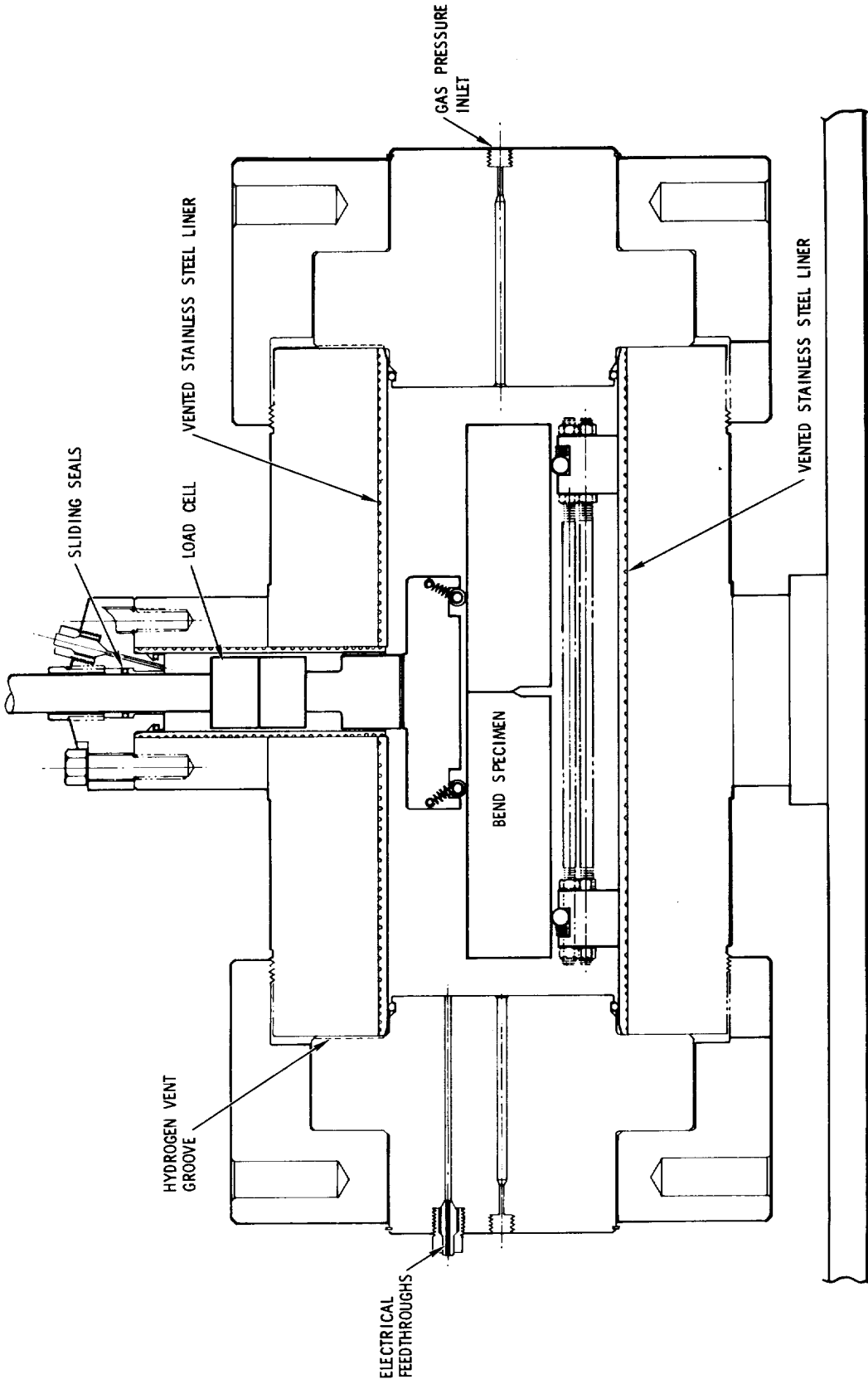


Figure 10. Vessel for performing bend tests in 15000-psi hydrogen environments.

A special pressure vessel was fabricated to abrade cylindrical tensile specimens in high-pressure hydrogen (Fig. 11). An abrading tool located at the longitudinal centerline around the vessel extends from the sides into the middle of the vessel to contact the tensile specimen. The specimen is abraded by rotating the specimen with the tool in contact with it. The electrical feed-through openings are to facilitate electrical resistivity measurements while the specimen is abraded, or during tensile or fatigue testing in high-pressure hydrogen.

To perform tests at cryogenic temperatures in high-pressure hydrogen, the pressure vessels are immersed in a cooling medium and the temperature inside the vessel is monitored. Metal-sheathed thermocouples can be inserted into the pressure vessels through high-pressure glands.

The sliding seal friction is considerably higher at cryogenic temperatures and this increased friction decreases the accuracy of the load measurements if a load cell is not located inside the test vessel. As an example of the magnitude of the sliding seal friction, the static friction on a 0.306-inch-(shaft) diameter specimen illustrated in Fig. 7 was measured to be 36, 83, 566, and 300 pounds at 140°, 74°, -109°, and -320°F. The measurements were made while the vessel was pressurized with 2000-psi helium and with the sliding seals tightened sufficiently to hold this pressure without measurable leakage. With increasing sliding seal area, the sliding seal friction would increase proportionately.

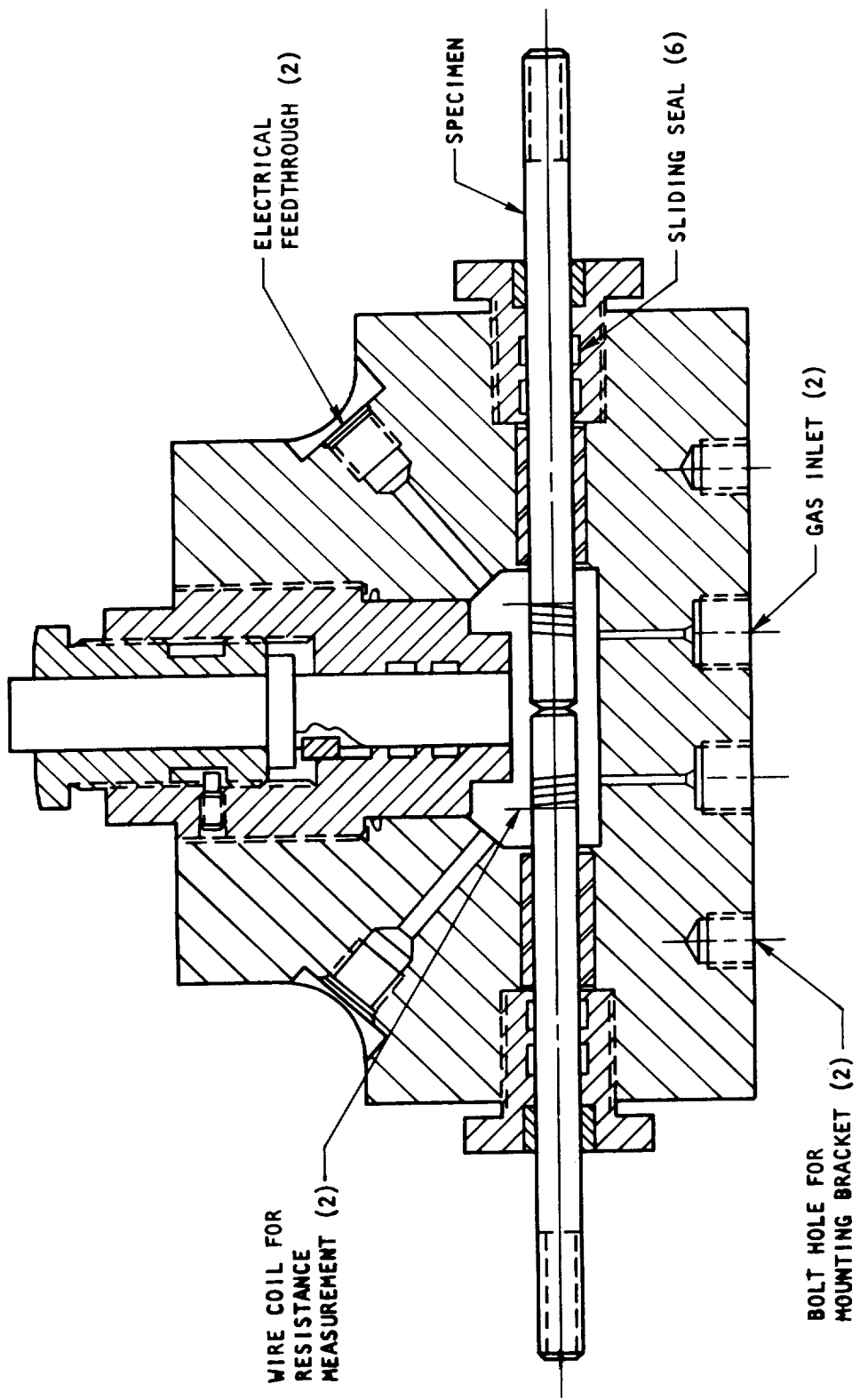


Figure 11. Device for abrading tensile specimens in high-pressure hydrogen (ref. 7).

With large pressure vessels, the compatibility of the pressure vessel material with the high-pressure hydrogen is an important consideration. The materials that are not embrittled (Ref. 7) by hydrogen are copper alloys, aluminum alloys, and the stable (will not transform to martensite during cold working) austenitic stainless steels. The smaller vessels, such as shown in Fig. 7 and 11, are constructed of AISI type 316 stainless steel. The large vessel shown in Fig. 10 contains a vented AISI 316 stainless-steel liner in contact with high-pressure hydrogen. The structural part of this vessel is constructed of low-alloy steel.

#### Mechanical Testing in Hydrogen at Elevated Temperatures

It is considerably more difficult to perform tests in high-pressure hydrogen at elevated temperatures than at lower temperatures. The problems are difficulty of transmitting the load into the vessel, and strength and compatibility of the vessel materials in contact with high-temperature, high-pressure hydrogen.

These problems, however, are not particularly severe for hydrogen pressures less than a few atmospheres. The high-vacuum system described in Fig. 5 can be used to 250°C (482°F) in low-pressure hydrogen. In this system, the specimen is heated by contact with a heat exchanger. In higher-pressure hydrogen, the hydrogen gas would quickly transfer the heat to the vessel wall because of the high thermal conductivity of gaseous hydrogen at high pressure.

A test apparatus designed for tensile testing at elevated temperatures in vacuum or inert-gas environments may not be suitable for testing in low-pressure hydrogen because the heat reflectors and heating elements are likely to be very reactive with hydrogen. Of the refractory metals (columbium, tantalum, molybdenum, and tungsten), columbium and tantalum are the easiest to fabricate into

heaters and heat reflectors, but these two metals will form hydride in the presence of hydrogen. Molybdenum and tungsten, which do not hydride, are therefore better suited for this type of service.

The most feasible method of performing tests in ambient-pressure hydrogen at elevated temperatures is by heating a tubular test chamber from the outside. Tensile tests at elevated temperatures (72° to 1500°F) in 1-atmosphere hydrogen (Ref. 37) and in precisely controlled ambient-pressure hydrogen/water vapor mixtures (Ref. 38) have been performed in this type of apparatus. The test chamber consisted of a nickel alloy tube with a removable water-cooled flange and a sliding seal at each end of the tube. For the hydrogen/water vapor tests, hot silicone oil was used in place of water as the coolant to prevent the water vapor from condensing.

The same basic method can be used for elevated-temperature testing in high-pressure hydrogen. Figure 12 is a schematic of a vessel to be used at Rocketdyne for performing fracture toughness tests on compact-tension and modified WOL specimens in 5000-psi hydrogen at cryogenic and elevated temperatures (-320° to 1200°F). The test specimens are anchored to the vessel cover and loaded by the ram, which extends through sliding seals located in the water-cooled necked region. It is advisable that the sliding seals be maintained at room temperature during cryogenic- and elevated-temperature testing because of increased sliding friction at cryogenic temperatures and the temperature limitations of sliding seal materials at elevated temperatures.

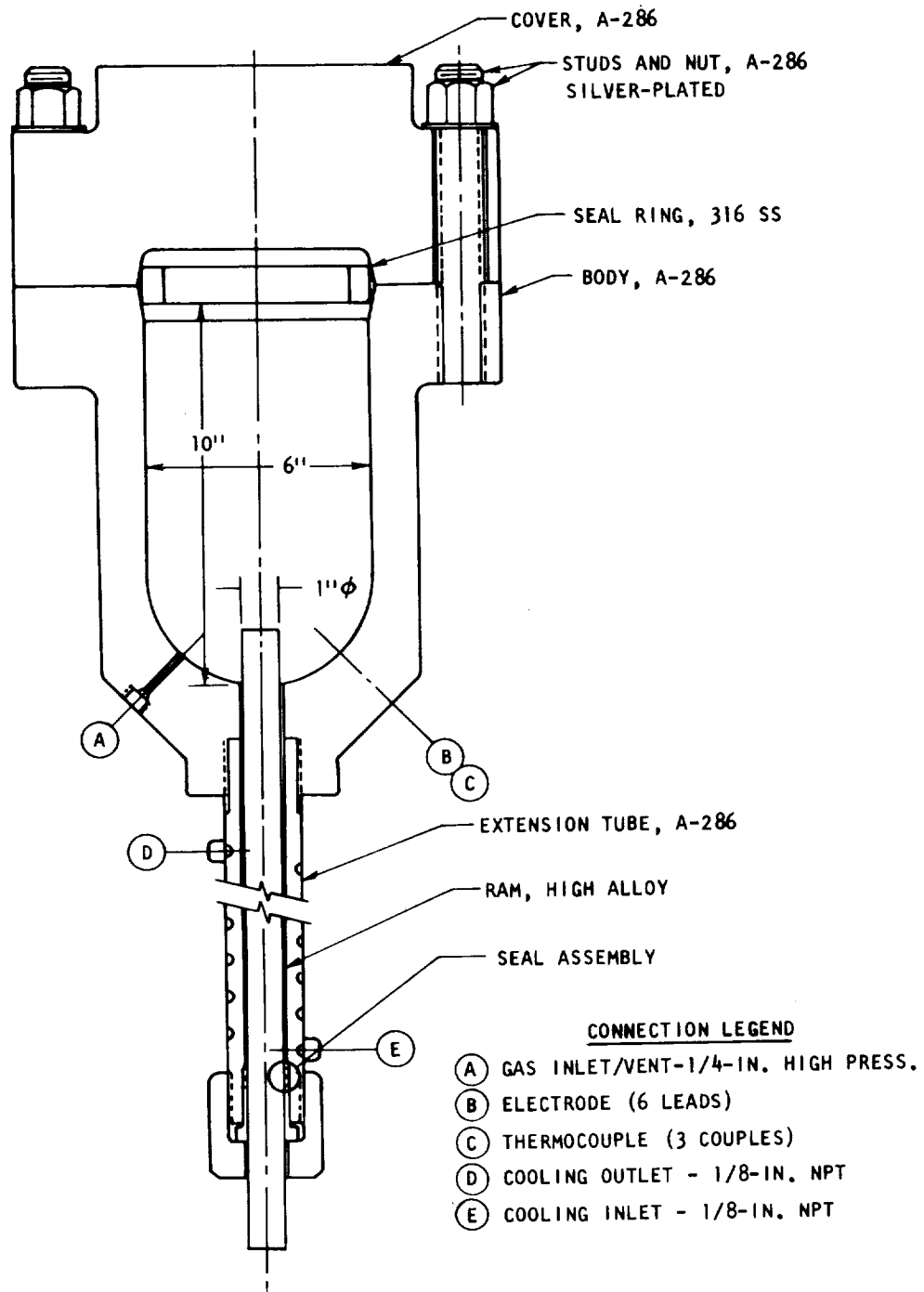


Figure 12. Pressure vessel used to test modified WOL specimens in high-pressure hydrogen at from  $-320^{\circ}$  to  $1200^{\circ}$  F.

The pressure vessel is constructed of A-286, a precipitation-hardened austenitic stainless steel. A-286 is not particularly high strength (125-ksi yield and 170-ksi ultimate), but it is the strongest alloy tested thus far which is not severely embrittled by high-pressure hydrogen. High-temperature pressure vessels would ordinarily be made of high-strength nickel-base alloys, but these are extremely embrittled (Ref. 7 ) by high-pressure hydrogen.

Materials limitations, therefore, place definite restrictions on the temperatures at which pressure vessel materials can be heated. To extend this range, it is necessary that the vessels contain an internal heater and that the vessel walls be water cooled. A system of radiation shields is not effective because of high heat transfer due to high thermal conductivity and rapid convection of gaseous hydrogen at high pressure. Outgassing from any ceramic insulation, however, would make it virtually impossible to maintain any degree of hydrogen purity unless the insulation is isolated from the test specimen.

The apparatus used at Rocketdyne for performing tensile tests on cylindrical specimens at temperatures up to 2000°F is shown schematically in Fig. 13 (Ref. 26). The test vessel has a double wall for water cooling, and includes a tube which separates the specimen cavity from the furnace cavity. A water-cooled lower extension of the vessel contains a load cell. The specimen cavity, furnace cavity, and load cell cavity are separated from each other by Viton-A O-ring seals. The same gas at the same pressures is fed into the three cavities during the tests in order to minimize gas passage across the O-rings. Self-aligning ball joints are located inside the vessel to ensure that a uniaxial load is applied to the specimen.

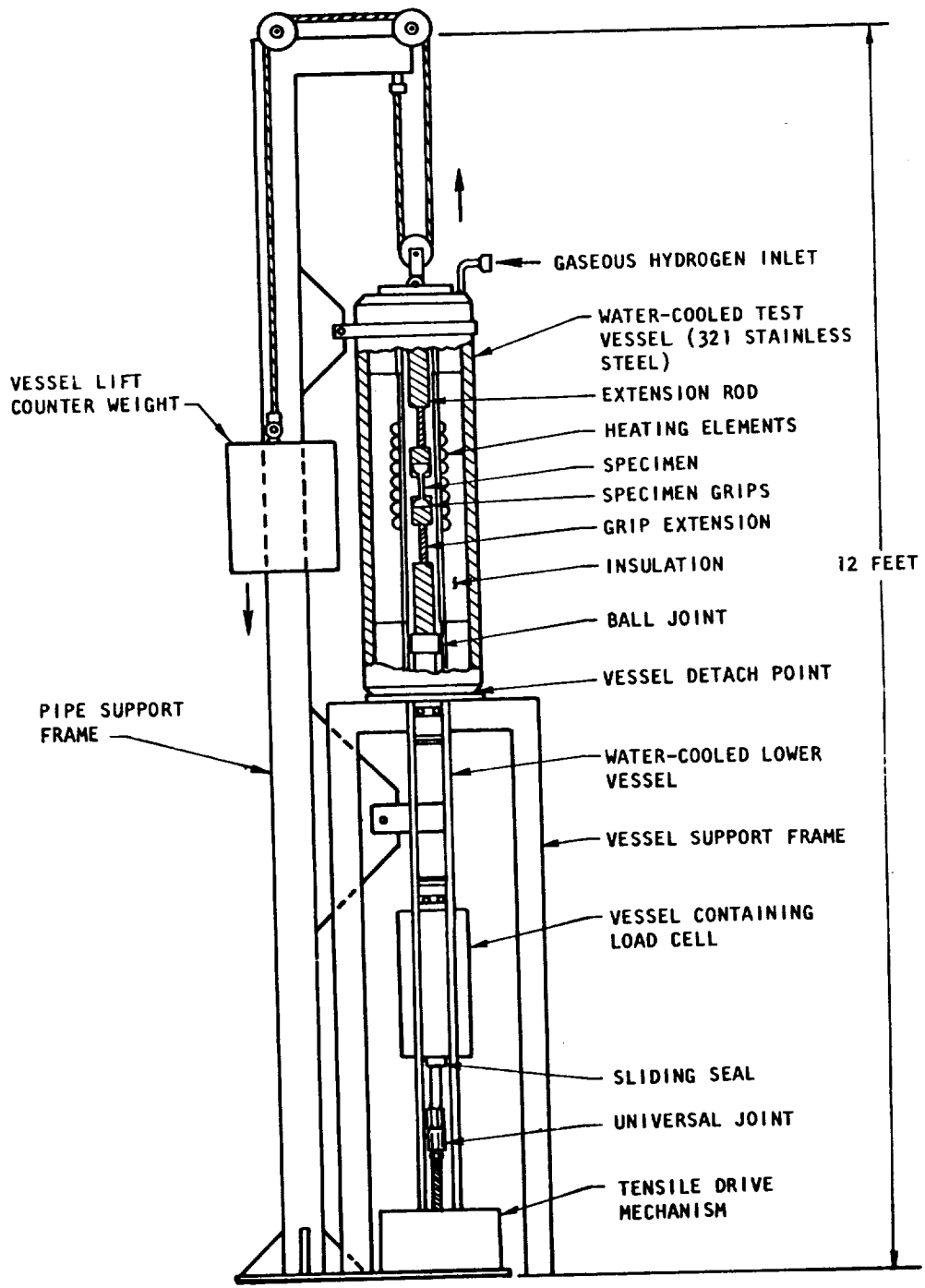


Figure 13. Apparatus for tensile-testing cylindrical specimens in high-pressure hydrogen at elevated temperatures.

Hollow specimens can be a convenient method for performing tests in high-pressure, high-temperature hydrogen; however, notching the inside of a cylindrical specimen is difficult. Considerable care must be exercised in preparation of the hole and its surface. A disadvantage of this type of specimen is data interpretation, since virtually all engineering data are determined on solid cylindrical specimens.



## CHAPTER 6. TENSILE PROPERTIES

This chapter reports the results of investigations on the tensile properties of various metals and alloys in gaseous hydrogen environments. All of these data cannot be collected into homogeneous figures and tables due to the wide variety of methods used by the different investigators. As described in Chapter 5, the test procedure can have a pronounced effect on the test results. For example, if the test cells are not evacuated prior to admitting hydrogen, the full extent of the embrittlement may not be observed. Some testing of tensile specimens has been performed with various hold times in the hydrogen environment prior to testing. This type of test has been performed with and without an applied stress present during the hold time. The data on the effect of temperature on the susceptibility to embrittlement are quite limited as is the effect of impurities in the hydrogen atmospheres. Factors such as these have not always been considered.

Among the materials that are embrittled by exposure to gaseous hydrogen are the high- and medium-strength steels, high-strength nickel-base alloys, pure nickel, some titanium and some cobalt alloys, and the metastable (with regard to the austenite-martensite transformation) 300-series stainless steels. These are the materials found to be susceptible to hydrogen-environment embrittlement, and it is by no means a complete list of materials which may be affected by gaseous hydrogen environments.

A large number of alloys have been investigated by Walter and Chandler, and on the basis of tensile tests on unnotched and notched specimens in 10 000-psi hydrogen at room temperature, they have classified the susceptibility to hydrogen-

environment embrittlement into four categories, viz., extreme, severe, slight, and negligible (Ref. 7). These categories are defined as follows and serve to orient further discussion.

1. Extreme embrittlement: High-strength steels and high-strength nickel-base alloys are in this category. Embrittlement is characterized by a large decrease of notch strength and ductility, and some decrease of unnotched strength. Large reductions of ductility are found for all three common measures of ductility (elongation and reduction of area of unnotched specimens, and reduction of area of notched specimens). Surface cracks are not usually found in failed specimens.
2. Severe embrittlement: The majority of the metals tested are in this category, including ductile, lower-strength steels, Armco iron, pure nickel, and the titanium-base alloys. Embrittlement is characterized by a considerable reduction of notch strength and ductility, but no reduction of unnotched strength. The measure of ductility most affected by the high-pressure hydrogen environment is the reduction of area of notched specimens. A large number of deep surface cracks occur in failed specimens.
3. Slight embrittlement: The nonstable AISI 300-series stainless steels (AISI 304L and 305), beryllium-copper, and commercially pure titanium are in this category. Embrittlement is characterized by a small decrease of unnotched ductility. Infrequent shallow surface cracks occur in failed specimens.

4. Negligible embrittlement: The aluminum alloys, stable austenitic stainless steels, A-286 (a precipitation-hardened austenitic stainless steel), and OFHC copper are in this category. Surface cracking is not observed in failed specimens.

The average ratio of tensile properties in hydrogen to helium are shown in Table 3 and this classification will be used wherever possible.

TABLE 3  
CHARACTERISTICS OF HYDROGEN-ENVIRONMENT EMBRITTLEMENT CATEGORIES

Category	Average Ratio of Tensile Properties in 10 000-psig Hydrogen to 10 000-psig Helium				
	Notched Specimens		Unnotched Specimens		
	Reduction of Area	Ultimate Strength	Reduction of Area	Elongation	Ultimate Strength
Extreme	0.16	0.29	0.11	0.07	0.77
Severe	0.51	0.75	0.62	0.79	1.0
Slight	0.80	0.91	0.96	0.98	1.0
Negligible	0.91	0.99	1.0	0.97	1.0

Tensile tests performed on columbium and tantalum in gaseous hydrogen environments resulted in severe embrittlement. However, embrittlement was associated with absorption of large quantities of hydrogen, and thus may be an internal-hydrogen rather than a hydrogen-environment phenomenon. Internal-hydrogen embrittlement of refractory metals has been reviewed by Chandler and Walter (Ref. 39).

#### Room-Temperature Results

Hofmann and Rauls performed the earliest experiments in which tensile tests were conducted in gaseous hydrogen. Their results on the effect of gaseous

hydrogen on a 0.22% carbon steel in 1961 are shown in Table 4 (Ref. 40). No strength values were reported. Purity of the hydrogen was 99.95%.

TABLE 4  
TENSILE PROPERTIES OF LOW-CARBON STEEL IN HYDROGEN

Room Temp.	UTS, ksi	% Elong.	Red. of Area, %
Air (ambient press.)	70.8	32	64
147 psig H <sub>2</sub>		34.5	52
294 psig H <sub>2</sub>		33	47
735 psig H <sub>2</sub>		30	50
1470 psig H <sub>2</sub>		30	36.5
2205 psig H <sub>2</sub>		26	28
1470 psig Argon		36	62

At 147 psig, many cracks formed, with increasing frequency of cracks to 2205 psig.

CK22 (0.22% C) steel normalized at 900°C, extension rate of 1.75 mm/sec, gage section 6mm x 30 mm.

In a second series of tests utilizing cold-drawn 0.22% carbon steel, Hofmann and Rauls (Ref. 41) investigated the effect on the degree of embrittlement occasioned by various hydrogen pressures and various additions of oxygen and nitrogen to the high-pressure hydrogen. This latter topic will be discussed later. A lowering of the ultimate tensile strength and rupture elongation with increasing hydrogen pressure was reported (Fig. 14). These authors also investigated (Ref. 42) the effect of strain rate on ductility at a pressure of 2205 psig (Fig. 15). The

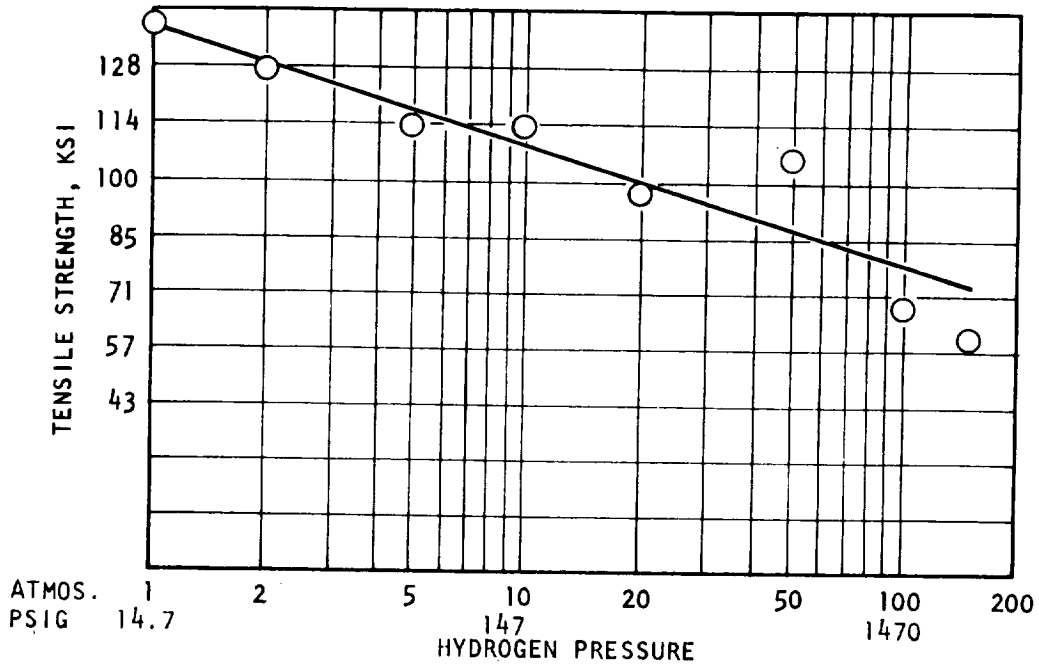


Figure 14. Effect of hydrogen pressure vs tensile strength.

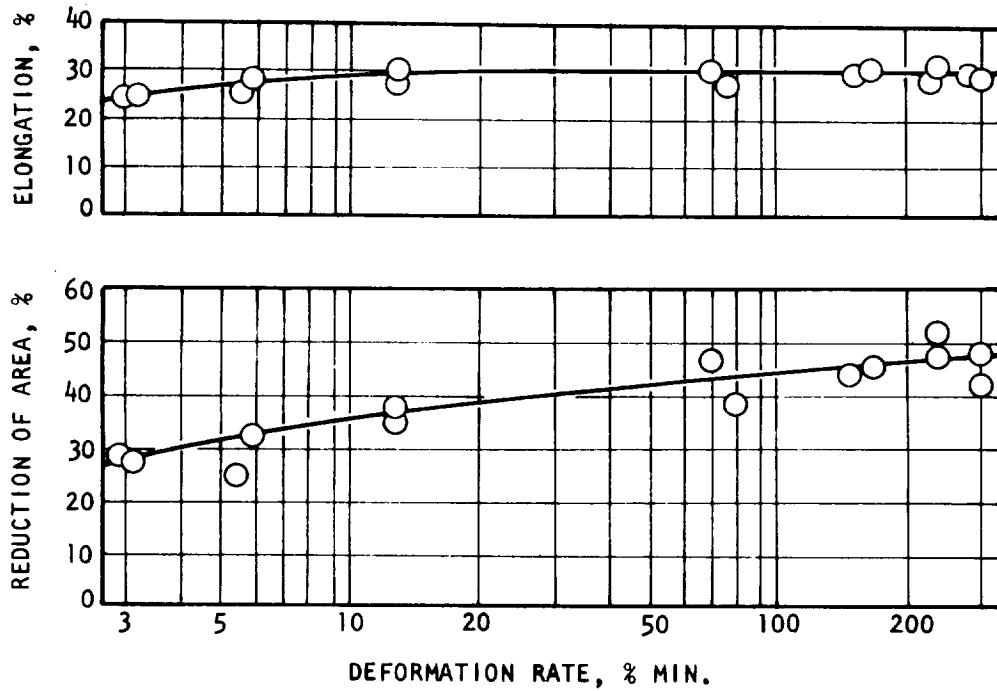


Figure 15. Effect of deformation rate on elongation (in 5D) and reduction in area (normalized CK22 steel, exposed to hydrogen pressure of 2205 psig).

largest effect of hydrogen is noted at the slowest strain rate and the effect decreases with increasing strain rate with, however, a significant effect still evident at the fastest strain rate.

These authors (Ref. 42) also reported on additional experiments with Armco iron and 0.45% carbon steel. The ductility of these steels in hydrogen environments from 14.7 to 2205 psig is shown in Fig. 16. The effect of a 2205-psig hydrogen environment on the ductility of various plain carbon steels is shown in Fig. 17.

Hofmann and Rauls further investigated the effect of gaseous hydrogen with notched tensile specimens of the 0.22% and 0.45% carbon steel and a high-strength steel specimen. For the carbon steel, the specimens were 8 mm in diameter with a circumferential notch of 60° included angle. The notch was 1-mm deep and had a root radius of 0.1 mm ( $K_t = 5.1$ ). For the high-strength steel the specimen was 4.3 mm in diameter with a 60° notch, a 1.15-mm notch depth, and a 0.08-mm root radius ( $K_t = 3.5$ ). Results are shown in Table 5.

TABLE 5. NOTCHED AND UNNOTCHED TENSILE STRENGTH IN AIR AND HYDROGEN (Ref. 42)

Material	UTS, ksi				Notch Strength Ratio H <sub>2</sub> /Air
	Air		2205-psig H <sub>2</sub>		
	UN	N	UN	N	
Armco Iron	51.4	71	48.6	51.4	0.72
0.22 C Normalized	71	102.8	71	76.6	0.75
0.45 C Normalized	96.2	119.6	96.2	93.4	0.79
High-Strength Steel*	233.3	312	233.3	156	0.50

\*In 1470-psig H<sub>2</sub>. Chemical composition: 0.71C; 0.65 Si; 1.24 Mn; 0.035 P; 0.028 S; 0.005 N; 0.006 Al

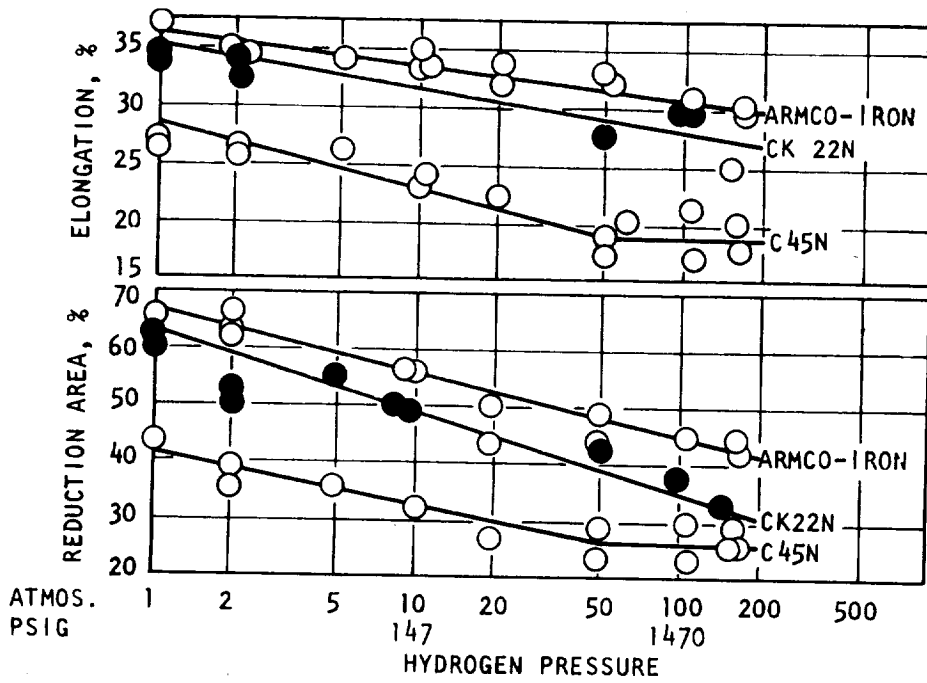


Figure 16. Effect of high-pressure hydrogen on elongation (in 5D) and reduction in area (Armco iron, CK 22 N, and C 45 N steels).

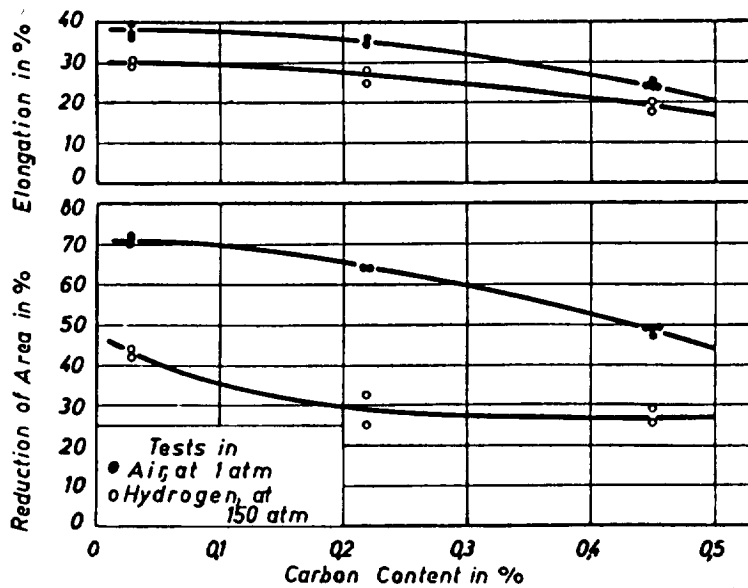


Figure 17. Effect of carbon content on elongation and reduction in area in air and in high-pressure hydrogen.

A series of tests was conducted at Rensselaer starting in about 1957 (Ref. 35). The test specimens used were cylindrical rods with threaded ends. The diameter was 0.306 inch, with a 60° V-notch at the midplane of the specimen. The diameter of the specimen at the root of the notch was 0.1500 inch, and the root radius was 0.0046 inch. This gave a stress concentration (after Peterson, Ref. 43) of  $K_t \approx 4.0$ . Most of the tests were conducted with a hold time in the hydrogen atmosphere and will be reported later. The purity of the hydrogen was not reported.

Cavett and Van Ness reported in 1963 that K-monel and quenched and tempered 4140 steel are severely embrittled as compared to normalized 4140 steel (Table 6, Ref. 44). Vennett and Ansell (Ref. 45) also investigated the effect of strain rate on the tensile strength and percent elongation of AISI 304L stainless steel. Their results are shown in Fig. 18. The degree of hydrogen-environment embrittlement is again observed to decrease with increasing strain rate.

In the most comprehensive series of tests, Walter and Chandler (Ref. 7) tested a large number of materials in 10 000-psig hydrogen, and the degree of hydrogen-environment embrittlement was determined by comparison with the mechanical properties determined in 10 000-psig helium. The test specimens were 9 inches long and 0.306 inch in diameter. The surface finish was 16 rms. The unnotched specimens had a 1.25-inch-long, 0.250-inch-diameter gage section. The notched specimens had a 60° notch at the midplane. Specimen diameter at the root of the notch was 0.150 inch, with a root radius of 0.00095. The stress concentration factor ( $K_t$ ) was approximately 8.5 (Ref. 43).

TABLE 6

NOTCHED ( $K_t \approx 4.0$ ) TENSILE STRENGTH IN NITROGEN  
AND HYDROGEN (Ref. 44)

	Air (UN)	Ultimate Tensile Strength, ksi			Ratio $H_2/N_2$ Notch Strength
		10K-psi $N_2$ (N)	6K-psi $H_2$ (N)	10K-psi $H_2$ (N)	
4140 Normalized	135	241	207	204	0.85
4140 Quenched & Tempered	228	362	121	89	0.25
C1025	65	106	--	80	0.76
K-Monel*	139	251	--	113	0.45
K-Monel**	100	144	--	105	0.73

\*Annealed

\*\*Precipitation hardened

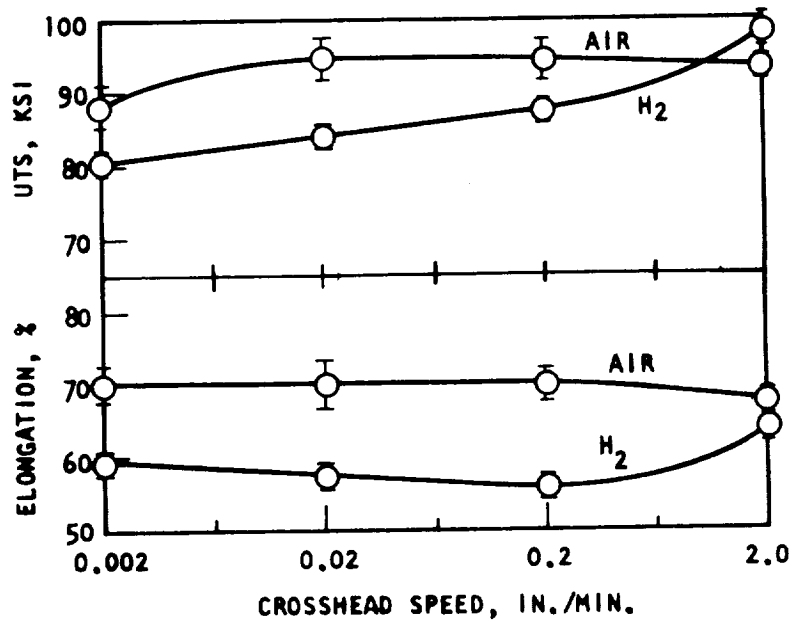


Figure 18. Tensile strength and elongation versus crosshead speed for notched ( $k_t$  4.0) specimens of 304L stainless steel tested in air and 10000 psi hydrogen at various strain rates. (Gage length is assumed to be 0.0985 in.)

The unnotched specimens of the AISI 304L stainless steel, AISI 305 stainless steel, and the OFHC copper had a gage section diameter of 0.150. The majority of the tests were conducted using a strain rate of  $0.002 \text{ min}^{-1}$  to the yield point and  $0.04 \text{ min}^{-1}$  from yield to fracture. The notched specimens were load paced at a rate corresponding to an unnotched strain rate of  $0.0007 \text{ min}^{-1}$ . The notched specimens of AISI 304L and 430F stainless steel and 6061-T6 aluminum alloy were tested with a strain rate corresponding to an unnotched strain rate of  $0.005 \text{ min}^{-1}$  and the notched A-286 stainless steel was tested with a loading rate corresponding to an unnotched strain rate of  $0.0014 \text{ min}^{-1}$ . The heat treatments of the alloys tested are given in Table 7. Purity of the hydrogen, after pressurization, was  $<0.5 \text{ ppm } O_2$ ,  $<5 \text{ ppm}$  total hydrocarbons,  $<0.5 \text{ ppm } CO + CO_2$ ,  $<0.5 \text{ ppm } H_2O$ , and  $2.6 \text{ ppm } N_2$ . The results of these tests are shown in Table 8.

The high-strength steels, AISI 1042 (quenched and tempered), AISI 4140, Fe-9Ni-4Co-0.20C, and 18 nickel (250) maraging steel, were all extremely embrittled by gaseous hydrogen as indicated by large reductions of notch strength and unnotched and notched ductility. Unnotched ductility of these specimens was reduced over 75 percent, and the notch ductility was essentially zero for all of the specimens tested in 10 000-psig hydrogen. Reduction of notch strength ranged from 60 percent for AISI 4140 to 88 percent for 18 nickel (250) maraging steel. The 18 nickel (250) maraging steel specimens were the most embrittled of all the materials tested. This steel had a 32-percent reduction in unnotched strength, as well as an 88-percent reduction in notched strength.

The 400-series stainless steels (AISI 410, 440C, and 430F) were among the most hydrogen-environment-embrittled steels tested. The AISI 410 and 440C are in the extremely embrittled category, while the 430F is in the severely

TABLE 7

## HEAT TREATMENT OF ROCKETDYNE MATERIALS (Ref. 7)

Material	Heat Treatment by Supplier (As-Received Condition)	Hardness	Heat Treatment at Rocketdyne	Hardness
Armco Iron	Annealed		None	
AISI 1042	Annealed		One set of specimens normalized at 1650°R for 1 hour and air cooled; one set normalized as above, then annealed at 1575°F for 1 hour, water quenched, tempered at 400°F for 2 hours, and air cooled	R <sub>c</sub> 52 R <sub>b</sub> 93.5
AISI 4140	Annealed	207 BHN	Annealed at 1550°F for 1 hour, water quenched tempered at 900°F for 2 hours	
HY 100	To MIL S-162166 dated 2-27-63		None	
ASTM A-372 Class IV (API N-80)	Tempered at 875°F		None	
Fe-9Ni-4Co-0.20C	Annealed	R <sub>c</sub> 30	Annealed at 1550°F for 1 hour, oil quenched; double tempered at 1000°F for 2 hours	
18 Nickel (250) Maraging Steel	Annealed		Aged at 900°F for 6 hours	
AISI Type 304L Stainless Steel	Annealed and cold drawn	170 BHN	Normalized at 1950°F for 1 hour, air cooled	R <sub>b</sub> 68
AISI Type 305 Stainless Steel	Annealed and cold drawn		None	
AISI Type 316 Stainless Steel	Annealed and cold drawn		None	
AISI Type 430F Stainless Steel	Annealed		None	
AISI Type 410 Stainless Steel	Annealed and cold drawn		Annealed at 1850°F for 1 hour, oil quenched; tempered at 1000°F for 1 hour	
AISI Type 440C Stainless Steel	Annealed and cold drawn	R <sub>b</sub> 99	Heated slowly to 1900°F for 1 hour, oil quenched; tempered at 400°F for 2 hours	R <sub>c</sub> 54.5
17-7PH Stainless Steel	Annealed	214 BHN	Annealed at 1950°F for 1 hour; air cooled; austenitized at 1400°F for 1-1/2 hours; air cooled to 60 to 60°F; held 30 minutes; immediately aged at 1050°F for 1-1/2 hours	
A-286 Stainless Steel	Solution treated at 1650 F for 2 hours; water quenched; aged at 1325 F for 16 hours; air cooled	321 BHN	None	R <sub>c</sub> 34.6
1100-O Aluminum	Zero temper		None	
7075-T73 Aluminum	Heat treated to -T73 temper		None	
6061-T6 Aluminum	Heat treated to -T6 temper		None	
Titanium, Commercially Pure	Hot rolled		None	
TI-5Al-2.5Sn ELI	Rocketdyne Spec RB0170-079		Vacuum annealed at 1400°F for 4 hours; argon cooled	
OFHC	Cold drawn		None	
Be-Cu Alloy 25	Condition H		None	
Nickel 270	Hot Rolled		None	
Rene 41	1975 F for 1 hour; water quenched	R <sub>c</sub> 29	1975°F for 1 hour; water quenched; aged at 1400°F for 16 hours; air cooled	
Inconel 718	Annealed		Annealed at 1750°F for 1 hour; air cooled; reheated to 1325°F for 8 hours; furnace cooled to 1150°F at 100°F/hr; held for 10 hours; air cooled	

TABLE 8

RESULTS OF TESTS ON VARIOUS ALLOYS AT ROCKETDYNE (REF. 7 )

Material	Environment		Unnotched Specimens					Notched Specimens			Degree of Embritt.
	Type	Press., psig	YS, ksi	UTS, ksi	Elong., %	Red. of Area, %	Strength Ratio H <sub>2</sub> /He	Red. of Area %	UTS, ksi	Strength Ratio H <sub>2</sub> /H <sub>e</sub>	
18% Ni (250) Maraging Steel	He	10 000	248	250	8.2	55.0	--	2.5	423	--	Extreme
	H <sub>2</sub>		---	171	0.2	2.5	0.68	0.0	50	0.12	
AISI Type 410 Stainless Steel	He		192	211	15.0	60.0	--	2.2	386	--	
	H <sub>2</sub>		---	166	1.3	12.0	0.79	0.6	82	0.22	
AISI 1042 Quenched & Tempered	He		165	---	---	---	--	0.6	236	--	
	H <sub>2</sub>		---	187	---	---	--	0.6	53	0.22	
17-7PH Stainless Steel	He		150	164	17.0	45.0	--	0.6	302	--	
	H <sub>2</sub>		---	151	1.7	2.5	0.92	0.4	70	0.23	
H-11	He		244	299	8.8	30	--	0.0	252	--	
	H <sub>2</sub>		---	171	0.0	0.0	0.57	0.0	63	0.25	
Fe-9Ni-4Co-0.2C	He		187	199	15.0	67.0	--	6.3	367	--	
	H <sub>2</sub>		---	175	0.5	15.0	0.86	0.2	89	0.24	
Rene 41	He		163	196	21.0	29.0	--	3.4	280	--	
	H <sub>2</sub>		---	165	4.3	11.0	0.84	0.2	77	0.27	
Electroformed Ni	He	7 000	---	---	---	---	--	31.0	120	--	
	H <sub>2</sub>		---	---	---	---	--	1.0	37	0.31	
AISI 4140	He	10 000	179	186	14.0	48.0	--	2.8	313	--	
	H <sub>2</sub>		---	178	2.6	8.8	0.96	0.9	125	0.40	
Inconel 718	He		182	207	17.0	26.0	--	1.7	274	--	
	H <sub>2</sub>		---	193	1.5	0.8	0.93	0.2	126	0.46	
AISI Type 440C Stainless Steel	He		236	293	--	3.2	--	0.2	149	--	
	H <sub>2</sub>		---	119	--	0.0	0.40	0.0	74	0.50	
Ti-6Al-4V (STA)	He		157	164	13.0	47.0	--	2.2	228	--	Severe
	H <sub>2</sub>		---	152	13.0	50.0	--	0.9	133	0.58	
AISI Type 430F Stainless Steel	He		72	80	22.0	64.0	--	1.9	152	--	
	H <sub>2</sub>		---	78	14.0	37.0	--	0.6	104	0.68	
Nickel 270	He		---	48	56.0	89.0	--	23.6	77	--	
	H <sub>2</sub>		---	50	52.0	67.0	--	6.9	54	0.70	
ASTM A-515 Gr. 70	He		45	65	42.0	67.0	--	8.1	106	--	
	H <sub>2</sub>		---	43	64	29.0	35.0	3.0	77	0.73	
HY-100	He		97	113	20.0	76.0	--	7.3	224	--	
	H <sub>2</sub>		---	115	18.0	63.0	--	3.8	164	0.73	
ASTM A-372-IV	He		82	118	20.0	53.0	--	2.0	200	--	
	H <sub>2</sub>		---	116	9.6	18.0	--	2.8	148	0.74	
Ti-6Al-4V (Annealed)	He		132	156	15.0	48.0	--	2.2	243	--	
	H <sub>2</sub>		---	159	15.0	48.0	--	1.0	183	0.79	
AISI 1042 Normalized	He		58	90	29.0	59.0	--	8.5	153	--	
	H <sub>2</sub>		---	89	22.0	27.0	--	2.8	115	0.75	
ASTM A-517-F (T-1)	He		109	118	18.0	65.0	--	7.4	226	--	
	H <sub>2</sub>		---	111	18.0	63.0	--	2.1	173	0.77	
ASTM A533-B	He		---	119	19.0	66.0	--	15.0	227	--	
	H <sub>2</sub>		---	116	17.0	33.0	--	2.8	176	0.78	
HY-80	He		82	98	25.0	70.0	--	8.6	190	--	
	H <sub>2</sub>		---	85	99	20.0	60.0	3.9	153	0.80	
AISI 1020	He		41	63	40.0	68.0	--	14.0	105	--	
	H <sub>2</sub>		---	40	62	32.0	45.0	6.2	83	0.79	
Ti-5Al-2.5Sn ELI	He		106	113	20.0	45.0	--	3.1	201	--	
	H <sub>2</sub>		---	114	18.0	39.0	--	1.8	162	0.81	
Armco Iron	He		54	56	18.0	83.0	--	6.4	121	--	Slight
	H <sub>2</sub>		---	57	15.0	50.0	--	1.7	105	0.86	
AISI Type 304L Stainless Steel	He		24	77	86.0	78.0	--	21.0	102	--	
	H <sub>2</sub>		---	76	79.0	71.0	--	11.0	89	0.87	
AISI Type 305 Stainless Steel	He		51	90	63.0	78.0	--	19.0	165	--	
	H <sub>2</sub>		---	87	65.0	75.0	0.97	17.0	147	0.89	
Be-Cu Alloy 25	He		79	94	22.0	72.0	--	12.0	195	--	
	H <sub>2</sub>		---	93	22.0	71.0	--	13.0	181	0.93	
Titanium (Commercially Pure)	He		53	63	32.0	61.0	--	10.0	126	--	
	H <sub>2</sub>		---	---	31.0	61.0	--	7.5	120	0.95	
AISI Type 310 Stainless Steel	He		---	77	56.0	64.0	--	20.0	116	--	Negligible
	H <sub>2</sub>		---	78	56.0	62.0	--	18.0	108	0.93	
A-286 Stainless Steel	He		123	158	26.0	44.0	--	5.6	233	--	
	H <sub>2</sub>		---	162	29.0	43.0	--	6.2	227	0.97	
7075-T73 Aluminum	He		54	66	15.0	37.0	--	3.8	116	--	
	H <sub>2</sub>		---	65	12.0	35.0	--	2.3	114	0.98	
6061-T6 Aluminum	He		33	39	19.0	61.0	--	9.5	72	--	
	H <sub>2</sub>		---	40	19.0	66.0	--	11.0	78	--	
1100-0 Aluminum	He		---	16	42.0	93.0	--	20.0	18	--	
	H <sub>2</sub>		---	16	39.0	93.0	--	21.0	25	--	
OFHC Copper	He		39	42	20.0	94.0	--	20.0	87	--	
	H <sub>2</sub>		---	41	20.0	94.0	--	24.0	86	--	
AISI Type 316 Stainless Steel	He		64	94	59.0	72.0	--	18.0	161	--	
	H <sub>2</sub>		---	99	56.0	75.0	--	19.0	161	--	

embrittled category. Among these steels, it appears that, the stronger the steel, the greater the hydrogen-environment embrittlement, although the results for AISI 440C are somewhat ambiguous because of its extreme notch sensitivity. The ultimate tensile strength of unnotched 440C was 293 ksi, while the notch strength in 10 000-psig helium was 149 ksi. In 10 000-psig hydrogen, the notch strength was 74 ksi, indicating a 50-percent reduction of notch strength.

There was also a reduction of strength of the unnotched specimens of the 400-series stainless steels in high-pressure hydrogen. Strength reductions were 2.5 percent for AISI 430F. Ultimate tensile strength reduction of unnotched specimens of AISI 440C was considerably greater (60 percent) than observed for any other material.

The low-alloy steels (Armco iron, AISI 1042 normalized, HY-100, and ASTM A-372) were in the category of severe embrittlement. Reduction of ductility of the unnotched specimen was greatest for ASTM A-372 class IV, and least for HY-100. Reduction of notch strength was about 27 percent for HY-100 and ASTM A533-B and 14 percent for Armco iron. Except for the ASTM A-372, the notch ductility of these steels was drastically reduced by the 10 000-psig hydrogen environment.

The AISI 304L and 305 stainless steels are in the slightly embrittled category. The reduction of area of unnotched AISI 304L specimens was reduced approximately 10 percent by the 10 000-psig environment. The notched specimens had a strength reduction between 10 and 17 percent and a ductility reduction of 50 percent due to the hydrogen environment. All of the specimens were reported to be magnetic after testing. Benson, et al. (Ref. 46) reported a similar effect with a 7.3-percent reduction of notched strength in AISI 304L stainless steel in 10 000-psig hydrogen. Specimens of AISI 305 stainless steel were reported to be very

slightly magnetic after testing; no surface cracking was observed, and there was only a slight indication of reduced ductility in the unnotched and notched specimens (Ref. 7). Only a small reduction (about 4 percent) of unnotched strength and 11-percent reduction of notch strength was observed. Thus, AISI 305 stainless steel was somewhat less embrittled by 10 000-psig hydrogen than was AISI 304L stainless steel, which showed a reduction of ductility as well as strength in high-pressure hydrogen. There was no indication of a reduction in strength or ductility in the unnotched and notched AISI 316 specimens because of exposure to the high-pressure hydrogen environment.

The precipitation-hardened austenitic stainless steel (A-286 stainless steel) showed negligible embrittlement in the 10 000-psig hydrogen environment. The tensile strength of the notched specimen was approximately 2-1/2 percent lower in hydrogen than it was in 10 000-psig helium; there was no decrease in ductility of the unnotched and notched A-286 alloy specimens.

Both nickel and nickel-base alloys were considerably embrittled by 10 000-psig hydrogen. Nickel 270 (99.4 percent Ni + Co) is severely embrittled in 10 000-psig hydrogen. The reduction of notch strength is approximately 30 percent when compared to results obtained in 10 000-psig helium. The reduction in unnotched tensile strength for Rene' 41 was 16 percent and, for notched specimens, the reduction of tensile strength was 73 percent. These reductions are based on tests conducted in 10 000-psig helium. As noted earlier, K-monel is also subject to hydrogen-environment embrittlement (Ref. 44).

In more intensive investigations, three heats of Inconel 718 were tested for hydrogen-environment embrittlement (Ref. 47). Five different heat treatments (Table 9) were used with these three heats (Table 10). The results of the tensile tests on unnotched and notched specimens of Inconel 718 are given in Table 11. The data for the room-temperature tests on notched specimens indicate that the reduction of notch strength by hydrogen is a function of the heat-heat treatment combination of the Inconel 718 tested. For example, specimens of heat C with heat treatment 5 showed a 49-percent reduction of notch strength in 500-psig hydrogen, while specimens of heat B with heat treatment 3 had only a 15-percent reduction of notch strength in 2000-psig hydrogen. From these results, it is obvious that the heat and/or heat treatment of Inconel 718 has a considerable effect on the degree of hydrogen-environment embrittlement. Walter and Chandler (Ref. 47) proposed that the lower embrittlement of heat B with heat treatment 3 was due to the high annealing and aging temperatures used. VanWanderham (Ref. 48) also concluded that this type of heat treatment yields Inconel 718 less susceptible to embrittlement by high-pressure hydrogen. However, the results of recent tests on heat C showed a high degree of embrittlement of specimens with heat treatment 5, which resembles heat treatment 3, and these specimens were more embrittled than specimens with heat treatment 4, with its lower annealing and aging temperatures. These data indicate that, for some as yet unknown reason, heat B had a relatively low susceptibility to hydrogen environment. It should be noted that the three heats tested were within composition specification limits for Inconel 718. There does not appear to be any correlation between the properties in helium for the different heats and heat treatments and the degree of hydrogen-environment embrittlement, although heat B did have the highest ductility and notch strength/unnotched strength ratio and lowest hydrogen-environment embrittlement. Additional work is in progress, see the Appendix.

TABLE 9

HEAT-TREAT CONDITION OF INCONEL 718 TEST MATERIALS (Ref. 47)

Heat Treatment	Heat Treatment					
	Solution Annealing (In Argon)		First Aging Temp.		Second Aging Temp.	
	°F	minutes	°F	hours	°F	hours
1	1750, air cool	60	1325	8	1150	10
2	1850, air cool	60	1360	10	1175	10
3	1900, air cool	20	1400	11	1200	9
4	1800, air cool	60	1325	8	1150	12
5	1950, air cool	60	1350	9	1200	11

TABLE 10

CHEMICAL COMPOSITION OF INCONEL 718 TEST MATERIALS (Ref. 47 )  
(Vendor Certified)

Heat	Elements														
	Ni	Fe	Cr	Cb/Ta	Mo	Ti	Al	Co	Si	Mn	Cu	C	P	S	B
A	51.11	19.81	18.37	5.39	3.13	0.92	0.52	--	0.33	0.16	0.12	0.04	--	0.007	--
B	52.50	Bal.	18.93	5.22	3.10	0.89	0.53	0.39	0.13	0.05	0.02	0.038	0.032*	0.006	0.004
C	51.44	18.22	19.69	5.23	2.80	1.01	0.39	0.06	0.18	--	--	0.042	0.003	0.009	0.00064
AMS Spec.**	50.00/ 55.00	Bal.	17.00/ 21.00	4.75/ 5.50	2.80/ 3.30	0.65/ 1.15	0.20/ 0.80	1.00	0.35	0.35	0.30	0.08	0.015	0.015	0.006

\*Analyzed at Rocketdyne to be 0.016.

\*\*Nos. 5662, 5663, and 5664. Compositions given as ranges or maximums.

TABLE 11  
 TENSILE PROPERTIES OF INCONEL 718 IN HIGH-PRESSURE HYDROGEN AND HELIUM AT ROOM TEMPERATURE (Ref. 47)

Material		Environment		Tensile Properties							
Heat (from Table 10)	Heat Treatment (from Table 9)	Type	Press., psig	Unnotched Specimens				Notched Specimens (K <sub>t</sub> ≈ 8.0)			
				YS, ksi	UTS, ksi	Elong., %	Red. Of Area, %	YS, ksi	UTS, ksi	Red. Of Area, %	Strength Ratio H <sub>2</sub> /He
A	1	Air	0	193	213	16	27	1.7	282	1.7	--
	1	He	10 000	183	208	18	26	1.7	274	1.7	--
	1	H <sub>2</sub>	10 000	182	193	1.5	0.8	0.2	126	0.2	0.46
B	2	Air	0	188	217	16	31	1.5	284	1.5	--
	2	He	1 000	194	216	17	32	1.4	282	1.4	--
	2	H <sub>2</sub>	1 000	186	215	17	28	1.3	169	1.3	0.60
C	3	Air	0	191	206	25	39	3.1	333	3.1	--
	4	He	100	192	208	25	40	3.4	333	3.4	--
		He	2 000	188	208	24	38	2.8	333	2.8	--
	5	H <sub>2</sub>	100	186	207	23	38	3.0	332	3.0	1.0
		H <sub>2</sub>	1 000	188	206	24	37	3.0	302	3.0	0.91
	5	H <sub>2</sub>	2 000	189	206	24	38	2.3	299	2.3	0.90
C	4	Air	0	189	206	24	38	1.1	282	1.1	0.85
	4	He	500						270		--
	4	H <sub>2</sub>	500						273		--
5	5	He	500						180		0.66
	5	H <sub>2</sub>	500						287		--
									146		0.51

The notched, commercially pure titanium specimens were slightly embrittled. Ti-6Al-4V and Ti-5Al-2.5Sn ELI notched specimens were severely embrittled in 10 000-psig hydrogen. The unnotched, commercially pure titanium and Ti-6Al-4V specimens were not embrittled by 10 000-psig hydrogen. Numerous surface cracks were present on the unnotched, commercially pure titanium specimens tested in hydrogen, but the cracks were not sufficiently deep to affect embrittlement, as will be discussed further in Chapter 8, Metallography. The large (45 percent) decrease of notch strength of Ti-6Al-4V (STA) in 10 000-psig hydrogen without a reduction of unnotched properties is unique for the materials tested.

The results of the tests on notched Ti-6Al-4V (STA) specimens should be noted because the mechanical properties show a very large dependency on the method of purging the test cells. Tests in 10 000-psig hydrogen preceded only by a pressurization/depressurization treatment did not cause embrittlement. The large reduction of notch strength occurred only when the test cells were previously evacuated. Thus, embrittlement of Ti-6Al-4V (STA) is evidently quite sensitive to hydrogen purity.

Unalloyed aluminum (1100-0 aluminum) was tested in 5000-psig hydrogen and there was no indication of embrittlement; 6061-T6 aluminum alloy was not embrittled in 10 000-psig hydrogen. The ultimate tensile strengths of both unnotched and notched 7075-T73 aluminum alloy were approximately the same in hydrogen and helium environments. However, the average ductility of the unnotched and notched specimens was slightly lower in 10 000-psig hydrogen than in 10 000-psig helium. In these tests, the test vessels were vacuum purged prior to pressurization with 10 000-psig hydrogen for the 1100-0 aluminum tests, but not for the other two aluminum alloys.

Results of tests on Be-Cu alloy 25 indicated no embrittlement of the un-notched specimens by high-pressure hydrogen. There was, however, a 7-percent reduction of notch strength in 10 000-psig helium containing 44-ppm hydrogen. Notch ductility was not affected by high-pressure hydrogen.

### Effect of Hydrogen Pressure (Room Temperature)

The effect of pressure on the degree of hydrogen embrittlement has been investigated for only a few alloys. Results of tests performed at various hydrogen pressures are shown in Table 12 (Ref. 7, 44, 46, and 49). The heat-treated condition of these alloys is shown in Table 13.

There is no evidence of any reduction of strength or ductility of the unnotched AISI 310 stainless steel due to hydrogen environment. However, there appears to be a small decrease of strength and ductility of the notched specimens, and the degree of embrittlement decreases with decreasing pressure. Data at hydrogen pressures less than 10 000 psi are possibly within experimental scatter. Benson, et al. (Ref. 46) report similar results for notched AISI 310 stainless steel, the degree of embrittlement at 10 000-psig hydrogen being less than 1 percent. The notch ductility at lower hydrogen pressures is somewhat lower on an average than the ductility in 10 000-psig helium, but this difference may have been the result of the increase of ductility in the 10 000-psig helium due to pressure effects.

A slight reduction of unnotched strength for ASTM A533-B specimens occurs when they are tested in 10 000-psig hydrogen. No strength reduction was observed for specimens tested in hydrogen at lower pressures. A substantial loss of ductility was noted in the unnotched and notched ASTM A533-B specimens tested in

TABLE 12

EFFECT OF HYDROGEN PRESSURE ON VARIOUS ALLOYS

Material	Environment		Unnotched Specimens				Notched Specimens				Ref.	
	Type	Press., psig	YS, ksi	UTS, ksi	Elong., %	Red. of Area, %	Red. of Area, %	UTS, ksi	Strength Ratio H <sub>2</sub> /He	~K <sub>t</sub>		
AISI Type 310 Stain- less Steel	He	0	33.5	89	55.0	66.5	--	--	--	8.0	7	
		100	--	--	--	--	--	--	--			
		1 000	35.0	90	54.0	67.5	--	--	--			
	H <sub>2</sub>	10 000	--	77	56.0	64.0	19.8	116	--	↓	41	
		0	35.0	87	53.5	65.5	18.7	124	0.98			
		100	36.3	87	52.3	66.0	18.0	123	0.98			
	He	1 000	34.0	89	55.0	67.0	16.0	123	0.98	↓	41	
		10 000	--	78	55.0	63.3	18.0	108	0.93			
		10 000	--	--	--	--	--	110	--			
	ASTM A533-B	He	0	118.0	118	28.0	70.0	12.0	216	--	8.0	7
100			--	--	--	--	--	--	--			
1 000			119.5	116	23.5	71.5	14.0	215	--			
H <sub>2</sub>		10 000	--	120	19.5	67.5	11.0	227	--	↓	41	
		0	115.0	118	21.0	68.3	7.1	235	0.99			
		100	118.0	120	22.3	67.3	7.4	212	0.98			
He		1 000	113.3	117	20.0	57.7	4.2	218	0.92	↓	41	
		10 000	36.0	116	16.7	32.7	2.9	176	0.78			
		10 000	--	--	--	--	--	--	--			
Ti-6Al-4V (STA)		Air	0	169.0	179	11.5	48.0	1.7	237	--	8.0	43
	1 000		166.0	178	11.0	45.5	3.4	249	--			
	He	2 000	166.5	177	13.0	46.0	3.2	251	--	↓	43	
		1 000	167.6	178	11.5	50.0	0.6	154.5	0.64			
	H <sub>2</sub>	2 000	164.3	175	11.3	49.0	0.6	150.0	0.60	↓	43	
		1 000	--	--	--	--	--	--	--			
Ti-5Al- 2.5Sn ELI	He	1 400	--	--	--	--	3.8	186	--	8.0	26	
		10 000	106.0	113	20.0	45.0	3.1	201	--			
	H <sub>2</sub>	1 400	--	--	--	--	--	3.4	168	0.90	↓	26
		10 000	--	114	18.0	39.0	1.8	162	0.81			
Inconel 718*	Air	0	187.5	217	16.0	31.0	1.5	284	--	8.0	42	
		1 000	194.0	216	16.5	32.0	1.4	282	--			
	He	1 000	186.3	215	17.3	28.0	1.3	169	0.58	↓	42	
		1 000	--	--	--	--	--	--	--			
Inconel 718**	Air	0	190.5	206	25.0	39.0	3.1	333	--	8.0	42	
		100	199.5	208	24.5	31.5	3.1	333	--			
		1 000	--	--	--	--	--	333	--			
		1 500	--	--	--	--	--	--	--			
	He	2 000	187.5	208	24.0	37.5	2.8	333	--	↓	42	
		100	199.5	208	24.5	31.5	3.1	332	1.00			
		1 000	--	--	--	--	3.0	302	0.91			
		1 500	208.0	206	24.3	37.5	2.6	299	0.90			
H <sub>2</sub>	2 000	--	206	24.0	37.5	1.7	282	0.85	↓	42		
	2 000	--	206	24.0	37.5	1.7	282	0.85				
4140 Low Strength†	Air	0	--	135	--	--	--	--	--	4.0	39	
		10 000	--	--	--	--	--	241	--			
	H <sub>2</sub>	6 000	--	--	--	--	--	207	--	↓	39	
		10 000	--	--	--	--	--	204	0.83			
4140 High Strength†	Air	0	--	228	--	--	--	--	--	4.0	39	
		10 000	--	--	--	--	--	362	--			
	H <sub>2</sub>	2 000	--	--	--	--	--	135	--	↓	39	
		6 000	--	--	--	--	--	121	--			
		10 000	--	--	--	--	--	89	0.22			

\*Heat Treatment 2 (Table XIII)  
 \*\*Heat Treatment 3 (Table XIII)  
 †Held in H<sub>2</sub> environment 24 hours before testing

TABLE 13

## HEAT TREATMENT OF MATERIALS

Material	Heat Treatment by Supplier (As-Received Condition)	Hardness	Heat Treatment by Rocketdyne	Hardness	Ref.
ASTM A533-B	Stress-relieved plate		Annealed at 1650°F for 1 hour; water quenched; tempered at 1270°F for 1 hour; air cooled		7
AISI Type 310 Stainless Steel	Annealed	R <sub>b</sub> 79	None	R <sub>b</sub> 79	→
Inconel 718 (Heat Treatment 2 Table 9)	Annealed	R <sub>c</sub> 24	Annealed at 1850°F for 1 hour; air cooled; reheated to 1360°F for 10 hours; furnace cooled to 1175°F; held for 10 hours; air cooled	R <sub>c</sub> 44	
Inconel 718 (Heat Treatment 3 Table 9)	1750°F for 1 hour; air cooled	R <sub>c</sub> 28	Annealed at 1900°F for 20 min- utes; argon cooled to 300°F; reheated to 1400°F for 11 hours; furnace cooled to 1200°F; held for 9 hours; air cooled	R <sub>c</sub> 40	49

hydrogen at 1000- and 10 000-psig pressures (Fig. 19) (Ref. 7). A decrease in the notched strength was also observed. The decrease in ductility and strength is a linear function of the square root of hydrogen pressure and extrapolates to zero effects at zero hydrogen pressure. It should be noted that surface cracking was observed on unnotched ASTM A533-B specimens tested at all hydrogen pressures. Surface cracking effects will be discussed in Chapter 8, Metallography.

The relationship between tensile properties and the square root of the hydrogen pressure is consistent with a hydrogen adsorption rate-controlled embrittlement process, as has been proposed by Williams and Nelson (Ref. 8). This point will be discussed later in Chapter 10, Technical Discussion.

The influence of pressure was also determined to a limited extent on Inconel 718 (Ref. 47 and 49). The results of a series of tests for Inconel 718 in 100- and 2000-psig hydrogen appear in Table 12.

These results indicate a small reduction of ductility for heat treatment 2, as measured by the reduction of area in the unnotched specimens during exposure to 1000-psig hydrogen, but no decrease is observed for heat treatment 3 at any pressure. It should be noted that this is a considerable difference from the almost zero ductility found for heat treatment 2 in tests conducted in 10 000-psig hydrogen (Table 8). Walter and Chandler (Ref. 7) observed that the reduction of ductility for the individual specimens in 1000-psig hydrogen was directly proportional to the size of the surface crack causing fracture.

The notch strength of specimens from heat treatment 2 was reduced approximately 40 percent in 1000-psig hydrogen, compared to approximately 55 percent in 10 000-psig hydrogen when compared to similar helium pressures. There was a small reduction in ductility of notched specimens from exposure to 1000-psig hydrogen, while the notched specimens tested in 10 000-psig

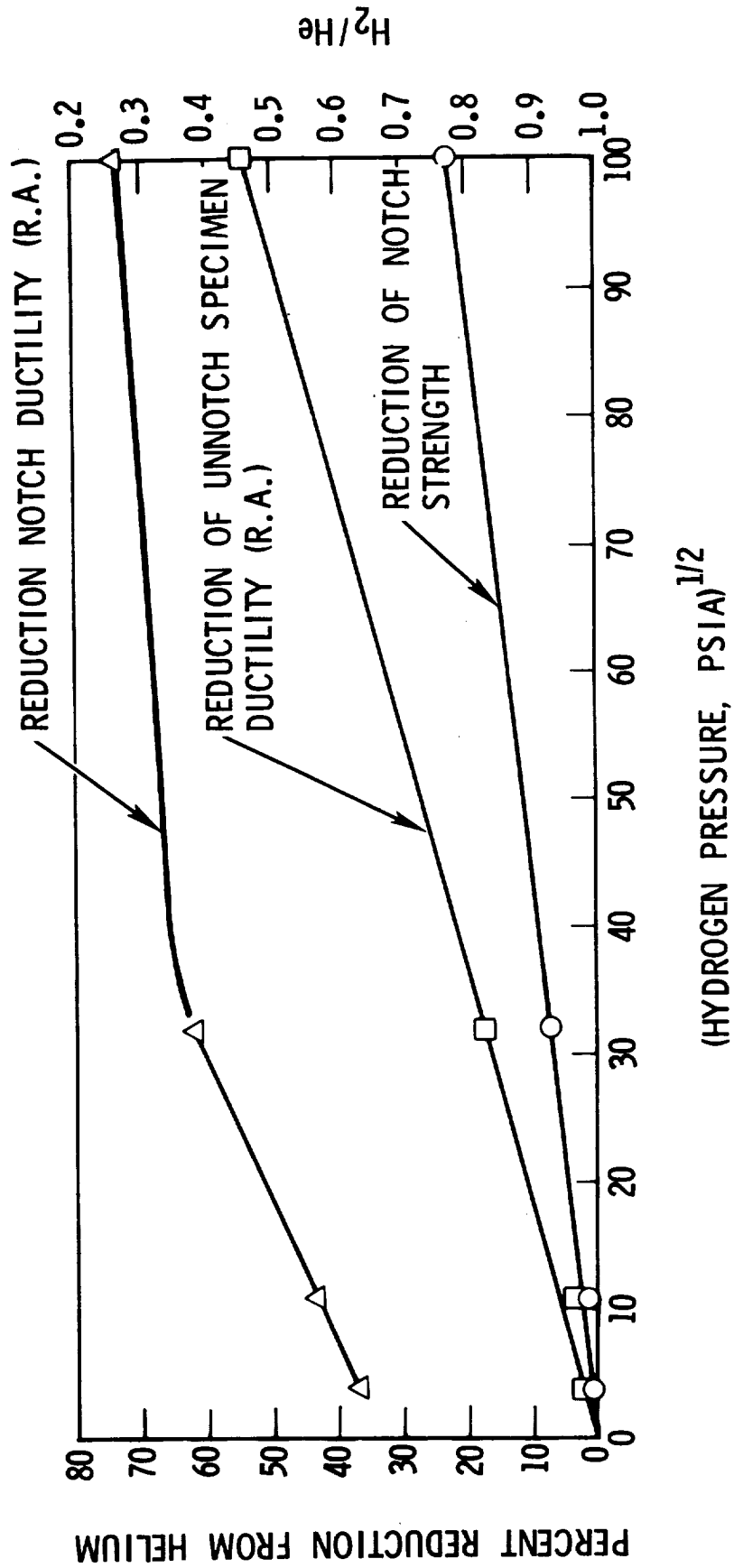


Figure 19. Reduction in tensile properties of ASTM A533-B specimens in hydrogen compared with that in helium as a function of hydrogen pressure.

hydrogen had almost zero ductility. For heat treatment 3, the notch strength was reduced only 15 percent at 2000-psig hydrogen. The reduction of notch strength for heat treatment 3 was a function of the square root of hydrogen pressure (as shown in Fig. 20) up to 2000-psig hydrogen pressure.

There was no reduction of unnotched strength or ductility at room temperature for Ti-6Al-4V (STA) in 1000- and 2000-psig hydrogen (Table 12). The reduction of notch strength was about 32 percent in 1000-psig hydrogen and about 45 percent at 2000-psig hydrogen. Accompanying the reduction of notch strength was a reduction of notch ductility. For Ti-5Al-2.5Sn ELI the reductions of notch strength in 1400-psig and 10 000-psig hydrogen were 10 and 19 percent, respectively.

#### Influence of Notch Severity

The effect of stress concentration factor on hydrogen-environment embrittlement has been investigated at Rensselaer (Ref. 50 and 51) and at Rocketdyne (Ref. 7). The work at Rensselaer is summarized in Table 14. Two steels were used, AISI 4140 and AISI 304L stainless steel. The 4140 was heat treated to two strength levels. Two specimen designs were used, one with a stress concentration factor of 2.0 and one with 4.0. The low-strength 4140 had approximately an 11-percent loss of strength for the  $K_t \approx 2.0$  specimen when tested in 10 000 psig hydrogen, with or without a hold time, when compared to a control specimen tested in air. The  $K_t \approx 4.0$  specimen, soaked in 10 000-psig hydrogen for 20 hours before testing, showed an 18-percent loss of strength when compared to the control specimen. The  $K_t \approx 4.0$  specimen without a hold time showed an anomalous 16-percent gain in strength.

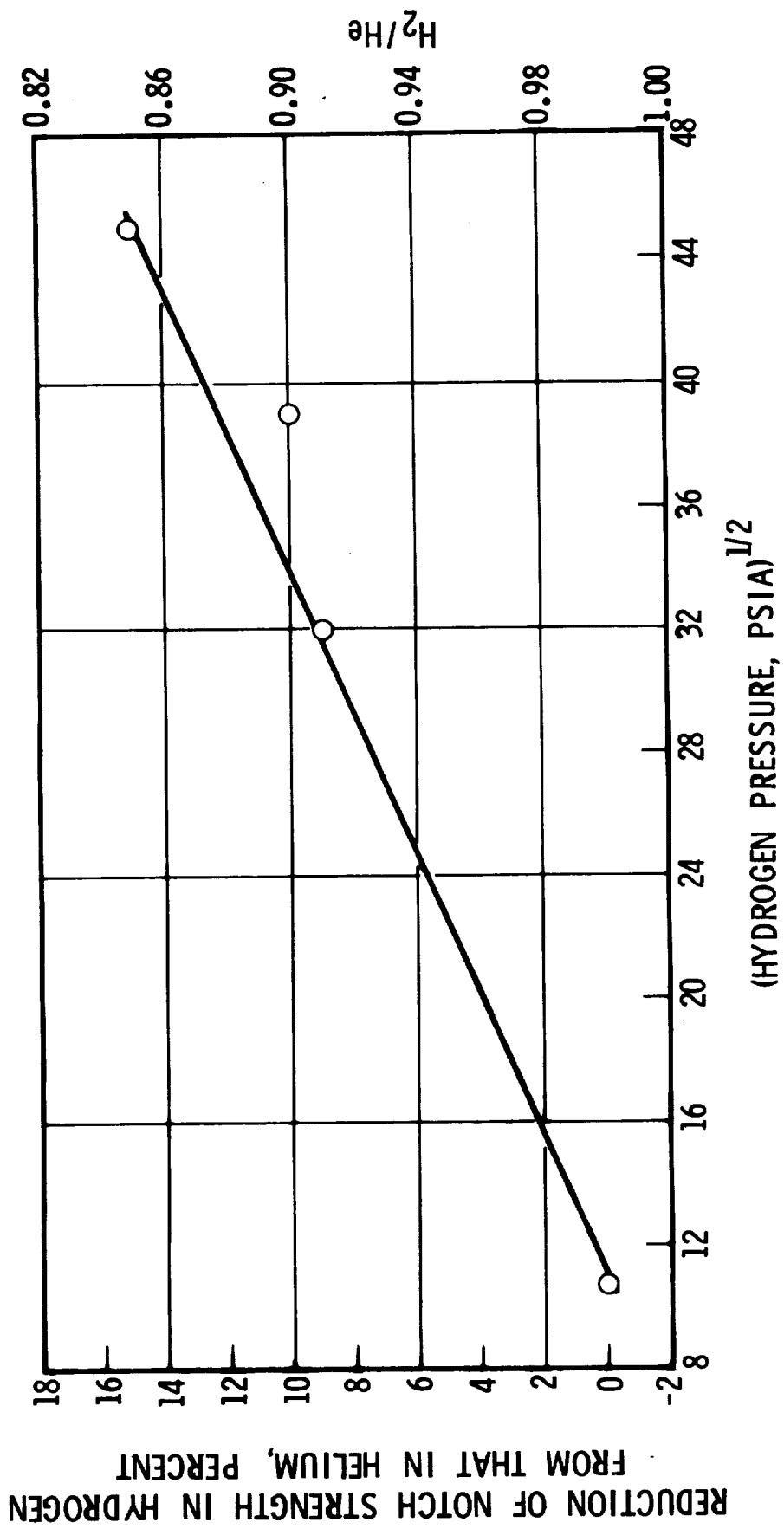


Figure 20. Reduction of notch strength of Inconel 718 in hydrogen compared with that in helium as a function of hydrogen pressure (room temperature).

TABLE 14

EFFECT OF NOTCH SEVERITY ON HYDROGEN-ENVIRONMENT EMBRITTLEMENT

Material	Exposure Time	~ Stress Concentration Factor, $K_t$	Test Condition			Test Results				Ref.
			Environ.	Press., psig	Strain Rate/Min	Strength		Ductility		
						UTS, ksi	Ratio H <sub>2</sub> /He (Air)	Ave. % Red. of Area	Ratio H <sub>2</sub> /He (Air)	
4140 Low strength	0	2.0	Air, RT	0	0.02 crosshead speed	287	--	--	--	50
	20 hr		H <sub>2</sub> , RT	10 000		254	0.89	--	--	
	3 min		H <sub>2</sub> , RT	10 000		252	0.88	--	--	
	0	4.0	Air, RT	0	0.02 crosshead speed	261	--	--	--	
	20 hr		H <sub>2</sub> , RT	10 000		215	0.82	--	--	
	3 min		H <sub>2</sub> , RT	10 000		304	1.16	--	--	
0	2 hr	Air, -321°F	0	0.02 crosshead speed	361	--	--	--		
2 hr		H <sub>2</sub> , -321°F	10 000		377	1.04	--	--		
4140 High Strength	0	2.0	Air, RT	0	0.02 crosshead speed	377	--	--	--	50
	20 hr		H <sub>2</sub> , RT	10 000		177	0.45	--	--	
	5 min		H <sub>2</sub> , RT	10 000		240	0.64	--	--	
	0	4.0	Air, RT	0	0.02 crosshead speed	375	--	--	--	
	20 hr		H <sub>2</sub> , RT	10 000		122	0.32	--	--	
	0		Air, -321°F	0		265	--	--	--	
20 hr	H <sub>2</sub> , -321°F	10 000	247	0.93	--	--	--			
AISI Type 304 L Stainless Steel	24 hr	2.0	Air	0	0.02 crosshead speed	107.0	--	60.0	--	7
	24 hr		N <sub>2</sub>	10 000		108.4	--	--	--	
	24 hr		H <sub>2</sub>	2 500		98.0	0.92	--	--	
	24 hr		H <sub>2</sub>	5 000		103.0	0.96	52.8	0.88	
	24 hr		H <sub>2</sub>	7 500		96.7	0.90	--	--	
	24 hr		H <sub>2</sub>	10 000		98.6	0.92	54.4	0.92	
	3 min	H <sub>2</sub>	10 000	102.2	0.96	--	--			
	24 hr	4.0	Air	0	0.02 crosshead speed	117.0	--	60.0	--	
	24 hr		N <sub>2</sub>	10 000		118.9	--	--	--	
	24 hr		H <sub>2</sub>	2 500		110.2	0.94	--	--	
	24 hr		H <sub>2</sub>	5 000		99.5	0.86	44.4	0.74	
	24 hr		H <sub>2</sub>	7 000		95.7	0.82	--	--	
	24 hr		H <sub>2</sub>	10 000		94.4	0.81	41.4	0.69	
	3 min	H <sub>2</sub>	10 000	100.8	0.86	--	--			
	24 hr	1.0	Air	0	0.02 crosshead speed	102.0	--	60.0	--	
24 hr	H <sub>2</sub>		5 000	89.0		0.87	45.7	0.76		
24 hr	H <sub>2</sub>		10 000	85.0		0.83	44.3	0.74		
AISI Type 310 Stainless Steel	0	0	He	10 000	0.0007	116.0	--	20.0	--	7
	0		H <sub>2</sub>	10 000		108.0	0.93	18.0	0.90	
	0		Air	0		125.0	--	27.0	--	
	0		He	10 000		111.5	--	29.0	--	
	0		H <sub>2</sub>	10 000		112.0	1.00	29.0	1.00	
	0		Air	0		112.0	--	37.0	--	
	0		He	10 000		111.0	--	32.0	--	
	0		H <sub>2</sub>	10 000		111.0	1.00	31.7	1.00	
ASTM A533-B	0	0	He	10 000	0.0007	227.0	--	11.0	--	7
	0		H <sub>2</sub>	10 000		176.0	0.97	2.8	0.26	
	0		Air	0		221.0	--	15.0	--	
	0		He	10 000		211.0	--	16.0	--	
	0		H <sub>2</sub>	10 000		168.0	0.80	4.9	0.31	
	0		Air	0		221.0	--	19.0	--	
	0		He	10 000		207.0	--	19.0	--	
	0		H <sub>2</sub>	10 000		177.0	0.86	4.9	0.26	
ASTM A-517 (T-1)	0	0	Air	0	0.0007	232.0	--	7.0	--	7
	0		He	10 000		221.5	--	5.7	--	
	0		H <sub>2</sub>	10 000		173.0	0.78	3.1	0.58	
	0		Air	0		243.0	--	11.0	--	
	0		He	10 000		229.5	--	11.5	--	
	0		H <sub>2</sub>	10 000		172.0	0.45	2.0	0.14	
	0		Air	0		243.0	--	13.0	--	
	0		He	10 000		226.5	--	12.0	--	
	0		H <sub>2</sub>	10 000		181.0	0.20	2.8	0.23	
	0		Air	0		128.0	--	65.0	--	
	0		H <sub>2</sub>	10 000		121.0	0.96	63.0	--	

Embrittlement for the high-strength 4140 was more spectacular. The  $K_t \approx 2.0$  specimen showed a 52-percent loss of strength, and the  $K_t \approx 4.0$  specimen showed a 68-percent loss of strength (as compared to air tests) when tested in 10 000-psig hydrogen after an approximately 20-hour soak.

The embrittlement of the AISI 304L stainless steel also showed a dependency on the degree of stress concentration. For the  $K_t \approx 2.0$  notch, the decrease in ductility was 12.0 percent at 5000 psig, and 8.0 percent at 10 000 psig. For the  $K_t \approx 4.0$  notch, the decrease in ductility was 26.0 percent at 5000 psig, and 31.0 percent at 10 000-psig hydrogen. These results show that for these two materials, there was a small dependence of ductility on hydrogen pressure, but the stress concentration factor had a pronounced effect.

Walter and Chandler (Ref. 7) have investigated the influence of notch geometry for ASTM A533-B, ASTM A-517, and AISI 310 stainless-steel specimens in 10 000-psig hydrogen. The notch geometries investigated had stress concentration factors ( $K_t$ ) of approximately 3.9, 5.9, and 8.4. The results are tabulated in Table 14. For AISI 310 stainless steel, no embrittlement was observed except for specimens with a  $K_t \approx 8.4$  for which the loss of notch strength was less than 10 percent.

The results for ASTM A533-B are plotted in Fig. 21, and for ASTM A-517 (T-1) in Fig. 22. The degree of embrittlement in 10 000-psig hydrogen increased for low values of  $K_t$ , reached a maximum at  $K_t \approx 8.0$  for ASTM A533-B and at  $K_t \approx 6.0$  for ASTM A-517 (T-1).

Also plotted in Fig. 21 and 22 is the reduction of strength for fatigue precracked specimens. The  $K_t$  value for a notch containing a fatigue-induced crack was arbitrarily assumed by Walter and Chandler to be between 19 and 20.

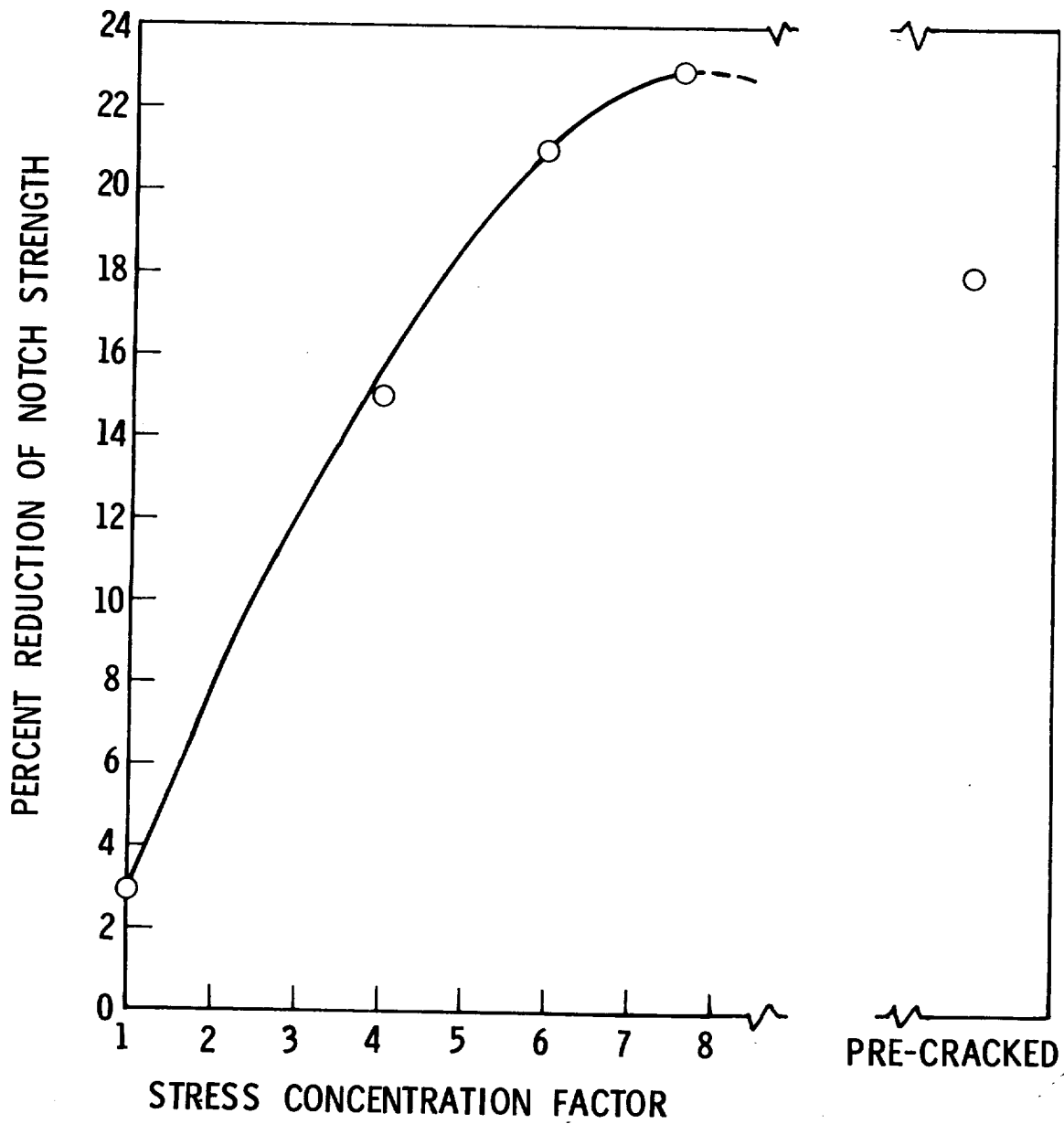


Figure 21. Reduction of Strength as a Function of Notch Severity for ASTM A533-B (ref. 7)

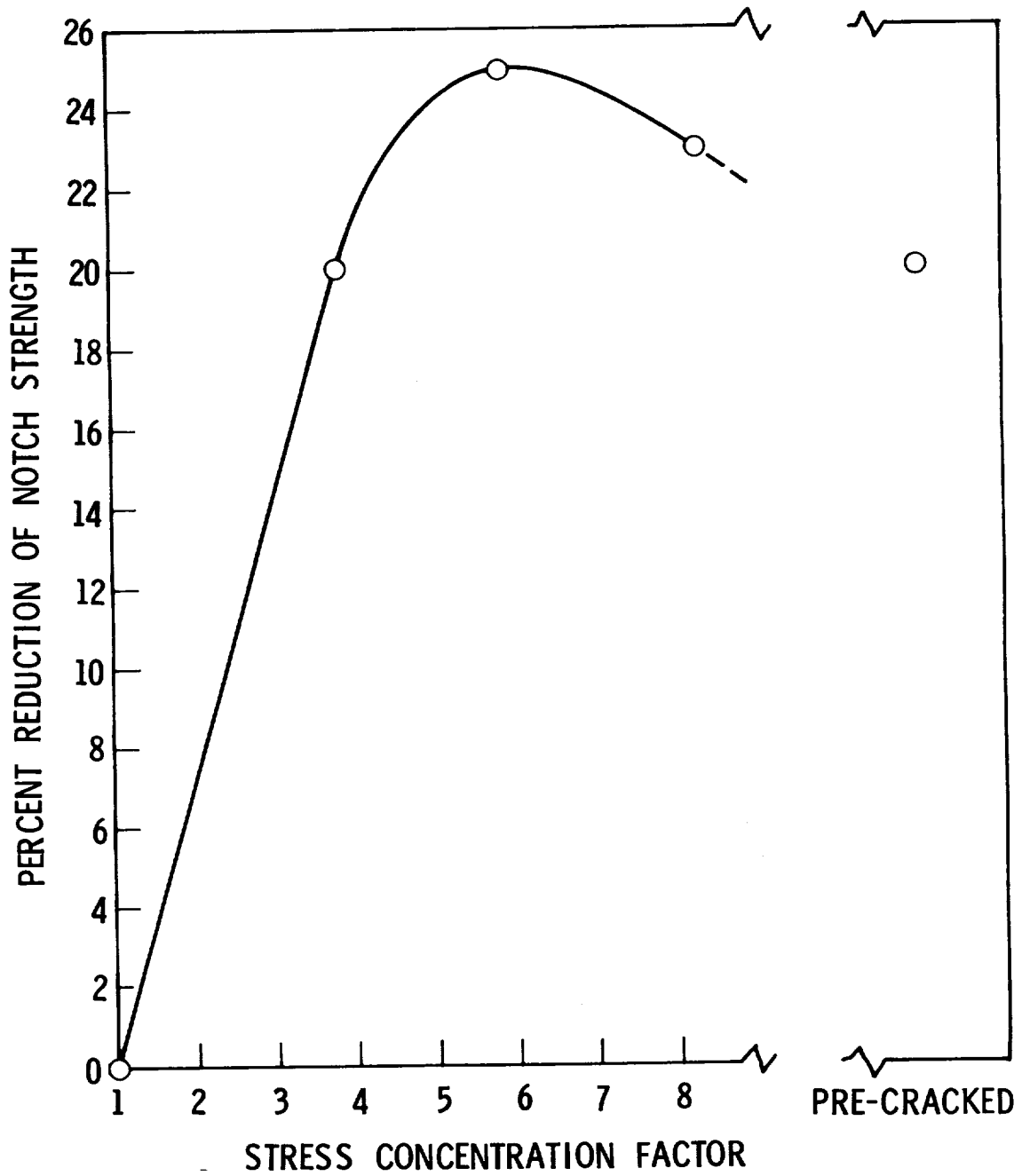


Figure 22. Reduction in Strength of ASTM A-517 as a function of notch severity.

The precracked specimens of both materials are not as embrittled by 10 000 psig hydrogen as the  $K_t \approx 6.0$  and  $8.0$  geometries, indicating that embrittlement does not increase indefinitely with decreasing notch radius.

#### Effect of Hold Time (Room Temperature)

Early experimental work on hydrogen-environment embrittlement employed an exposure time (unstressed) in the gaseous hydrogen prior to conducting tensile tests in the environment (Ref. 50). Later work was done in which a stress was applied during the hold time in hydrogen (Ref. 7).

All of the hold-time data (Table 15) with no applied stress showed that the amount of hydrogen-environment embrittlement was not a function of the hold time in the environment. Some of the data indicate that an inverse relation between hold time and the degree of embrittlement exists, i.e., the longer the hold time, the less the degree of embrittlement (Ref. 7). The inverse relationship was attributed to a buildup of oxygen contamination on the surface of the sample during the hold period (Ref. 7). The effect is evident from the data in Table 15 for the AISI 310 stainless steel, where the degree of embrittlement with no hold time is 7 percent and is approximately 0 as the hold time increases. These tests were run in test cells which had been pressurized/depressurized with hydrogen but had not been evacuated. For titanium, data are available (Table 15) for pressurized/depressurized test cells and for test cells which were evacuated prior to testing. In both cases, the degree of embrittlement is much greater with no hold time than with prolonged exposure.

TABLE 15

EFFECT OF TIME OF EXPOSURE TO HYDROGEN ON THE TENSILE PROPERTIES OF THREE ALLOYS  
 AT ZERO HOLD STRESS IN 10 000-PSIG HYDROGEN AND HELIUM (Ref. 7)

Material	Environment		Unnotched Specimens				Notched Specimens			
	Type	Hold Time, hours	YS, ksi	UTS, ksi	Elong., %	Red. of Area, %	Red. of Area, %	UTS, ksi	Strength Ratio H <sub>2</sub> /He	~K <sub>t</sub>
AISI Type 310 Stainless Steel	He H <sub>2</sub>	0	---	77	56	64	20.0	116	--	8.0
		0	---	78	56	62	18.0	108	0.93	↓
		1	---	78	56	62	17.0	112	0.97	
		8	---	79	56	68	15.0	119	1.03	
		24	---	83	55	69	17.0	113	0.97	
ASTM A533-B	He H <sub>2</sub>	0	---	119	19	66	15.0	227	--	8.0
		0	---	116	17	33	2.8	176	0.78	↓
		1	---	119	16	37	4.0	173	0.76	
		8	---	118	16	37	3.5	179	0.79	
		24	---	118	17	33	3.7	182	0.79	
Ti-6Al-4V Annealed	He H <sub>2</sub>	0	132	156	15	48	2.2	243	--	8.0
		0	---	159	15	48	1.0	183	0.75	↓
		1	---	158	16	48	--	---	--	
		24	---	151	15	51	3.0	220	0.91	
Ti-6Al-4V (STA)	He H <sub>2</sub>	0	156	164	13	46	--	227	--	8.0
		0	---	171	13	50	1.1	136	0.60	↓
		24	---	165	11	46	2.5	192	0.85	

From the data in Table 16, no effect on the degree of hydrogen-environment embrittlement of various steels and K-monel could be attributed to holding specimens under stress in 10 000-psig hydrogen for periods up to 100 days before tensile testing. The yield strength of unnotched AISI 1020 specimens increased with hold time when held at a stress below the yield strength; however, the specimens had been prestrained and the yield strength increase was attributed to strain aging. Yield strengths of unnotched HY-80 and ASTM A-515 specimens, which had not been prestrained, were not affected by holding at a stress below the yield strengths. When unnotched AISI 1020, ASTM A-515, and HY-80 specimens were tensile tested after holding at a stress above the yield strength, a new yield point was found that increased with hold time. This increase in yield strength was attributed to strain or stress aging.

The degree of hydrogen-environment embrittlement, as measured by reduction of notch strength in 10 000-psig hydrogen compared to that in 10 000-psig helium, decreased with increasing exposure duration for the prestrained, notched AISI 1020 specimens. It was suggested (Ref. 7 ) that this embrittlement decrease related to an increase of yield strength/ultimate strength ratio, resulting from strain aging during the hold period. Evacuation of the test vessels prior to pressurization/depressurization purging led to increased embrittlement from the 10 000-psig hydrogen environment in tests involving no hold period. The increased embrittlement was attributed to a reduction in the concentration of oxygen adsorbed on the specimen surface. After holding for 1 day or longer, the embrittlement in 10 000-psig hydrogen was the same whether or not the test vessels had been evacuated.

**TABLE 16**  
**EFFECT OF EXPOSURE TIME AND HOLD STRESS IN HYDROGEN**  
**ON THE TENSILE PROPERTIES OF VARIOUS METALS**

Material	Test Environment			Hold Stress	Unnotched Specimens					Notched Specimens			~k <sub>t</sub>	Ref.	
	Type	Press. psig	Hold Time, days		YS, ksi	UTS, ksi	Elong., %	Red. of Area, %	Strength Ratio H <sub>2</sub> /He	Red. of Area, %	UTS, ksi	Strength Ratio H <sub>2</sub> /He			
AISI 1020 (Prestrained)	Air	0	0	0	54	71	--	65	--	12.0	114	--	8.0	7	
		He	10 000	0	0	41	63	40.0	68	--	14.0	105			--
			10 000	1	35.5	47	64	34.0	68	--	--	--			--
			10 000	1	53.0	53	63	37.0	71	--	--	--			--
			10 000	10	53.0	71	72	31.0	69	--	--	--			--
			10 000	1	76.0	--	--	--	--	--	19.0	101			--
	10 000	10	76.0	--	--	--	--	--	14.0	103	--				
	H <sub>2</sub>	10 000	0	0	40	62	32.0	45	--	8.2	84	0.80			
		10 000	1	35.5	46	63	33.0	45	--	--	--	--			
		10 000	100	35.5	52	66	25.0	49	--	--	--	--			
		10 000	1	53.0	64	65	30.0	45	--	--	--	--			
		10 000	100	53.0	72	73	30.0	54	--	--	--	--			
		10 000	1	76.0	--	--	--	--	--	--	101	0.96			
		10 000	1	76.0	--	--	--	--	--	--	104	0.99			
10 000		100	76.0	--	--	--	--	--	--	--	--				
ASTM A515	Air	0	0	0	49	73	--	66	--	--	--	--	8.0	7	
		10 000	0	0	--	65	42.0	67	--	8.1	106	--			
	H <sub>2</sub>	10 000	0	0	--	64	29.0	35	--	3.4	74	0.68			
		10 000	1	32.3	44	67	28.0	34	--	--	--	--			
		10 000	100	32.3	45	66	27.0	38	--	--	--	--			
		10 000	1	54.0	63	67	29.0	36	--	--	--	--			
		10 000	100	54.0	69	71	27.0	47	--	--	--	--			
		10 000	1	67.0	--	--	--	--	--	3.4	83	0.78			
		10 000	1	67.0	--	--	--	--	3.7	83	0.78	--			
		10 000	100	67.0	--	--	--	--	--	--	--	--			
HY-80	Air	0	0	0	93	107	--	64	--	--	--	--	8.0	7	
		10 000	0	0	--	98	23.0	70	--	8.6	190	--			
	H <sub>2</sub>	10 000	0	0	85	99	20.0	60	--	3.9	151	0.80			
		10 000	1	64.4	85	99	22.0	62	--	--	--	--			
		10 000	100	64.4	85	101	22.0	66	--	--	--	--			
		10 000	1	92.5	98	101	20.0	58	--	--	--	--			
		10 000	100	92.5	102	105	17.0	58	--	--	--	--			
		10 000	1	136.0	--	--	--	--	--	4.2	161	0.85			
		10 000	1	136.0	--	--	--	--	4.3	155	0.82	--			
		10 000	100	136.0	--	--	--	--	--	--	--	--			
H-11 Tool Steel	Air	0	0	0	165	299	13.0	30	--	--	--	--	8.0	7	
		10 000	0	0	--	299	8.8	30	--	0.0	252	--			
	H <sub>2</sub>	10 000	0	0	--	171	0	0	0.62	0.0	57	0.23			
		10 000	1	128.0	153	172	0	0	0.62	--	--	--			
		10 000	100	128.0	146	167	0	0	0.60	--	--	--			
		10 000	1	54	--	--	--	--	--	0.0	78	0.31			
		10 000	1	54	--	--	--	--	--	0.0	112	0.44			
		10 000	100	54	--	--	--	--	--	--	--	--			
4140 Low Strength	Air	0	0	0	--	--	--	--	--	287	--	2.0	44		
	H <sub>2</sub>	10 000	0	0	--	--	--	--	--	252	0.88				
	H <sub>2</sub>	10 000	0.83	0	--	--	--	--	--	254	0.89				
4140 High Strength	Air	0	0	0	--	--	--	--	--	377	--	2.0	45		
	H <sub>2</sub>	10 000	0	0	--	--	--	--	--	240	0.64				
	H <sub>2</sub>	10 000	0.83	0	--	--	--	--	--	177	0.48				
AISI Type 304L Stainless Steel	Air	0	0	0	--	93	--	60	--	60.0	107	--	2.0	36	
	Air	0	0	0	--	--	--	--	--	60.0	117	--			
	H <sub>2</sub>	5 000	1	0	--	89	--	45.7	0.95	52.8	106	0.99			
	H <sub>2</sub>	5 000	1	0	--	--	--	--	--	44.4	101	0.86			
	H <sub>2</sub>	10 000	1	0	--	86	--	44.3	0.92	54.4	101	0.96			
C-1025	Air	0	0	0	--	65	--	--	--	--	--	4.0	36		
	N <sub>2</sub>	10 000	1	0	--	--	--	--	--	106	--				
	H <sub>2</sub>	10 000	1	0	--	--	--	--	--	80	0.76				
K-Monel Precip. Hardened	Air	0	0	0	--	139	--	--	--	--	--	4.0	36		
	N <sub>2</sub>	10 000	1	0	--	--	--	--	--	251	--				
	H <sub>2</sub>	10 000	1	0	--	--	--	--	--	113	0.45				
K-Monel Annealed	Air	0	0	0	--	100	--	--	--	--	--	4.0	36		
	N <sub>2</sub>	10 000	1	0	--	--	--	--	--	144	--				
	H <sub>2</sub>	10 000	1	0	--	--	--	--	--	105	0.74				
SAE 4140 *	Air	0	0	0	--	--	--	--	--	257	--	t/r=3	47		
	↓	6 000	25	33	--	--	--	--	--	165	0.64				
	↓	6 000	50	33	--	--	--	--	--	170	0.66				
SAE 1018*	Air	0	0	0	--	--	--	--	--	169	--				
	↓	6 000	25	16.5	--	--	--	--	--	169	--				
	↓	6 000	50	16.5	--	--	--	--	--	170	--				

\*Tests performed in air after exposure to 6000-psig hydrogen

The strength of notched Ti-6Al-4V specimens was considerably lower in 10 000-psig hydrogen as compared to 10 000-psig helium. In almost all cases, both annealed and STA Ti-6Al-4V notched specimens failed in hydrogen shortly after a hold stress was established, rather than while the specimens were being loaded. Once cracking was initiated in hydrogen, failure was rapid. There was no indication of hydrogen-environment embrittlement of unnotched Ti-6Al-4V STA specimens, but an increase of yield strength occurred during the hold period and was attributed to strain or stress aging.

Thus, no effect of hold time or applied stress on the degree of hydrogen-environment embrittlement is evident from these results. Similar results were found (Ref. 52) from an investigation of the effect of hold times of 1, 10, and 100 days on tensile properties in hydrogen of parent- and weld-metal specimens of ASTM A-517, ASTM A515, and ASTM A533-B.

In all cases reported, the degree of embrittlement of notched specimens was approximately the same for the various hold times at constant applied stress in 10 000-psig hydrogen. The degree of embrittlement has always been found to be less for the long hold times, probably because of increased impurity effects.

In recent tests, Owens (Ref. 53) tested in air specimens that had been exposed to 6000-psig hydrogen. Results obtained for notched specimens ( $t/r \sim 3$ ) of SAE 4140 and 1018 steels showed essentially no effect of hold time under an applied stress at 6000-psig hydrogen pressure. The hold stresses were 33 000 and 16 500 psi, respectively. The specimens were exposed to 6000-psig hydrogen for 25 and 50 days, taken out of the vessel, and tested immediately. In addition, some specimens were allowed to remain out of storage for 1 and 10 days prior to testing. The results are shown in Table 16. The results show that SAE 4140 was

embrittled by this procedure while the SAE 1018 was not. It is of interest to note that for specimens exposed for 25 days to 6000-psig hydrogen, the ultimate tensile strength was restored to the original value after 10 days storage at ambient temperature.

No comprehensive study has been made on the effect of hold stress and hold time. The limited data to date (Table 16) indicate that there is probably no effect from these variables. Whatever effect might occur, however, may be masked by the effect of contamination buildup during the course of these types of tests.

#### Effect of Temperature

The data available on the tensile properties in hydrogen as a function of temperature are limited. The data available are from the work of Hofmann and Rauls (Ref. 42) and from Walter et al. on Inconel 718 and Ti-6Al-4V (Ref. 26, 47, and 49).

Hofmann and Rauls investigated the effect of temperature on hydrogen-environment embrittlement between  $-130^{\circ}\text{F}$  ( $-90^{\circ}\text{C}$ ) and  $338^{\circ}\text{F}$  ( $170^{\circ}\text{C}$ ) at 2205 psig pressure for cold-drawn and normalized CK 22. The tensile deformation rate was 5%/min. No effect on the ultimate tensile strength was observed at any of the test temperatures. The effect on ductility (percent elongation and reduction of area), however, was pronounced, as shown in Fig. 23 and 24. In the cold-drawn CK 22, the maximum degradation value of reduction of area occurred at  $0^{\circ}\text{C}$  in hydrogen, while in the normalized CK 22, the maximum degradation occurred at  $-40^{\circ}\text{C}$ .

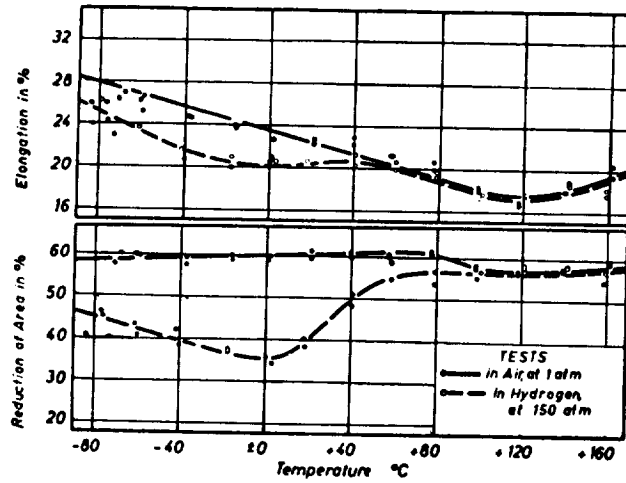


Figure 23. Effect of temperature on elongation and reduction of area of cold-drawn CK 22 steel in air and in hydrogen.

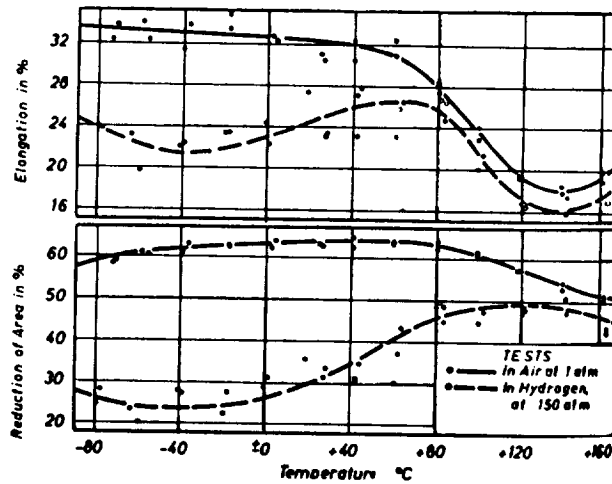


Figure 24. Effect of temperature on elongation and reduction of area of normalized CK 22 steel in air and in hydrogen.

As can be seen from the data in Table 17 and Fig. 25, the reduction of notch strength of Inconel 718 for heat B and heat treatment 3 specimens tested in 2000-psig hydrogen was essentially zero at  $-109^{\circ}$  and  $-320^{\circ}$ F, and was essentially the same (approximately 15 percent) at room temperature and  $140^{\circ}$ F. The reduction of notch strength of heat C with heat treatment 4 specimens by 500-psig hydrogen decreased from 34 percent at room temperature to 14 percent at  $400^{\circ}$ F, and down to zero at  $1200^{\circ}$ F. Results from  $1200^{\circ}$ F tests may be invalid because of oxygen contamination of the hydrogen, as was evidenced by surface discoloration of the specimens. As discussed earlier, the susceptibility of heat B and heat treatment 3 specimens to a hydrogen-environment embrittlement was much less than other heat-heat treatment combinations of Inconel 718. Thus, greater temperature dependence may be realized with other heat-heat treatment combinations (Ref. 47).

A limited number of hydrogen-environment embrittlement tests at temperatures above room temperature also have been performed on Waspaloy, another nickel-base alloy. The reduction of notch strength for Waspaloy in 500-psig hydrogen was approximately 36 percent at room temperature, 26 percent at  $400^{\circ}$ F, and 6 percent at  $1200^{\circ}$ F. Again, the results from  $1200^{\circ}$ F tests might be affected because of contamination. In any case, the data indicate that the hydrogen-environment embrittlement of Inconel 718 (and probably other nickel-base alloys) is a maximum in the vicinity of room temperature.

The results of the tensile tests of Ti-6Al-4V(STA) in hydrogen and helium at various pressures and temperatures are given in Table 18 and Fig. 26. The loss of notch strength in hydrogen at room temperature is severe. The sharp reduction in the hydrogen-environment embrittlement of Ti-6Al-4V(STA) as the

TABLE 17

TENSILE PROPERTIES OF NICKEL-BASE ALLOY AS A FUNCTION OF TEMPERATURE

Material		Environment			Tensile Properties								Ref.	
					Unnotched Specimens				Notched Specimens					
					YS, ksi	UTS, ksi	Elong., %	Red. of Area, %	YS, ksi	UTS, ksi	Red. of Area, %	Strength Ratio H <sub>2</sub> /He		
Heat (From Table X)	Heat Treat (From Table IX)	Press., psig	Temp., °F											
Inconel 718	3	He	100	-320	229	249	20	34	3.1	388	--		42	
B	1	H <sub>2</sub>	100	-320	223	244	19	33	3.2	377	1.0			
		He	2000	-320	229	257	20	39	2.8	377	--			
		H <sub>2</sub>	2000	-320	221	247	22	33	3.7	375	1.0			
		Air	0	RT	180	215	21	37	2.5	281	--			
		Air	800	-260	191	244	23			308	--			
		He	800	-260	173	246	20	35	2.5	313	--			
		H <sub>2</sub>	800	-260	195	250	20	33	2	321	1.0			
		He	2000	-109	--	--	--	--	3.4	355	--			
		H <sub>2</sub>	2000	-109	--	--	--	--	3.9	351	1.0			
		H <sub>2</sub>	2000	RT	189	206	24	38	1.1	282	0.85			
		He	100	140	182	203	24	38	3.4	324	--			
		H <sub>2</sub>	100	140	182	204	24	40	3.9	320	1.0			
		He	2000	140	185	202	24	41	3.1	330	--			
		H <sub>2</sub>	2000	140	185	200	24	40	3.0	283	0.86			
		He	500	RT	--	--	--	--	--	273	--			
		H <sub>2</sub>	500	RT	--	--	--	--	--	180	0.66			
		He	500	400	--	--	--	--	--	237	--			
		H <sub>2</sub>	500	400	--	--	--	--	--	205	0.86			
		He	500	1200	--	--	--	--	--	180	--			
		H <sub>2</sub>	500	1200	--	--	--	--	--	184	1.0			
		He	500	RT	--	--	--	--	2.4	214	--		26	
		H <sub>2</sub>	500	RT	--	--	--	--	0.95	137	0.64			
		He	500	400	--	--	--	--	2.5	191	--			
		H <sub>2</sub>	500	400	--	--	--	--	0.8	141	0.74			
		He	500	1200	--	--	--	--	4.3	192	--			
		H <sub>2</sub>	500	1200	--	--	--	--	4.3	180	0.94			
Waspaloy														

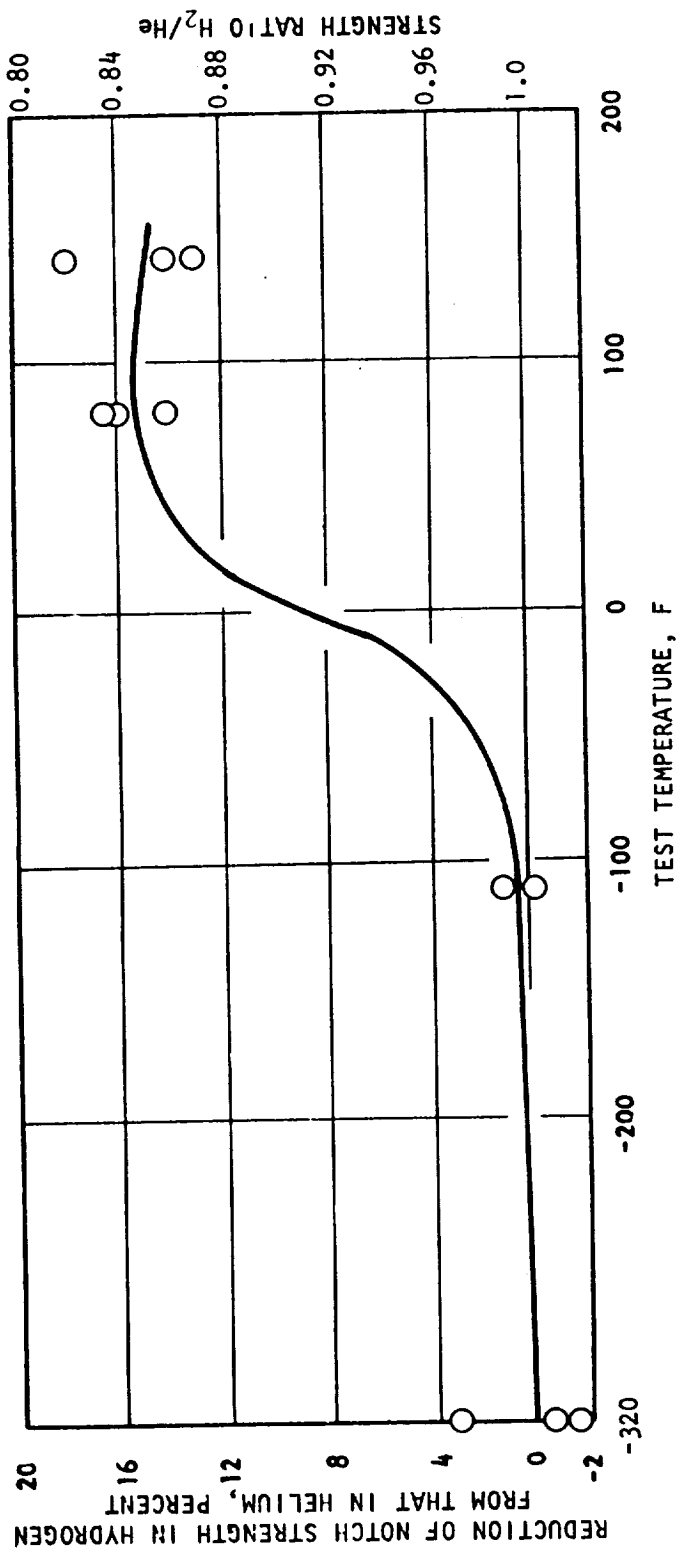


Figure 25. Reduction in strength of notched Inconel 718 specimens in 2000-psi hydrogen compared with that in 2000-psi helium as a function of temperature (ref. 43).

TABLE 18

TENSILE PROPERTIES OF Ti-6Al-4V (STA)\* IN HIGH-PRESSURE HYDROGEN AND HELIUM AT ROOM AND CRYOGENIC TEMPERATURES (Ref.49)

Environment			Tensile Properties									
Type	Press., psig	Temp., °F	Unnotched Specimens					Notched Specimens ( $K_t=8.0$ )				
			No. of Tests	YS, ksi	UTS, ksi	Elong., %	Red. of Area, %	No. of Tests	Red. of Area, %	UTS, ksi	Strength Ratio H <sub>2</sub> /He	
Air	0	RT	2	169	179	12	48	2	1.7	237	--	
He	1000	RT	2	166	178	11	46	2	3.4	249	--	
H <sub>2</sub>	1000	RT	3	168	178	11	49	3	0.8	169	0.68	
He	1000	-320	1	242	251	6.6	37	2	0	236	--	
H <sub>2</sub>	1000	-320	3	241	251	6.1	33	3	0.6	222	0.94	
He	2000	RT	2	167	177	13	46	2	3.2	251	--	
H <sub>2</sub>	2000	RT	3	164	175	11	48	3	0.4	136	0.54	
He	2000	-109	2	190	201	9.7	40	2	2.0	228	--	
H <sub>2</sub>	2000	-109	3	184	195	7.9	37	3	1.9	210	0.91	
He	2000	-320	2	240	254	5.5	36	2	0.3	229	--	
H <sub>2</sub>	2000	-320	3	243	253	6.7	33	3	1.3	234	--	

\*Supplier-certified STA spec. AMS 4965 (1750°F solution annealed for 1 hr; water quenched; aged 4 hrs at 1000°F)

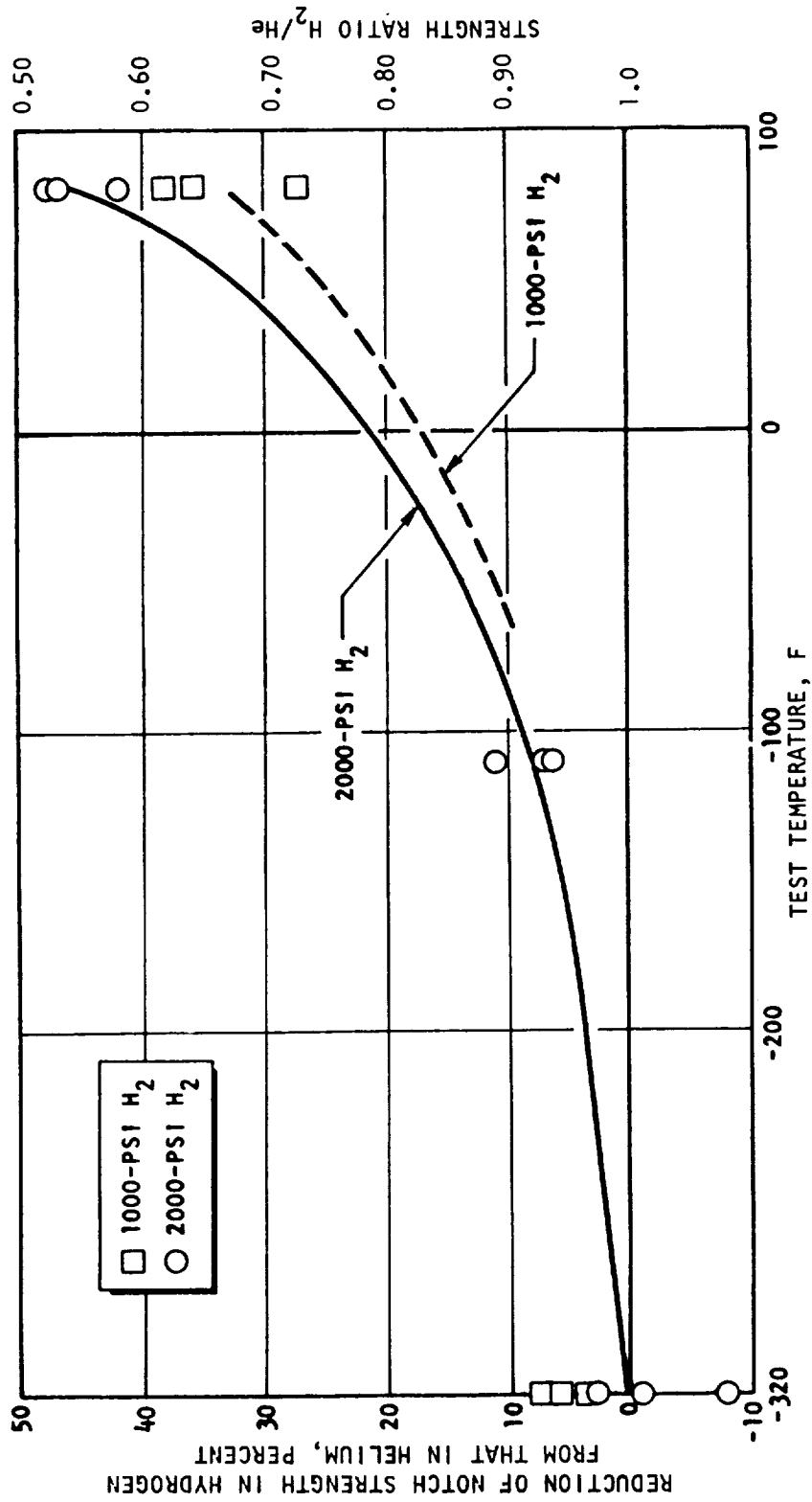


Figure 26 Reduction in strength of notched ( $K_t \approx 8.0$ ) Ti-6Al-4V (STA) specimens in hydrogen compared with that in helium as a function of temperature

test temperature is reduced below room temperature is evident from Fig. 26. Some loss of notch strength occurred at  $-109^{\circ}\text{F}$ , but virtually none at  $-320^{\circ}\text{F}$ .

#### Embrittlement of Welds in Pressure Vessel Steels

The effect of high-pressure hydrogen on weldments and parent metal of three pressure-vessel steels has been investigated by Walter and Chandler (Ref. 52). The ASTM designations of the steels tested were: A-302-56 Gr. B modified with nickel (A-302), A-517-64 Gr. F (T-1), and A-212-61T Gr. B-FB (A-212). The A-302 steel has since been redesignated A533-B and the A-212 steel as A515. The newer designations are used in this report. Both longitudinal and girth welds were tested, except for A515 in which the girth and longitudinal welds were similar. The welded plates simulated actual pressure-vessel plates in thickness, weld geometry, weld procedure, and heat treatment. The thickness of the plates tested were: A533-B, 5-1/2 inches; A-517, 1-3/8 inches; and A515, 4 inches. Both unnotched and notched specimens were tested. The notched specimens had a  $K_t \approx 4.2$  (Ref. 43). The specimens from the weld panels were taken normal to the longitudinal and the girth welds, and the notches were located either in the weld zone or in the heat-affected zone. Tests were conducted with various hold times (1, 10, and 100 days) and at various hold stresses in the hydrogen atmosphere. No effect of hold time or hold stress on embrittlement was observed. The results of short-time tests are tabulated in Table 19.

No difference was observed between the strength of the unnotched specimens tested in 10 000-psig hydrogen and in 10 000-psig helium for any of the three alloys, or for the parent metal and the weld specimens. However, exposure to high-pressure hydrogen resulted in a decrease in the reduction of area of approximately 33 percent for the A533-B longitudinal welds and 50 percent for the A533-B

TABLE 19

TENSILE PROPERTIES OF UNNOTCHED AND NOTCHED WELD SPECIMENS  
IN 10 000-PSIG HYDROGEN AND HELIUM (Ref. 52)

Material	Type	Type of Environment	Pressure, psig	Hold Time, days	Hold Stress, ksi	Unnotched Specimens			Notched Specimens			Ratio (H <sub>2</sub> /He)		
						YS, ksi	UTS, ksi	Elongation, %	Reduction of Area, %	Hold Stress, ksi	Reduction of Area, %		UTS, ksi	
A533-B	Parent Metal, Longitudinal Direction	He	10 000	0	0	--	106	22	68.0	--	17.0	198	--	
		H <sub>2</sub>	10 000	1	78	--	106	22	57.0	123	5.3	172	0.87	
	Parent Metal, Transverse Direction	He	10 000	0	0	--	101	22	62.0	--	17.0	196	--	
		H <sub>2</sub>	10 000	0	--	--	--	--	--	--	9.8	190	0.97	
	Longitudinal Weld	He	10 000	0	0	91	105	24	65	--	10.0	205	--	
		H <sub>2</sub>	10 000	1	78	--	113	18	43	123	1.6	171	0.83	
	Longitudinal Weld, Heat-Affected Zone	He	10 000	0	--	--	--	--	--	--	13.0	197	--	
		H <sub>2</sub>	10 000	1	--	--	--	--	--	123	5.6	194	0.98	
	Girth Weld	He	10 000	0	0	94	107	18	53.0	--	5.5	208	--	
		H <sub>2</sub>	10 000	1	78	--	115	11	22.0	123	2.0	173	0.83	
	Girth Weld, Heat-Affected Zone	He	10 000	0	--	--	--	--	--	--	3.3	232	--	
		H <sub>2</sub>	10 000	1	--	--	--	--	3.3	123	3.7	143	0.62	
A-517-64 (T-1)	Parent Metal, Longitudinal Direction	He	10 000	0	0	96	116	18	49.0	--	3.1	204	--	
		H <sub>2</sub>	10 000	1	87	103	115	16	25.0	151	1.2	185	0.91	
	Longitudinal Weld	He	10 000	0	0	99	109	17	62.0	--	11.0	210	--	
		H <sub>2</sub>	10 000	1	87	101	115	11	29.0	151	2.5	147	0.70	
	Longitudinal Weld, Heat-Affected Zone	He	10 000	0	--	--	--	--	--	--	1.2	216	--	
		H <sub>2</sub>	10 000	1	--	--	--	--	--	151	0.8	163	0.75	
	Girth Weld	He	10 000	0	0	86	106	17	63.5	--	7.9	202	--	
		H <sub>2</sub>	10 000	1	--	--	--	--	--	139	2.2	162	0.80	
	Girth Weld, Heat-Affected Zone	He	10 000	0	0	0	--	--	--	--	8.4	210	--	
		H <sub>2</sub>	10 000	1	--	--	--	--	--	139	0.0	178	0.85	
	A515	Parent Metal, Longitudinal Direction	He	10 000	0	0	38	67	40	57.0	--	12.0	125	--
			H <sub>2</sub>	10 000	1	34	46	65	29	34.0	91	2.3	89	0.71
Longitudinal Weld		He	10 000	0	0	58	71	23	64.0	--	19.0	142	--	
		H <sub>2</sub>	10 000	1	53	61	72	17	48.0	91	4.5	135	0.95	
Longitudinal Weld, Heat-Affected Zone	He	10 000	0	0	--	--	--	--	--	11.0	146	--		
	H <sub>2</sub>	10 000	1	--	--	--	--	--	91	2.3	119	0.82		

girth welds, the A-517 longitudinal welds, and the A515 parent metal. The longitudinal weld of the A515 showed a 25-percent decrease in the reduction of area. A small effect of the hydrogen environment was observed for all materials except the A533-B girth weld and A515 parent metal. The reduction of area data are shown in Fig. 27. The notched specimens that were tested in the hydrogen environment showed a reduction of both strength and ductility compared to specimens tested in helium. The smallest strength reduction occurred in the A533-B parent-metal specimens. The transverse parent-metal specimens had almost no strength reduction, while the strength of the longitudinal weld was more embrittled than the parent metal. The girth-weld, heat-affected zone was the most embrittled by the hydrogen environment. The A515 parent-metal specimens showed a greater strength reduction than did specimens from the other two parent-metal materials. The welds of A515 were not as embrittled as the parent metal. There was a small effect of 10 000-psig hydrogen on the A-517 parent metal in the A-517 longitudinal weld and longitudinal weld heat-affected zones. The A-517 girth welds were not as embrittled as the longitudinal welds.

Tests also were performed at 3000-, 5000-, and 7500-psig hydrogen pressures on notched longitudinal parent-metal and notched longitudinal weld-metal specimens of these three materials. Only for the notched A515 parent metal and the A515 specimens containing a notch in the longitudinal-weld metal was there a significant decrease of embrittlement as the hydrogen pressure was reduced from 10 000 to 3000 psig. The specimens tested at 3000 and 5000 psig had significantly higher strengths than those tested at higher pressures. The ultimate strength of the A515 notched parent-metal specimens was reduced by 10 percent in 3000-psig

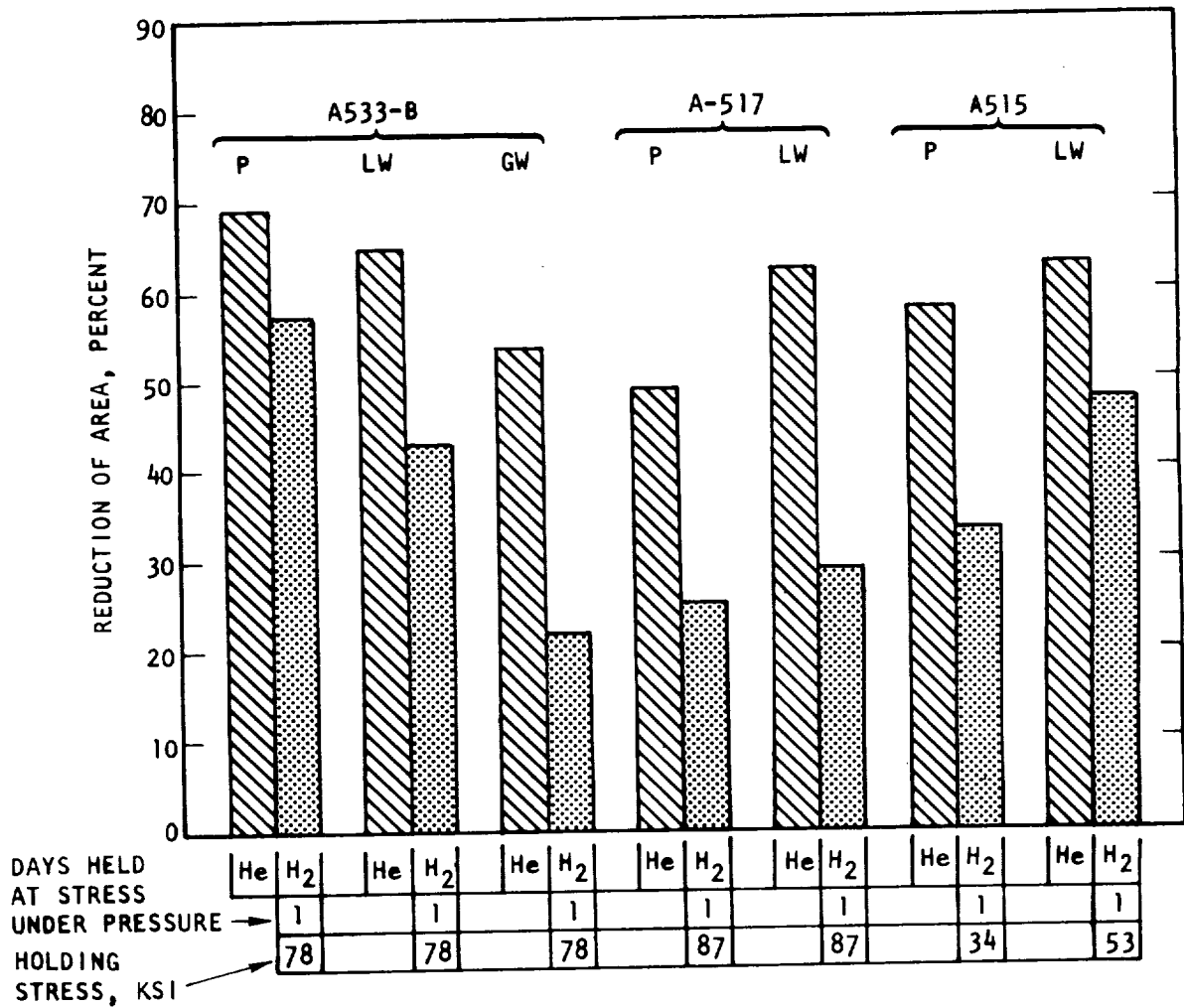


Figure 27. Reduction of area of unnotched parent metal and weld specimens in 10000-psi hydrogen and helium. (P = parent metal, LW = longitudinal weld; GW = girth weld.)

hydrogen and by 30 percent in 10 000-psig hydrogen compared to helium at corresponding pressures. There was a correspondingly higher ductility of the A-515 notched specimens tested at 3000- and 5000-psig pressures than at higher hydrogen pressures (Ref. 52).

Pittinato (Ref. 54) has determined the properties of Ti-6Al-4V ELI weldments in forged plate, and found no environmental effects when testing in 14.7- and 50.0-psia pressure hydrogen. The ultimate strength was lowered at the most by 2 percent by the hydrogen gas. The results are shown in Table 20. Pittinato also investigated the effect of prestrain and abrasion with iron on the tensile properties and found only an additional 1-percent loss of tensile strength (total loss 3 percent) from prestraining and abrasion.

#### Effect of Hydrogen on Stress-Strain Curves

An interesting effect of hydrogen on the stress-strain curves for OFHC copper and high-purity silicon iron has been observed by Vennett and Ansell (Ref. 55) and Bernstein (Ref. 56). These results are shown in Fig. 28 and 29. For OFHC copper, an approximate loss of 16 percent in the ultimate tensile strength occurs in 10 000-psig hydrogen. The hydrogen "damage" apparently begins before the onset of necking (before the ultimate is reached) and most likely is related to the onset of plastic deformation. The fracture surface also changes remarkably in 10 000-psi hydrogen, as shown in Fig. 30. The "double cup" geometry generally found in ductile materials disappears in 10 000-psig hydrogen. The fracture surface in both instances was ductile. For silicon iron, the stress-strain curves were almost identical, but the elongation and ductility changed drastically.

TABLE 20  
 TENSILE PROPERTIES OF WELDED Ti-6Al-4V ELI  
 FORGED PLATE AT AMBIENT TEMPERATURE (Ref. 54)

Environment		Dry Box Atm. ppm		Hold Time, days	Hold Stress	Unnotched Specimens		
Gas	Press. (absolute)	O <sub>2</sub>	H <sub>2</sub> O			Yield ( $\sigma_y$ ), ksi	Ultimate, ksi	Elongation, % in 1 in.
He	14.7			0	0	131.9	154.9	7.3
H <sub>2</sub>	14.7	≤1.4	≤0.8	0	0	131.3	152.9	7.0
H <sub>2</sub>	50.0	≤1.3	≤0.7	0	0	129.8	152.0	7.2
H <sub>2</sub>	14.7	≤1.2	≤0.5	1	0.75 $\sigma_y$	130.2	153.5	7.1
H <sub>2</sub>	50.0	≤1.2	≤0.6	1	0.75 $\sigma_y$	129.4	152.1	6.4

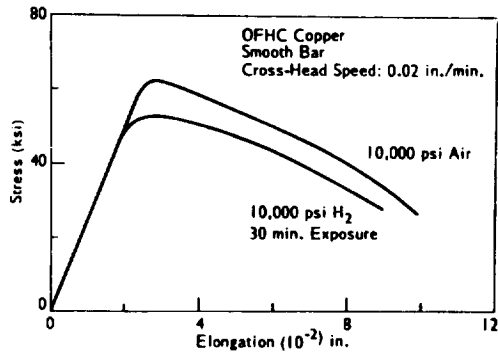


Figure 28. Engineering stress vs elongation observed OFHC copper tested in air and hydrogen.

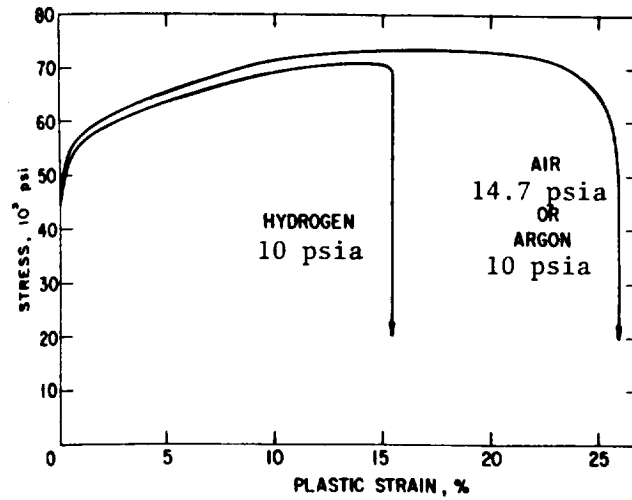


Figure 29. Effect of environment on ductility of iron-3% silicon polycrystals.

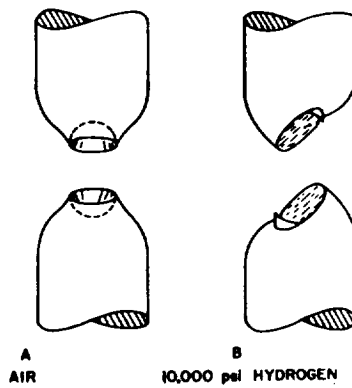


Figure 30. OFHC copper tensile specimens-- smooth-bar fractures in air and in hydrogen at 10000 psig.

Also, the fracture mode changed appreciably. For the sample tested in air, a significant amount of ductility occurred and the major part of the brittle region of the fracture surface was intergranular. In the sample tested in the 10-psig hydrogen environment, there was no localized deformation, and the fracture mode was predominately cleavage. This was particularly true near the fracture initiation site.

## CHAPTER 7. OTHER MECHANICAL PROPERTIES

With the exception of tensile properties, the majority of mechanical property data in hydrogen is on crack growth in hydrogen environments at various pressures. Extremely limited data exist on creep, stress-rupture, fatigue life, and fracture mechanics.

### Creep and Stress Rupture

Klima, Nachtigall, and Hoffman (Ref. 57) investigated the effect of hydrogen on the stress-rupture properties of an iron-base alloy (A-286), a nickel-base alloy (Inconel 700), and a cobalt-base alloy (S-816). The test specimens were hollow tubes into which hydrogen gas (99 percent purity,  $-70^{\circ}\text{C}$  dewpoint) was supplied at 500 psig from pressurized cylinders. Comparative tests were run with air at 500 psig. The results are given in Table 21. The  $1500^{\circ}\text{F}$  stress-rupture strength of S-816 was significantly less in hydrogen than in air.

Hofmann, Rauls, and Vogt (Ref. 58) have shown that failure in smooth specimens of a 0.7% carbon reinforcing steel occurred within a few minutes to several hours in hydrogen at an applied stress of 200 ksi at  $40^{\circ}\text{C}$ . Failure did not occur within a 1000-hour test period when the same material was tested in air. The 0.02% yield stress of this alloy was 208 ksi. The results are shown in Fig. 31. Tests with notched specimens of the same steel showed a sharp increase in time to failure at a critical stress at  $-4^{\circ}\text{F}$  ( $-20^{\circ}\text{C}$ ) (Fig. 32). At  $68^{\circ}\text{F}$  ( $+20^{\circ}\text{C}$ ), no effect was observed.

### Fatigue Properties

The effect of hydrogen at 1000 and 10 000 psig on the low-cycle fatigue (tension-tension) strength of unnotched and precracked cylindrical specimens was determined for AISI 310 stainless steel, ASTM A533-B, and ASTM A-517 steels (Ref. 7)

TABLE 21

STRESS-RUPTURE LIVES OF THREE HIGH-TEMPERATURE  
ALLOYS IN 500-PSIG GAS (Ref. 57)

Alloy	Internal Gas	Stress, psi	Temperature, °F	Average Life, hr	Standard Deviation, hr	Confidence Level, percentile
A-286	Air	57 000	1200	264	±32	83
	H <sub>2</sub>	57 000	1200	215	±90	
Inconel 700	Air	40,000	1500	209	±15	20
	H <sub>2</sub>	40 000	1500	206	±40	
S-816	Air	19 000	1500	215	±32	98
	H <sub>2</sub>	19 000	1500	151	±31	

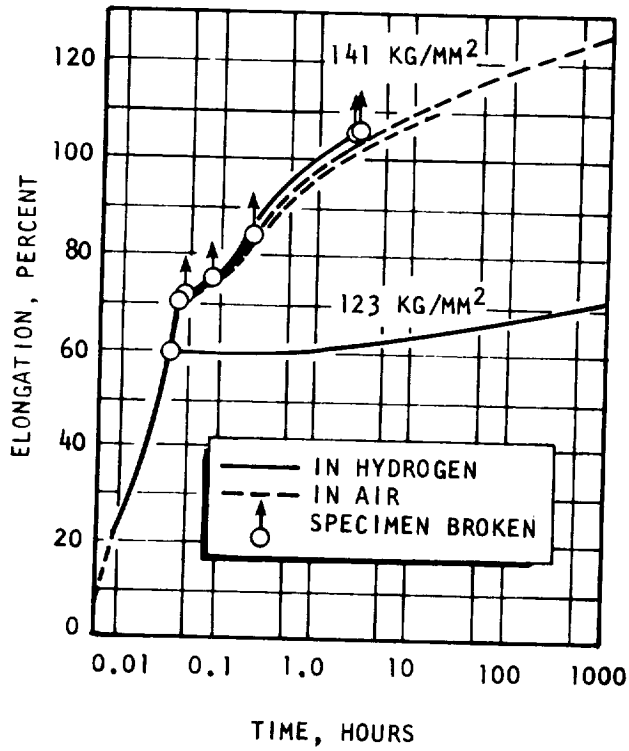


Figure 31. Creep of reinforcing steel at 104° F (40° C) in air and in 1470-psia hydrogen.

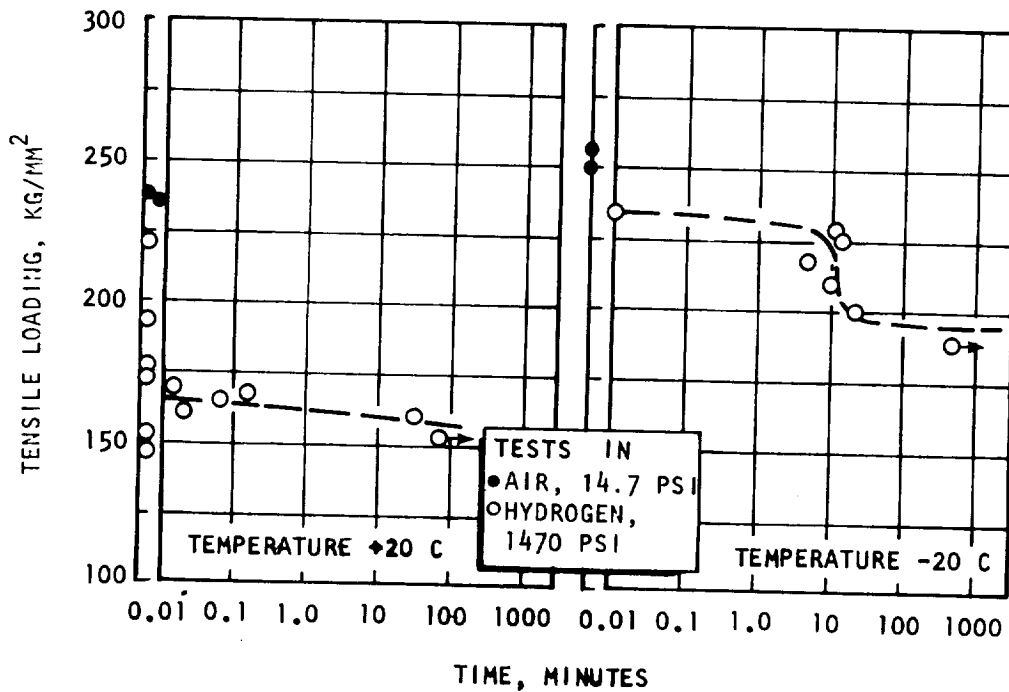


Figure 32. Creep of reinforcing steel with round notch in 1470-psia hydrogen at 68° F (20° C), and -4° F (-20° C). Tensile properties in air are shown for comparison.

It should be noted that the results from precracked specimens do not represent conventional fatigue life, but represent comparative rates of cyclic crack growth in the test environment. Low-cycle fatigue strengths of unnotched specimens of all three materials and of precracked, AISI 310 stainless-steel specimens were about the same as their tensile strengths in the same environment. The low-cycle fatigue properties of the precracked ASTM A533-B (Fig. 33) and ASTM A-517 (Fig. 34) specimens were quite similar to each other in all environments. For both materials, the 1000-cycle fatigue strength in 10 000-psig hydrogen was about 1/3 that in 10 000-psig helium; and for the 10 000-psig hydrogen tests there appeared to be a low-cycle fatigue limit that first occurred between 1000 and 2000 cycles. The fatigue strengths of precracked ASTM A533-B and ASTM A-517 specimens in 1000-psig hydrogen were about midway between the strengths in 10 000-psig hydrogen and that in 10 000-psig helium.

The unnotched specimens were load cycled between zero load and a load in the vicinity of their yield strengths. The results showed no environmental influence on the fatigue life of these specimens.

Results of low-cycle fatigue tests on precracked specimens for Inconel 718 at room temperature are plotted in Fig. 35 (Ref. 49). Essentially no difference exists between the fatigue strength in 100-psig hydrogen at room temperature and that in air at 14.7-psia pressure. The fatigue strength for 100 cycles to failure was 22 percent lower in 2000-psig hydrogen than in 2000-psig helium at room temperature. Results of fatigue tests at  $-260^{\circ}\text{F}$  on precracked specimens of Inconel 718, with a different heat treatment, are plotted in Fig. 36 (Ref. 59). At  $-260^{\circ}\text{F}$ , the fatigue strength is essentially the same in 800-psig hydrogen as in 800-psig helium.

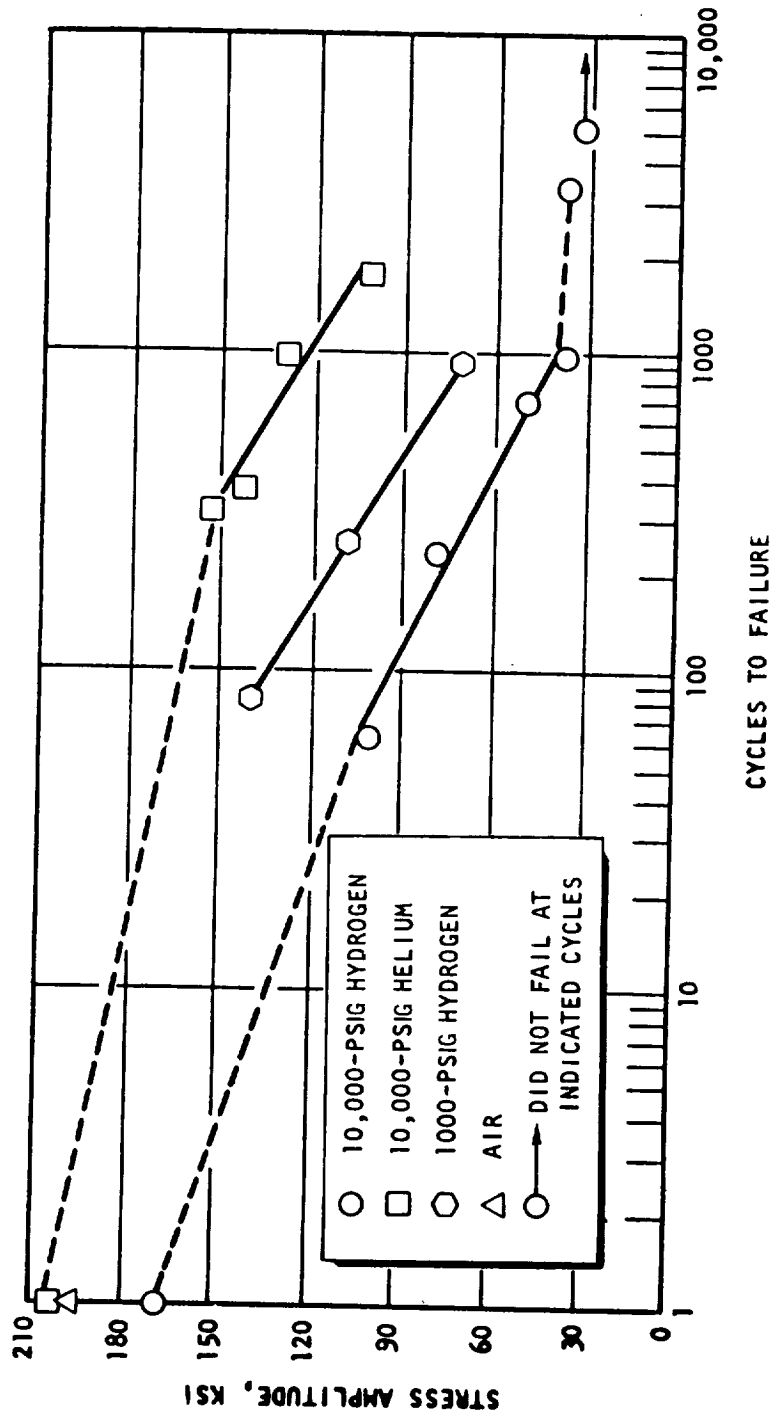


Figure 33. Effect of high-pressure hydrogen environment on low-cycle fatigue strength of precracked ASTM A533-B steel specimens. Stress was calculated using diameter after specimen was precracked (ref. 7).

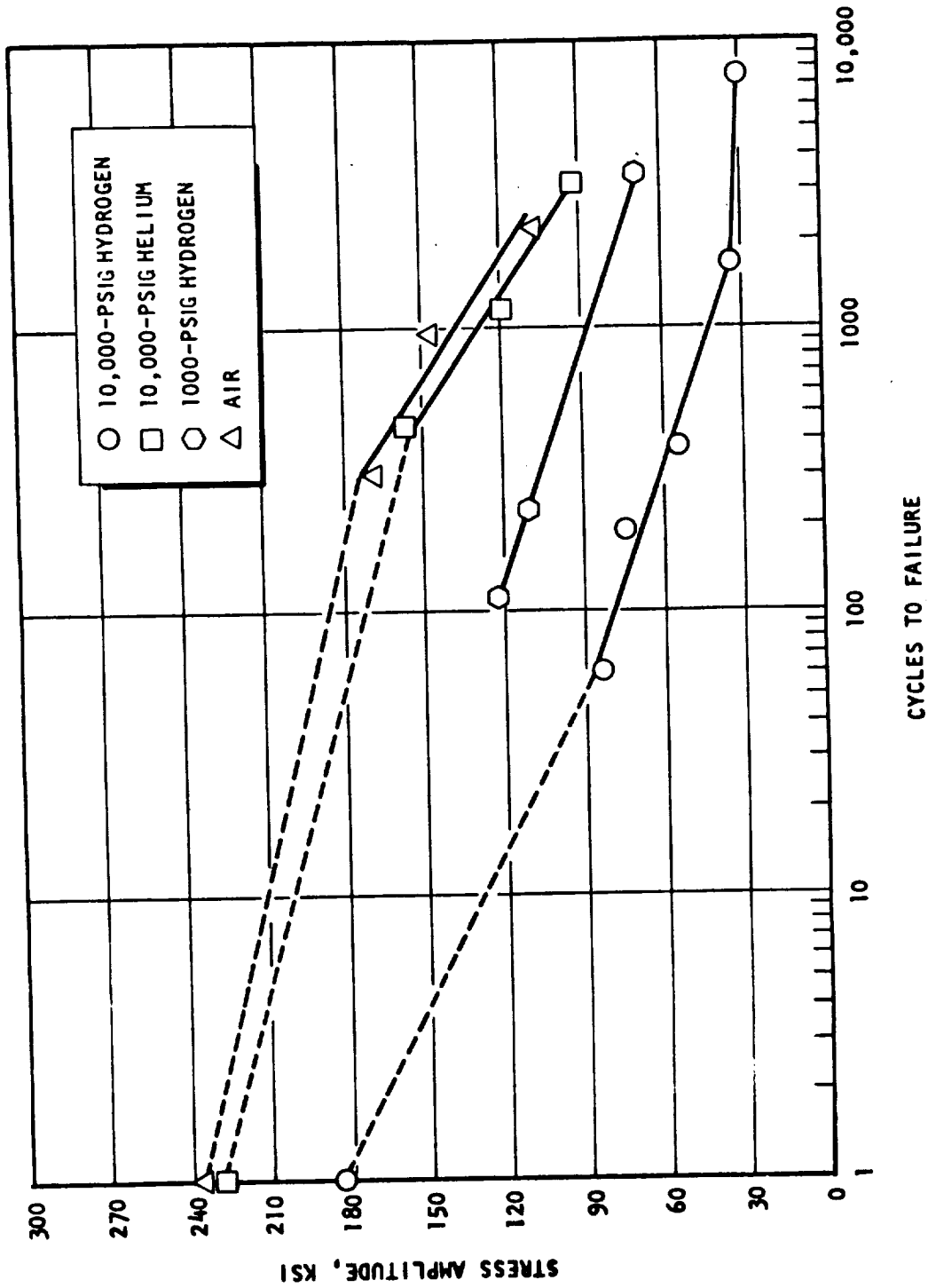


Figure 34. Effect of high-pressure hydrogen environment on low-cycle fatigue strength of precracked ASTM A-517 specimens. Stress was calculated using diameter of notched specimen prior to precracking (ref. 7).

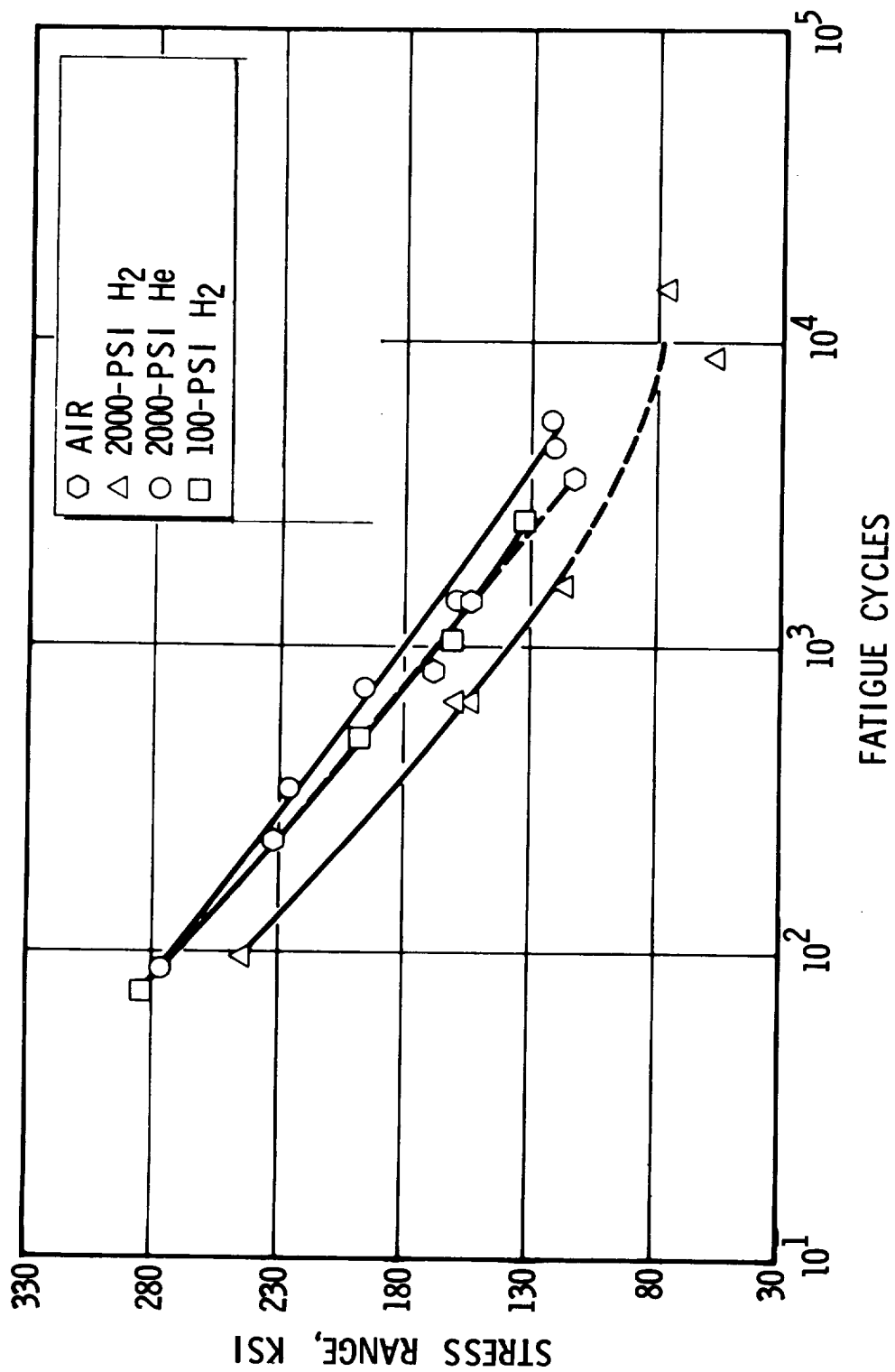


Figure 35. Effect of various environments on the low-cycle fatigue strength of precracked specimens of Inconel 718 (heat B, heat treatment 3) at room temperature. (See tables IX and X for heat and heat treatment.)

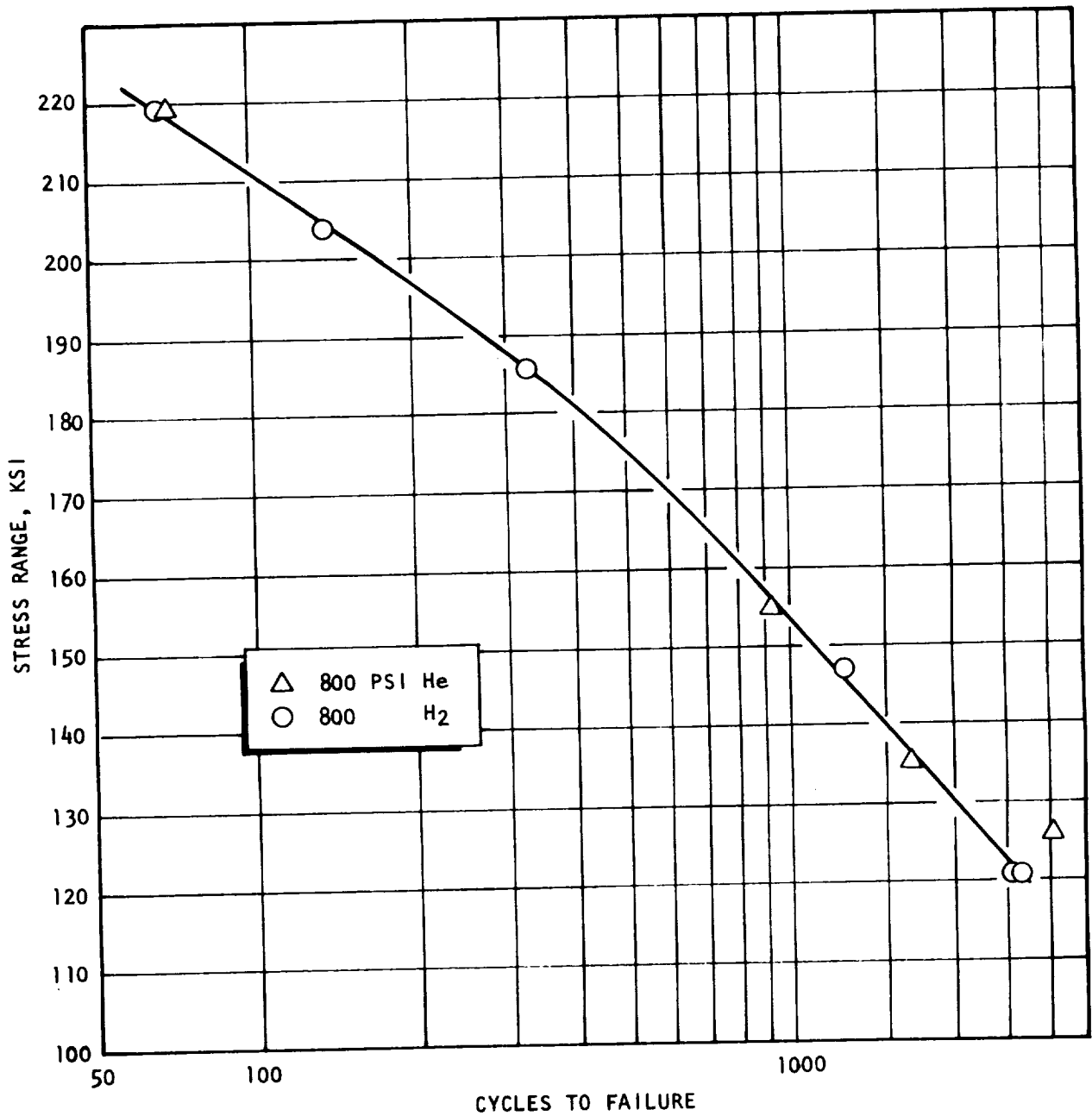


Figure 36. Effect of 800-psi hydrogen and helium on the low-cycle fatigue strength of precracked specimens of Inconel-718 (heat B, heat treatment 1) at  $-260^{\circ}$  F. (See Tables IX and X for heat and heat treatment.)

Pittinato (Ref. 60) has also investigated the influence of gaseous hydrogen on the fatigue life of Ti-6Al-4V using precracked specimens. Tests were conducted in high-purity hydrogen, liquid hydrogen, liquid nitrogen, and helium for comparative purposes. The results are shown in Fig. 37. The number of cycles to failure was less in hydrogen than in nitrogen or helium at temperatures between  $-100^{\circ}\text{F}$  and room temperature.

Van Wanderham and Harris (Ref. 61) have studied conventional low-cycle fatigue in hydrogen. Results were obtained at 5000 psig using both hollow specimens that were internally pressurized with hydrogen or helium and solid specimens in a hydrogen-filled pressure vessel. Axial strain was measured and controlled by means of a proximity probe extensometer.\* The chemical composition of the materials tested at Pratt and Whitney are given in Table 22. The type of specimens used by these authors is shown in Fig. 38.

Results for 5000-psig hydrogen and helium are given in Fig. 39 for two heats of Inconel 718. Considerable degradation of fatigue properties is evidenced from these data for heat code LDUL. For example, at a 1-percent total strain range with hollow specimens from heat code LDUL, a life of approximately 3000 cycles would be predicted for helium while in hydrogen the life would be only 150 cycles (Fig. 39). Data are not yet available for heat code BVTO in helium.

Figures 40 and 41 show the results of low-cycle fatigue tests for Inconel 625 conducted at  $78^{\circ}\text{F}$  and  $1250^{\circ}\text{F}$ , respectively. At room temperature and a 1-percent total strain range, a fatigue life of 2000 cycles in helium and 500 cycles in hydrogen is indicated. At  $1250^{\circ}\text{F}$  and a 1-percent total strain range, a fatigue life of 1000 cycles in helium and of approximately 250 cycles in hydrogen would be predicted. At a 1-percent plastic strain range, a life of

---

\*Patent applied for by M. C. VanWanderham, J. A. Harris, Jr., and R. Bogart.

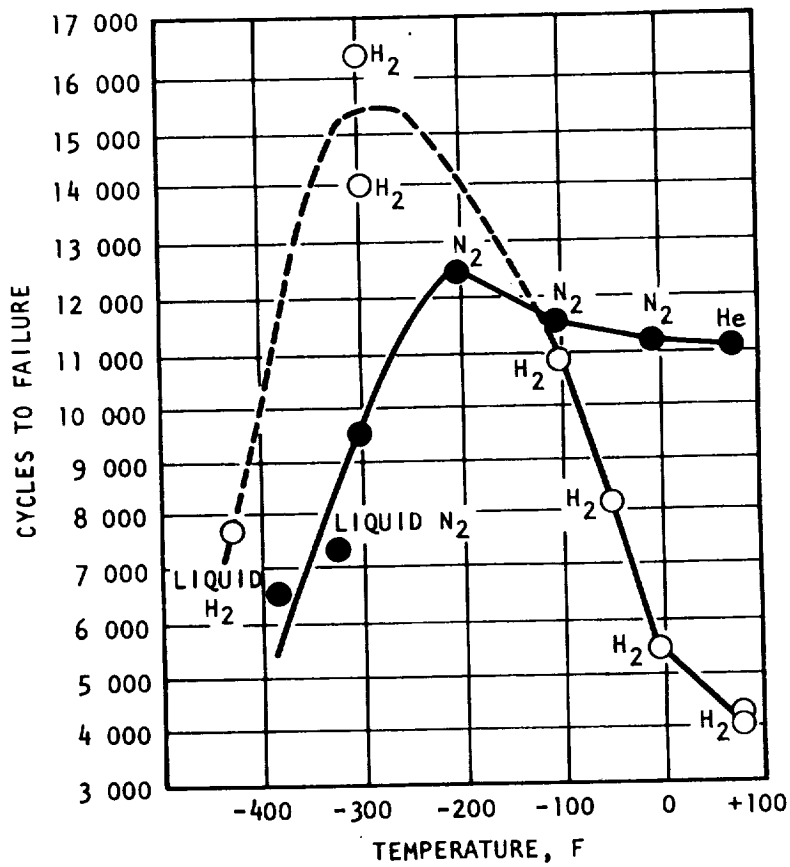


Figure 37. Fatigue curves of precracked Ti-6Al-4V tested under tension-tension loading using a lower stress of 12.5 ksi and an upper stress of 62.5 ksi.

TABLE 22

CHEMICAL COMPOSITIONS OF THE FIVE MATERIALS SUBJECTED TO  
LOW-CYCLE FATIGUE TESTS IN HIGH-PRESSURE HYDROGEN (Ref. 61)

Material	Chemical Composition, percent															
	C	Mo	Si	Cr	Ni	Co	Cb and Ta	Ti	Al	B	Cu	Fe	Zr	Mn	La	W
Inconel 718	0.07	3.1	0.35*	19.0	52.5	1.0*	5.3	0.90	0.60	0.006*	0.10*	Bal	--	0.35*	--	--
Inconel 625	0.10*	9.0	0.50*	21.5	Bal	1.0*	3.65	0.40*	0.40*	--	--	5.0*	--	0.50*	--	--
Waspaloy	0.07	4.25	0.15*	19.5	Bal	13.5	--	3.0	1.4	0.007	0.10*	2.0*	0.05	0.50*	--	--
Haynes 188	0.10	--	0.50*	22.0	22.0	Bal	--	--	--	0.015*	--	2.0*	--	0.75	0.08	14.5
CG-27	0.05	5.0	--	13.0	38.1	--	0.70	2.5	1.63	0.01	--	Bal	--	--	--	--

\*Maximum

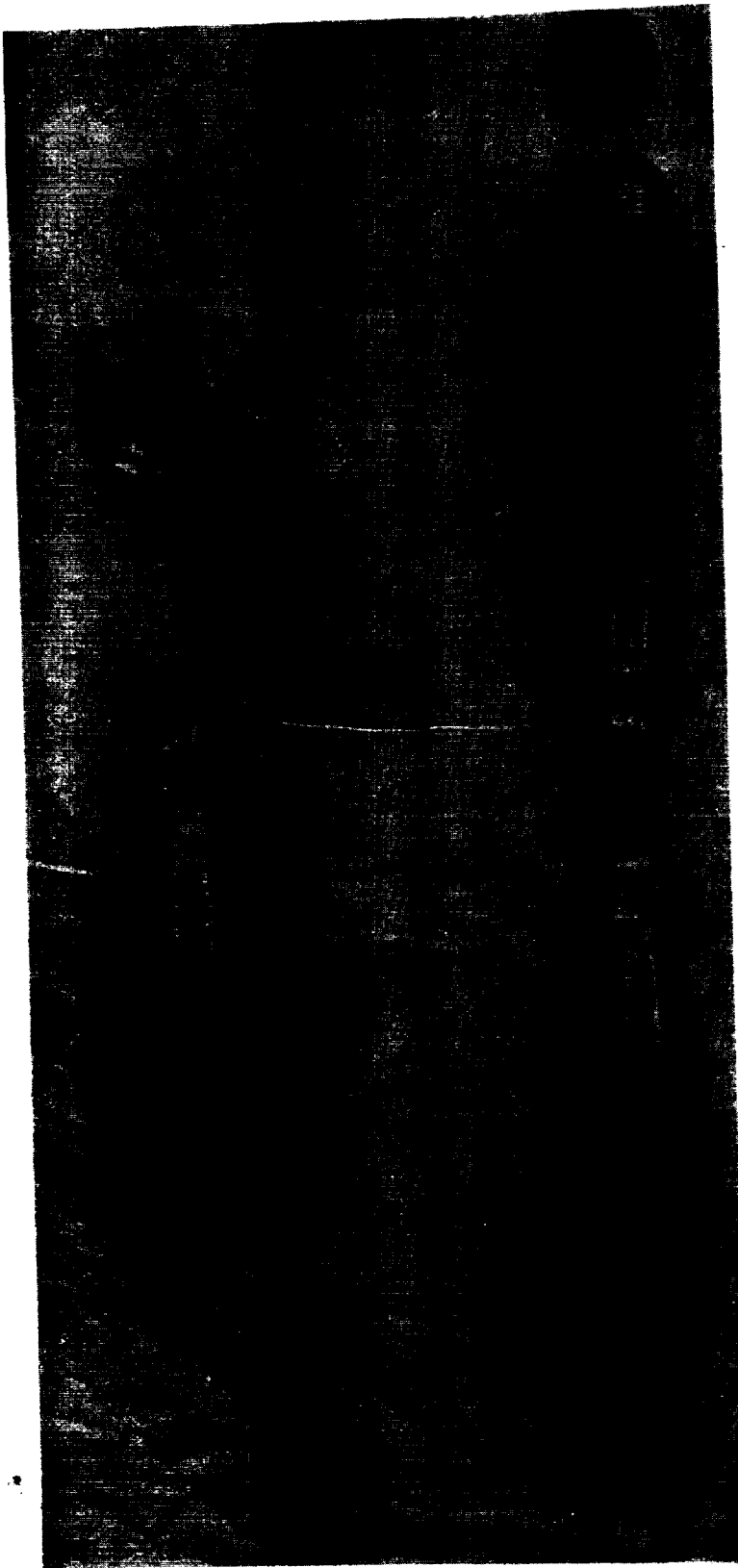


Figure 38. Test specimen used for low-cycle fatigue tests conducted in 5000-psig hydrogen.

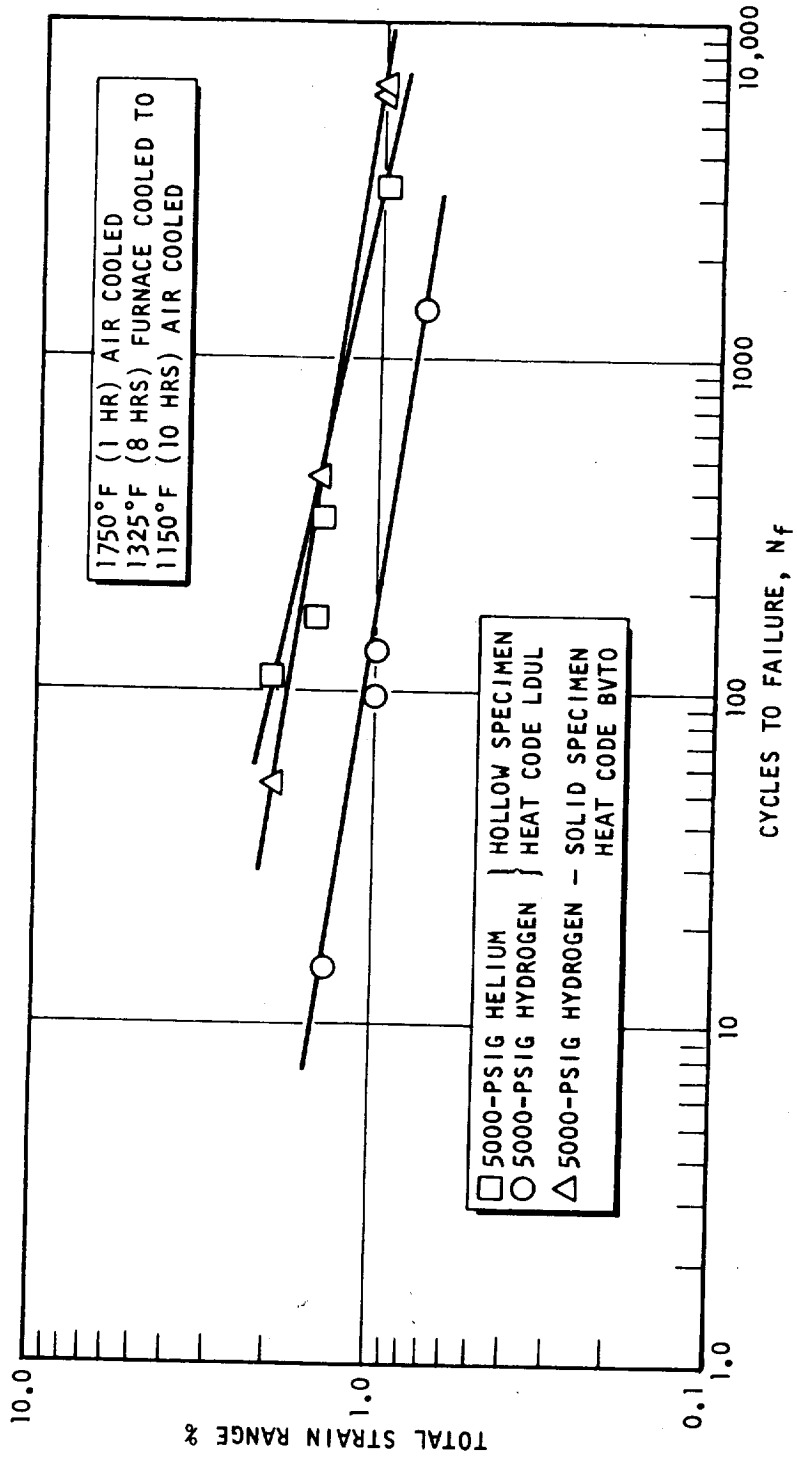


Figure 39. Effect of cyclic total strain on fatigue life at 76° F of Inconel 718.

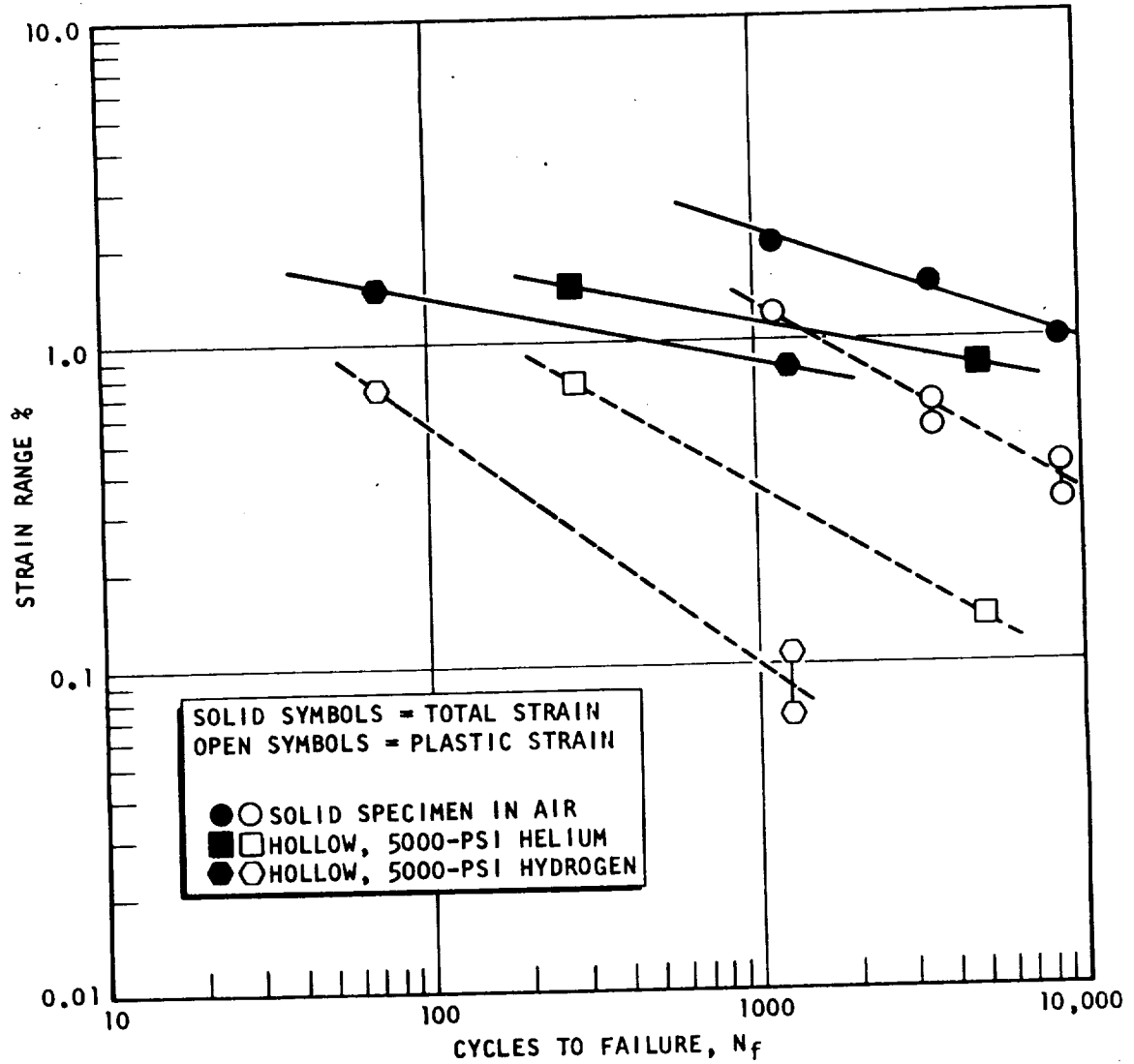


Figure 40. Effect of cyclic strain on fatigue life at 78° F of Annealed Inconel 625 (PWA 1040 Heat Code BUDQ).

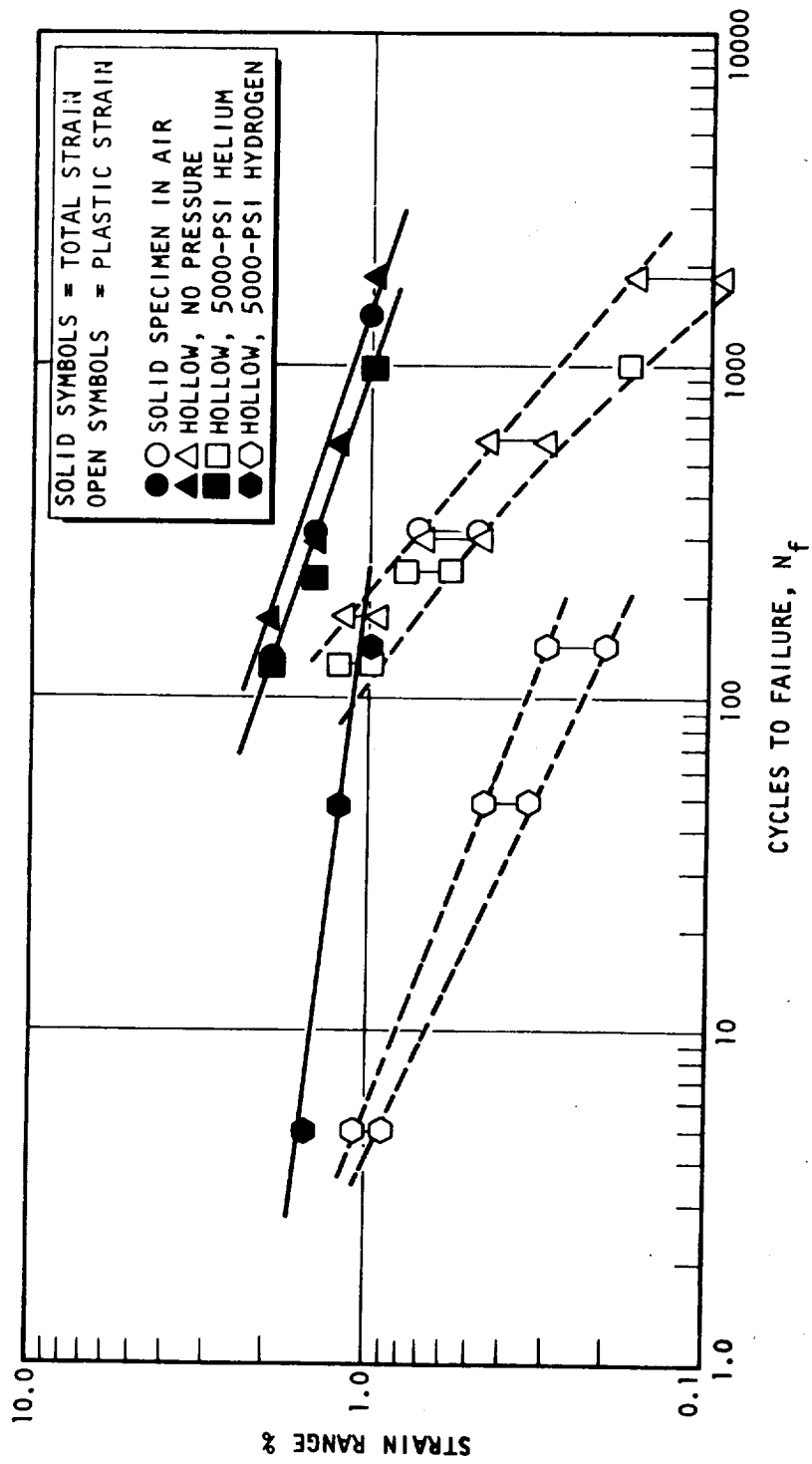


Figure 41 Effect of cyclic strain on fatigue life at 1250° F of annealed Inconel 625 (PWA 1040 Heat Code BLDQ).

less than 50 cycles in hydrogen would be predicted at room temperature and of less than 10 cycles at 1250 F. The two data points at a given  $N_f$  value for plastic strain range in Fig. 40 through 46 do not indicate data scatter, but represent the observed change in the plastic strain range for that specimen.

Figures 42 and 43 show the low-cycle fatigue behavior of PWA 1027 Waspaloy at room temperature and 540°F, respectively. At room temperature and at a 1-percent total strain range, a life of 7000 cycles would be predicted for helium and a life of 1000 cycles for hydrogen. At 540°F and at the same total strain, a life of approximately 2250 cycles in helium and of approximately 200 cycles in hydrogen would be predicted.

Degradation of fatigue properties by 5000-psig hydrogen also was encountered in the cobalt base alloy Haynes 188 (Fig. 44). The degradation observed was not as severe as in the nickel-base alloys. For the Haynes 188 alloy at 1-percent total strain range, a life of approximately 6000 cycles would be predicted for specimens in helium while in hydrogen a life of approximately 2500 cycles would be predicted. At a 1-percent plastic strain, a fatigue life of between 500 and 600 cycles would be predicted in hydrogen.

Degradation of fatigue properties was not as severe in the Crucible Steel Company Alloy CG-27 at room temperature as in the nickel-base alloys. At a 1-percent total strain range, a fatigue life in helium and hydrogen of 4000 cycles and 1100 cycles, respectively, would be predicted (Fig. 45). At 540°F and the same total strain, a fatigue life of 5000 cycles would be predicted in helium while, in hydrogen, a fatigue life of 1000 cycles would be expected. This would indicate that degradation is more severe at 540°F than at room temperature (Fig. 46).

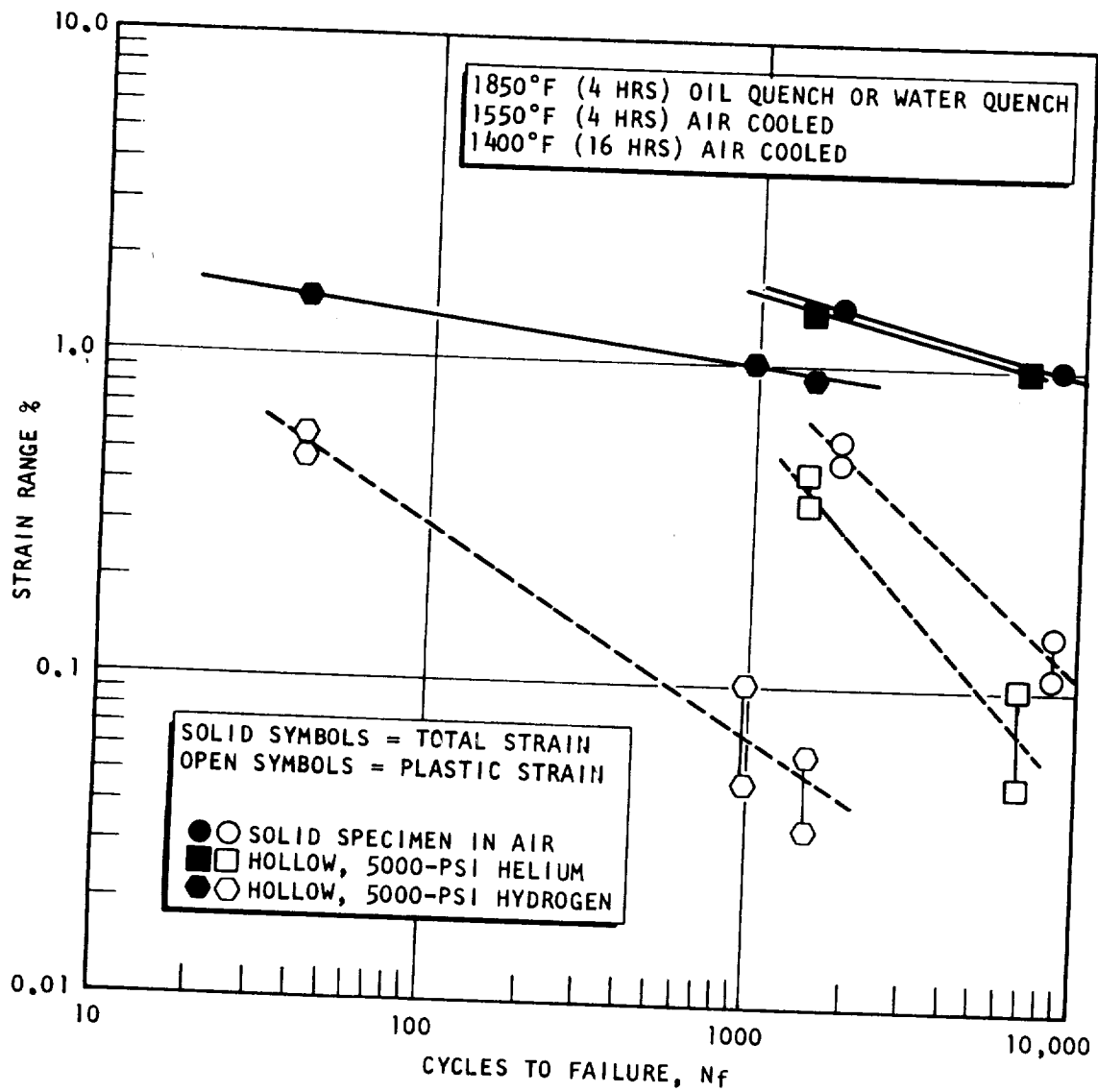


Figure 42. Effect of cyclic strain on fatigue life at 78° F of Waspaloy (PWA 1027 Heat Code LCCS).

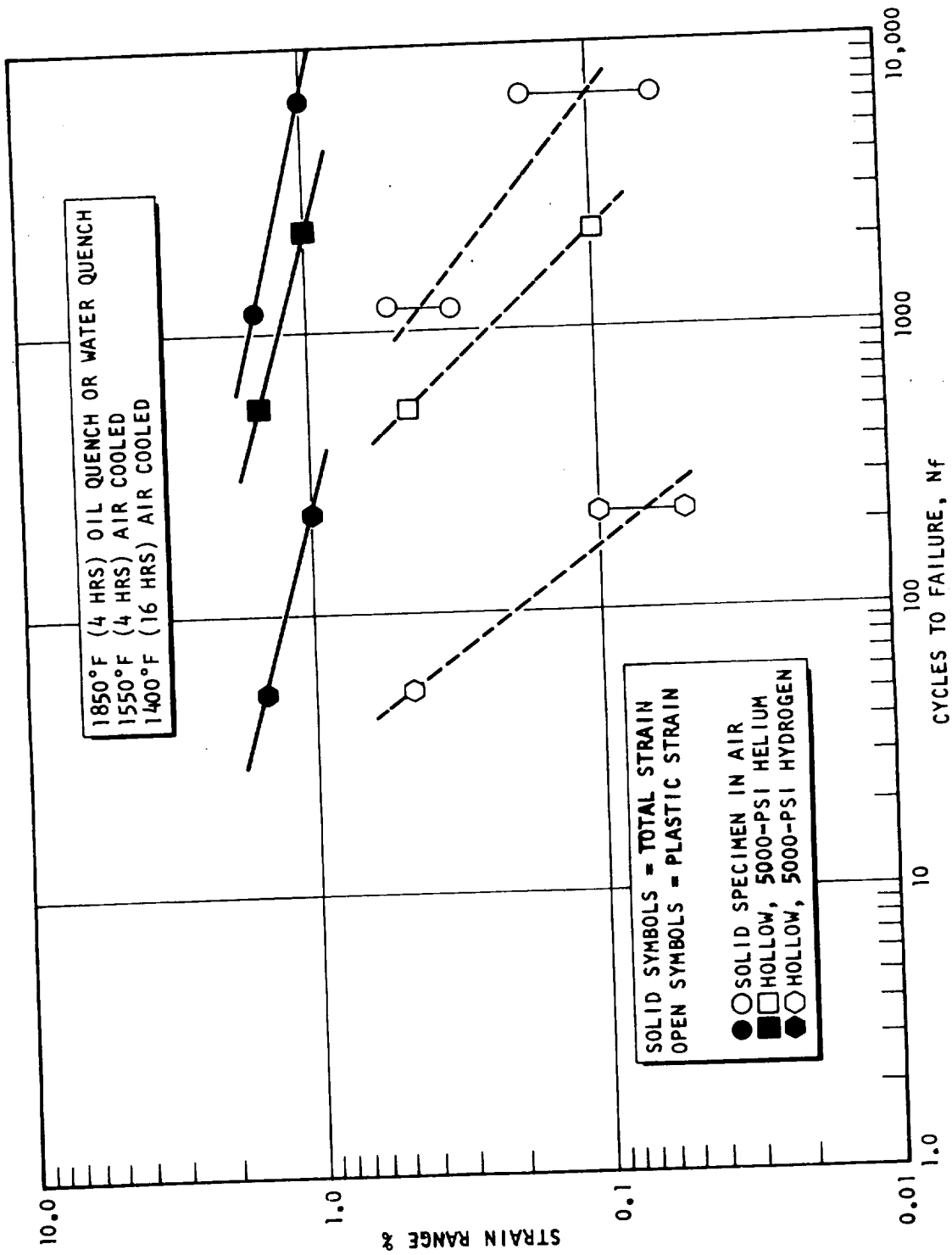


Figure 43. Effect of cyclic strain on fatigue life at 540° F of Waspalloy (FWA 1027 Heat Code LCCS).

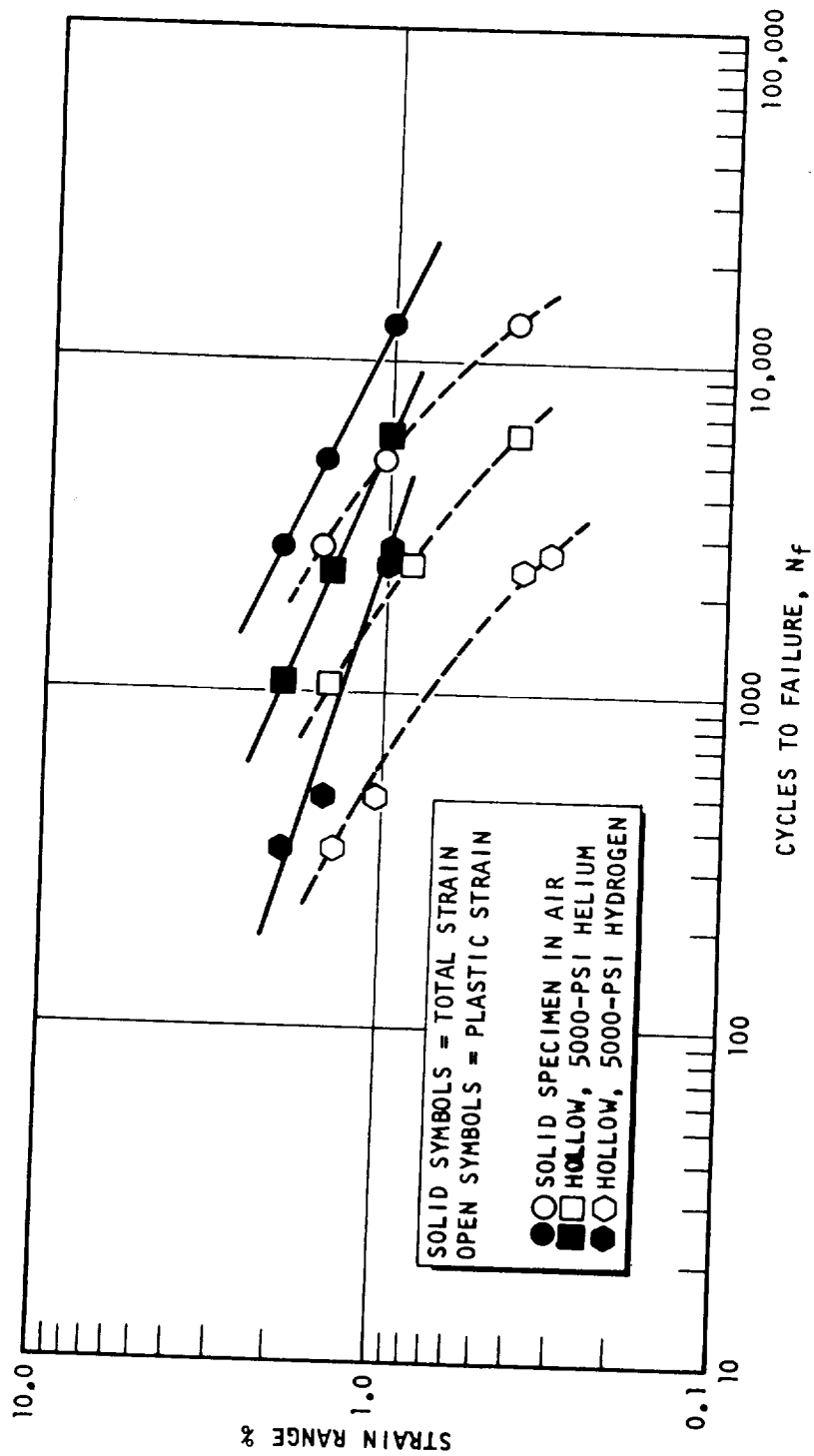


Figure 44. Effect of cyclic strain on fatigue life at 78° F of annealed Haynes 188 alloy.

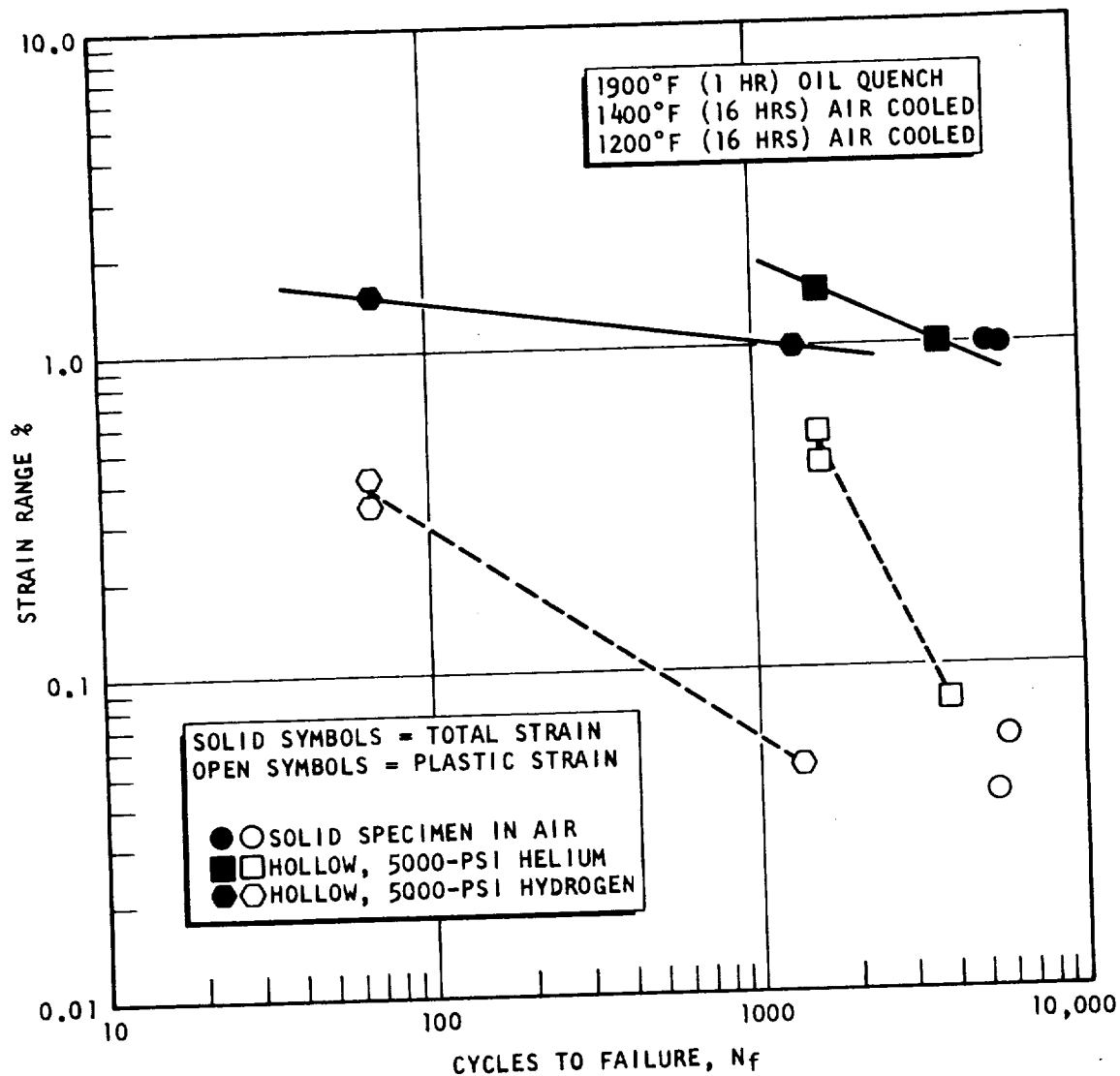


Figure 45. Effect of cyclic strain on fatigue life at 78° F of CG-27 alloy.

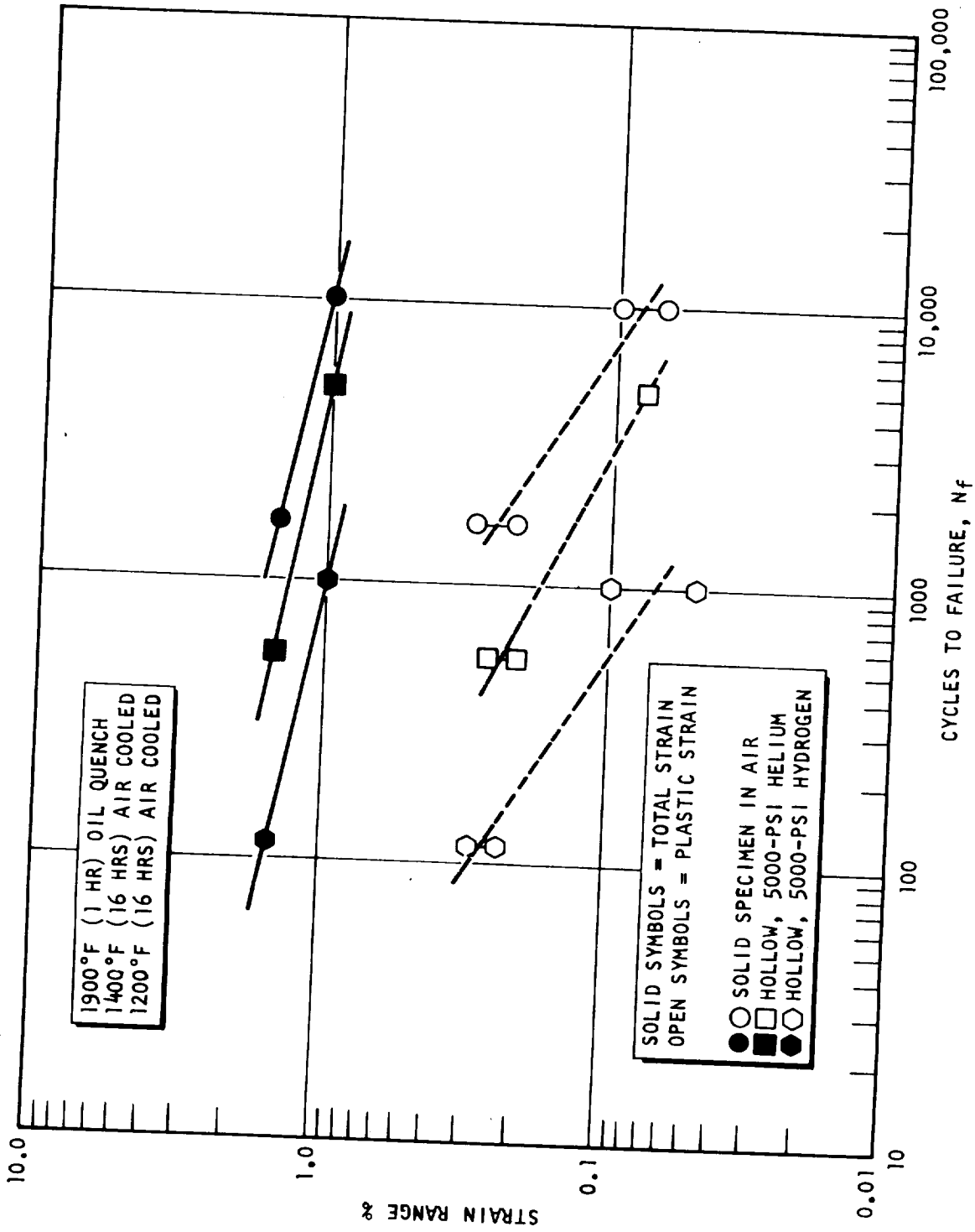


Figure 46. Effect of cyclic strain on fatigue life at 540° F of CG-27 alloy.

Figure 47 summarizes data for tests at a 1% total strain range. It can be seen that all the alloys except A-286 had more than a 60% reduction in fatigue life in 5000-psig hydrogen with Inconel 718 having the most severe reduction of fatigue life. The ratio of the cycles to failure in helium to the cycles to failure in hydrogen at 5000 psig also is shown in Fig. 47. The data shown for A-286 were obtained from tests run at 1% total strain range only.

#### Fracture Mechanics

Threshold fracture toughness ( $K_{th}$ ) values have been determined in high-pressure hydrogen for Inconel 718 and 2219-T6E46 aluminum by Lorenz (Ref. 62). This program was undertaken to determine which of these materials would be the best for use in hydrogen pressure vessels on the Mariner '69 space vehicle.

Lorenz (Ref. 62) found for the Inconel 718 alloy that  $K_{Ic}$  (in air) was 150 ksi  $\sqrt{\text{in.}}$  based on the results for one specimen that fractured below the yield strength of the material. For Inconel 718 weldments, the  $K_{Ic}$  value was 95.0 ksi  $\sqrt{\text{in.}}$ .

Sustained flaw growth data derived from surface-flawed specimens tested in 5200-psig hydrogen indicated a  $K_{th}$  of 22 ksi  $\sqrt{\text{in.}}$  for Inconel 718 (Fig. 48) and 21.0 ksi  $\sqrt{\text{in.}}$  for Inconel 718 weldments (Fig. 49).

The  $K_{Ic}$  value (in air) for the 2219-T6E46 aluminum base metal was 35.7 ksi  $\sqrt{\text{in.}}$ , and 32.0 ksi  $\sqrt{\text{in.}}$  for the weldments. Sustained flaw growth data are shown in Fig. 50 and 51 and the data indicate  $K_{th}$  values of 28.0 ksi  $\sqrt{\text{in.}}$  and 26.0 ksi  $\sqrt{\text{in.}}$ , for the base metal and the weldments, respectively. Thus, it

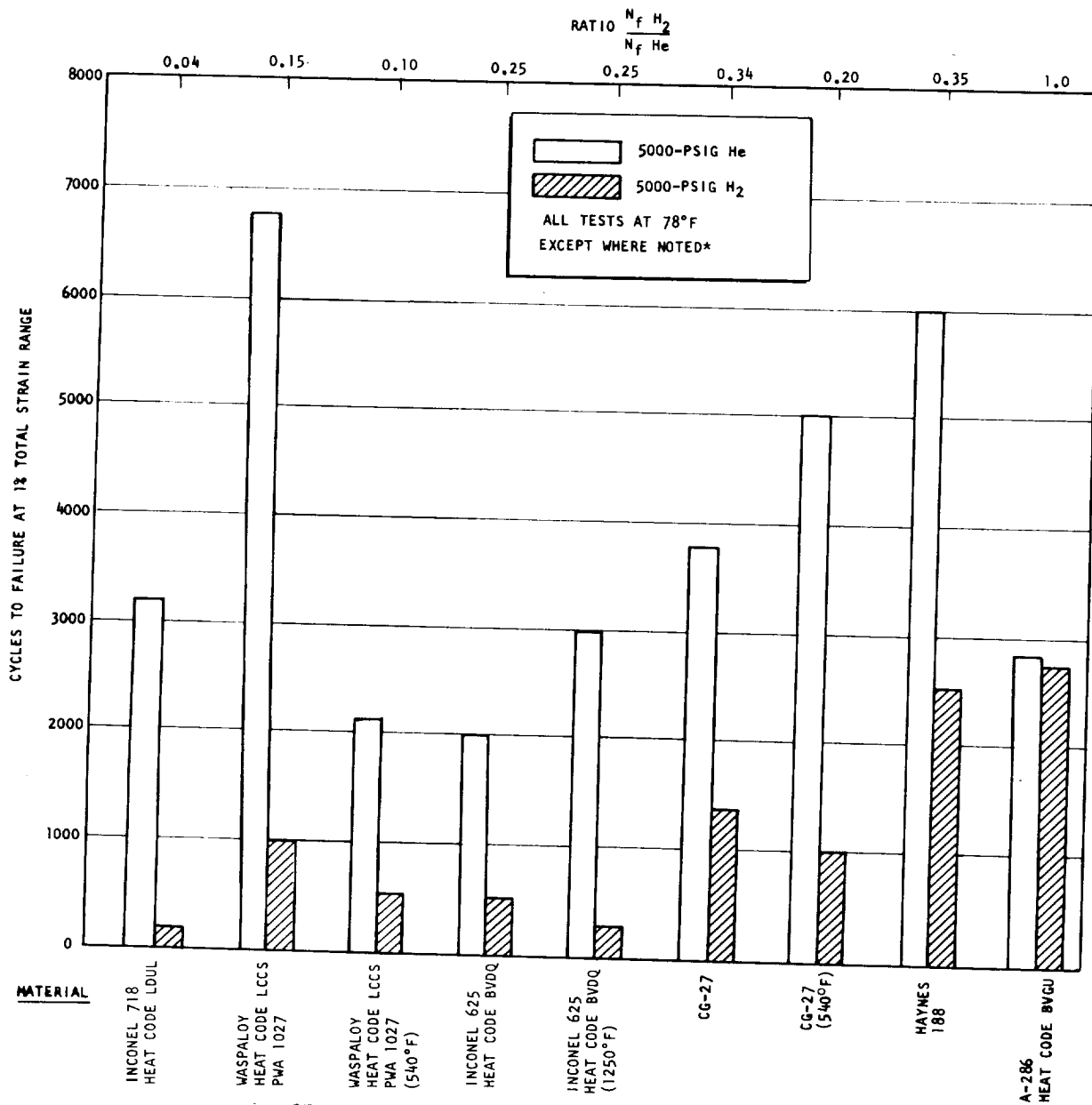


Figure 47. Relative low-cycle fatigue life at 1-percent total strain.

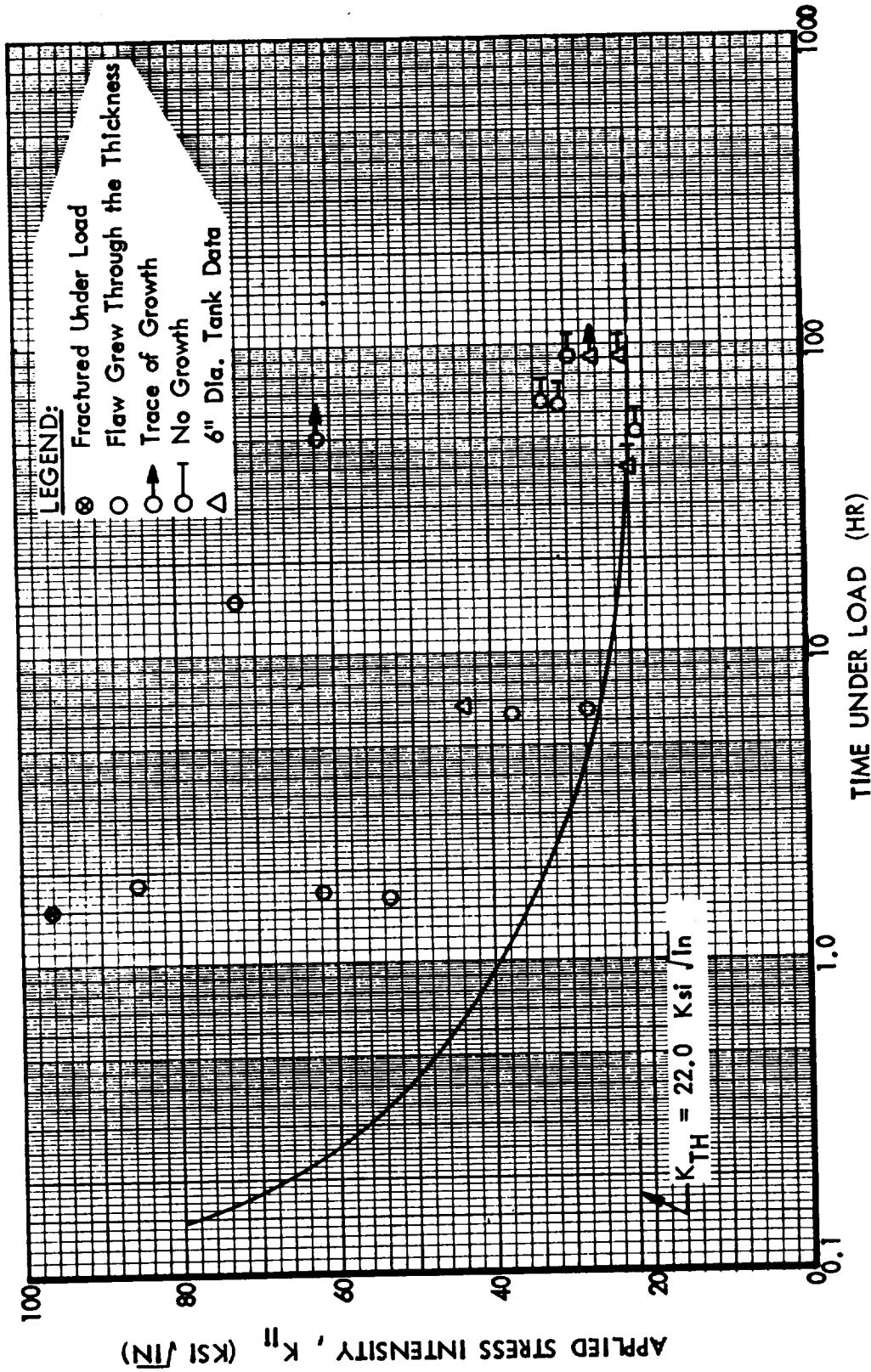


Figure 48. Sustained flaw-growth data for Inconel 718 base metal.

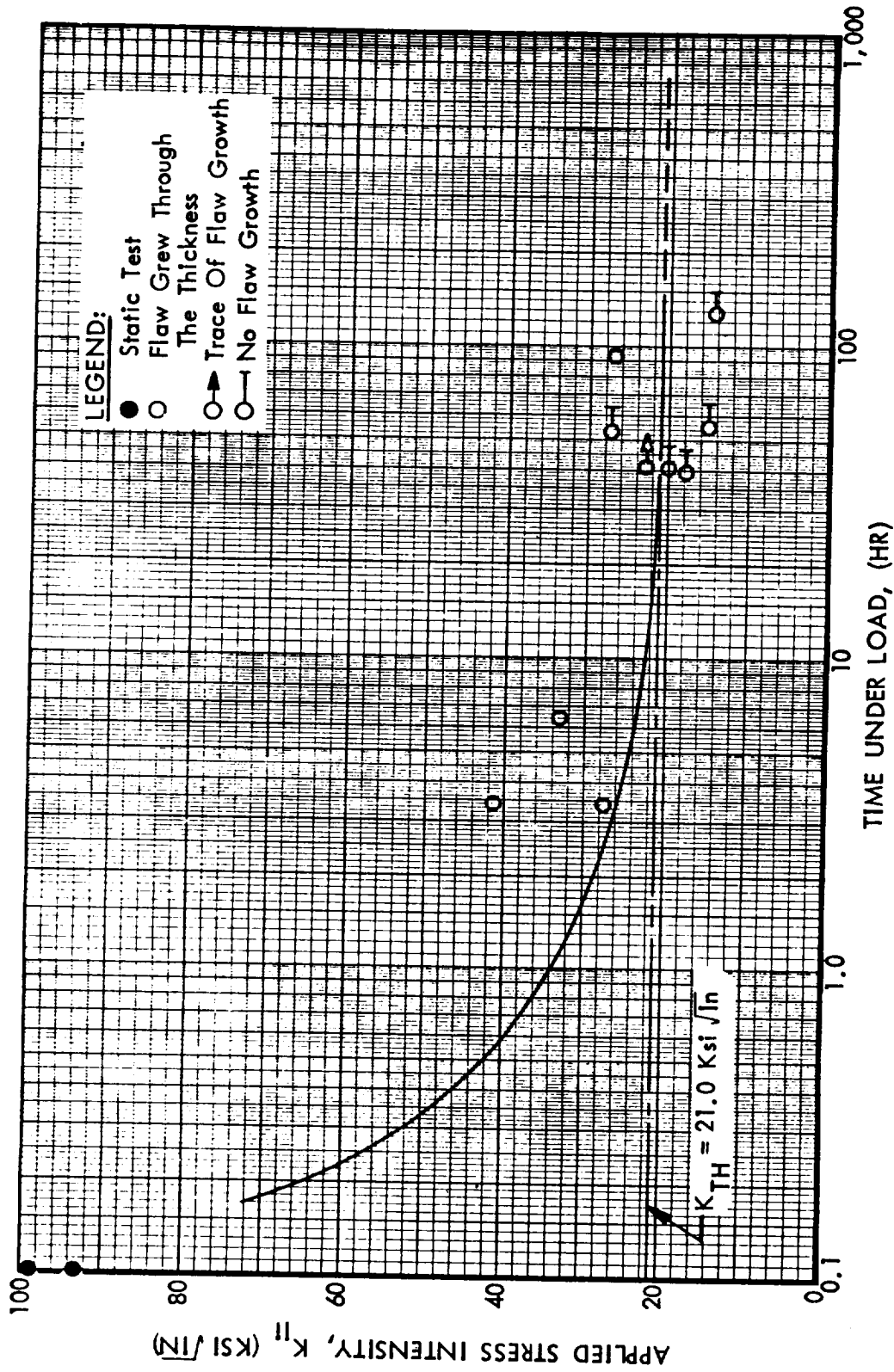


Figure 49. Sustained flaw-growth data for Inconel 718 weldment.

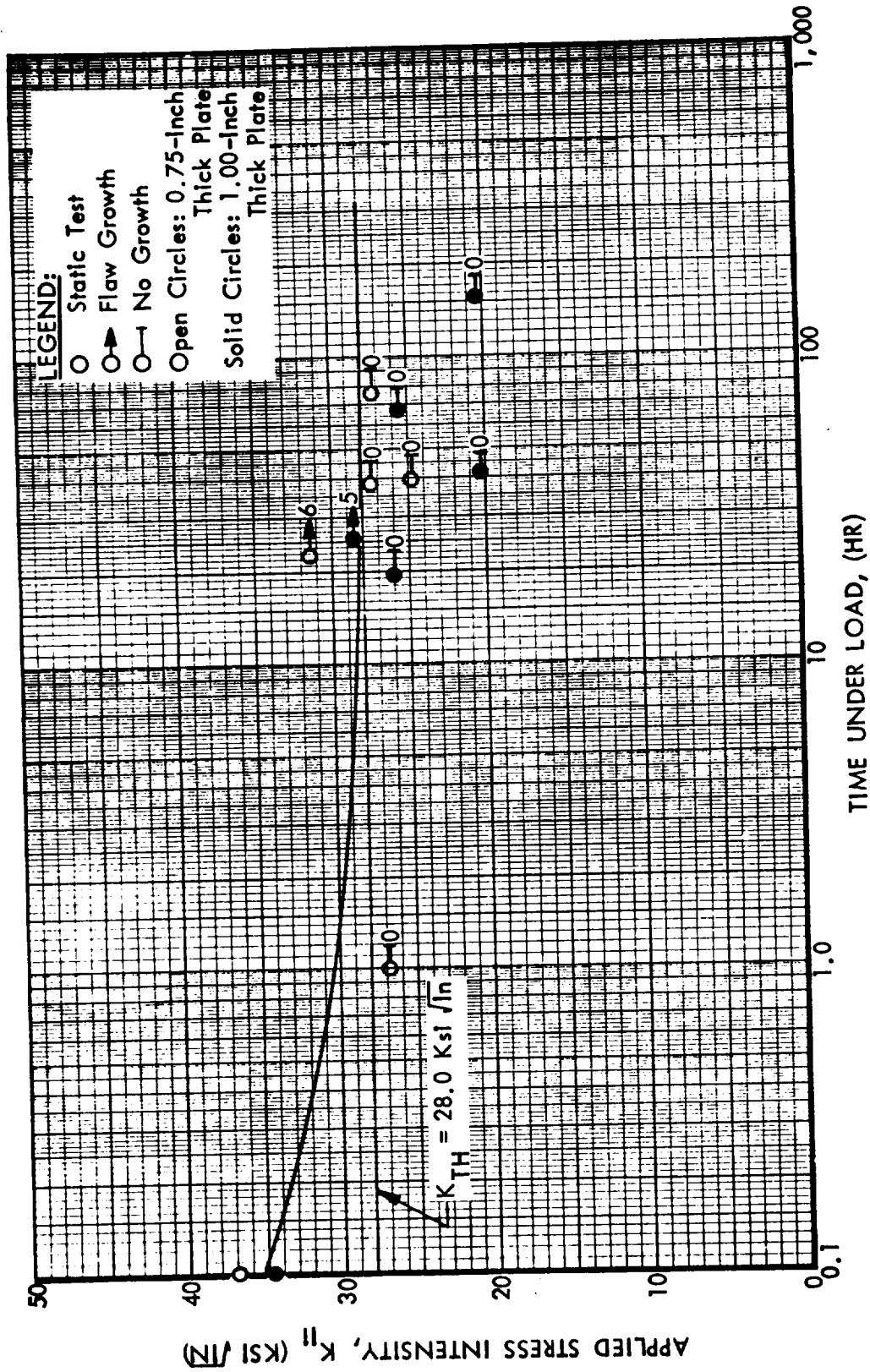


Figure 50. Sustained flaw-growth data for 2219-T6E46 aluminum base metal.



can be seen that the aluminum retains its load-carrying capability in 5200-psig hydrogen at stress-intensity levels of more than 80% of the  $K_{IC}$  fracture toughness values, while the Inconel 718 is drastically affected by hydrogen.

#### Crack Growth

Hancock and Johnson (Ref. 63); Spitzig et al. (Ref. 64); Walter and Chandler (Ref. 47); Marcus and Stocker (Ref. 30); Williams and Nelson (Ref. 8); and Nelson et al. (Ref. 65) have investigated the effect of gaseous hydrogen on crack growth rate in steels, nickel and nickel-base alloys, and a copper-base alloy. Accelerated crack growth was found in hydrogen in all cases except in the copper-base alloy.

Hancock and Johnson (Ref. 63) investigated the effect of hydrogen at atmospheric pressure on crack growth in H-11 tool steel. They found that subcritical crack growth initiated in hydrogen at lower stress field intensities and propagated at faster rates than in wet argon, as shown in Table 23 and Fig. 52. Hancock and Johnson further showed that additions of small amounts of oxygen (0.6%) to the gaseous hydrogen environment completely stopped crack growth. This effect is shown in Fig. 53. At the lower stress intensities, there appears to be an incubation period before crack growth begins. This emphasizes the importance of having clean initial cracks at the beginning of a test in hydrogen.

Spitzig et al. (Ref. 64) investigated the effect of dry and humid hydrogen environments on crack growth in 18 Ni(250) maraging steel. The results are shown in Fig. 54 in terms of  $(1/c_0 - 1/c) \text{ in.}^{-1}$  versus the number of cycles  $N$ ,

TABLE 23

CRACK INITIATION ( $K_{I1}$ ) AND UNSTABLE FRACTURE ( $K_{Ic}$ )  
STRESS FIELD INTENSITIES

	Hydrogen	Wet Argon	Dry Argon
$K_{I1}$ (ksi in.)	11	18	40
$K_{Ic}$ (ksi in.)	(1)	40	40

(1)

Because of the long subcritical crack,  $K_{Ic}$  could not be measured.

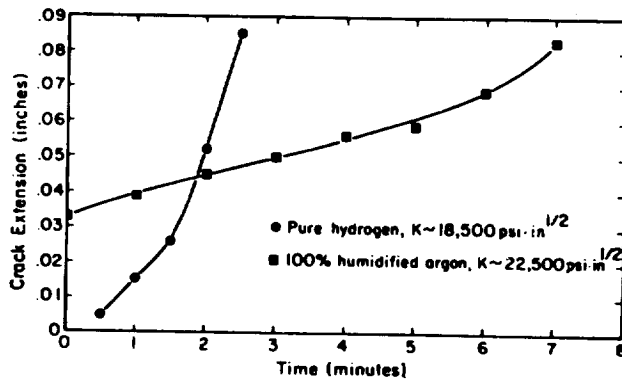


Figure 52. Subcritical crack growth of H-11 steel in molecular hydrogen and humidified argon.

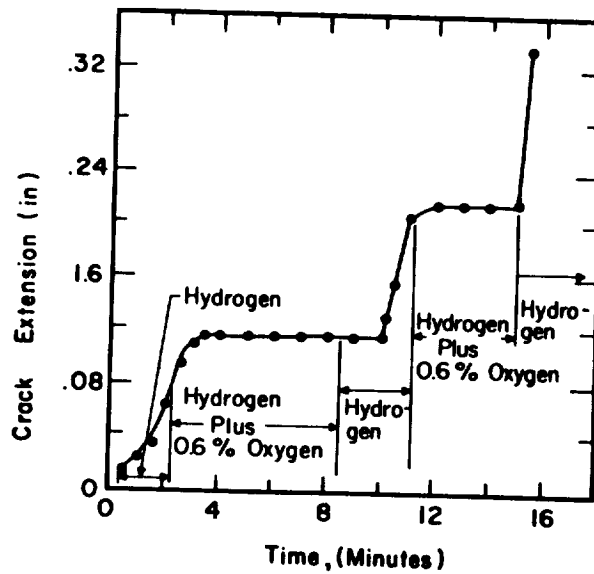


Figure 53. Subcritical crack growth of H-11 steel in hydrogen-oxygen mixtures.

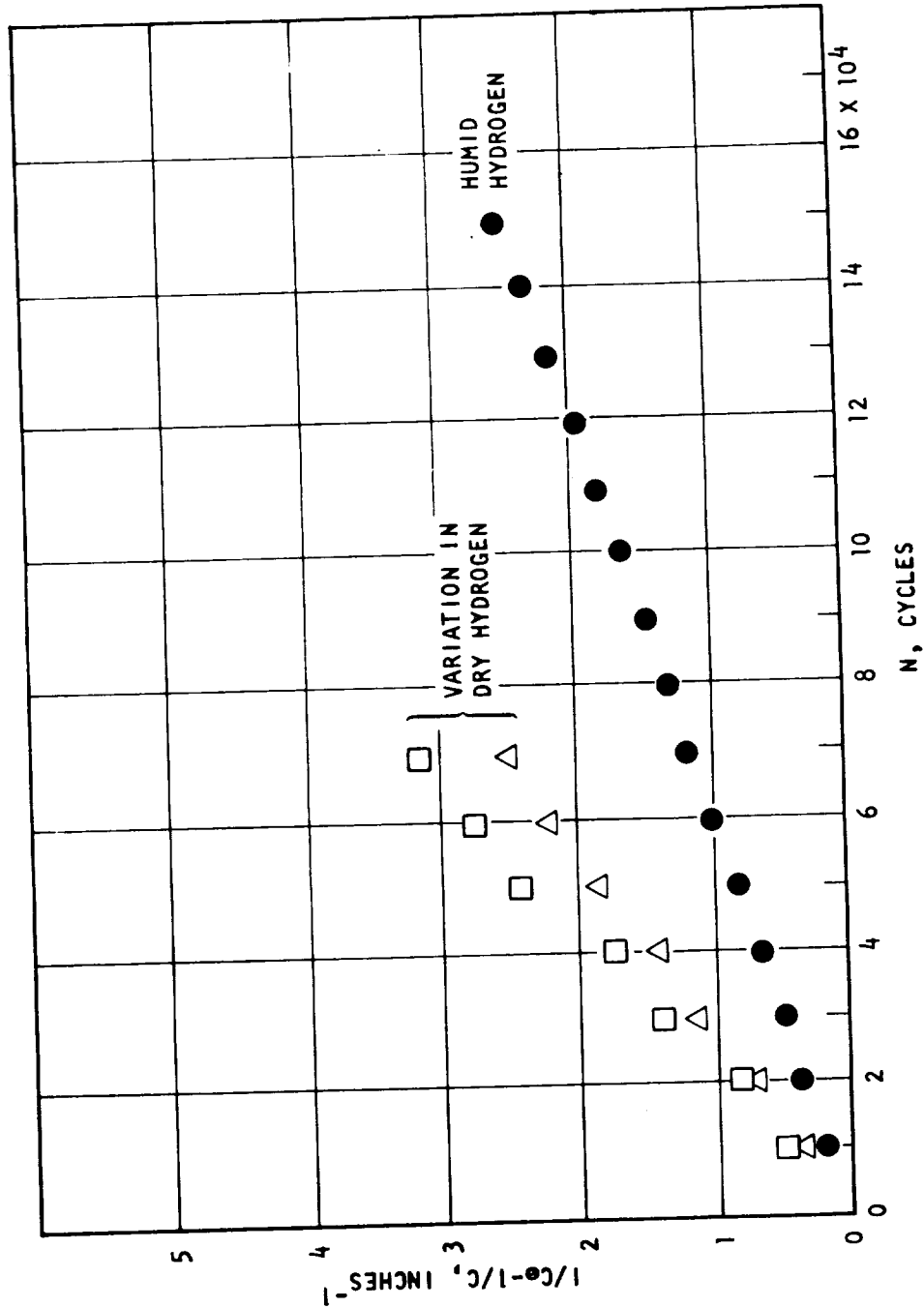


Figure 54. Fatigue-crack growth in 18Ni (250) maraging steel tested in hydrogen.

where  $c$  is the equivalent half-crack length (Ref. 66 and 67) and  $c_0$  is the initial equivalent half-crack length. The variation in the crack growth rate for the "dry" hydrogen is believed to be caused by variations in the amount of water contained in the hydrogen used. Duplicate tests in the humid hydrogen environment showed negligible differences.

Walter and Chandler (Ref. 47) have shown that cyclic crack growth rates in Inconel 718 are faster in 2000-psig hydrogen than in 2000-psig helium and ambient air. Their results are shown in Fig. 55. The chemistry and heat treatment of the Inconel 718 used are given in Tables 9 and 10, Heat B, heat treatment 3. Crack growth rates were determined by an electrical resistivity method. Hydrogen purity was  $<0.5$  ppm  $O_2$ ,  $<0.5$  ppm  $H_2O$ , and 2.6 ppm  $N_2$ .

Walter and Chandler (Ref. 7) used electrical resistivity measurements to determine the onset of crack growth in tensile tests on notched cylindrical specimens of ASTM A-517, Inconel 718, and Ti-6Al-4V. These results are presented in Table 24.

TABLE 24  
CRACK GROWTH DURATION DURING TENSILE TESTS OF NOTCHED SPECIMENS  
TESTED IN HIGH-PRESSURE HYDROGEN

Specimen	Pressure, psi	Notch Strength in He, ksi	Notch Strength in $H_2$ , ksi	Stress at Which Crack Initiation Occurred, ksi	Time Period Over Which Crack Growth Occurred, sec
A-517	10 000	251	183	173*	39*
Inconel 718	2 000	333	286	249	25
Ti-5Al-4V	2 000	250	132	114	40

\*The crack growth resolution during this test was quite marginal and thus considerable crack growth may have occurred past this time period and before this stress is reached.

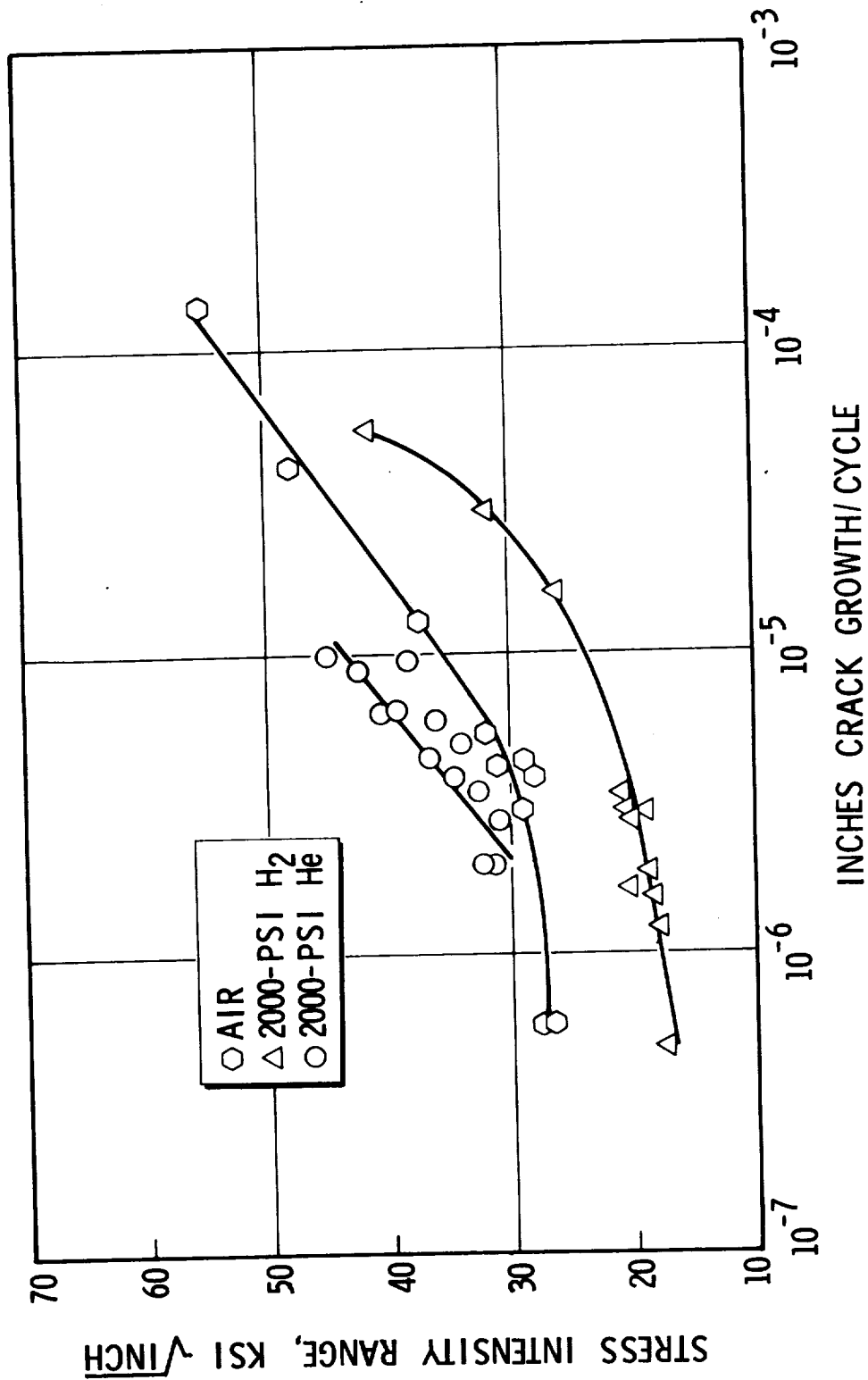


Figure 55. Cyclic crack growth versus stress intensity range during fatigue tests of Inconel 718 at room temperature.

The results indicate that failure is preceded by a considerable period of crack growth for all three materials. The hydrogen-affected region as determined from fractographic examination (see Chapter 8, Metallography) was, therefore, formed over a significant period of the total time during which the applied load was continually increasing.

The electrical resistivity was also monitored during comparative air and helium tests. The results showed that failure occurred almost immediately following the first indication of crack formation.

Marcus and Stocker (Ref. 30) have investigated the effect of hydrogen on crack growth rates in the pressure range of  $10^{-8}$  to 150 torr for Ni-200 and a copper alloy, NARloy-Z\*, using tapered double-cantilever beam specimens (TDCB). The apparatus used in the foregoing experiments has been described previously in Chapter 5, Test Procedure. Tests were conducted at room temperature at a frequency of 2 cycles per second with a maximum stress intensity of 27 ksi  $\sqrt{\text{in.}}$  and a cyclic stress intensity of 11 ksi  $\sqrt{\text{in.}}$ . The crack propagation rate of Ni-200 was 0.02  $\mu/\text{cycle}$  at  $10^{-9}$  torr pressure, and increased to 0.16  $\mu/\text{cycle}$  in hydrogen at a pressure of 150 torr. A crack growth rate of 0.2  $\mu/\text{cycle}$  was established for the NARloy-Z in the  $10^{-10}$  torr vacuum environment; this rate remained essentially the same in the hydrogen environments tested. Further tests on crack growth rates in Ni-200 at 150 torr hydrogen pressure between 77<sup>o</sup>F (25<sup>o</sup>C) and -58<sup>o</sup>F (-50<sup>o</sup>C) showed that the rate of crack growth was a maximum in the vicinity of -13<sup>o</sup>F (-25 C). The crack growth rates were relatively frequency independent in the range of 0.2 to 5 cps.

---

\*Trademark of North American Rockwell Corporation

Similar increases in crack growth rates were observed in hydrogen at room temperature for titanium alloys (Ti-6Al-4V, Ti-8Al-1Mo-1V, and titanium 75A) (Ref. 30). Measurable increases in the crack growth rates were observed at hydrogen pressures as low as 1 torr. For annealed Ti-6Al-4V in 150 torr hydrogen, with a cyclic stress intensity  $K$  of 13 ksi  $\sqrt{\text{in.}}$ , crack growth rates increased in a linear fashion from 0.6 to 3.3  $\mu/\text{cycle}$  as the stress intensity maxima were increased from 20 to 30 ksi  $\sqrt{\text{in.}}$ . The crack growth rate in vacuum ( $10^{-10}$  torr) and 14.7-psia air was 0.4  $\mu/\text{cycle}$  at a  $K$  max of 37 ksi  $\sqrt{\text{in.}}$ .

Attempts to determine crack growth rates with TCDB specimens of columbium (niobium) resulted in formation of cracks in the grip section and fracture of the specimen normal to the desired direction. Any region of the sample which was stressed beyond the yield point resulted in the formation of microcracks.

Williams and Nelson (Ref. 8) measured the stress intensity factors required for the initiation of measurable slow crack growth ( $K_{\text{SCG}}$ ) in fully hardened, stress-relieved 4130 steel as a function of displacement rate. The results for tests in air and at hydrogen pressures ranging from 127 to 709 torr are shown in Fig. 56. At low-displacement rates, the  $K_{\text{SCG}}$  values in hydrogen are about one-half those in air. The  $K_{\text{SCG}}$  values for air and for hydrogen at the faster displacement rates are equal to the critical stress intensity factor  $K_{\text{C}}$ . The maximum embrittlement in low-pressure gaseous hydrogen was observed to occur at slow strain rates.

Figure 57 shows the results of Williams and Nelson (Ref. 8) for crack propagation rates as a function of the reciprocal of the absolute temperature. Each datum point is the result of two measurements at the indicated temperature. All measurements were taken using the same specimen. Crack growth began immediately

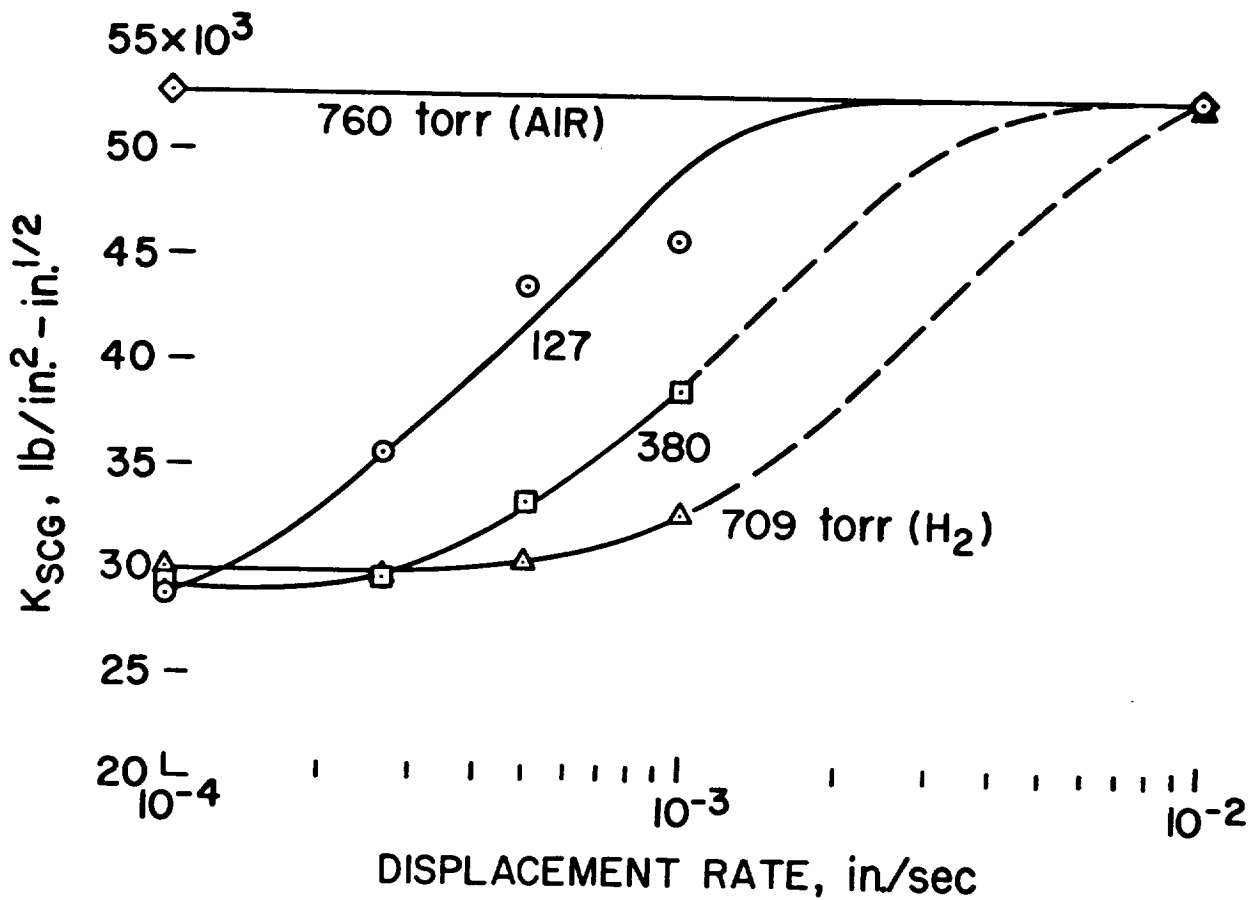


Figure 56 Effect of hydrogen pressure and displacement rate on the embrittlement of 4130 steel.

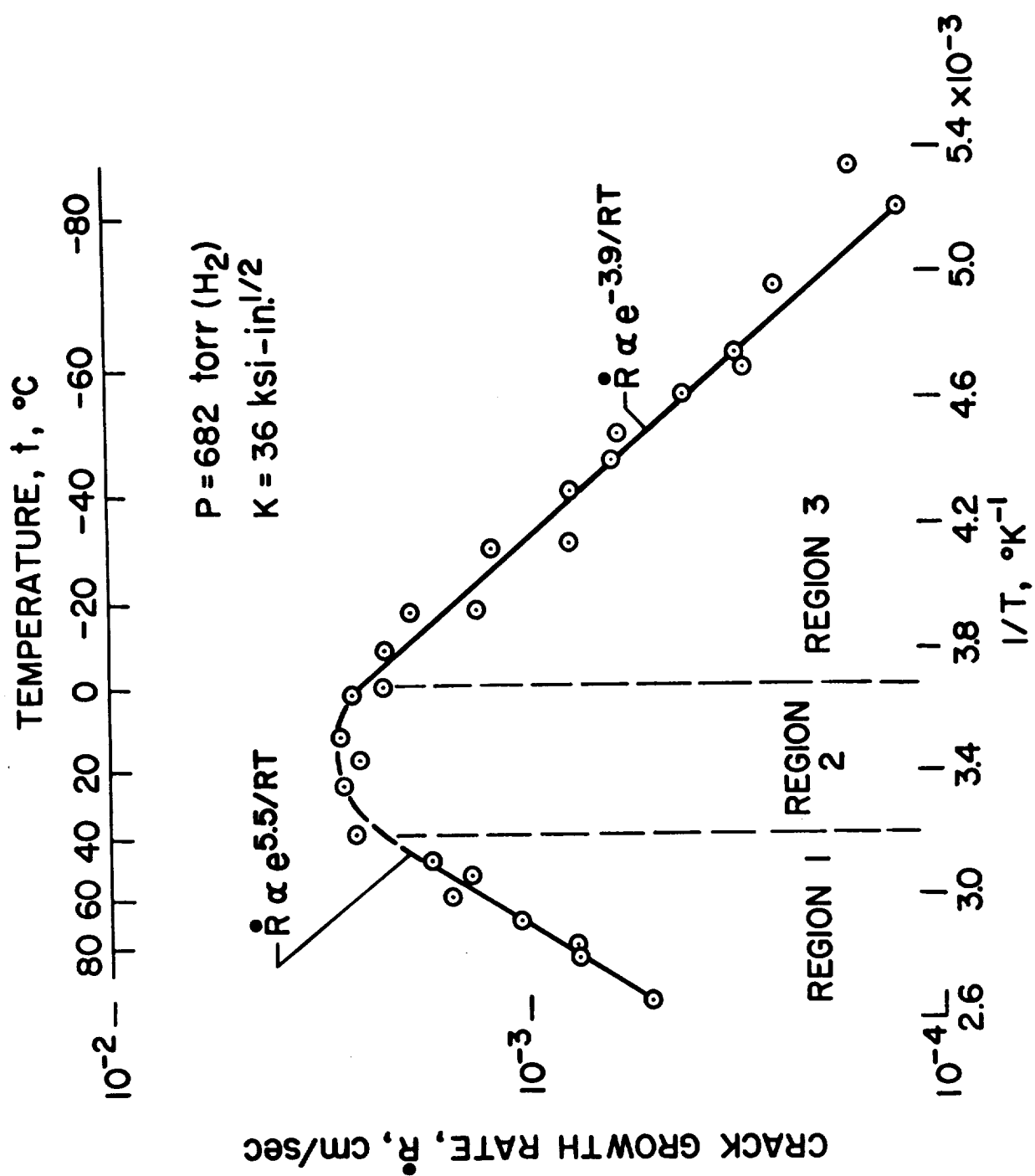


Figure 57. Temperature dependence of the slow crack-growth rate of 4130 steel.

after loading with no indication of an incubation period. From Fig. 57 it is observed that the maximum crack propagation rate occurs near room temperature. A similar temperature dependence has also been observed for internal-hydrogen embrittlement (Ref.68). Figure 58 shows the results for crack propagation rates as a function of pressure in the temperature range of  $-76^{\circ}\text{F}$  ( $-60^{\circ}\text{C}$ ) to  $140^{\circ}\text{F}$  ( $60^{\circ}\text{C}$ ).

Nelson et al. (Ref. 65) investigated the effect of partially dissociated hydrogen on embrittlement. Figure 59 shows the effect of temperature on  $K_{\text{SCG}}$  in various environments. Again,  $K_{\text{SCG}}$  in air is nearly independent of temperature in the range studied. In a molecular hydrogen environment the results are similar to those in Fig. 56. In an atomic-molecular hydrogen environment the temperature dependence and the magnitude of  $K_{\text{SCG}}$  vary significantly from those in molecular hydrogen. Figure 59 shows that  $K_{\text{SCG}}$  is pressure dependent in the vicinity of room temperature. The nature of this pressure dependence near room temperature is shown in Fig. 60, where  $K_{\text{SCG}}$  is shown as a function of molecular hydrogen pressure. The results of crack-growth studies in an atomic-molecular hydrogen environment at a constant hydrogen pressure of  $8 \times 10^{-3}$  torr are given in Fig. 61. The apparent activation energy of 6800 cal/g-atom was found for crack growth in a partially dissociated hydrogen environment. The significance of these results will be discussed in Chapter 10, Discussion.

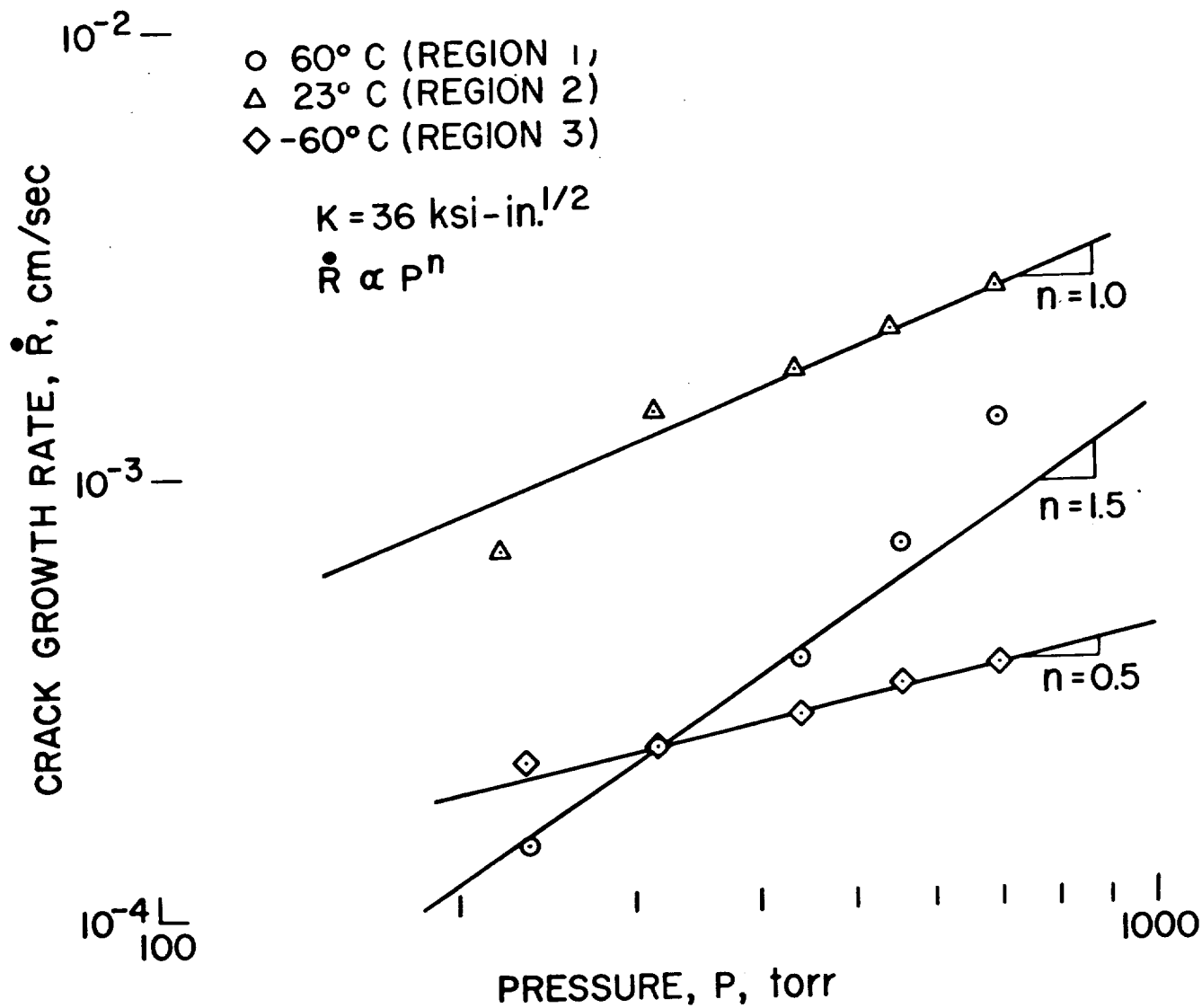


Figure 58. Effect of hydrogen pressure on the slow crack-growth rate of 4130 steel.

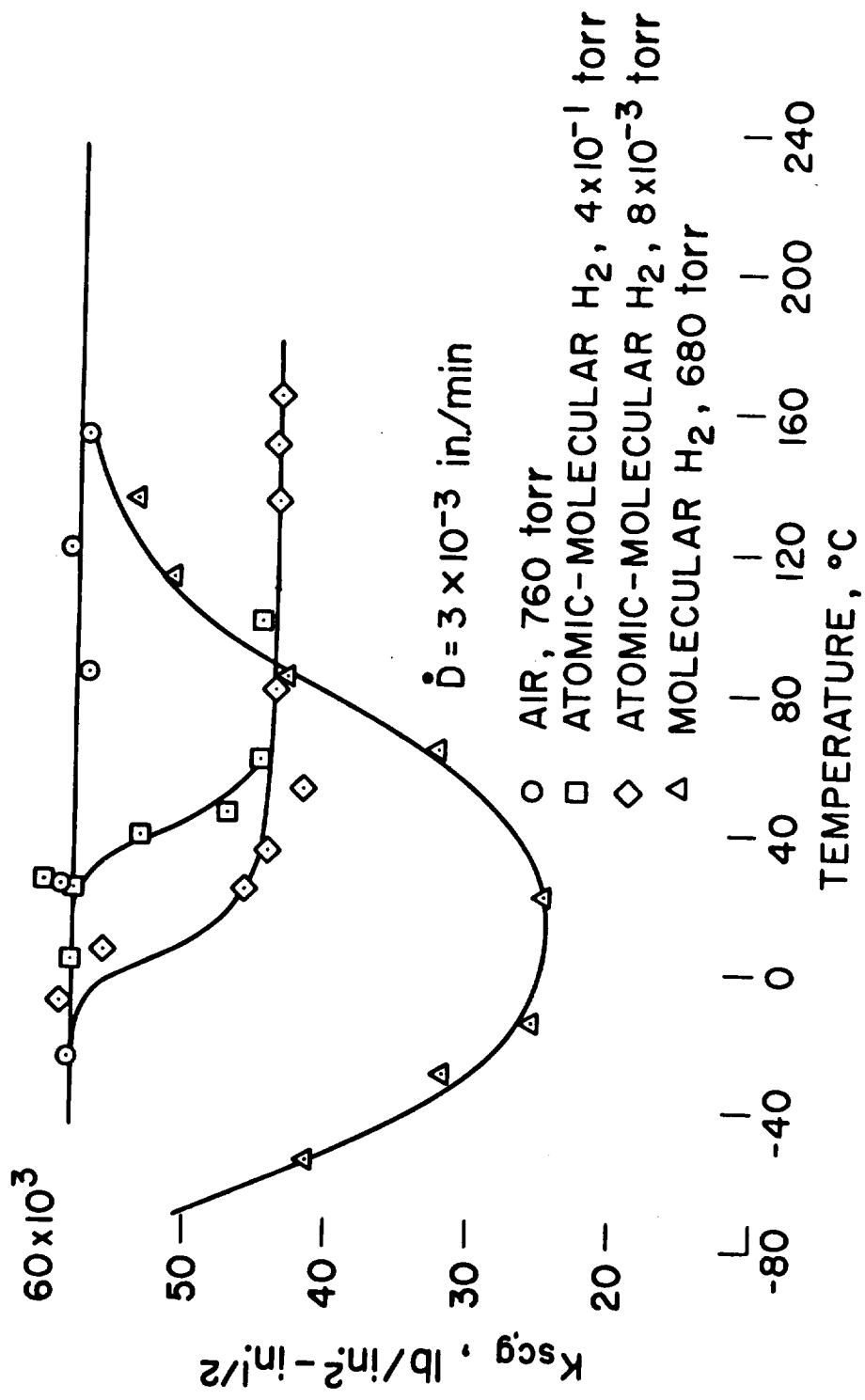


Figure 59. Effect of temperature on slow crack growth ( $K_{SCG}$ ) of 4130 steel in air, molecular hydrogen, and atomic-molecular hydrogen.

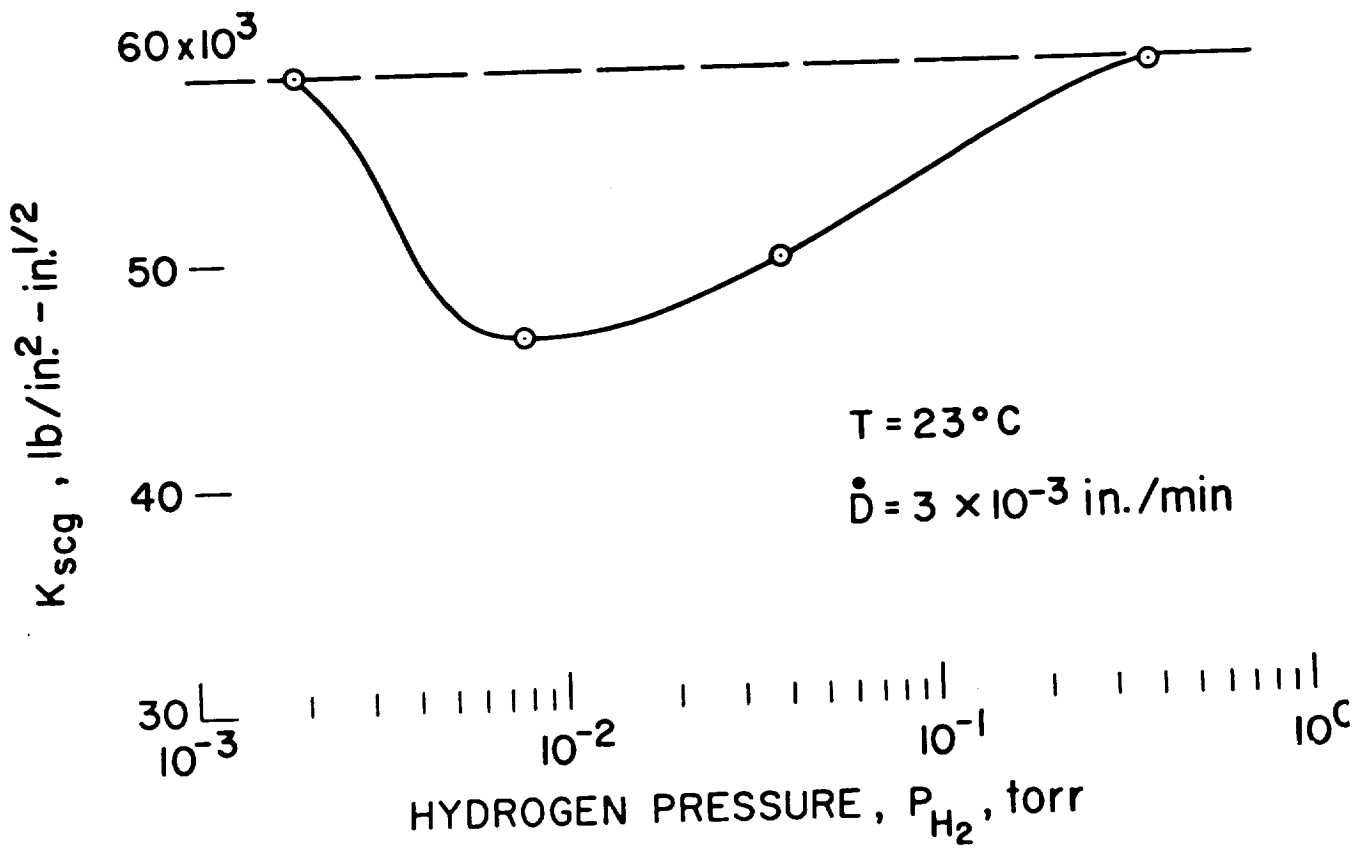


Figure 60. Dependence of embrittlement of 4130 steel on molecular hydrogen pressure in an atomic-molecular hydrogen environment.

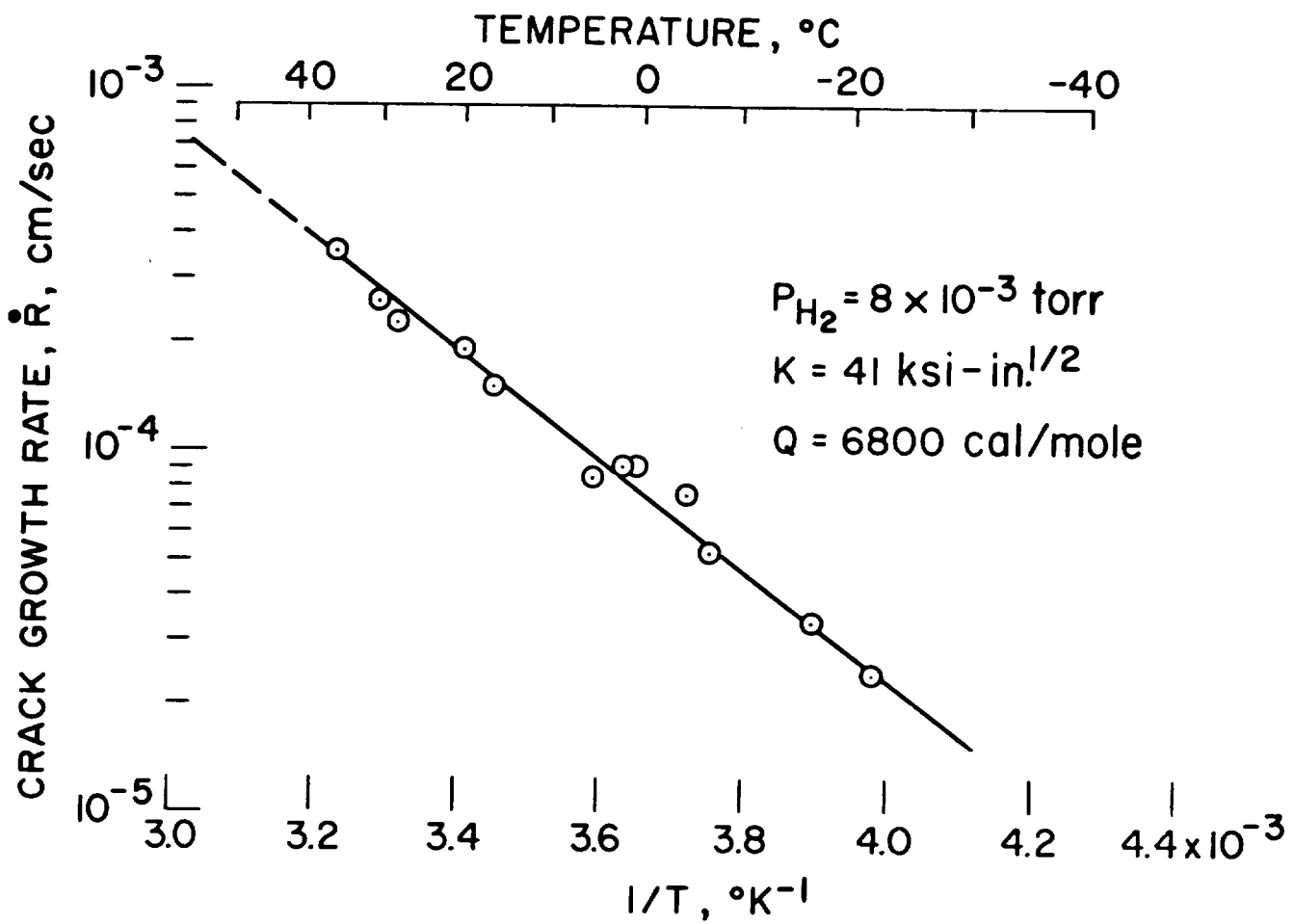


Figure 61. Dependence of slow crack-growth rate in 4130 steel on temperature in an atomic-molecular hydrogen environment.



## CHAPTER 8. METALLOGRAPHY

The results of metallographic and fractographic examination of specimens tested in hydrogen environments are described in this chapter. Hydrogen environment embrittlement results from the formation of a surface crack or cracks and the propagation of these cracks in a brittle manner. In the majority of embrittled metals, extensive surface cracking is observed near the fracture of unnotched specimens. Hofmann and Rauls (Ref. 40) were the first to observe these surface cracks; they associated the cracks with gaseous hydrogen pockets, "fish-eyes," that form internally in steels containing internal hydrogen.

Walter and Chandler (Ref. 7) examined the surface of unnotched specimens of 32 alloys tensile tested at ambient temperatures in air (ambient pressure), 10 000-psig helium and 10 000-psig hydrogen environments. Surface cracks, oriented approximately parallel to the fracture surface, were apparent on all the specimens embrittled by 10 000-psig hydrogen. No cracks were observed on specimens tested in air or in 10 000-psig helium. It was shown (Ref. 7) that the metallographic characteristics associated with hydrogen-environment embrittlement can be categorized according to the four embrittlement categories presented earlier (Table 8). The results for unnotched and notched specimens are presented together and are described as a function of the degree of embrittlement.

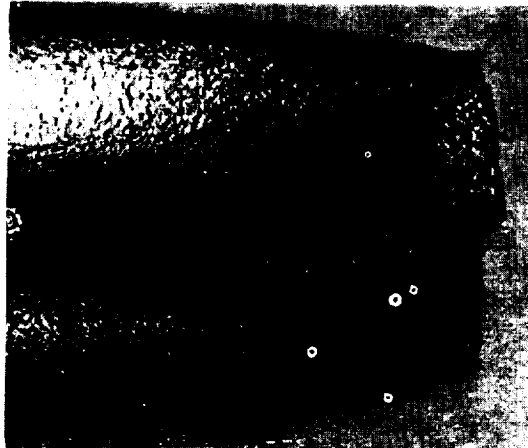
The metallography shown in this chapter is taken, except where noted, from Walter and Chandler (Ref. 7). The specimens tested in 10 000-psig hydrogen which were negligibly embrittled did not contain surface cracks and the fracture mode of these specimens appeared to be ductile.

### Slightly Embrittled Specimens

The slightly embrittled group of metals either had no surface cracks, as observed for Be-Cu Alloy 25, or contained a large number of very small surface cracks, as observed on titanium and AISI 304L stainless steel. The results for commercially pure titanium are illustrated in Fig. 62. Figure 62(A) and (B) show that the surface cracks on unnotched specimens were numerous, shallow, and blunt. The fracture of the unnotched specimens did not, however, appear to originate from these surface cracks. There was no measurable reduction of ductility, and the shear lips were well-formed indicating that the fracture initiated within the specimens.

An electron fractograph of the machined surface/fractured surface interface of a notched titanium specimen tested in 10 000-psig hydrogen is shown in Fig. 62(C). The fracture is brittle and transgranular with a considerable amount of secondary cracking perpendicular to the fracture surface. The depth of the brittle region was approximately 0.02 inch.

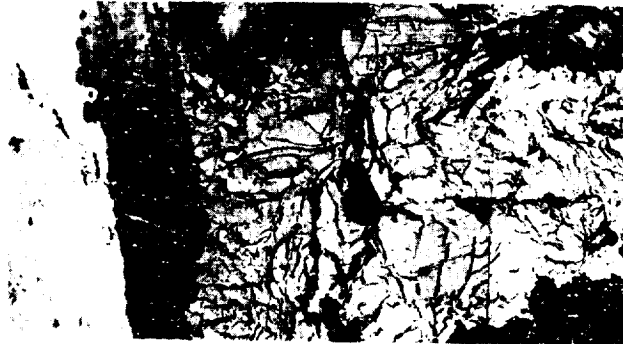
The surface cracks on AISI 304L stainless steel were similar in shape to those observed on commercially pure titanium. The cracks were sufficiently deep, however, to cause a slight (8 to 9 percent) reduction of ductility and the shear lips on these specimens were somewhat discontinuous. Benson et al. (Ref. 46) attributed the nucleation of surface cracks on AISI 304L stainless-steel specimens tested in 10 000-psig hydrogen to strain-induced martensite platelets. Blunting of the cracks was observed in the more ductile austenite matrix.



(A) 10X



(B) 110X



(C) 1000X

Figure 62. Metallography of Commercially Pure Titanium Specimens Tested in 10 000 psig Hydrogen ((A) Photomicrograph (10X) Showing Multitude of Small Surface Cracks; (B) Photomicrograph (110X) of Surface Cracks; (c) Electron Fractograph (1000X) of Notched Specimen at the Machined Surface/ Fractured Surface Interface)

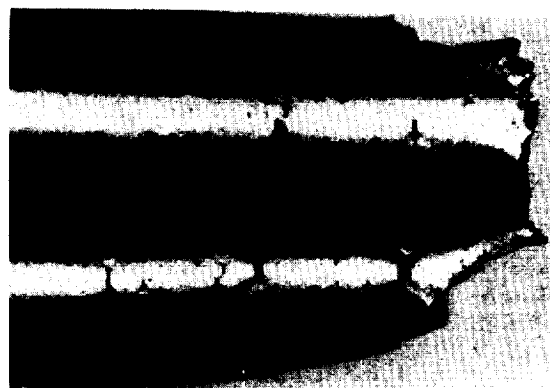
### Severely Embrittled Specimens

The majority of metals tested by Walter and Chandler (Ref. 7) were in the severely embrittled category. The surface cracks on specimens of metals in this category were less numerous than for the slightly embrittled metals, but were larger and easily visible to the naked eye. The density and size of the cracks increased with the degree of plastic strain, i.e., there were few cracks located outside the necked-down region and most were located close to the fracture.

It appears that a critical plastic deformation is required to initiate surface cracking. This critical deformation could be associated with rupturing surface protective layers to expose a metal surface to the hydrogen. Abrading ASTM A-517 specimens in hydrogen prior to testing increased the number of surface cracks formed, but plastic deformation was still required before surface cracks were initiated.

Figure 63 illustrates surface cracking of ASTM A533-B steel specimens tested in 10 000-psig, 1000-psig, and 14.7-psia hydrogen environments. The cracks were sufficiently deep to initiate fracture at the higher hydrogen pressures. There were indications of surface cracks on the specimen tested in 14.7-psia hydrogen, although the cracks were not sufficiently deep to affect ductility; however, shear lips were complete. It appears from Fig. 63 that the amount of plastic deformation needed to form a surface crack increases with decreasing hydrogen pressure.

The metallography of several severely embrittled specimens is illustrated in Fig. 64. Fracture of unnotched specimens generally involved formation of several surface cracks as is illustrated in Fig. 64(A). These surface cracks



(A)

10X



(B)

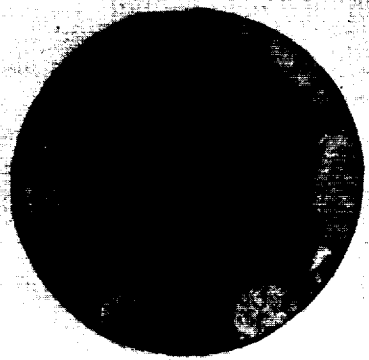
10X



(C)

10X

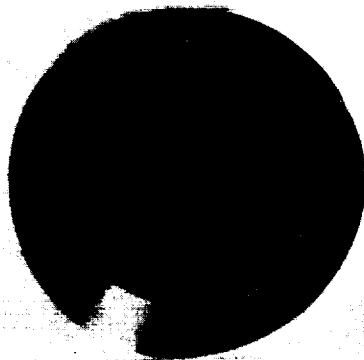
Figure 63. Photomicrographs (10X) of ASTM A533-B Specimens Tested in Hydrogen at Various Pressures ((A) 10 000-psig Hydrogen; (B) 1000-psig Hydrogen; (C) 14.7-psia Hydrogen)



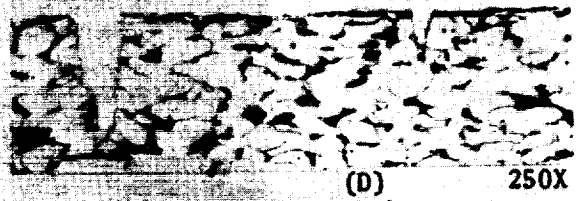
(A) 10X



(B) 10X



(C) 10X



(D) 250X

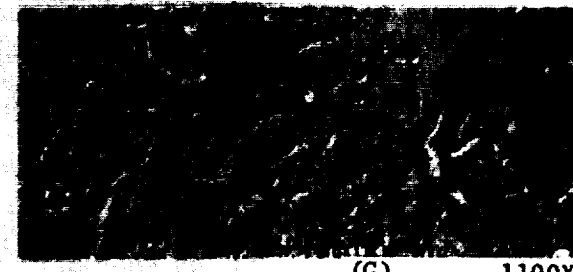


(E) 100X

Machined Fracture



(F) 1300X



(G) 1100X

Figure 64. Metallography of Severely Embrittled Specimens Tested in 10 000-  
psig Hydrogen (Photomicrographs Showing Fracture Origins (A) AISI  
1020 Unnotched Specimen; (B) ASTM A533-B Notched Specimen; (C)  
Ti-6Al-4V (STA) Notched Specimen; Photomicrographs of Surface  
Cracks in (D) AISI 1020 (E) AISI 430F; Electron Fractographs of  
(F) AISI 1042 Notched Specimen at the Machined Surface/Fractured  
Surface Interface and (G) Ti-6Al-4V (STA) Notched Specimen at  
Region Adjacent to Machined Surface)

appeared as small, half-moon-shaped areas normal to the surface and gave the appearance of radial growth of a crack which initiated at the surface. In many cases, the surface cracks were not distinct because of crack overlap. Shear lips were not formed on specimens in this embrittlement category.

The surface cracks of metals in the severely embrittled category were considerably sharper than those found in slightly embrittled metals. Figure 64 shows cracking in AISI 1020 (D) and AISI 430F stainless steel (E). The surface cracks were somewhat sharper in the more embrittled AISI 430F stainless steel.

Crack branching is extensive in the severely embrittled category. As shown in Fig. 64(E), branching can cause the crack to change direction toward the tensile axis, which decreases the stress intensity at the crack tip, and causes the crack to cease propagating.

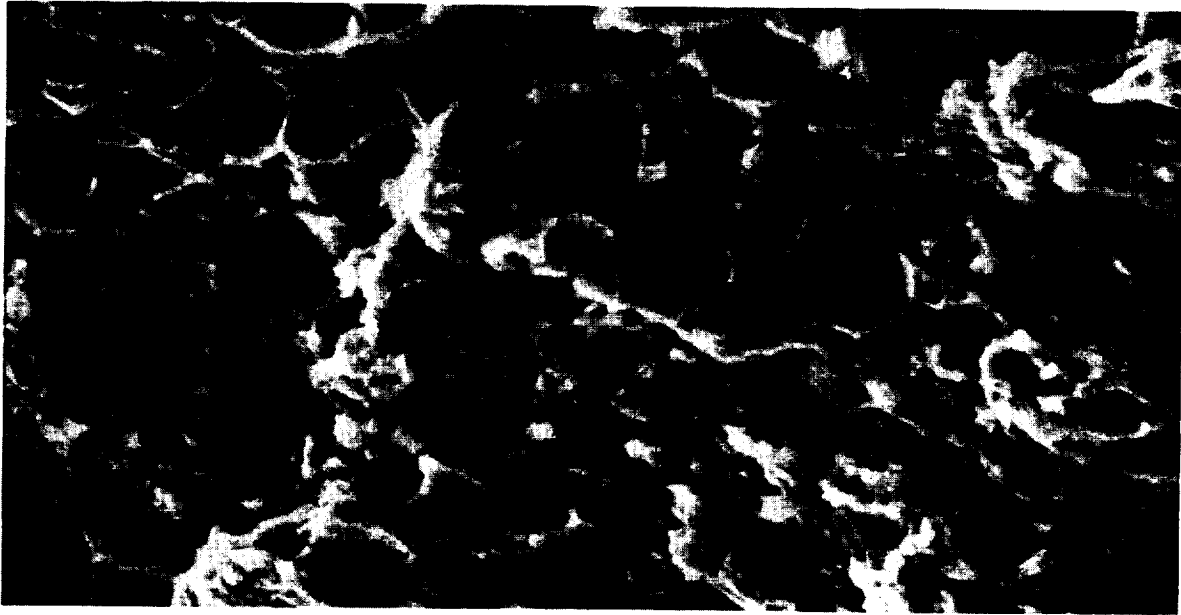
The brittle region extends uniformly around the entire fracture periphery in the notched low- and moderate-strength low-alloy steels tested in 10 000-psig hydrogen as illustrated in Fig. 64(B). The brittle outer region corresponds to the region of surface cracking of the unnotched specimens, and evidently, several surface cracks formed the brittle periphery. If the fracture had proceeded from a single surface crack, the brittle region would have been restricted to one side of the specimen. Figure 64(F) is an electron fractograph showing the machined surface (far left side)/fractured surface interface of a notched AISI 1042 specimen tested in 10 000-psig hydrogen. The brittle region is transgranular with secondary cracking (cracks into the fracture surface) that corresponds to branching of the surface cracking in unnotched specimens.

The fracture appearance of commercially pure titanium and the titanium-base alloy specimens was somewhat different from that of the other severely embrittled specimens. The brittle, hydrogen-affected region appeared as a dark band (Fig. 64(C)), often of crescent shape, on one side of the fracture periphery. There was no shear lip on the regions containing the dark band; however, there was a thin, sometimes broken shear lip on the remainder of the specimen. The size of the band appeared to be directly proportional to the degree of embrittlement. That is, the specimens with the most strength reduction also had the largest dark band.

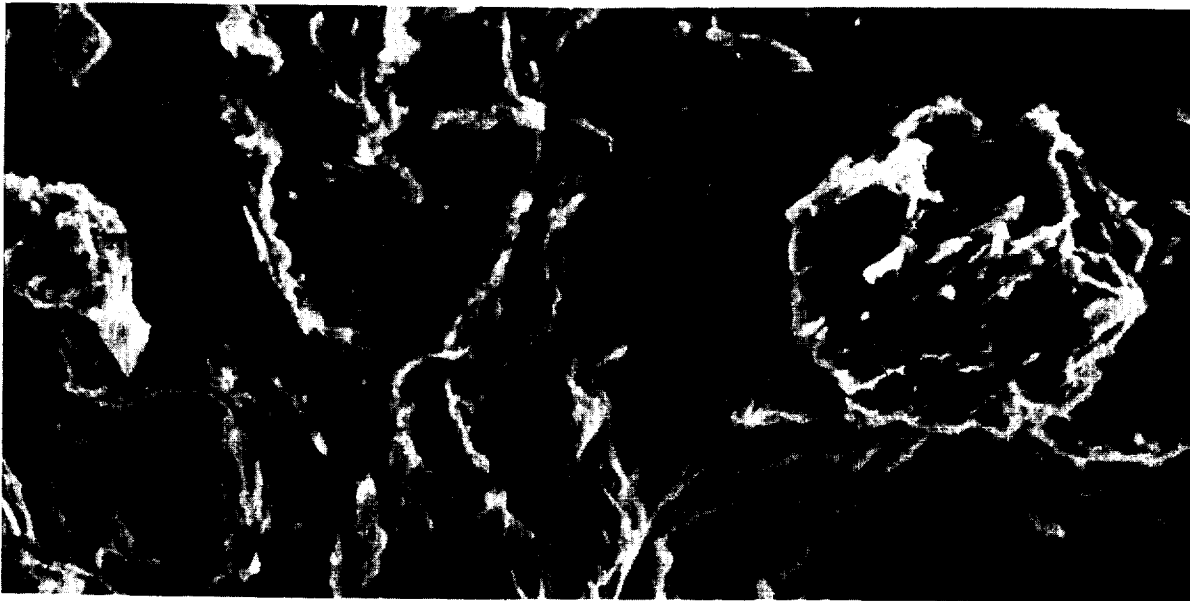
Figure 64(G) is an electron fractograph from the dark region (Fig. 64(C) of the fracture of a Ti-6Al-4V (STA) notched specimen tested in 10 000-psig hydrogen. The fracture is brittle and transgranular. The electron fractography did not show any evidence of a second phase (hydride); however, it is difficult to detect the hydride phase, and hydride formation is usually characterized by intergranular failures (Ref. 69).

Williams and Nelson (Ref. 31) have examined Ti-6Al-4V specimens that were bend tested in hydrogen at 14.7-psia pressure. In the solution-treated and aged condition, the specimens were little affected by the hydrogen environment, and the overall appearance of the fracture indicates primarily a shearing mode of failure (Fig. 65(A)). Figure 65(A) also shows small amounts of intergranular and transgranular fracture and large amounts of transgranular secondary cracking.

Ti-6Al-4V, solution treated and stabilized to form a microstructure containing equiaxed and some acicular  $\alpha$  in a  $\beta$  matrix, exhibited a large degree of embrittlement in hydrogen, Figure 65(B), a fractograph of the fracture, shows numerous regions of intergranular fracture along both the acicular and equiaxed  $\alpha$  -  $\beta$  boundaries.

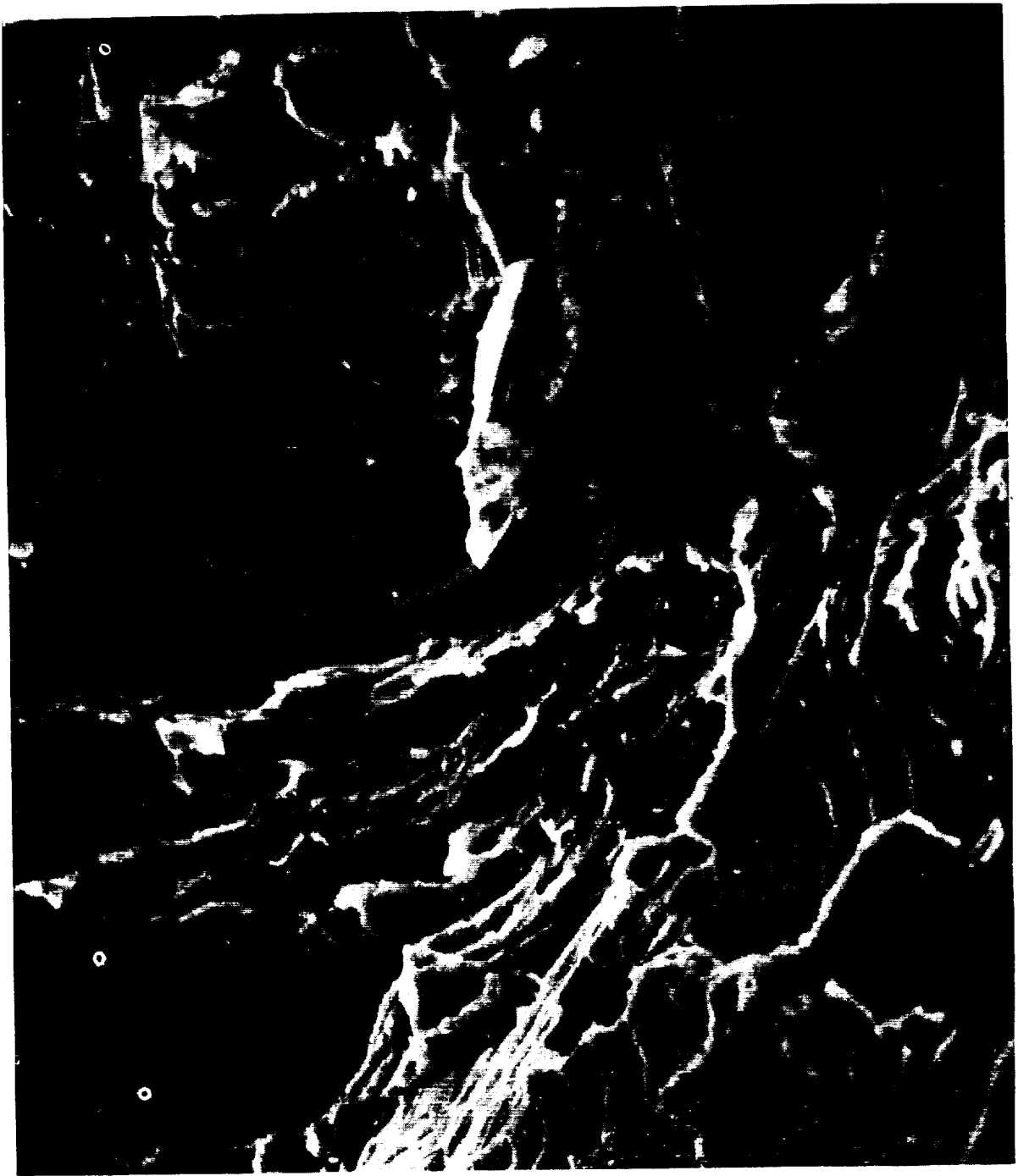


(A) STANDARD SOLUTION-TREATED AND AGED CONDITION



(B) SOLUTION-TREATED AND STABILIZED TO OBTAIN A MICROSTRUCTURE  
CONSISTING OF EQUIAXED AND ACICULAR  $\alpha$  IN A  $\beta$  MATRIX

Figure 65. Scanning Electron Fractographs of Ti-6Al-4V Specimens Bend Tested  
in a 14.7 psi Hydrogen Environment, Ref. 31 (2200X)



(C) SOLUTION-TREATED IN THE  $\beta$  FIELD AND STABILIZED TO OBTAIN COMPLETELY ACICULAR  $\alpha$  IN A  $\beta$  MATRIX

Figure 65 (Concluded)

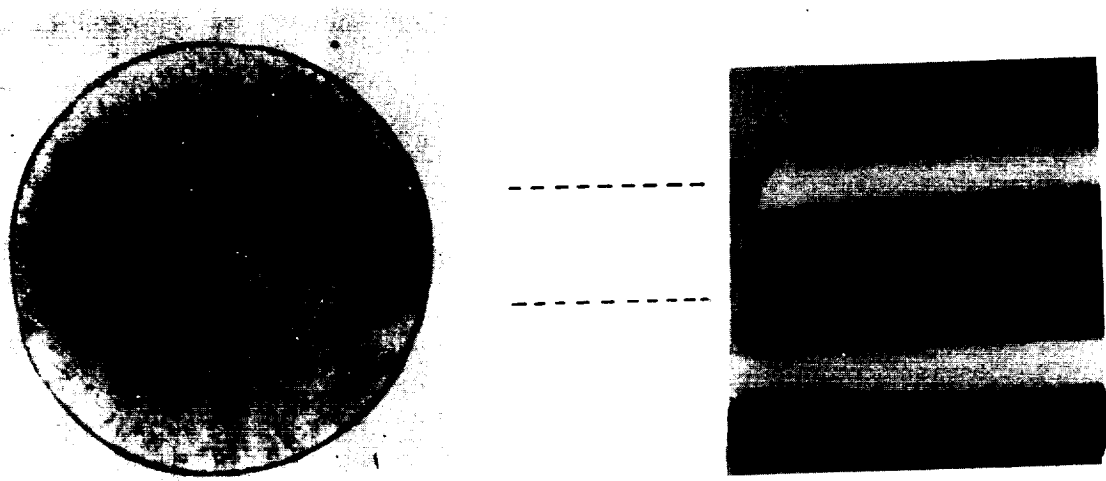
Figure 65(C) shows the fracture of a specimen which had been solution treated and stabilized to form completely acicular  $\alpha$  in a  $\beta$  matrix. The prime mode of failure was along prior  $\beta$  grain boundaries and along acicular  $\alpha$  -  $\beta$  boundaries with significant amounts of transgranular, secondary cracking. An interesting feature common to fracture of this structure in hydrogen is the fan-shaped, terraced structure which, according to Williams and Nelson (Ref. 31), is indicative of a stepwise crack growth process.

#### Extremely Embrittled Specimens

Metals extremely embrittled by hydrogen, are likely to form only one surface crack which propagates to failure. Figures 66(A) and (B) are end and side views of an unnotched Inconel 718 specimen showing the surface crack that initiated fracture. In each of the extremely embrittled metals, thin shear lips were observed which were complete except for the location of the single surface crack. Specimens of the alloys tested in air or 10 000-psig helium had complete shear lips.

Formation of surface cracks other than the one leading to failure was infrequent in the extremely embrittled alloys. Two surface cracks in an AISI 4140 specimen are shown in Fig. 66(C). The cracks appear to be fairly broad initially, but then narrow and remain sharp during propagation. Typically, surface cracks in the extremely embrittled metals are initially sharp and remain sharp or become sharp during propagation. Branching does not significantly impede crack propagation in these materials.

Electron fractographic examination of notched specimens in this embrittlement category showed the fractures to be very brittle near the region of fracture origin. Steinman, Van Ness and Ansell (Ref. 50) have shown that the brittle regions in notched AISI 4140 specimens tested in 10 000-psig hydrogen are characterized by transgranular cleavage. Figure 67 shows scanning electron fractographs



(A) 10X

(B) 10X

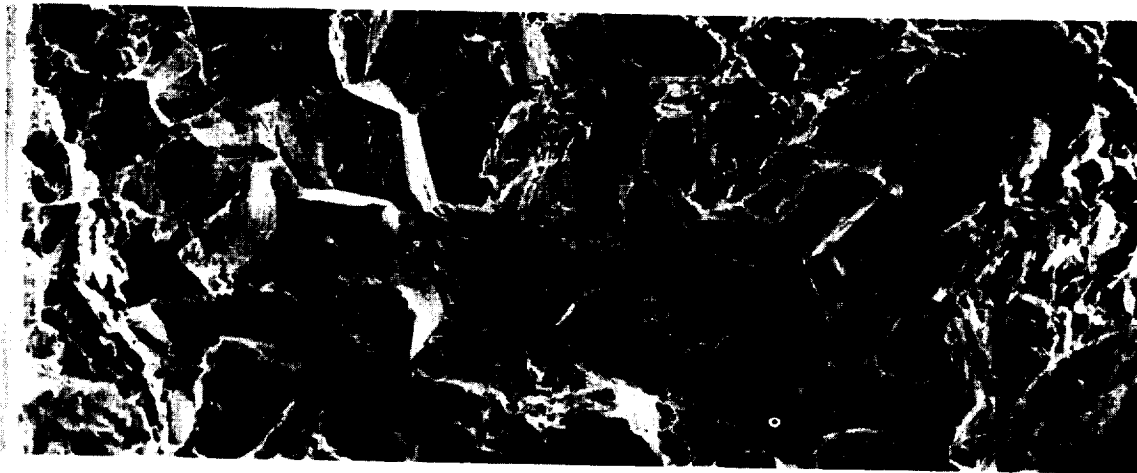


(C) 300X

Figure 66. Metallography of Extremely Embrittled Specimens Tested in 10 000-psi Hydrogen ((A) and (B) are Orthographic Projections of Un-notched Inconel 718 Specimen Showing Surface Crack that Initiated Fracture (Surface Crack is Dark Region Without the Shear Lip in (A) and Flat Region in (B)); (C) is Photomicrograph of Surface Cracks in an AISI 4140 Specimen)



(A) Ni-4.5% Al TESTED IN 14.7 PSI PRESSURE HYDROGEN, REF. 31 (160X)



(B) INCONEL 718 TESTED IN 2000-PSIG HYDROGEN, REF. 70 (750X)

Figure 67. Scanning Electron Fractographs of Nickel-Base Alloys Tested in Hydrogen [The machined surface is at the right in (A), and at the far left in (B).]

of Ni-4.5% Al (A) tested by Williams and Nelson (Ref. 31) in 14.7-psia hydrogen and of an Inconel 718 specimen (B) tested by Walter and Chandler in 2000-psig hydrogen. The fractographs are from the machined surface/fractured surface interface and show that the hydrogen-affected region is intergranular with deep secondary cracking. The layer of fine grains shown on the Ni-4.5% Al fractograph was caused by deformation during machining and subsequent recrystallization during heat treating. The depth of the brittle region and the sharp transition between the brittle and ductile regions are illustrated in the Inconel 718 fractograph.

Walter and Chandler (Ref. 70) measured the brittle crack depth for Inconel 718 as a function of hydrogen pressure. It was found that increasing the hydrogen pressure increased the depth of the brittle fracture but did not change its appearance. Figure 68 shows that the brittle crack depth was a linear function of the square root of hydrogen pressure and extrapolated to zero at zero hydrogen pressure. Embrittlement, as measured by reduction of notch strength, of these specimens was also found to be a linear function of the square root of hydrogen pressure.

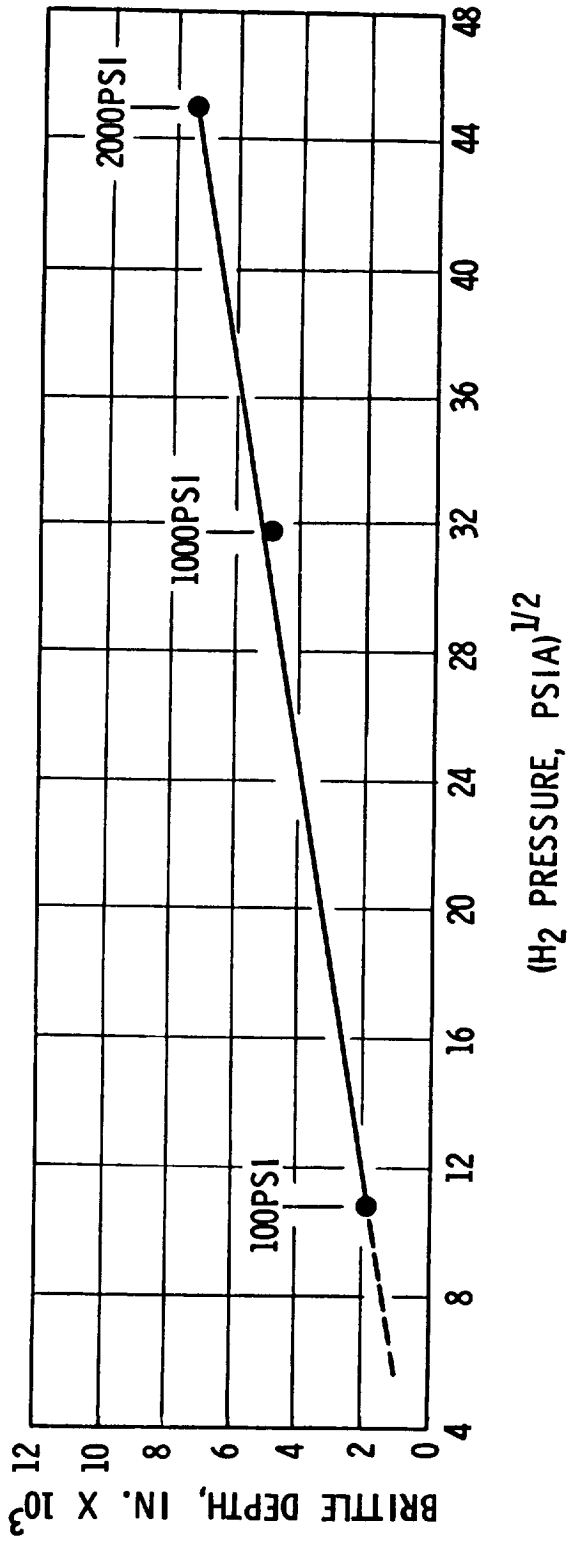


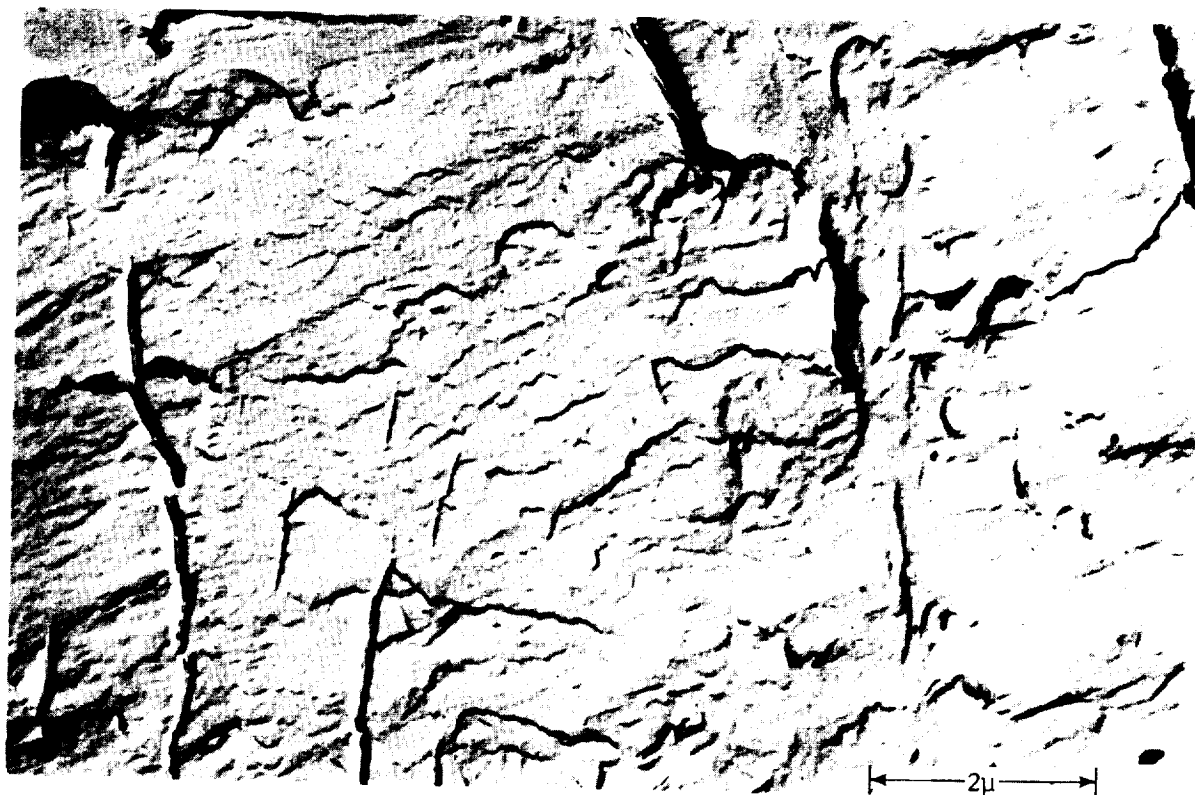
Figure 68. Brittle fracture depth of notched Inconel 718 specimens tested in high-pressure hydrogen.

## Fractography of Specimens Fatigue Tested in Hydrogen

Hydrogen environments reduce the fatigue strength and enhance the rate of crack growth in those metals that are susceptible to hydrogen-environment embrittlement. Marcus et al (Ref. 71) have shown that hydrogen, even at pressures considerably less than 14.7 psia, increases the rate of crack propagation for tapered DCB specimens during high-cycle fatigue in Ti-6Al-4V annealed. The fracture of a tapered DCB specimen tested in 150 torr hydrogen is illustrated in Fig. 69. Secondary cracks are quite numerous, but the orientation of the cracks is random to the direction of crack propagation. Fatigue striations were not observed.

Electron fractography examination was made by Walter and Chandler (Ref. 7 and 70) on several precracked notched specimens tested in low-cycle fatigue. The results are presented in Table 25. The fatigue strengths of the ASTM A-517 and ASTM A533-B specimen in 10 000-psig hydrogen were about 1/3 that in 10 000-psig helium. The Inconel 718 specimens were tested in 2000-psig helium and hydrogen environments. The fatigue strength was 22 percent less in hydrogen than in helium.

Examination of the fatigue-induced fractures indicated close similarity between the specimen tested in air and helium environments; however, the regions of fatigue crack growth were considerably more brittle in the specimens tested in hydrogen than in those tested in air and helium environments. In fact, the hydrogen-affected regions appeared essentially the same in the tensile- and fatigue-type failures. Secondly, fatigue striations were easily seen in those specimens fractured in air and helium, but were not observed in the low-alloy steel specimens fractured in 10 000-psig hydrogen, and were only faintly seen



(A) Electron Fractograph



(B) Scanning Electron Fractograph

Figure 69. Fracture Surface From Annealed Ti-6Al-4V Fatigued in 150 Torr H<sub>2</sub> Gas (Ref. 71)

TABLE 25

RESULTS OF ELECTRON FRACTOGRAPHY EXAMINATION OF SPECIMENS  
TESTED IN LOW CYCLE FATIGUE (Ref. 7 and 70)

Material	Test Environment	Initial Stress, ksi	Cycles to Failure	Fracture Description
ASTM A-517	10 000-psig Helium	206	438	Fatigue striations observable.
ASTM-A-517	10 000-psig H <sub>2</sub>	117	191	Transgranular, brittle or quasi-cleavage. No fatigue striations observable.
ASTM A533-B	10 000-psig H <sub>2</sub>	75	3 281	Transgranular, brittle or quasi-cleavage. No fatigue striations observable.
Inconel 718	Air (14.7 psia)	118	3 576	Fatigue striations clearly observable
Inconel 718	2000-psig Helium	132	4 575	Fatigue striations clearly observable
Inconel 718	2000-psig H <sub>2</sub>	77	8 780	Intergranular and transgranular brittle fracture; faint indications of fatigue striations.
Inconel 718	2000-psig H <sub>2</sub>	87	14 919	Intergranular and transgranular brittle fracture; faint indications of fatigue striations.

in the Inconel 718 specimens fractured in 2000-psig hydrogen. Figure 70(A) and (B) illustrate striations formed in Inconel 718 in air and hydrogen environments. Those in Fig. 70(B) are the most evident striations seen on the hydrogen embrittled specimens.

These observations agree with those of Spitzig, Talda, and Wei (Ref. 64) who studied crack growth during fatigue testing of 18 Ni (250) maraging steel 1/4-inch-thick center-notched plate specimens while exposed to hydrogen at 14.7 psia. They observed that hydrogen considerably increased the rate of crack growth in this material. Fractographic examination revealed that the hydrogen-affected regions were quite brittle without indications of fatigue striations.

The relative absence of fatigue striations on the specimens tested in hydrogen environments suggests that the mechanism proposed by Laird and Smith (Ref. 72) is the most applicable of those which have been postulated to explain fatigue striations. According to these authors, the striations form from plastic deformation at the crack tip. The hydrogen environment reduces fracture ductility and thereby reduces striation formation.

Meyn (Ref. 73) suggested that the brittle striation regions produced during a low-amplitude fatigue are predominantly the result of environmental reaction at the crack tip, and presumably fatigue striations in low-amplitude fatigue would not occur in vacuum. Pelloux (Ref. 74) has shown that fatigue striations are not found in certain aluminum and titanium alloys during fatigue crack growth in vacuum environments. Pelloux theorized that fatigue striations occur because oxidation prevents reversible slip, and reversible slip is not prevented in vacuum environments. According to Meyn and Pelloux, an embrittling environment should,

therefore, delineate striations and accelerate crack growth which, of course, is not in accordance with what is observed from fatigue failure in hydrogen. It should be noted, however, that the fatigue striations may have been present but obscured by the brittle nature of the fractures.

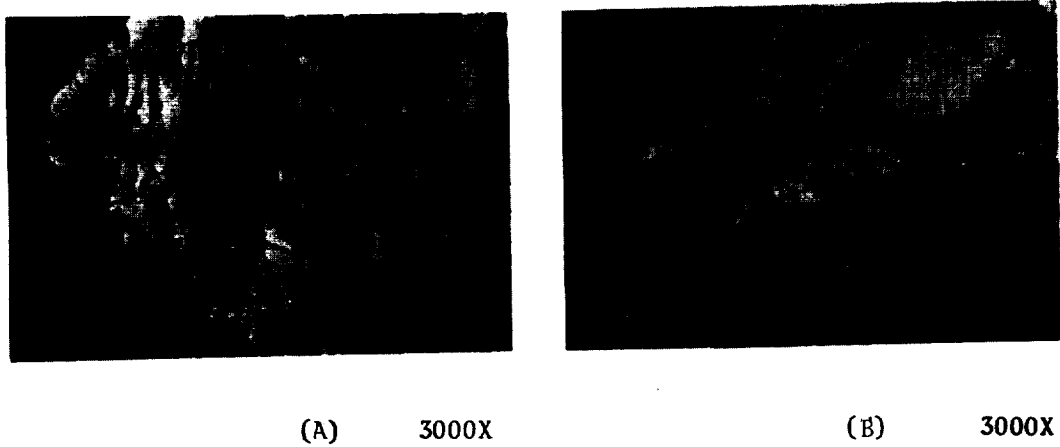


Figure 70. Electron Fractograph of Fatigue Tested Inconel 718 Specimens ((A) 3576 Cycles to Failure in Air; (B) 8780 Cycles to Failure in 2000-psig Hydrogen)

Walter and Chandler (Ref. 37), and Walter and Ytterhus (Ref. 78) tested various coatings to determine their effectiveness as hydrogen barriers. The coatings were applied to tantalum and Ta-10W and columbium and B-66 (columbium alloy), sheet (1/2 x 2-1/8 x 0.03 inches) specimens. The specimens were heat treated in purified hydrogen at atmospheric pressure. The exposure consisted of thermally cycling the specimens three times between 800<sup>o</sup> and 1500<sup>o</sup>F, holding at 800<sup>o</sup>F for 1 hour, and quenching in oil at room temperature. The total elapsed time for each heat treatment was approximately 6-1/2 hours.

The results of these tests are listed in Table 26. The coatings that were effective hydrogen barriers were vapor-deposited tungsten, Sylcor R-505, tin-aluminum, and Sylcor R-508 silver-silicon. The vapor-deposited tungsten and Sylcor R-505 coatings were only 0.001 inch thick. Carburizing B-66 by vacuum heat treating at 2000<sup>o</sup>F (1093<sup>o</sup>C) to 2500<sup>o</sup>F (1371<sup>o</sup>C) in contact with carbon also formed a protective hydrogen barrier. However, a surface network of intergranular carbides formed during carburization and subsequent heat treatment in hydrogen, and this carbon penetration caused a fairly low bend ductility (30<sup>o</sup> bend angle) following hydrogen exposure.

Many of the coatings were not adequate hydrogen barriers because of cracking in the intermetallic coatings and/or incomplete adherence of the coating to the substrate. It was observed that complete adherence was necessary for a coating to be an effective hydrogen barrier.

Fidelle et al. (Ref. 79) evaluated a series of coatings for protecting high-strength steels from hydrogen embrittlement. Uncoated disks of the steels were burst with hydrogen at room temperature. The effectiveness of the protective coatings was evaluated by subjecting the disks on the coated side to a

## CHAPTER 9. PREVENTIVE MEASURES

Nearly all of the high-strength metallic materials investigated have been found to be embrittled when exposed to high-pressure hydrogen. Thus, there is a severe limitation on the combination of properties for metals that can be used in highly stressed structures in contact with high-pressure hydrogen. If existing high-strength alloys are to be used to their full potential in hydrogen, it is necessary that methods of prevention of hydrogen-environment embrittlement be established.

Two basic methods by which this embrittlement can be prevented are the use of protective coatings and the addition of inhibitors to the hydrogen. Despite the importance, the literature is quite limited regarding methods for preventing embrittlement.

### Coatings

Most of the published literature on hydrogen barrier coatings deals with the permeability of hydrogen through various metals and nonmetallic compounds. Generally, those metals with low hydrogen solubilities and covalent and ionic-bonded materials, such as oxides and carbides, have low hydrogen permeabilities. The aluminum and silicon intermetallic compounds also have been found to be hydrogen barriers. The available data (Ref. 75 through 77) indicate that the following materials have low hydrogen permeabilities in order of increasing permeability: aluminum oxide (lowest permeability), tungsten, gold, various glasses, tungsten and molybdenum silicides, molybdenum, nickel aluminide, aluminum Solaramic enamel, copper, platinum, and nickel.

TABLE 26

CHARACTERISTICS OF COATINGS AS HYDROGEN BARRIERS (Ref. 37 and 78)

FROM 800° TO 1500°F\*

Coating	Substrate			
	B-66	Ta-10W	Tantalum	Columbium
Oxidized Surface	Poor	Good	--	--
Anodized Surface	Poor	Poor	--	--
Carburized Surface	Excellent	Poor	--	--
Copper Strike-Nickel Strike-Gold Electrolytic Deposition	--	Good	--	--
Ni(0.001") W(0.0005-0.002") Electrolytic Deposition	Poor	Poor	--	--
Tungsten (Vacuum Deposited)	Promising	Poor	--	--
Tungsten (Vapor Deposited)	Excellent	Excellent	--	--
Platinum	Poor	Poor	--	--
Aluminized (Los Angeles Div.)	Promising	Poor	--	--
Aluminized-Siliconized Surface	Poor	Poor	--	--
Aluminized (Atomics Int'l.)	Poor	Promising	--	--
Tin-Aluminum R-505 Sylcor Coating	Excellent	Excellent	Excellent	--
Silver-Silicon R-508 Sylcor Coating	--	--	--	Excellent
Siliconized	Poor	Promising	--	--
W (Vacuum Deposited) and Siliconized	Poor	Promising	--	--

\*Barriers evaluated by measuring hydrogen absorbed in specimen substrate. Coating resistance ranked as follows:

Excellent: essentially no hydrogen absorption at 800°F heat treatments

Good: measurable hydrogen absorption but the amount absorbed would not be expected to appreciably affect the mechanical properties

Promising: the amount of hydrogen absorbed considerably less than would be absorbed without the coating (without improvement, the coating would probably not be an adequate barrier)

Poor: no significant reduction in hydrogen absorption due to the coating

hydrogen pressure which would lead to immediate failure in the absence of the coating. The effectiveness of the coatings was evaluated by observing the time to failure. The influence of surface conditions on embrittlement was also evaluated. It was found that a rough surface accentuated embrittlement, and that surface compression by shot peening decreased embrittlement.

Fidelle and co-workers found that protection from high-pressure hydrogen was obtained with gold, aluminum, cadmium, and, to a lesser extent, tin, but not with nickel, zinc, chromium, or copper. Rupture of the protected disks occurred after several months' exposure and after absorption of approximately 1-ppm hydrogen in the steel.

Fidelle et al. (Ref. 79) assumed that the failure of the coated disks was caused by an internal-hydrogen embrittlement delayed failure mechanism. It is possible, however, that the time delay was that needed to obtain sufficient quantities of hydrogen at the coating/substrate interface to cause hydrogen-environment embrittlement.

The disks that were uncoated or coated with a nonprotecting coating failed during application of pressure or soon after the pressure was established. Coatings were not protective if they contained microscopic porosity and lacked good adherence. The nickel coating was ineffective because it was embrittled by high-pressure hydrogen. Chromized coatings were evaluated because of the protective chromium oxides. The chromized surfaces were brittle, however, and failure occurred at hydrogen pressures about 1/2 the hydrogen burst pressure of uncoated disks.

The Sylcor R-505 tin-aluminum and vapor-deposited tungsten coatings (which, as indicated above, are barriers to hydrogen) were further evaluated by Walter et al. (Ref. 37 and 78) to determine their effectiveness for preventing embrittlement of B-66 and Ta-10W during tensile testing in hydrogen. Coated sheet (0.003-inch thick) tensile specimens were exposed to flowing hydrogen at 14.7-psia pressure. When the test environment and temperature had been established, a tensile stress of 50 percent of the room temperature yield strength was applied. This stress was maintained for 30 minutes, then the specimens were tensile tested to failure. The results indicated that the Sylcor R-505 tin-aluminum coating was not particularly effective for preventing embrittlement at room temperature and 400°F. The change of hydrogen barrier characteristics at 400°F was associated with the 442°F tin-aluminum eutectic temperature. Below that temperature, the coating was not self-healing to cracks present in the aluminide intermetallic diffusion zone. These cracks may have formed during application and solidification, because cracking and absorption of hydrogen occurred at ambient temperature even in undeformed specimens.

Similar tensile tests were performed at room temperature on vapor-deposited tungsten-coated B-66 and Ta-10W specimens. The tungsten coating was not ductile at this temperature, as evidenced by flaking of the coating during tensile deformation and, as a result, this coating also was not protective.

Experiments are being conducted at Rocketdyne for developing a technique to protect electroformed nickel during ambient-temperature exposure to 1200- and 7000-psig hydrogen. The results indicate that copper and gold coatings prevent embrittlement of unnotched specimens tensile tested in these hydrogen environments. The coatings, however, gave limited protection to notched specimens.

The investigations that have been performed to prevent embrittlement by gaseous hydrogen indicate that protective coatings must have the following characteristics:

1. Low hydrogen permeability
2. Nonporous, i.e., free of defects
3. Completely adherent to the substrate
4. Ductile or self-healing

Coatings that have shown the most potential for preventing hydrogen-environment embrittlement are copper, gold, cadmium, and perhaps the Sylcor R-508 silver-silicon coating and, for elevated-temperature service, the Sylcor R-505 tin-aluminum coating.

#### Impurity Additions to Hydrogen

Hofmann and Rauls (Ref. 42) performed a series of tests to evaluate the influence of air, nitrogen, oxygen, and argon on embrittlement by gaseous hydrogen. The tests were performed at ambient temperature on CK 22, a 22-percent carbon, plain carbon steel in 1470 psia hydrogen.

Their results are shown in Fig. 71 and 72. Additions of argon and purified nitrogen to hydrogen did not reduce embrittlement. However, the addition of 5-percent nitrogen (not shown in Fig. 71), which was not prepurified, partially eliminated embrittlement. It was suggested that oxygen impurities in the nitrogen were responsible for the embrittlement reduction. The minimum oxygen content needed to initiate reduction of embrittlement by the hydrogen environment was about  $10^{-4}$  volume percent (1 ppm) and embrittlement was completely eliminated by 1-percent oxygen.

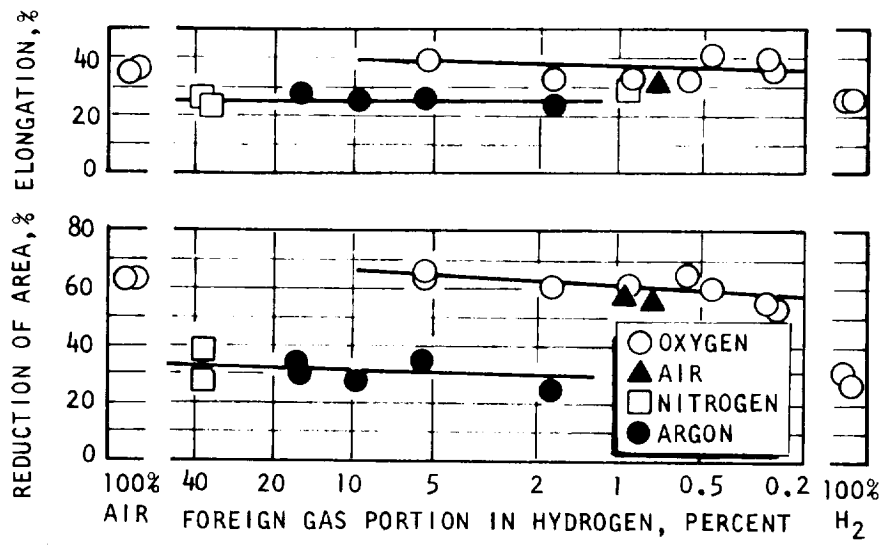


Figure 71. Effect of trace impurities in hydrogen under 100-atm partial pressure on the elongation and reduction in area of CK 22 N steel.

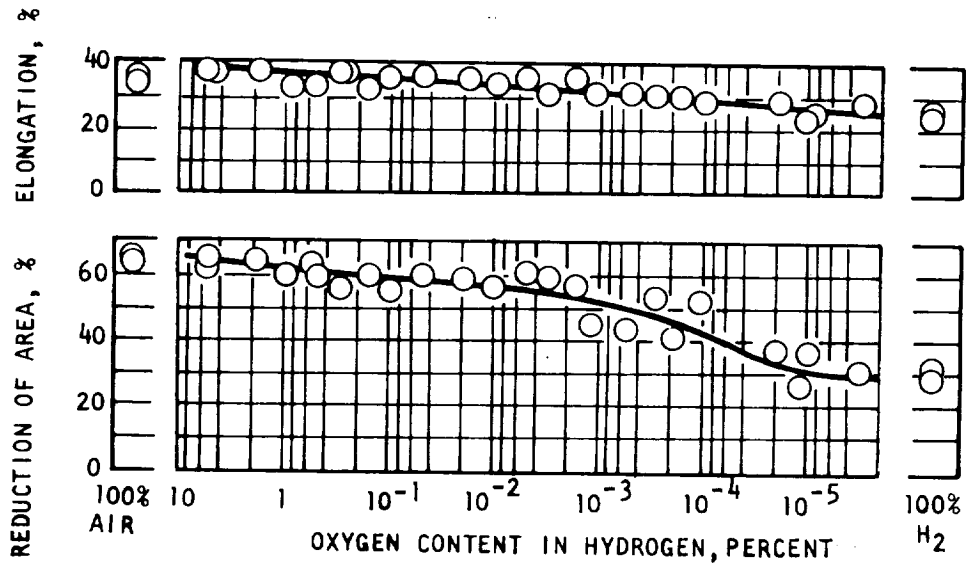


Figure 72. Effect of oxygen additions to hydrogen under 100-atm partial pressure on the elongation and reduction in area of CK 22 N steel.

At the other extreme, Walter and Chandler (Ref. 7) showed that measurable reductions in strength and ductility of notched high-strength steels and nickel-base alloys occurred during tensile tests conducted in 10 000-psig helium containing 44-ppm (0.44-psi) hydrogen. Thus, hydrogen-environment embrittlement is a function of the partial pressure of the hydrogen and is not affected by dilution with inert gases.

In a qualitative manner, investigators have observed that hydrogen-environment embrittlement is reduced when impurities are present in the hydrogen environment. Williams and Nelson (Ref. 31) have performed tests in low-pressure ( $\leq 14.7$  psia) hydrogen on iron, nickel, and titanium-base alloys and have observed that impurities affect the degree of embrittlement of titanium alloys more than the other two. Similarly, Walter and Chandler (Ref. 7) observed that embrittlement of Ti-6Al-4V during tensile testing in 10 000-psig hydrogen will occur only if the test cells are evacuated and purged several times prior to testing. On the other hand, purging by pressurization/depressurization without evacuation is sufficient to obtain near-maximum embrittlement of iron and nickel-base alloys by 10 000-psig hydrogen (see Chapter 5, Test Procedures).

Hydrogen-environment embrittlement of high-strength steels appears to be least influenced by hydrogen impurities. Sawicki and Johnson (Ref. 80) found that embrittlement of high-strength steels by hydrogen at 14.7-psia pressure is not influenced by oxygen contents of less than 200 ppm. This relatively high oxygen contamination level suggests that the inhibiting influence of oxygen is a function of its absolute partial pressure regardless of the total pressure of the system. That is, the higher the hydrogen pressure, the less the oxygen content required to decrease or eliminate the embrittling influence of hydrogen.

## CHAPTER 10. DISCUSSION

### General

As described in previous chapters, a wide variety of metals and alloys are embrittled by hydrogen environments. The embrittlement increases with increasing hydrogen pressure and occurs over a range of temperatures, but is most severe in the vicinity of room temperature. The general characteristics of hydrogen-environment embrittlement are: (1) the effect is one of embrittlement while in the hydrogen environments; (2) it is a surface effect; and (3) it is an immediate effect.

The elastic properties, yield strength and, in many cases, the ultimate tensile strength of unnotched specimens are the same in hydrogen as in air or inert environments. The most significant effects of the hydrogen environments are on tensile ductility, notch strength, and crack behavior. More precisely, the effect of the hydrogen environment is to embrittle the surface. The embrittled "surface" may be the immediate surface or a surface layer of some finite but limited thickness. The metal surface in hydrogen cannot undergo plastic deformation to the same degree as it can in air or inert environments or, for that matter, as can the interior of the metal whose surface is in contact with hydrogen. When a susceptible metal is stressed in tension in hydrogen to some critical amount of plastic deformation, the surface fractures, i.e., a surface crack forms, while the interior of the metal is still capable of undergoing considerable additional deformation. This surface cracking provides some of the most dramatic visual evidence of hydrogen-environment embrittlement. For a susceptible metal, an

existing crack or one formed in the hydrogen environment will propagate at a lower stress intensity and at a more rapid rate in hydrogen than in air or inert environments.

The effect of the hydrogen environment is, for all practical purposes, immediate, i.e., as soon as a susceptible metal is placed in the hydrogen it is embrittled. No hold time in the hydrogen environment is required. This does not mean that failure is immediate. Time to failure obviously will depend on the type and rate of stress application and other factors. But, as soon after exposure to hydrogen as the required critical surface deformation can be applied, the surface will crack. The actual formation of the crack will take a finite but very short time. Also, propagation of any existing crack will be more rapid as soon as the hydrogen contacts the true metal surface. Crack propagation will be complicated by the presence of surface layers, such as self oxides, which will have to be broken to establish the hydrogen/metal contact. The extremely short time required to establish the effect of the hydrogen environment is not inconsistent with the fact that the degree of hydrogen-environment embrittlement is greater at slower strain rates and may not occur at rapid strain rates. This results simply from the fact that the hydrogen embrittling effects of surface crack formation and crack propagation take a certain time and, at very rapid strain rates, they do not have time to occur before failure due to tensile overload.

The amount of hydrogen-environment embrittlement of susceptible metals is highly influenced by the nature of the surface cracking and crack propagation in hydrogen. Extreme embrittlement is associated with the formation of a sharp surface crack(s) and with the crack(s) remaining sharp during propagation. Lesser

degrees of embrittlement are associated with the formation of surface cracks which are blunt and/or the blunting or branching of cracks during propagation.

Hydrogen-environment embrittlement is an environmental effect and occurs only while the metal is in contact with hydrogen. A metal that is exposed to hydrogen but then removed from the hydrogen is not subject to hydrogen-environment embrittlement. It may not seem necessary to dwell on the environmental nature of hydrogen-environment embrittlement, except that the thinking on this embrittlement tends to be colored by the long-standing familiarity with, and the massive literature on, embrittlement resulting from hydrogen charging. Thus, questions continually arise as to the required time of exposure and many tests have been performed on specimens soaked in hydrogen, even at ambient temperatures, but removed before testing. Obviously, exposure to hydrogen can result in other forms of hydrogen embrittlement subsequent to removal from the hydrogen. Depending on the pressure, temperature, and time of exposure, sufficient hydrogen could be absorbed to result in internal-hydrogen embrittlement or the hydrogen could react with the metal to form a hydride or with carbon or oxygen to form high-pressure gas pockets and thus embrittle the metal even after it is removed from the hydrogen. Embrittlement due to previously absorbed hydrogen may add to, or synergistically interact with, hydrogen-environment embrittlement.

#### Tensile Tests

Much of the information on the characteristics of hydrogen-environment embrittlement has come from tensile tests performed on unnotched and notched specimens in hydrogen at ambient temperatures. The results of such tests will be considered in this section to clarify or expand on some of the characteristics noted above and to assist in understanding the meaning of the data obtained from these tests.

As noted, no effects of hydrogen environments at ambient temperatures on elastic properties or yield strength have been found. The deformation capability of the metal surface is lower in hydrogen than in air or inert environments. The interior of the metal is, of course, unaffected by the environment. Thus, as the tensile test proceeds, a critical surface deformation is reached at which the surface fractures in a brittle manner and a surface crack is formed. The most direct evidence for the environmental nature of the embrittlement in hydrogen is the brittle appearance of the fracture at the surface of unnotched and notched specimens (as discussed in Chapter 8, Metallography) and the cracks formed on the surface in deformed regions of unnotched specimens of susceptible metals. In notched specimens, the region of highest deformation is so localized at the base of the notch that surface cracks, other than those resulting in failure, are normally not found.

From the time at which surface cracking begins, the test is no longer a normal tensile test but is a rather complex test of a cracked specimen and this must be considered in assessing the meaning and usefulness of the strength and ductility data obtained from these tests. In alloys that are placed in the extremely embrittled category (Table 8) the first surface crack to form propagates to failure, usually without the formation of additional surface cracks. This crack propagates at some finite rate that is more rapid in hydrogen than it would be in air or an inert environment. Because the test is being conducted as a tensile test, and the load is continuing to be increased, and because of the deepening of the crack, the stress intensity in front of the propagating crack is increasing rapidly during the test. The crack propagates until the remaining area fails due to tensile overload. The final catastrophic failure is a ductile failure apparently unaffected by the hydrogen environment. It can be seen that the

"ultimate tensile strengths" and "ductilities" determined from such tests on unnotched and notched specimens of metals that are extremely embrittled in hydrogen are determined by the load or strain rate, the time (plastic deformation) at which the surface crack is formed, and the rate of propagation of the crack in hydrogen. Thus, these properties are far more sensitive to load or strain rates than are tensile properties determined in air or inert environments.

For alloys in the severely or slightly embrittled categories (Table 8) the first surface crack to form does not propagate to failure. The surface cracks in these alloys are blunt as formed or tend to blunt or branch during propagation in hydrogen. The first surface crack forms, propagates in a brittle manner to some extent, blunts or branches, and stops. A second crack forms and the process continues until, finally, the remaining area has been reduced by the series of surface cracks (e.g., AISI 1020, Fig. 64) so that catastrophic, ductile, tensile overload failure occurs. The properties determined from these tests will be a function of the same factors as listed in the above paragraph for the extremely embrittled metals, and also will be a function of the extent of crack propagation before the crack is stopped by blunting or branching.

From the above discussion, it can be inferred that the different tensile properties will show differing degrees of sensitivity to the hydrogen environments. The degrees of sensitivity in decreasing order are: fracture mode (effects on the appearance of the fracture have been noted when only negligible change of properties occurred), reduction of area of notched specimens, ultimate strength of notched specimens, reduction of area of unnotched specimens, elongation of unnotched specimens, and ultimate strength of unnotched specimens. Only for

metals in the extremely embrittled category is there a reduction of ultimate tensile strength of unnotched specimens in hydrogen. The fact that this property is not affected by hydrogen for metals in the other embrittlement categories simply reflects the relationship noted above between rate of loading (straining) and the time for crack initiation and extension, remembering that crack blunting and branching slow crack growth considerably in these metals. In fact, it appears that in most cases, surface cracks do not form until the ultimate tensile strength is reached, i.e., necking begins.

Although the ultimate strengths and ductilities determined from tensile tests in hydrogen on unnotched and notched specimens of susceptible materials are of limited direct usefulness in design, these tensile tests are valuable as rapid and economical screening tests which provide a good indication of the relative degrees of embrittlement of different metals by hydrogen environments, e.g., as shown in Table 8. For design purposes, the tensile properties determined in hydrogen can be used as a guide for establishing additional safety factors to compensate for hydrogen-environment embrittlement.

#### Surface Cracking in Hydrogen

Metals susceptible to hydrogen-environment embrittlement undergo surface cracking when stressed in hydrogen while nonsusceptible metals do not. The fact that failure of susceptible metals in ambient temperature hydrogen initiates with brittle surface cracking (as discussed in Chapter 8, Metallography) is convincing evidence of the environmental nature of the embrittlement (Ref. 7). Failure initiates with brittle surface cracking in other forms of environmental embrittlement i.e., stress corrosion and liquid metal embrittlement. Without environmental effects, tensile failures initiate inside the metal in the region of highest

triaxial stress and the fracture propagates back to the surface in a ductile manner forming the typical ductile shear lip. This behavior holds even for metals embrittled by charging with hydrogen but tested in air. Troiano (Ref. 6), by optical metallography, and Phillips, Kerlins, and Whiteson (Ref. 81), by electron fractography, showed that in hydrogen-charged specimens tested in air, brittle cracks formed inside the metal and propagated inward in a brittle manner. The fracture finally propagated back to the surface in a ductile manner and shear lips were formed.

All results to date show that surface cracking in hydrogen does not begin until the yield strength has been exceeded and plastic deformation has occurred. No investigations have been reported in the literature of the amount of plastic deformation which takes place before surface cracking begins. It has been postulated (Ref. 52) that a critical plastic deformation is required to initiate surface cracking in hydrogen and the important deformation is, of course, that at the surface.

For hydrogen to cause surface cracking, it seems axiomatic that the hydrogen must be brought to the metal surface and adsorbed, dissociated, and possibly absorbed into the metal surface. If the metal has its normal oxide layer, the hydrogen can reach the actual metal surface either by diffusing through the oxide or by making direct contact with the surface after the oxide is ruptured. Most metal oxides are good barriers to hydrogen and the diffusion of hydrogen through the oxide is rather slow, particularly at ambient temperatures. The amount of hydrogen which could reach the metal surface by diffusion through the oxide is believed too small to cause significant embrittlement for most of the tensile tests performed in hydrogen because of the short exposure times. Thus, it appears reasonable that the critical surface deformation for initiation of

surface cracking in hydrogen is, at minimum, that surface deformation required to rupture the oxide layer so that the hydrogen can contact the metal surface. As discussed in Chapter 8, Metallography, specimens tensile tested in hydrogen after abrasion in hydrogen to remove the oxide layer had a much larger number of surface cracks than specimens abraded in air before testing in hydrogen (Ref. 7). The amount of plastic deformation at crack initiation was not determined. However, a certain amount of plastic deformation of the metal surface still was required before surface cracking initiated in specimens abraded in hydrogen to remove the oxide before beginning the tensile test.

The abrading tests were performed on ASTM A-517, a steel placed in the severely embrittled category. The more numerous surface cracks resulting from abrading in hydrogen did not result in a greater degree of embrittlement as measured by strength and ductility. This is attributed to the crack blunting that occurs in such metals and results in slower crack propagation which then determines the degree of embrittlement more than does crack initiation. It should be cautioned that abrading in hydrogen of the metals in the extremely embrittled category may increase significantly the amount of embrittlement because crack blunting does not occur in these metals.

The surface deformation required for surface crack initiation in hydrogen is undoubtedly a function of many factors. The following are suggested: the metal, metal condition (e.g., heat treatment and fabrication method), the nature of the oxide (how adherent and protective it is, and how able it is to deform with the metal), temperature (effects on metal, oxide, and rate of adsorption, dissociation, and absorption of hydrogen into metal surface) hydrogen pressure (higher pressures may be able to increase rate of movement of hydrogen through protective surface layers and rate of hydrogen adsorption, etc.), prior surface

work hardening, surface preparation (surface finish, chemical polishing, oxide removal, vacuum treatment, etc.), stress concentration factor (required surface deformation may be different at base of notch than on unnotched specimen), strain or load rate, crystal plane exposed, direction of loading relative to direction of prior cold working, and hydrogen purity. There may be others.

#### Crack Propagation in Hydrogen

All metals susceptible to hydrogen-environment embrittlement undergo surface cracking in hydrogen, but the degree of embrittlement in tensile tests is determined by the rate of crack propagation and the tendency for the crack to blunt or branch to reduce the applied stress intensity. Metals in the slightly embrittled category form very rounded cracks which tend to propagate very little, and effects on properties due to hydrogen are small. In fact, in pure titanium, the effect of the very shallow, very rounded surface cracks is so small that a ductile shear lip is formed. Metals in the severely embrittled category form sharp surface cracks, but they tend to branch. The metals in the extremely embrittled category form sharp surface cracks and these tend to remain sharp and not branch as they propagate.

As discussed in Chapter 7, Other Mechanical Properties, crack behavior in hydrogen has been investigated with precracked specimens for a number of metals. In a few instances, the tests were designed to develop valid fracture mechanics data and were performed in high-pressure hydrogen. However, most tests on precracked specimens have been conducted to develop more fundamental information on the effect of various parameters on crack growth rates in hydrogen. Almost all

of these latter tests were performed in hydrogen at pressures near 14.7 psia and below and at temperatures near room temperature. As to be expected, crack growth rates were considerably faster in hydrogen than in air or inert environments for materials classified from tensile tests as extremely or severely embrittled (Table 8). Crack behavior of an aluminum alloy and a copper alloy was found to be essentially unaffected by hydrogen environments, which is consistent with the negligible embrittlement found for aluminum- and copper-base materials from tensile tests in hydrogen.

The fracture toughness parameter,  $K_{IC}$ , is generally considered to be a property of a given material and not affected by the environment, including hydrogen environments. Direct evidence that  $K_{IC}$  is not affected by hydrogen environments, particularly high-pressure hydrogen environments, is very limited. From crack growth studies in hydrogen at pressures near 14.7 psia, Sawicki and Johnson for H-11 tool steel (see Appendix) and Williams and Nelson for AISI 4130 steel (Ref. 8) have rather definitive evidence that  $K_{IC}$  is not affected by hydrogen environments at these pressures. Bixler (Ref. 28) conducted tests on surface-flawed Inconel 718 and Ti-5Al-2.5Sn ELI specimens in 1400-psig hydrogen at ambient temperatures, and concluded that  $K_{IC}$  was not affected by the environment. However, the evidence is somewhat ambiguous since valid  $K_{IC}$  values were not obtained. Thus, it is believed that additional experiments are required to determine if  $K_{IC}$  is affected by high-pressure hydrogen environments. A program including such tests is in progress (see Appendix). The definition of  $K_{IC}$  is important in this respect. A  $K_{IC}$  determined using the secant intercept method may well be affected by a high-pressure hydrogen environment and the time to perform the  $K_{IC}$  test may be more critical in hydrogen than in air or inert environments. In the determination of

$K_{IC}$ , it is important that the precrack be extended by cycling at low stress levels in hydrogen before beginning the  $K_{IC}$  test. Otherwise, the initiation of crack movement in hydrogen would be a function of the rupturing of the surface oxide layer. Extension of the crack by fatiguing in hydrogen brings the added complication that the amount of this extension will be difficult to measure visually or metallographically because there is little difference in the appearance of fracture surfaces produced by tensile loading or fatiguing in hydrogen (see Chapter 8, Metallography).

As expected, considerable effects of high-pressure hydrogen on  $K_{th}$ , the threshold stress intensity for sustained-load flaw growth, have been found. Ratios of  $K_{th}$  in high-pressure hydrogen at 70 F to  $K_{IC}$  in air were shown to be less than 20 percent for both Inconel 718 (Ref. 28 and 62) and Ti-5Al-2.5Sn ELI (Ref. 28). Conversely, this ratio was found to be about 80 percent for the 2219-T6E46 aluminum alloy. Sawicki and Johnson (see Appendix) have found that  $K_{th}$  for H-11 tool steel in hydrogen decreases with increasing pressure for pressures near 14.7 psia. As with  $K_{IC}$  tests, it is important in  $K_{th}$  tests that the precrack be fatigue extended in hydrogen before the start of the  $K_{th}$  test. As an example, if the bolt-loaded modified WOL specimen is used, the stress intensity required to initiate crack movement in air (or even in hydrogen but with the oxide present) may be large enough to lead to specimen failure in the hydrogen. Even if failure does not occur, the crack will extend much further, which leads to a greater probability that the crack will branch from the plane of crack growth which complicates  $K_{th}$  determinations. This is especially true because, in some steels, the tendency for crack branching is greater in hydrogen than in inert environments (Ref. 7).

As noted in Chapter 7, Other Mechanical Properties, crack growth rates have been found to be considerably greater in hydrogen environments, even at very low pressures, than in air or inert environments for various high-strength steels, pure nickel, nickel-base alloys, and titanium-base alloys, but not for a copper-base alloy. These investigations were conducted in almost all cases with hydrogen pressures of 14.7 psia and below, in most cases with sustained rather than cyclic loading, and were designed to develop information on the nature of hydrogen-environment embrittlement and parameters affecting it.

Williams and Nelson (Ref. 8) investigated sustained load, slow crack growth of AISI 4130 steel in hydrogen at pressures below 14.7 psia, and at temperatures from approximately -122 F (-80°C) to 176°F (80°C). They found the crack growth rate to be a function of  $1/T$ , where  $T$  is in °K, to be a maximum near room temperature, and to be a function of  $P_{H_2}^{1.5}$  at higher temperatures and  $P_{H_2}^{0.5}$  at lower temperatures.

Sawicki and Johnson (see Appendix) found a similar temperature relationship for H-11 tool steel. To explain their results, Williams and Nelson developed a hypothesis that a thermally activated chemisorption process is rate controlling for crack growth in hydrogen. Their theory predicts that crack growth rates would be a function of  $P_{H_2}^{0.5}$  at high pressures.

The investigations of Nelson et al. (Ref. 65) on crack behavior of AISI 4130 steel in partially dissociated hydrogen at low pressure showed that the presence of the atomic hydrogen in the environment considerably increased crack growth rates and altered the kinetics. They postulated that the presence of atomic

hydrogen served to bypass the chemisorption rate-controlling process discussed above and the rate-controlling process then became the absorption of the atomic hydrogen into the metal.

#### Effect of Hydrogen Environments on Other Properties

Hydrogen environments most severely degrade the properties of precracked specimens and thus have the large effects on  $K_{th}$  and crack growth rates described in Chapter 7, Other Mechanical Properties. As discussed above, with smooth specimens, the most severe property degradation will occur in tests involving plastic strain. Thus, the considerable reductions of stress-rupture strengths and cycles-to-failure in strain cycling tests in hydrogen are not surprising.

High-cycle fatigue tests in hydrogen have not been reported although some are planned (see Appendix). However, it is expected that the effect of hydrogen environments on high-cycle fatigue will not be as significant. In high-cycle fatigue, the strain per cycle is small, and thus the effect of hydrogen on the number of cycles to crack initiation may be small and the main effect of the hydrogen would be on crack propagation. But generally, in high-cycle fatigue, approximately 90 percent of the time-to-failure is occupied with crack initiation.

#### Metals Susceptible to Hydrogen-Environment Embrittlement

A wide variety of metals, which unfortunately includes almost all of the high-strength structural alloys, are susceptible in some degree to hydrogen-environment embrittlement. Iron, nickel, and titanium and alloys based on these metals and on cobalt have been found to be embrittled by hydrogen environments. Thus, susceptible metals include those with body-centered-cubic, face-centered-cubic, and hexagonal structures. Metals not embrittled are copper and aluminum

and their alloys, and the most stable stainless steels, i.e., those that remain austenitic and do not transform to martensite during deformation.

The only apparent common denominator separating susceptible and nonsusceptible metals is that all metals found to be susceptible to date are transition elements and their alloys. Metals not susceptible are not transition metals, the exception being the austenitic stainless steels. In this regard, it is simply noted that magnetic behavior is associated with transition metals, and the ferromagnetic behavior of iron alloys is not present in the austenitic stainless steels, which thus have lost one of the characteristics of transition metal behavior. The less stable stainless steels tend to partially transform to martensite during deformation and, where martensite forms on the surface, surface cracking occurs in hydrogen (Ref. 46).

Within the group of metals susceptible to hydrogen-environment embrittlement, the degree of embrittlement is not particularly predictable. In general, higher strength alloys are more embrittled than lower strength alloys. However, one of the most embrittled metals is electroplated nickel, as plated. Also, in an investigation of three pressure vessel steels, the lowest strength one, a plain carbon steel, was the most embrittled in tensile tests (Ref. 52). The difference between yield and ultimate strengths was small in the two higher-strength steels, but relatively large in the lower-strength steel. In accord with the earlier discussions of surface cracking, the larger reduction of properties in hydrogen for the lower-strength steel was attributed to the initiation of surface cracks at a stress which was low relative to the ultimate tensile strength.

Different heats and different heat treatments for a given alloy can show significant differences in the degree of embrittlement by hydrogen environments. In the most striking instance, the reduction of notch strength of Inconel 718 in

1000-psig hydrogen at ambient temperatures was 40 percent for one heat-heat treatment combination and only 10 percent for a different heat and heat treatment. There was no obvious compositional or structural difference to which the difference in embrittlement could be attributed, but the less embrittled material did have the higher ductility and notch strength/unnotched strength ratio. In general, for a given alloy, heat treating to a higher strength level results in a greater degree of hydrogen-environment embrittlement.

As noted in the earlier discussion of surface crack formation and propagation, both the nature of the surface crack formed and the way in which it propagates play a crucial role in determining the degree of hydrogen-environment embrittlement of a material. The most extremely embrittled materials form sharp cracks which remain sharp during propagation in hydrogen. Lesser degrees of embrittlement are associated with the initial formation of blunt cracks and with crack blunting or branching during propagation.

#### Effect of Various Parameters on Degree of Hydrogen-Environment Embrittlement

Hydrogen Pressure.— The degree of hydrogen-environment embrittlement increases with increasing hydrogen pressure. However, sizable effects, e.g., increases in crack growth rates, occur in hydrogen at pressures below 14.7 psia. From their investigations of slow crack growth rates of AISI 4130 steel in hydrogen environments at pressures of 14.7 psia and less, and at temperatures near room temperature, Williams and Nelson (Ref. 8) found that the crack growth rates were a function of  $P_{H_2}^{0.5}$  at temperatures below room temperature, and of  $P_{H_2}^{1.5}$  at temperatures above room temperature. From their hypothesis of a

rate-controlling, thermally activated chemisorption process, Williams and Nelson further concluded that crack growth rates are a function of  $P_{H_2}^{0.5}$  at high pressures and/or low temperatures, and a function of  $P_{H_2}^{1.5}$  at low pressures and/or high temperatures.

As discussed in Chapter 6, Tensile Properties, an apparent relationship was found between the tensile properties of ASTM A533-B steel and Inconel 718 in hydrogen and  $P_{H_2}^{0.5}$  (Ref. 47 and 70). This may be explained as follows if one accepts the hypothesis of Williams and Nelson. Tensile tests of susceptible materials in hydrogen are ultimately complex tests of cracked specimens and the properties measured are a function of the rate of testing, the plastic deformation at which surface cracks initiate, and the rate of crack growth. The same rate of testing was used for the tests at the different pressures. If the amount of plastic deformation at which surface cracks initiate is relatively insensitive to hydrogen pressure, which does not appear to be an unreasonable assumption for the oxide-covered specimens, then the measured tensile properties will essentially be a function of crack growth rates and, from Williams and Nelson,  $P_{H_2}^{0.5}$ . Such a relationship may not hold for specimens with a clean metal surface unless the time, i.e., critical plastic deformation, for surface crack initiation is also a function of  $P_{H_2}^{0.5}$  or insensitive to pressure, which seems unlikely.

In tensile tests on electroformed nickel at pressures from 14.7 to 7000 psig, the degree of embrittlement in hydrogen increased with increasing pressure, but was a function not of  $P_{H_2}^{0.5}$ , but more nearly the  $\ln P_{H_2}$ . With either relationship, the increase in the degree of embrittlement with a given increase of pressure is much greater at low pressures than at high pressures.

It has been suggested (Ref. 31) that the effect of hydrogen pressure is more significant for normal surfaces, i.e., surfaces covered with oxide and adsorbed gases than for clean metal surfaces. It may be, especially for clean surfaces, that the effect of pressure will reach a maximum and embrittlement will not increase significantly above a certain high pressure.

Temperature.— There have been only very limited investigations of the relationship between hydrogen-environment embrittlement and temperature. However, all the data obtained to date indicate that the degradation of mechanical properties, e.g., tensile, fatigue, or crack growth rate, by hydrogen environments is a maximum near room temperature. It also appears that the degree of embrittlement decreases more rapidly as the temperature is lowered below room temperature than when it is raised an equivalent amount above room temperature. It should be noted that the hydrogen environments considerably reduce the cycles-to-failure in strain cycling tests at temperatures as high as 1250°F (677°C) (Ref. 61). As discussed earlier, Williams and Nelson (Ref. 8) determined the effect of temperature on the sustained load, slow crack growth rate of AISI 4130 steel in hydrogen at pressures below 14.7 psia and temperatures from approximately -112°F (-80°C) to 176°F (80°C). They found the crack growth rate to be maximum near room temperature and to be a function of  $1/T$  (°K) at lower and higher temperatures. The temperature at which the maximum crack growth rate occurred increased with pressure. A similar relationship between crack growth rate and temperature was found by Sawicki and Johnson (Ref. 80) for H-11 tool steel in a similar temperature/pressure regime. It might be expected that surface crack initiation is a function of temperature, but no investigations have been conducted.

Hydrogen Purity.— The degree to which a metal will be embrittled by a hydrogen environment is a function of the purity of the hydrogen, particularly with regard to oxygen content. Hofmann and Rauls (Ref. 42) found that the minimum oxygen content at which a reduction in the embrittlement of a plain carbon steel by 1470-psig hydrogen occurred was approximately  $10^{-4}$  volume percent (1 ppm) and embrittlement was completely eliminated by 1-percent oxygen. Conversely, Sawicki and Johnson (Ref. 80) found that crack growth rates of H-11 tool steel in 14.7-psia hydrogen were not influenced by oxygen contents of less than approximately 200 ppm. Although comparisons between these two sets of results are somewhat questionable because of the differences in tests performed, the results do suggest that the inhibiting effect of oxygen is more a function of absolute quantity present, i.e., partial pressure, than of the percentage content. Thus, the higher the hydrogen pressure, the lower the percentage oxygen content that will inhibit the hydrogen embrittlement. Such gases as nitrogen and argon (Ref. 42) or helium (Ref. 7) do not inhibit hydrogen-environment embrittlement, so their presence as an impurity in the hydrogen would not affect results. It would be expected that other oxidizing gases, such as  $\text{CO}_2$  and  $\text{H}_2\text{O}$ , would inhibit hydrogen-environment embrittlement, but preliminary indications are that  $\text{H}_2\text{O}$  is not as effective an inhibitor as expected.

Surface Condition.— Because hydrogen-environment embrittlement is a surface effect, the condition of the surface would be expected to affect the degree of embrittlement. Important factors would be surface finish; method of surface finishing, i.e., mechanical or chemical machining, electroplating, swaging, shot

peening, etc.; thickness and adherence of oxide; vacuum treatment; and degree of work hardening. Investigations of the effect of these factors are very limited. Walter and Chandler (Ref. 7) did find that abrading a steel in hydrogen to remove the oxide prior to tensile testing in hydrogen increased the number of surface cracks formed in the necked-down region.

### Mechanism

The mechanism for hydrogen-environment embrittlement may be divided into two areas for discussion: (1) the mechanism(s) for the transfer of hydrogen from the gas phase to the metal at the location and in the form in which it can embrittle the metal, and (2) the mechanism by which the hydrogen actually causes the metal to be embrittled. The first of these, which will be designated as the transfer mechanism, is at present better understood than the second, which will be designated as the embrittlement mechanism. It is generally agreed that hydrogen-environment embrittlement is a surface or near-surface effect. If the embrittlement results from penetration of hydrogen into and embrittlement of a surface layer, the depth of that layer is very small.

In the discussion, hydrogen-environment embrittlement and internal-hydrogen embrittlement will be covered. These two terms refer only to the source of the hydrogen for embrittlement. In the first case, the hydrogen comes from the environment and, in the second, the hydrogen is dispersed through the metal but may have to be concentrated in certain locations for embrittlement to occur. The transfer mechanisms are obviously not identical for the two types of embrittlement. However, the actual embrittlement mechanism may be the same, and many investigators have found it attractive to so postulate such a unifying mechanism.

The transfer of hydrogen to or into a metal will involve molecular hydrogen adsorption, which may be separated into physisorption and chemisorption, dissociation of molecular hydrogen to atomic hydrogen, and possibly absorption of the atomic hydrogen into the surface of the metal and diffusion into the metal to the extent necessary. As discussed previously, Williams and Nelson (Ref. 8) have concluded that chemisorption of hydrogen is the rate-controlling transfer mechanism for embrittlement in a hydrogen atmosphere. By studying crack growth rates using dissociated hydrogen, thereby eliminating the controlling adsorption reaction  $H_2 \rightarrow 2H^+ + 2e^-$ , they concluded that embrittlement was controlled by absorption of hydrogen into the metal surface. For internal-hydrogen embrittlement, the movement of hydrogen through the metal has been shown to be the rate-controlling process. Thus, for hydrogen-environment embrittlement, adsorption of hydrogen has been postulated to be the rate-controlling transfer mechanism while, for internal-hydrogen embrittlement, the movement of hydrogen may be rate controlling; this does not, however, in any way determine the final embrittlement mechanism.

Bulk diffusion cannot be the transfer mechanism for the rapid embrittlement encountered in hydrogen environments unless the embrittlement mechanism can be operative in the surface layer. Williams and Nelson (Ref. 8) have estimated that the observed crack growth rates of 4130 using TDCB specimens in gaseous hydrogen are two to five orders of magnitude faster than the bulk diffusion rates to be expected, and they concluded that bulk transport cannot be a necessary step in gaseous hydrogen environment. It is evident, therefore, that embrittlement is not due to the buildup of hydrogen in solution at a significant distance ahead of the propagating crack. Walter, et al. (Ref. 9) have estimated

the rate of movement of hydrogen in the metal as being faster than the rate of propagation of cracks in tensile tests of unnotched specimens in 10 000-psig hydrogen. If, however, embrittlement is confined to a surface layer, diffusion in the surface layer (which can be considerably more rapid than bulk diffusion) could allow the buildup of sufficient hydrogen in front of the crack to cause embrittlement.

The exact mechanism by which hydrogen embrittles a metal has been the subject of many investigations. To date, no embrittlement mechanism has been widely accepted for the actual embrittlement process. Some of the failure mechanisms that have been suggested for internal-hydrogen embrittlement are:

1. Planar-pressure theory
2. Addition of hydrogen electrons to the 3-d band of the metal
3. Lowering of surface energy by hydrogen adsorption

The pressure theory, as originally proposed by Zappfe (Ref. 82) and modified by many investigators, e.g., Tetelman and Robertson (Ref. 83), cannot be applicable to hydrogen-environment embrittlement since hydrogen pressures of less than 1 atmosphere have been found to increase the rate of crack propagation. For specimens totally immersed in a hydrogen environment, the hydrogen present in internal voids cannot have pressures greater than the applied hydrostatic pressure. Therefore, the external pressure must be at least equal to the pressure in the gas pockets, and the pockets would have no tendency to enlarge due to a pressure differential.

Troiano (Ref. 6) has suggested that for iron-base alloys the increase of energy due to the presence of hydrogen results from the addition of electrons from the hydrogen atoms to the 3-d electron bands. The repulsive forces determining the interatomic distances in transition metals are due to overlapping of these 3-d electron bands; increasing the number of electrons in the 3-d band would increase the repulsive forces and thus lower the fracture resistance of the metal. Such a mechanism may be applicable to both types of hydrogen embrittlement since transition metals are observed to be the most susceptible to each type. Nelson, et al. (Ref. 65) have related embrittlement to the solubility of hydrogen in the metal surface, and thus a failure mechanism based on Troiano's suggestion may be applicable.

Petch and Stables (Ref. 84) and Petch (Ref. 85) suggested that the failure mechanism occurs by lowering the surface energy of internal cracks by adsorption of hydrogen onto the crack surface and lowering the surface energy of the crack. This theory is an extension of the Griffith crack theory for fracture of brittle materials. Petch (Ref. 85) calculated the energy to initiate fracture in hydrogen-charged and hydrogen-free steels, and found that the energy difference was comparable with the energy of hydrogen adsorption. Walter, et al. (Ref. 9) and Williams and Nelson (Ref. 8) have postulated that this embrittlement mechanism can also be applicable to hydrogen-environment embrittlement wherein the energy of adsorption of hydrogen at the crack tip compensates for the energy required to form a new surface.

Thus, the embrittlement mechanism by which final failure occurs may be the same for hydrogen-environment embrittlement as for internal-hydrogen embrittlement. There is no evidence to indicate that the failure mechanism must be

different, and none to indicate they are the same. One difference that must be explained by any mechanism is why some metals are more embrittled by hydrogen environments than by internal-hydrogen charging. Nickel is a good example of this. Nickel-base alloys are among the most embrittled by hydrogen environments, while they are generally not subject to internal-hydrogen embrittlement when charged to higher hydrogen contents than can be absorbed from the embrittling hydrogen environment. Table 27 shows a comparison between the susceptibilities to each type of hydrogen embrittlement for a number of alloys (Ref. 9).

TABLE 27  
 SUSCEPTIBILITY OF VARIOUS MATERIALS TO INTERNAL-HYDROGEN  
 EMBRITTLEMENT AND HYDROGEN-ENVIRONMENT EMBRITTLEMENT

Degree of Embrittlement	Internal Hydrogen Electrolytically Charged (Ref. 12)	Gaseous Hydrogen Environment (Ref. 9)
Extreme	H-11 Tool Steel 17-4 PH Stainless Steel	18 Ni(250) Maraging Steel AISI Type 410 Stainless Steel H-11 Tool Steel 17-7 PH Stainless Steel René 41 Inconel 718
Severe	AM 355 Stainless Steel 18-Ni(250) Maraging Steel AISI E 8740	HY 100 Nickel 270
Slight	17-7 PH Stainless Steel	AISI Type 304L Stainless Steel
Negligible	Inconel 718 René 41	A-286 Super-Strength Alloy AISI Type 316 Stainless Steel

Internal-hydrogen embrittlement can be caused by a small amount of hydrogen in high-strength steels. Figure 73, from Farrell and Quarrel (Ref. 86), shows the effect of hydrogen concentration on the reduction of area (R.A.) for a number of steels with various initial ultimate tensile strengths. Walter and Chandler (Ref. 52) and Benson, et al. (Ref. 46) have shown that hydrogen-environment embrittlement occurs with final hydrogen concentrations as low as 0.1 to 1.0 ppm. Data for the R.A. of unnotched specimens tested in 10 000-psig helium and hydrogen at room temperature are also plotted in Fig. 73. It can be observed that the high-strength steels are quite affected by internal-hydrogen contents of less than 1.5 ppm, while lower-strength steels are not as affected at this hydrogen concentration. The data for specimens tested in 10 000-psig helium and hydrogen at room temperature show that the R.A. is significantly affected for both high- and low-strength steels by external hydrogen. Walter and Chandler (Ref. 7), Hoffman and Rauls (Ref. 41), and Ansell, et al. (Ref. 50 and 51) have shown that a hold period in hydrogen (either at zero hold stress or at a tensile hold stress) at room temperature prior to testing in hydrogen has no effect on the amount of embrittlement, indicating that no significant pickup of hydrogen occurs.

As shown in Fig. 73, embrittlement in the environment is much greater than can be explained on the basis of internal-hydrogen embrittlement because of the very small quantities of hydrogen that can be absorbed from these environments. It has generally been found that the hold time in the hydrogen environment has no effect on the degree of embrittlement. This is not to say there cannot be synergistic effects between hydrogen-environment embrittlement and internal-hydrogen embrittlement resulting from previously absorbed hydrogen or absorption of hydrogen prior to exposure to the hydrogen environment.

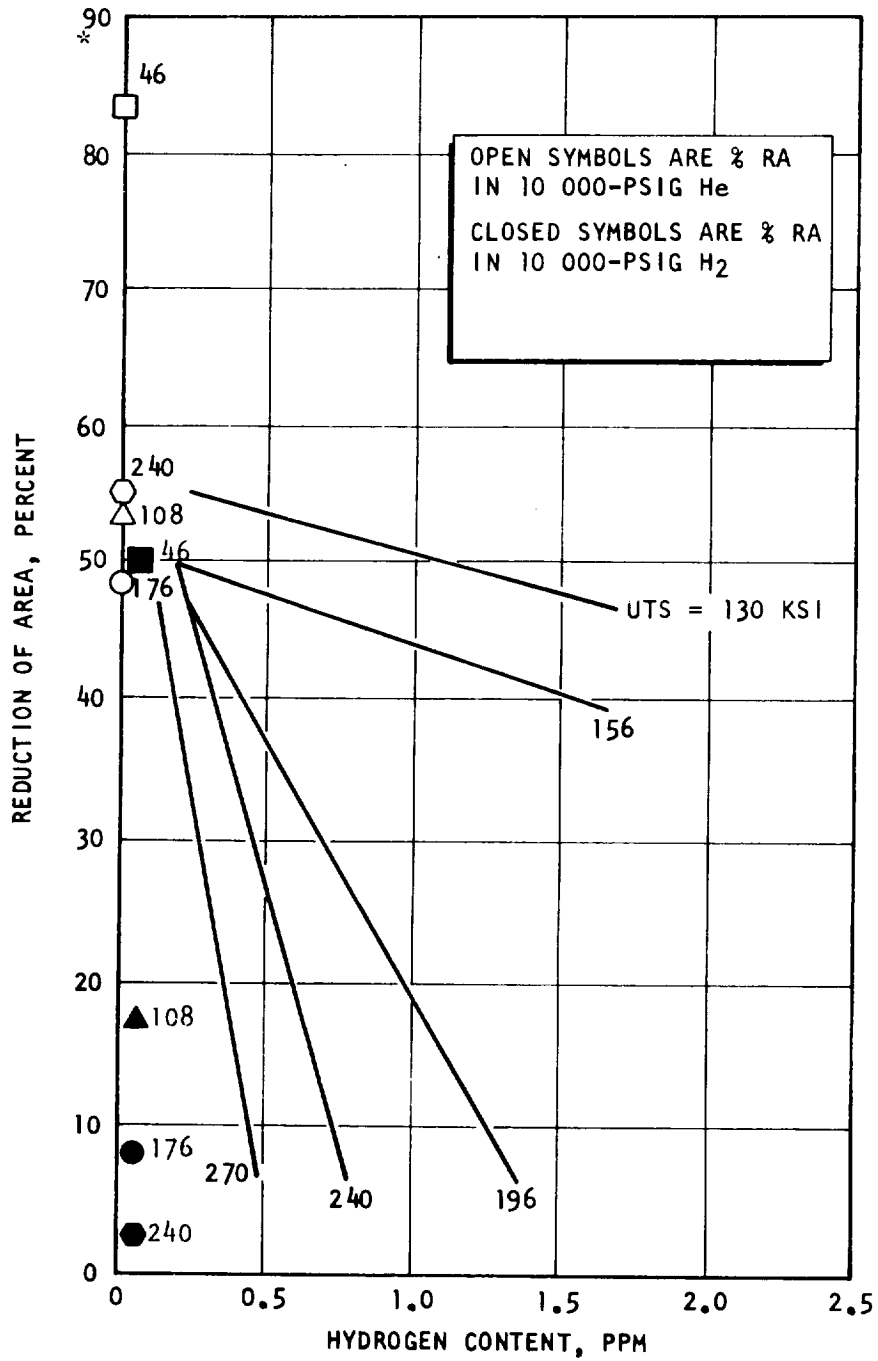


Figure 73. Effect of hydrogen content on the tensile ductility of high-strength steel (hydrogen content after exposure to 10000-psig hydrogen is approximately 0.1 ppm).

In summary, the rate controlling transfer mechanism in hydrogen environments is probably the adsorption of hydrogen onto the metal surface. In internal-hydrogen embrittlement, it has been concluded to be the movement of hydrogen through the lattice to concentrate the hydrogen in front of a crack. In both types of embrittlement, the failure mechanism has been hypothesized only, and no definite conclusions can be reached as to whether the failure mechanism is the same or different for hydrogen-environment embrittlement and internal-hydrogen embrittlement. Also, it is not possible to establish whether hydrogen-environment embrittlement is simply a surface effect or if it involves absorption of hydrogen into the metal to some limited depth.

## CHAPTER 11. SUMMARY

A wide variety of pure metals and alloys has been found to be susceptible to hydrogen-environment embrittlement. The embrittlement is an environmental effect so that, as soon as a susceptible metal comes in contact with the hydrogen environment, the surface of the metal behaves in a brittle manner once a certain amount of plastic deformation has occurred. Elastic properties, yield strength, and, in many cases, the ultimate tensile strength are not affected by the hydrogen environment. The most significant effects of the hydrogen environment are on tensile ductility, notch strength, and crack behavior.

Four categories of embrittlement, based on the results of tensile tests conducted in 10 000-psig hydrogen, have been established for classifying this susceptibility of metals to hydrogen-environment embrittlement. These are:

1. Extreme embrittlement: Embrittlement is characterized by a large decrease of notch strength and ductility and some decrease of unnotched strength in 10 000-psig hydrogen. High-strength steels and high-strength nickel-base alloys are in this category.
2. Severe embrittlement: Embrittlement is characterized by a considerable reduction of notch strength and ductility, but no reduction of unnotched strength. The majority of the metals tested are in this category, including ductile lower-strength steels, Armco iron, pure nickel, and the titanium-base alloys.
3. Slight embrittlement: Embrittlement is characterized by a small decrease of notch strength and a small or negligible decrease of unnotched ductility. The nonstable AISI type 300 series stainless steels (AISI types 304L and 305), beryllium-copper, and commercially pure titanium are in this category.

4. Negligible embrittlement: The aluminum alloys, stable austenitic stainless steels, A-286 (a precipitation-hardened austenitic stainless steel), and OFHC copper are in this category.

The effects of hydrogen environments on the tensile properties of metals have been investigated as a function of the following test variables:

1. Deformation Rate--The degree of embrittlement decreases with increasing rates of deformation. There are indications that no embrittlement is observed at sufficiently fast testing speeds.
2. Hydrogen Pressure--The degree of embrittlement increases with increasing hydrogen pressure, but can be considerable in some alloys even at 14.7-psia pressure.
3. Notch Severity--The hydrogen-environment embrittlement of low-alloy steels is a function of stress concentration factor ( $K_t$ ), increasing with  $K_t$  at low  $K_t$ , passing through a maximum for  $K_t \approx 6$  to 9, and then decreasing with  $K_t$  for higher  $K_t$  values.
4. Exposure Time in Hydrogen--Most investigations indicate that the degree of hydrogen-environment embrittlement is essentially independent of hold time or stress for both notched and unnotched specimens.
5. Temperature--Hydrogen-environment embrittlement is greatest in the vicinity of room temperature. The embrittlement decreases rapidly with decreasing temperature, and less rapidly with increasing temperatures. Embrittlement has been observed at temperatures as high as 1250°F. Crack growth measurements indicate that the rate of crack growth is proportional to  $1/T$ , where T is the absolute temperature.

6. Weldments--The effects of hydrogen on the mechanical properties of metals may vary appreciably between the parent metal, heat-affected zone, and weld metal. The weld zone and the heat-affected zone may be more affected or less affected than the parent metal.

Low-cycle fatigue and fracture toughness measurements also have been performed in hydrogen environments. Cyclic crack propagation rates are considerably increased by hydrogen environments. As an example, the 1000-cycle, ambient temperature fatigue strength of precracked, notched ASTM A533-B and ASTM A-517 specimens was reduced by about 65 percent in 10 000-psig hydrogen. Tests conducted on Inconel 718 and Ti-6Al-4V (STA) indicate that the effect of hydrogen on the fatigue strength is also a maximum at room temperature and decreases with decreasing temperature. Very low hydrogen pressures also can increase the rate of cyclic crack growth. For example, measurable increases of cyclic crack growth rates were observed in titanium at hydrogen pressures as low as 1 torr.

Hydrogen can increase the sustained as well as cyclic crack growth rate. The sustained crack growth rate in 4130 steel was considerably increased by hydrogen at 14.7-psia pressure. The threshold stress intensity,  $K_{th}$ , which is the minimum stress intensity required for sustained flaw growth, also can be considerably reduced by hydrogen environments. For example,  $K_{th}$  of Inconel 718 in 5200-psig hydrogen was determined to be 22 ksi  $\sqrt{\text{in.}}$  compared to a  $K_{Ic}$  of 150 ksi  $\sqrt{\text{in.}}$  in air.

Two methods for the prevention of hydrogen-environment embrittlement are the use of protective coatings and the addition of inhibitors to hydrogen. Coatings that have shown the most potential for preventing hydrogen-environment embrittlement are copper, gold, cadmium, and perhaps Sylcor R-508 (a silver-

silicon coating) and Sylcor R-505 (a tin-aluminum coating) for elevated-temperature service. The degree of hydrogen-environment embrittlement decreases with the amount of oxygen in the hydrogen. For example, the addition of 1-percent oxygen has been shown to prevent embrittlement of a 0.22-percent carbon steel by high-pressure hydrogen.

Metallographic studies have shown that fracture initiation in high-pressure hydrogen occurs at the metal surface. The fracture can be transgranular or intergranular. The surface-cracking characteristics are similar for metals in the same embrittlement categories regardless of base metal, crystal structure, or hydrogen adsorption capacities. The appearance of the brittle surface region was found to be independent of hydrogen pressure, but the depth of the brittle region was a linear function of the square root of hydrogen pressure.

The mechanism by which gaseous hydrogen embrittles metals has not been established, but there are certain aspects regarding it that are known. Basically, hydrogen-environment embrittlement is believed to be a surface or near-surface phenomenon. It has been shown that fracture initiation in hydrogen occurs at the surface and after a certain amount of plastic deformation has occurred.

## CHAPTER 12. RECOMMENDATIONS

This chapter contains recommendations for those concerned with the application of structural materials in contact with hydrogen and, in particular, with high-pressure hydrogen.

In designing structures for service in hydrogen, the use of materials embrittled by hydrogen should be avoided. However, this will be possible only in a limited number of structures and, in general, it will be necessary to use materials affected to some degree by hydrogen. The method used for factoring the environmental effect into the design will depend on the loading characteristics of the structure. In some cases, the degradation of a given mechanical property, e.g., low-cycle fatigue, can be used for establishing the design. However, the problem is more difficult for designs based on tensile properties.

As discussed in Chapter 10, Technical Discussion, tensile tests in hydrogen are actually complex crack propagation tests, and it is difficult to use "tensile properties" from such tests in normal design procedures. However, in some cases, it may be appropriate to use degradation of properties, i.e., reduction of notch strength, to establish a safety factor to compensate for the effects of the hydrogen environment. Hydrogen-environment embrittlement (excluding high-cycle fatigue) should not occur if one can truly design so that there is no material yielding and the design is based on the yield strength rather than on the ultimate strength of the material.

The most significant effect of environmental hydrogen on metals involves crack initiation and brittle crack propagation. Therefore, fracture mechanics, which is the study of crack behavior, is an attractive approach in designing for

service in hydrogen environments. The useful life of the structure can be predicted from proof tests in air, which measure the maximum existing flaw size, and from the threshold stress intensity ( $K_{th}$ ) for crack growth and/or cyclic flaw growth data obtained from tests conducted in hydrogen environments.

It has been shown that most structural alloys are embrittled by hydrogen environments; therefore, those alloys (particularly those based on transition metals) that have not been tested in hydrogen should be assumed to be susceptible to hydrogen environment embrittlement.

Good design practices are especially important for the design of structures for service in hydrogen environments. Notches or stress concentrations should be reduced and, if possible, eliminated; surface finishes should be tightly controlled; and all surface material defects removed. Inspection techniques should be thorough and periodic to determine if sustained or cyclic flaw growth is occurring after the structure has been placed in service.

It is evident that only properties measured in hydrogen environments should be used in designing structures for use in hydrogen. The apparatus and procedures for hydrogen environmental testing have been described in Chapter 5, Test Procedures. The hydrogen used during the tests should have the same purity as the highest hydrogen purity the structures would see in service. Prior to conducting the tests, the test system should be thoroughly purged by evacuation and pressurization/depressurization cycling. Removal of adsorbed gases from the test specimen simulates the condition of structures that will be exposed to high-purity hydrogen or to flowing hydrogen. The cracked specimens used for fracture mechanics testing should be cycled at low stress intensity amplitudes to extend

the cracks in hydrogen prior to performing the tests. This is to ensure that a clean crack will be exposed to hydrogen so that the true crack behavior in hydrogen will be measured.

In some instances, it may be possible to prevent embrittlement of a susceptible material by coatings or by inhibition (impurity additions to the hydrogen environment). Investigations or inhibition have been limited. If coatings are used, extreme care must be taken to ensure that the coatings remain intact because hydrogen will initiate and propagate cracks when contact is made with the metal surface. Vented, stainless-steel liners have proved to be effective for the protection of structural steels in high-pressure hydrogen storage vessels.



## REFERENCES

1. Lessing, L.: Fortune, May 1961, 152.
2. Nelson, G. A.: Proc. Am. Pet. Inst., 29M(III), 1949, 163.
3. Bentle, G., and W. T. Chandler: Effects of Hydrogen Environments on Columbium and Tantalum Alloys, Rocketdyne, a division of North American Rockwell Corporation, Canoga Park, California, AFML-TR-66-322, Part II, Wright-Patterson AFB, Ohio, September 1968.
4. Dann, A. W., F. J. Shortsleeve, and A. R. Troiano: Trans. AIME, 203, 1955, 895.
5. Frohberg, R. P., W. J. Barnett, and A. R. Troiano: Trans. ASM, 47, 1955, 892.
6. Troiano, A. R.: Trans. ASM, 52, 1960, 54.
7. Walter, R. J., and W. T. Chandler: Effects of High-Pressure Hydrogen on Metals at Ambient Temperature, Final Report, Contract NAS8-19, NASA, MSFC, Huntsville, Alabama, Rocketdyne, a division of North American Rockwell Corporation, Canoga Park, California, Report R-7780-1, 2, 3, 1969.
8. Williams, D. P., and H. G. Nelson: Met. Trans., 1, 1970, 63.
9. Walter, R. J., R. P. Jewett, and W. T. Chandler: Mater. Sci. Eng., 5, 1969/70, 99.
10. Lounamaa, K., and G. Braggstrom: J. Iron Steel Inst., (London), 203, 1965, 702.

11. Schaller, F. W., and A. R. Troiano: Hydrogen Embrittlement in Face-Centered Cubic Alloys of Nickel, ARL-133, Wright-Patterson AFB, Ohio, December 1961.
12. Groenveld, T. P., E. E. Fletcher, and A. R. Elsea: A Study of Hydrogen Embrittlement of Various Alloys, Summary Report, Contract NAS8-20029, NASA, MSFC, Huntsville, Alabama, 1966.
13. Tardif, H. P., and H. Marquis: High Pressure Hydrogen Effects on Steel, CARDE Tech. Memo 609/61, May 1961.
14. Mills, R. L., and F. J. Edeskuty: Chem. Eng. Progress, 52 (11), 1956, 477.
15. Dodge, B. F.: Trans. ASME, 75, 1953, 331.
16. Bridgeman, P. W.: "The Compressibility of Five Gases to High Pressure," Proceedings of the American Society of Arts and Sciences, 59, 1924, 173.
17. Poulter, T. C.: Trans. ASME, J. Appl. Mech., 64, 1942, A31.
18. Nelson, G. A., and R. T. Effinger: Welding J., 1955, 12s
19. Cooper, C. M.: Chem. and Eng. News, 30, 1952, 2942.
20. Van Ness, H. C., and B. F. Dodge: Chem. Eng. Prog., 51 (6), 1955, 266.
21. Perlmutter, D. D., and B. F. Dodge: Ind. and Eng. Chem., 48 (5), 1956, 885.
22. Laws, J.S., V. Frick and J. McConnell, Hydrogen Gas Pressure Vessel Problems in the M-1 Facilities, NASA CR-1305, March 1969. (Aerojet-General Report 8800-67, April 1966.)
23. Engelhard Industries, Inc. Sales Brochures, 113 Astor St., Newark, New Jersey.
24. "Molecular Sieves for Selective Adsorption," Data Sheet No. 51 Linde Co. New York, New York (1957).

25. Walter, R. J.: Instrumentation Technology, 14 (9), 1967, 84.
26. Walter, R. J., H. G. Hayes, and W. T. Chandler: Mechanical Properties of Inconel 718, Waspaloy, A-286, and Ti-5Al-2.5Sn ELI in Pure Gaseous H<sub>2</sub>, Prepared for Aerojet General Corp., Sacramento, California, Rocketdyne, a Division of North American Rockwell Corporation, Canoga Park, California Report No. R-8187, 10 April 1970.
27. Dessau, P. P.: Aerojet Nuclear Systems Company, Sacramento, California Personal communication.
28. Bixler, W. D.: Flaw Growth of Inconel 718 and 5Al-2.5Sn (ELI) Titanium in a High Purity Gaseous Hydrogen Environment, Boeing Document D180-10142-1, Prepared for Aerojet General Corporation, Sacramento, California, Contract L-80076, The Boeing Company, Seattle, Washington.
29. Lysyj, I.: "An Apparatus for the Determination of the Ortho-Para Isomer Ratio and the Detection of Trace Impurities in Cryogenic Samples of Hydrogen," ISA Proceedings, 1963, 41.
30. Marcus, H. L., and P. J. Stocker: North American Rockwell Science Center, Thousand Oaks, California, Personal communication.
31. Williams, D. P., and H. G. Nelson: NASA Ames Laboratory, Moffett Field, California, Personal communication.
32. Wei, R. P.: Lehigh University, Bethlehem, Pennsylvania, Personal communication.
33. Forman, R. G.: NASA, MSC, Houston, Texas, Personal communication.

34. Hydrogen Embrittlement Tests of Pressurized Cylindrical and Tensile Specimens Including Conventional Tensile Tests on ASTM A-302-B Steel, Nickel Modified  
NASA, Kennedy Space Center TR-451, October 1966.
35. Honnigford, J.B.: M.S. Thesis, Rensselaer Polytechnic Institute, Troy, New York, 1958.
36. Lorenz, P. M.: Effect of Pressurized Hydrogen Upon Inconel 718 and 2219 Aluminum, ASM Report No. W9-13.2, ASM Report System, Metals Park, Ohio.
37. Walter, R. J., and W. T. Chandler: AIAA J., 4 (2), February 1966, 302.
38. Walter, R. J., J. A. Ytterhus, R. D. Lloyd, and W. T. Chandler: Effect of Water Vapor/Hydrogen Environments on Columbium Alloys, AFML-TR-66-322, Part I, Air Force Materials Laboratory, Wright-Patterson Air Force Base, Ohio, December 1966.
39. Chandler, W. T. and R. J. Walter: "Hydrogen Effects in Refractory Metals and Alloys," Refractory Metals and Alloys, Ed. by I. Machlin, R. T. Begley, and E. D. Weisert, Plenum Press, New York, 1968, 197.
40. Hofmann, W., and W. Rauls: Archiv für das Eisenhüttenwesen, Marz 1961, 1.
41. Hofmann, W., and W. Rauls: Dechema Monograph 45, 1962, 33.
42. Hofmann, W., and W. Rauls: Welding J., May 1965, 225-S.
43. Peterson, R. E.: Stress Concentration Design Factors, John Wiley and Sons, New York, 1953.
44. Cavett, R. H., and H. C. Van Ness: Welding J., July 1963, 316-S.
45. Vennett, R. M., and G. S. Ansell: Trans. Quart. ASM, 62, 1969, 1007.

46. Benson, R.B., R.K. Dann, and L.W. Roberts, Jr.: Trans AIME, 242, 1968, 2199.
47. Walter, R.J. and W.T. Chandler: Effect of Hydrogen Environments on Inconel 718 and Ti-6Al-4V (STA), Paper presented at AIME Meeting, Las Vegas, Nevada, May 11-14, 1970.
48. VanWanderham, M.C., Pratt and Whitney Aircraft, W. Palm Beach, Fla.,  
Personal communication.
49. Walter, R. J., and W. T. Chandler: Effect of Hydrogen Environment on Inconel 718 and Ti-6Al-4V Under Simulated J-2 Engine Operating Environments, R-7920, Rocketdyne, a division of North American Rockwell, Canoga Park, California, Contract NAS8-19C, NASA, MSFC, Huntsville, Alabama, 30 June 1969.
50. Steinman, J. B., H. C. Van Ness, and G. S. Ansell: Welding J, May 1965, 221-S.
51. Vennett, R. M., and G. S. Ansell: Trans. ASM, 60, 1967, 242.
52. Walter, R. J., and W. T. Chandler: Effect of High-Pressure Hydrogen on Storage Vessel Materials, Paper presented at WESTEC Conference, Los Angeles, Calif., ASM Report No. W 8-2.4, ASM Report System, Metals Park, Ohio, 44073, March 1968.
53. Owens, W. H.: Effect of High Pressure Hydrogen on SAE 4140 and SAE 1018 Steels at Ambient Temperatures, AEDC-TR-66-269, Arnold Engineering Development Center, Arnold Air Force Station, Tennessee, December 1966.
54. Pittinato, G. F.: The Effects of a Hydrogen Environment on the Mechanical Properties of Forged Ti-6Al-4V ELI Weldments, McDonnell Douglas Corp., Huntington Beach, Calif., Contract NAS8-21470, NASA, MSFC, Huntsville, Alabama, November 1969.

55. Vennett, R. M., and G. S. Ansell: Trans. Quart. ASM, 62, 1969, 100/.
56. Bernstein, I. M.: Mat. Science and Eng., 6, 1970, 1.
57. Klima, S. J., A. J. Nachtigall, and C. A. Hoffman: Preliminary Investigation of Effect of Hydrogen on Stress-Rupture and Fatigue Properties of an Iron-, a Nickel-, and a Cobalt-Base Alloy, NASA TN D-1458, December 1962.
58. Hofmann, W., W. Rauls, and J. Vogt: Acta. Met., 10, (7) 1962, 688.
59. Walter, R. J., and W. T. Chandler: Effect of High-Pressure Hydrogen on Inconel 718 at -260°F, Research Report RR 70-3, Rocketdyne, a division of North American Rockwell Corporation, Canoga Park, California, 1 June 1970.
60. Pittinato, G. F.: Trans. Quart. ASM, 62, 1969, 410.
61. VanWanderham, M.C., and J.A. Harris, Jr.: Pratt and Whitney Aircraft, West Palm Beach, Florida, Private communication.
62. Lorenz, P. M.: Effect of Pressurized Hydrogen Upon Inconel 718 and 2219 Aluminum, Boeing Document D2-114417-1, The Boeing Company, Seattle, Washington, February 1969.
63. Hancock, G. G., and H. H. Johnson: Trans. AIME, 236, 1966, 513.
64. Spitzig, W. A., P. M. Talda, and R. W. Wei: Eng. Frac. Mechn., 1, 1968, 155.
65. Nelson, H. G., D. P. Williams, and A. S. Tetelman: "Embrittlement of a Ferrous Alloy in a Partially Dissociated Hydrogen Environment," Paper accepted for publication in Met. Trans.
66. Isida, M., and Y. Itagaki: Stress Concentration at the Tip of a Transverse Crack in a Stiffened Plate Subjected to Tension, 4th U.S. Congress Applied Mechanics, 1962, 955.

67. Paris, P. C., and G. C. Sih: ASTM STP No. 381, Philadelphia, Pa., 1965, 30.
68. Toh, T., and W. M. Baldwin: Stress Corrosion Cracking and Embrittlement, John Wiley and Sons, New York, 1956, 176.
69. Williams, D. N.: J. Inst. Metals, 91, 1962-63, 147-152.
70. Walter, R. J., and W. T. Chandler: Metallography of Alloys Fractured in Gaseous Hydrogen Environments, Paper presented at AIME Meeting, Las Vegas, Nevada, 11-14 May 1970.
71. Marcus, H. L., B. S. Hickman, J. C. Williams, G. Garmon, and P. Stocker: Slow Crack Growth in Titanium Alloys Exposed to Low Pressure of H<sub>2</sub> Gas, Paper presented at AIME Meeting, Las Vegas, Nevada, 11-14 May 1970.
72. Laird, C., and G. C. Smith: Phil. Mag., 7, 1962, 847.
73. Meyn, D. A.: Trans. ASM, 61, 1968, 42.
74. Pelloux, R. M.: Trans. ASM, 62, 1969, 281.
75. Martini, W. R.: Flame Heated Thermionic Converter Research, Final Report (July 1961-June 1963), Contract No. DA-36-039 SC-88982, Report AI-8681, Atomics International, a division of North American Rockwell, Canoga Park, California.
76. Steigerwald, E. A.: The Permeation of Hydrogen Through Materials for the Sunflower System, Final Report on Project No. 512-278131-08, 15 November 1963, TRW Electromechanical Division Report ER-5623.

77. Dushman, S.: Scientific Foundations of Vacuum Technique, 2nd Edition, John Wiley and Sons, New York, 1962.
78. Walter, R. J., and J. A. Ytterhus: Behavior of Columbium and Tantalum in Hydrogen Environments, Research Report No. 67-7, Rocketdyne, a division of North American Rockwell, Canoga Park, California.
79. Fidelle, J. P., J. M. Deloron, C. Roux, and M. Rapin: "Influence of Surface Treatments and Coatings on the Embrittlement of High-Strength Steels by Hydrogen Under Pressure," Case of 35 NiCrMo 16 Steel. Reprint from Proceedings of Interfinish '68 (7th International Congress on Metal Surface Treatment, Hanover, 5-9 May 1968).
80. Sawicki, V., and W. Johnson, Cornell University, Private communication.
81. Phillips, A., V. Kerlins, and B. V. Whiteson: AFML-TDR-64-416, Wright-Patterson Air Force Base, Ohio, 1965.
82. Zappfe, C. A.: Mater. Methods, 32, 1950, 58.
83. Tetelman, A. S. and W. D. Robertson: ActaMet, 11, 1963, 415.
84. Petch, N. J. and P. Stables: Nature, 169, 1952, 842.
85. Petch, N. J.: Phil.Mag. 1, 1956, 331.
86. Farrell, K. and A. G. Quarrell: J. Iron Steel Inst. (London) 202, 1964, 1002.

APPENDIX: WORK IN PROGRESS

Rocketdyne,  
a division of North American Rockwell Corporation  
Canoga Park, California

Program Title: Influence of Gaseous Hydrogen on Metals

Principal Investigators: R. J. Walter and W. T. Chandler

Funding Agency: NASA under contract NAS8-25579

The program is designed to provide data on the mechanical properties of candidate structural alloys in hydrogen under simulated Space Shuttle Engine operating conditions. Testing will be conducted in 5000-psig hydrogen and helium environments. The program is divided into the following three phases. Phase I consists of determining the variation of hydrogen-environment embrittlement with the material condition of Inconel 718. Three material heats in three different heat-treatment conditions will be evaluated by tensile testing in the two environments. Inconel 718 weldments will also be tested.

Phase II consists of performing tensile tests at room temperature and -200°F on Inconel 718, Inconel 625, AISI 321 stainless steel, A-286 stainless steel, Ti-5Al-2.5Sn ELI, 2219-T87 aluminum alloy, and OFHC copper specimens.

Phase III consists of measuring the threshold stress intensity,  $K_{th}$  at room temperature and -200°F on Inconel 718, Inconel 625, AISI 321 stainless steel, A-286 stainless steel, Ti-5Al-2.5Sn ELI, 2219-T87 aluminum alloy, and OFHC copper specimens.

Program Title: Space Shuttle Engine and Breadboard Thrust Chambers

Funding Agency: NASA

Severe hydrogen-environment embrittlement has been observed in electroformed nickel used to close out the coolant passages in hydrogen-fueled rocket engine thrust chambers. A program is being conducted to determine the mechanical properties of electroformed nickel in 1200- and 7000-psi hydrogen at  $-320^{\circ}$  to  $400^{\circ}$ F. In 1200-psi hydrogen at room temperature, electroformed nickel has practically no ductility, and the notched strength is reduced about 70 percent compared to that in air. These results are particularly interesting because electroformed nickel is very ductile in air and in comparative helium environments. Annealing decreases the embrittling effect of hydrogen and, as is mentioned in Chapter 9, Preventive Measures, copper and gold coatings are partially effective for preventing embrittlement.

Work is continuing to better define the properties of electroformed nickel in these hydrogen environments by determining its fatigue strength, cyclic crack growth rate, and fracture toughness. Experiments also are being conducted to improve techniques for preventing embrittlement.

Pratt & Whitney Aircraft, Florida Research  
and Development Center,  
Division of United Aircraft Corp.  
West Palm Beach, Florida

Program Title: Influence of Elevated Temperature on Metals In Gaseous Hydrogen

Responsible Engineer: J. A. Harris, Jr.

Funding Agency: NASA under contract NAS8-26191

The program consists of performing fatigue, fracture toughness, creep rupture, and tensile tests in 5000-psi hydrogen and helium environments, according to the matrix in Table 28.

TABLE 28

## TEST PROGRAM (PRATT &amp; WHITNEY AIRCRAFT)

Material	Temp. °F	Low Cycle Fatigue (H <sub>2</sub> /H <sub>e</sub> )	High Cycle Fatigue (H <sub>2</sub> /H <sub>e</sub> )	Fracture Toughness (H <sub>2</sub> /H <sub>e</sub> )	Creep Rupture (H <sub>2</sub> /H <sub>e</sub> )	Notched Tensile (H <sub>2</sub> /H <sub>e</sub> )	Smooth Tensile (H <sub>2</sub> /H <sub>e</sub> )
Inconel 718*	75	X	X	X		X	X
	1250	X	X		X	X	X
Inconel 718**	-320	X					
	75	X	X	X		X	X
	1250	X	X		X	X	X
Inconel 718 Welds**	75			X		X	X
Inconel 625	75	X		X		X	X
	1250				X	X	X
Inconel 625 Welds	75			X		X	X
A-286	75	X		X		X	X
	1250	X			X	X	X
AISI 347	-320					X	X
	75	X	X	X		X	X
	1250				X	X	X
Hastelloy X	75	X				X	X
	1250					X	X
Ti-6Al-4V	75	X		X		X	X
	200	X			X	X	X
(or maximum feasible temperature)							
Ti-5Al-2.5Sn	75	X	X	X		X	X
	200	X			X	X	X
(or maximum feasible temperature)							

\*Anneal at 1750°F for 1 hour; air cooled, plus aged at 1325°F for 8 hours; furnace cooled to 1150°F; held at 1150°F for a total aging time of 18 hours; air cooled

\*\*Solution at 1950°F for 1 hour; air cooled, plus aged at 1400°F for 10 hours; furnace cooled to 1200°F; held at 1200°F for a total aging time of 20 hours; air cooled

OR

Solution at 1900°F for 1 hour; air cooled 50°F/minute or faster, plus aged at 1325°F for 8 hours; furnace cooled to 1150°F; held at 1150°F for total aging time of 18 hours; air cooled. Recent data indicate solution at 1900°F provides less hydrogen degradation in low cycle fatigue than anneal at 1750°F or solution at 1950°F.

NASA, Ames Research Center  
Moffett Field, California

Program Director: D. P. Williams

The mechanical properties of dispersion-strengthened nickel-base alloys are being measured in hydrogen environments. The purpose of the program is to study the intrinsic nature of embrittlement of nickel. Tests performed on Ni-4.5%Al, which contained a fine dispersion of an aluminum-rich phase in an essentially pure-nickel matrix, has shown considerable embrittlement. Fractography of one of these specimens is presented in Chapter 8.

The energy of adsorption of hydrogen on metal surfaces is being measured by two methods: (1) measuring the energy needed to remove adsorbed hydrogen by ion bombardment; (2) evaporating and condensing a metal inside a calorimeter in vacuum and hydrogen environments. The differences between the surface energy in these environments is a measure of the heat of hydrogen adsorption.

The influence of straining in hydrogen on the surface dislocation morphology of AISI 1020 steel is being determined. Cracks are propagated slowly in low-pressure hydrogen, and the fracture surfaces are examined by transmission electron microscopy.

NASA, Manned Spacecraft Center

Houston, Texas

Principal Investigator: R. G. Forman

The sustained flaw growth in surface-flawed sheet specimens of parent metal and weld metal Inconel 718 was measured in 700- to 1000-psi hydrogen and helium environments. The fracture toughness  $K_{Ic}$  of these specimens in air as a function of specimen strength is shown in Fig. 74. Even though a magnification factor was used, the calculated fracture toughness of the parent metal specimens decreased with increasing crack depth.  $K_{Ic}$  in air was about 100 ksi  $\sqrt{\text{in.}}$  for the parent metal and 55 ksi  $\sqrt{\text{in.}}$  for the weld material.

The time to failure for specimens held under load at  $-100^{\circ}\text{F}$  in hydrogen is shown in Fig. 75. The threshold stress intensity, designated as  $K_{Isc}$ , is about 18 ksi  $\sqrt{\text{in.}}$  for the weld metal and 25 ksi  $\sqrt{\text{in.}}$  for the parent metal. The crack growth rate at  $-100^{\circ}\text{F}$  in these hydrogen environments is shown as a function of stress intensity in Fig. 76.

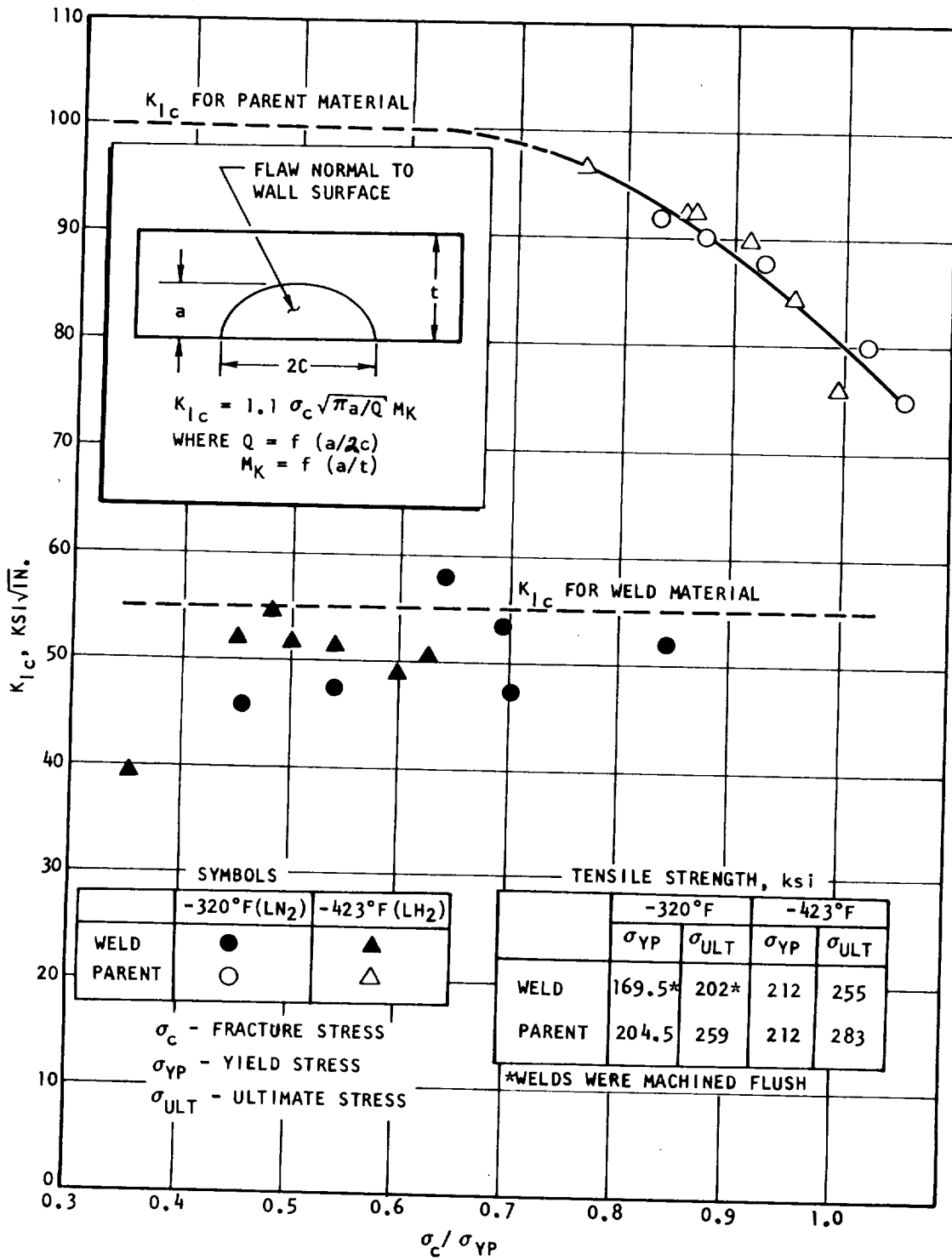


Figure 74. Fracture toughness and tensile strength of Inconel 718.

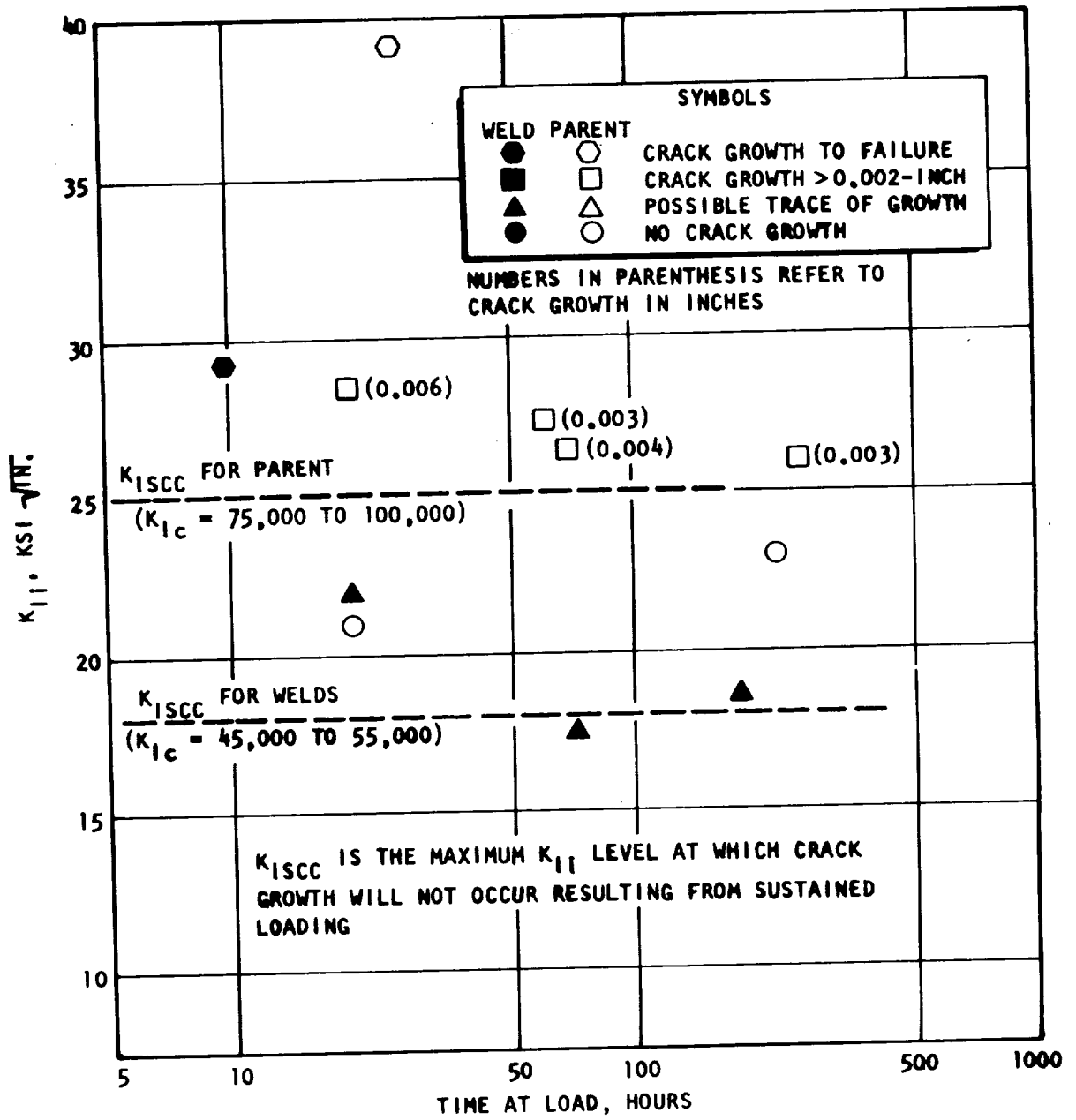


Figure 75. Crack-growth behavior of surface-flawed Inconel 718 specimen tested under sustained load in gaseous hydrogen at  $-100^{\circ}$  F.

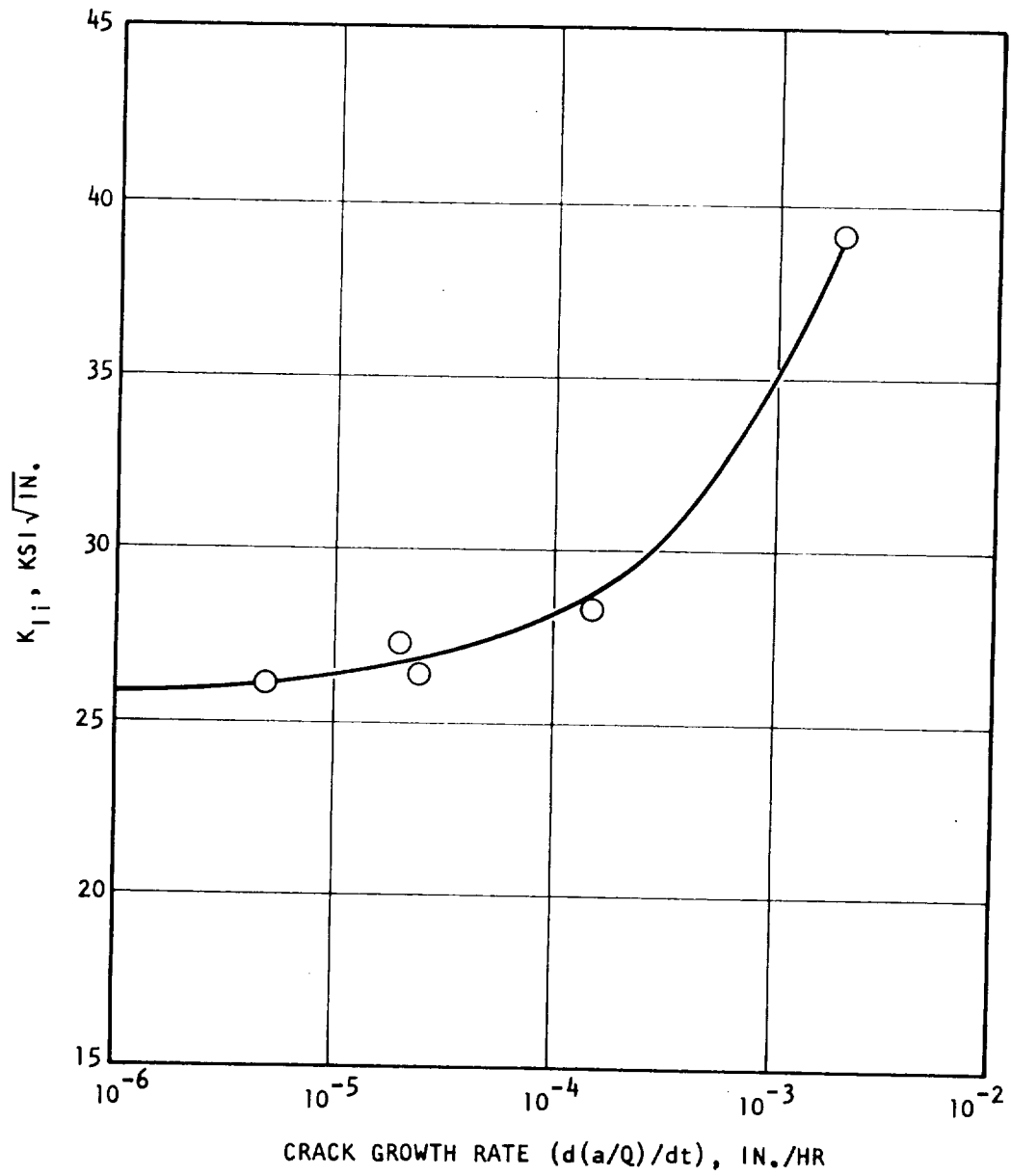


Figure 76. Crack-growth rate of Inconel 718 parent metal under sustained load in gaseous hydrogen at  $-100^{\circ}$  F.

The Boeing Company  
Space Division  
Seattle, Washington

Program Title: Flaw Growth of Inconel 718 and 5Al-2.5Sn (ELI) Titanium in a High-Purity Gaseous Hydrogen Environment

Principal Investigator: W. D. Bixler

Report No.: Boeing Document D180-10142-1, prepared for Aerojet-General Corp.

Contract: L-80076, September 1970

This work has been completed but the final report was received too late to be included in the text. Tests were conducted on surface-flawed Inconel 718 and Ti-5Al-2.5Sn ELI sheet specimens in 1400-psi hydrogen at 70°F, -100°F, and -160°F. The results indicated sustained-load threshold intensities in Inconel 718 of 19.8,  $\approx$ 30, and 99.4 at 70, -100, and -160°F, respectively. Similarly, the sustained-load threshold intensities of Ti-5Al-2.5Sn ELI were 21.5,  $\approx$ 45, and 53.3 at 70, -100, and -160°F, respectively. The threshold intensities for cyclic flaw growth was not measured but was determined to be less than the sustained load threshold values.

A continuation of this work will be performed under a direct NASA contract. Sustained and cyclic flaw growth measurements will be performed on Ti-5Al-2.5Sn ELI specimens in 300- to 400-psi hydrogen at -100 to -423°F.

Aerojet Nuclear Systems Company  
Sacramento, California

Principal Investigator: P. P. Dessau

Funding Agency: NASA

A series of fracture mechanics-type measurements are being planned in 1400-psi hydrogen at room temperature. The tests will be conducted on Fe-22Cr-13Ni-9Mn, titanium, Inconel 718 and A-286 stainless steel. Measurements will include plane strain and cyclic flaw growth tests on compact tension and through cracked-sheet specimens and threshold measurements using the Novak-Rolfe modified WOL-type specimen technique.

U. S. Steel Corporation  
Applied Research Laboratory  
Monroeville, Pennsylvania

Principal Investigator: A. W. Loginow

The threshold stress intensity on various steels in high-pressure hydrogen is being measured by placing preloaded WOL-type specimens in high-pressure hydrogen for relatively long durations.

Cornell University  
Ithaca, New York

Principal Investigator: V. Sawicki

Program Manager: H. H. Johnson, Department Materials Science and Engineering

Funding Agency: AEC

Professor Johnson is continuing his investigations into the influence of environments on crack propagation. Tests are being conducted in 1-atmosphere to 200-mm Hg on H-11 steel specimens. The work includes measuring  $K_{Ic}$ ,  $K_{th}$ , and the influence of temperature, stress intensity, and oxygen impurity content on the rate of crack extension. Investigations are being made to determine whether hydrogen penetration into the metal ahead of the crack is involved in crack growth.

Some of the significant though preliminary results are (1)  $K_{th}$  decreases as the hydrogen pressure increases, (2) the effect of temperature on crack growth rate is essentially the same as observed by Williams and Nelson\* on AISI 4130 steel, (3) the crack growth rate increases with increasing stress intensity but appears to reach saturation at high stress intensities and, (4) oxygen impurity levels of less than 300 to 500 ppm in 1-atmosphere hydrogen did not affect the measured  $K_{th}$ .  $K_{th}$  increased with increasing oxygen content for oxygen contents greater than 500 ppm.

$K_{Ic}$  was measured by noting the stress intensity at which the sustained or slow flaw growth rate reached instability. By this method  $K_{Ic}$  was found to be independent of hydrogen pressure.

\*Williams and Nelson results were discussed earlier in this report.

Lehigh University  
Bethlehem, Pennsylvania

Program Manager: R. P. Wei, Department of Mechanical Engineering and  
Mechanics Funding Agency: ARPA

Professor Wei is continuing his investigations into the influence of environments on crack growth. An interesting observation is that cyclic crack growth rate in  $\approx 0.060$ -inch-thick Inconel 718 plate appears to be the same in a 1-atmosphere hydrogen as in a 1-atmosphere argon environment.

Westinghouse Electric Corporation

Astronuclear Laboratory

Pittsburgh, Pennsylvania

Principal Investigator: R. L. Kesterson

Funding Agency: NASA

A program has commenced in which  $K_{th}$  is being measured in hydrogen at atmospheric pressure and temperatures ranging from  $-320^{\circ}\text{F}$  to  $+300^{\circ}\text{F}$ . The materials are beryllium, TZM molybdenum alloy, tungsten, stainless steels, and some copper and aluminum alloys.

A program is being scheduled to determine the influence of an ionized hydrogen environment on the mechanical properties of beryllium, beryllium copper, tungsten alloys, A-286 stainless steel, Cu-B<sup>10</sup> mixtures, BATH (aluminum mixture), aluminum alloys, graphites, and AISI 301, 302, and 304 stainless steels.

Aerojet Nuclear Systems Company  
Sacramento, California

Principal Investigator: C. E. Dixon

Funding Agency: NASA

Notched specimens of four materials will be irradiated in water (150°F) prior to room-temperature tensile testing in 500- and 1500-psig hydrogen. Control tests also will be conducted in helium after irradiation. The four materials to be tested are: Inconel 718, Ti-5Al-2.5Sn, A-286 stainless steel (bolt material), AISI type 301 stainless steel (full hard).

AEC, Savannah River Laboratory  
Aiken, South Carolina

Principal Investigator: J. A. Donovan

Funding Agency: NASA

The purpose of this program is to develop fundamental knowledge about the mechanism of hydrogen damage in metals at near-ambient temperatures. Initial work has concentrated on the hydrogen solubility, diffusivity, and permeation in high-purity iron and nickel.

